

thesisMPX_optimised.pdf

by Miguel Perez Xochicale

Submission date: 02-Nov-2018 02:18PM (UTC+0000)

Submission ID: 93819749

File name: 181102-19289-2larco_attachment_634819220181102-19289-1tkjnsh.pdf (15.78M)

Word count: 45372

Character count: 239469

NONLINEAR ANALYSES TO QUANTIFY MOVEMENT VARIABILITY IN HUMAN-HUMANOID INTERACTION

by

MIGUEL XOCHICALE

¹⁷
A thesis submitted to
The University of Birmingham
for the degree of
DOCTOR OF PHILOSOPHY

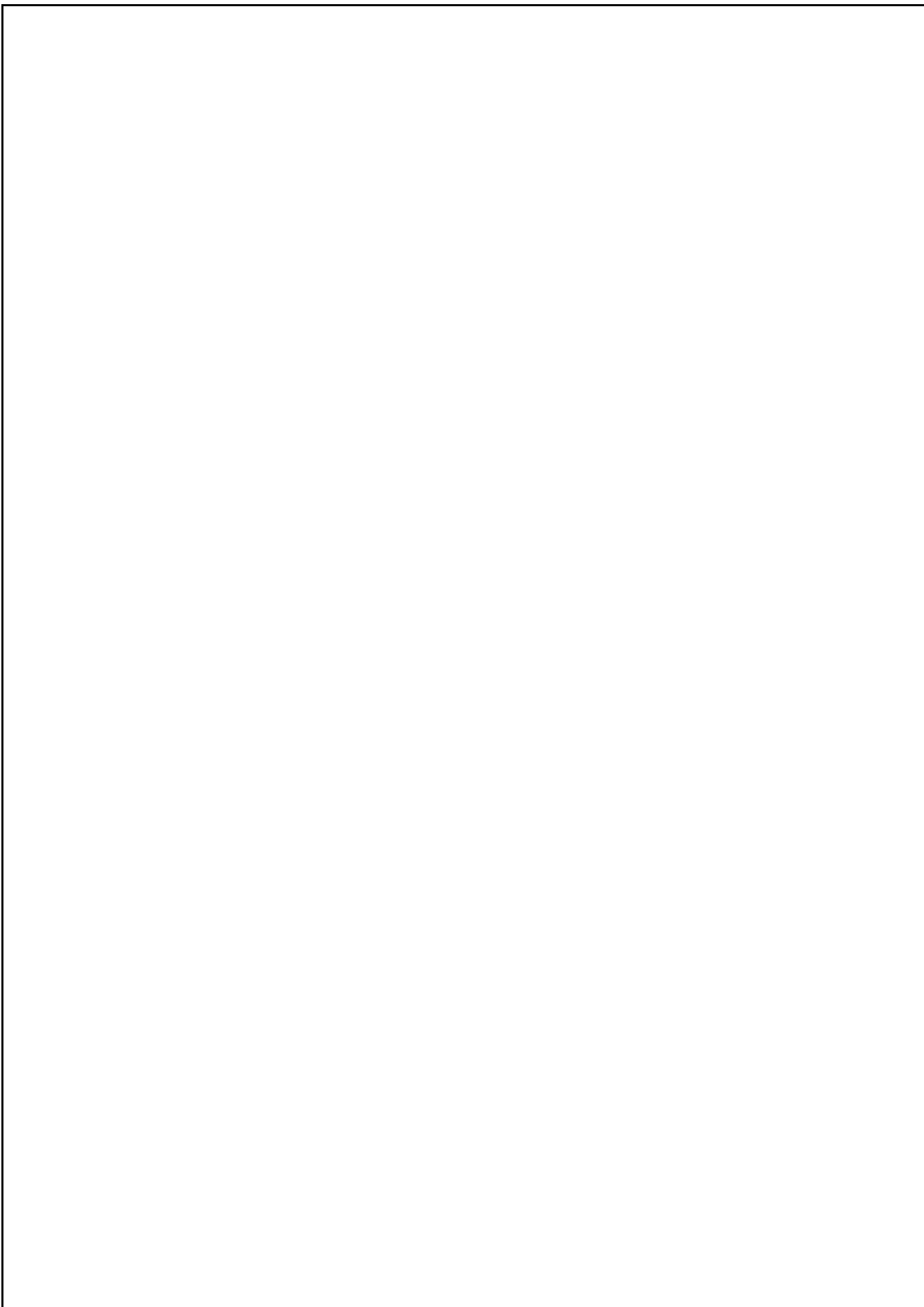
School of Engineering
College of Engineering and Physical Sciences
The University of Birmingham
26 October 2018

Abstract

Nonlinear analyses investigate the dynamics of observed time-ordered data. Such dynamics, for this thesis, are complex systems of sensorimotor variables of movement variability (MV) in the context of human-humanoid interaction. Hence, this dissertation not only explores questions such as what to quantify in MV?, or which nonlinear tools are appropriate to quantify MV?, but also how nonlinear analyses are affected with real-world time series data (e.g. nonstationary, data length limitations, sampling rate changes or noisiness). Particularly, I review nonlinear tools such as methods to determine embedding parameters, Reconstructed State Spaces (RSSs), Recurrence Plots (RPs) and Recurrence Quantification Analyses (RQAs). To my knowledge, I can conclude that, no scientific work has been reported regarding nonlinear analyses (e.g. RSSs with UTDE, RPs and RQAs) to quantify movement variability in the context of human-humanoid interaction. Also, we created 3D surfaces of RQA values considering the variation of embedded parameters and recurrence thresholds to show that 3D surfaces of RQA ENTR might be a better approach to provide understanding on the dynamics of different characteristic of real-world time series data. I can foresee many areas of applications where humanoids robots can be pre-programmed with nonlinear analyses algorithms to evaluate the improvement of movement performances, to quantify and provide feedback of skill learning or to quantify movement adaptations and pathologies.



$$\min_G \max_X F(G,X)$$



Acknowledgements

308

I would like to acknowledge to the Mexican National Council of Science and Technology (CONACyT) that funded my curiosity-driven research which allow me to quench this endless thirst for new knowledge during my PhD degree at The University of Birmingham, UK. To Professor Chris Baber for supervising my scientific endeavours and who wisely looses the leash in any of my explorations so as to take me back at the right time to write up this thesis. To Professor Martin J Russell who, in the first year of my PhD, helped with his acute comments and critics to make a better use of the language or mathematics. To Mourad Oussalah who kindly dedicate his time to discuss my research interest and our collaboration which were published in three peer-review confereces. I would also like to thank to Dr. Dolores Columba Perez Flores for her valuable comments that help me to have a better insight on nonlinear analyses, and to Constantino Antonio Garcia Martinez for developing the `nonlinearTseries` R package that was of significant help to accelerate the results of this thesis.

Miguel Xochicale

Birmingham, UK

October 2018



⁴² Table of contents

List of figures	xv
1 Introduction	1
1.1 Background	1
1.2 Movement Variability	3
1.2.1 Modelling Human Movement Variability	4
1.2.2 Movement Variability in Human-Humanoid Interaction	9
²⁰² 1.3 Research questions	13
1.4 Outline of the thesis	15
1.5 Publications	17
2 Quantifying Movement Variability	19
2.1 Introduction	19
2.2 Fundamentals of time-series analysis	19
2.2.1 Linear and nonlinear systems	20
2.2.2 Stationary and nonstationary signals	20
¹⁸⁶ 2.2.3 Deterministic and stochastic systems	20
2.2.4 Deterministic chaotic time series	21
2.3 Quantifying Movement Variability with Nonlinear Dynamics	21
2.3.1 Introduction	21

Table of contents

2.3.2	What to quantify in MV?	23
2.3.3	Which nonlinear tools are appropriate to quantify MV?	24
2.4	Nonlinear analyses with real-world data	27
2.4.1	Nonsationarity	28
2.4.2	Data length	29
2.4.3	Sampling rate	29
2.4.4	Noise	30
2.5	Final remarks	32
3	Nonlinear Analyses	33
3.1	Introduction	33
3.2	State Space Reconstruction Theorem	34
3.3	Uniform Time-Delay Embedding (UTDE)	35
3.4	Estimation of Embedding Parameters	37
3.4.1	False Nearest Neighbours (FNN)	37
3.4.2	Average Mutual Informationi (AMI)	41
3.4.3	Overall minimum embedding parameters	44
3.5	Reconstructed State Space with UTDE	44
3.6	Recurrence Plots (RP)	45
3.6.1	Structures of Recurrence Plots	47
3.7	Recurrence Quantifications Analysis (RQA)	48
3.7.1	Measures of RP based on the recurrence density	48
3.7.2	Measures of RP based on diagonal lines	49
3.7.3	Some weaknesses and strengths of RP and RQA.	50
3.8	Final remarks	52
4	Experiments	53

Table of contents

4.1	Aims	53
4.2	Participants	53
4.2.1	Human-Image Imitation Activities	54
4.2.2	Human-Humanoid Imitation Activities	54
4.3	Equipment	54
4.4	Ethics	55
4.5	Experiments	55
4.5.1	Human-Image Imitation Activities	55
4.5.2	Human-Humanoid Imitation Activities	59
4.6	Processing of time series	60
4.6.1	Raw time-series	60
4.6.2	Postprocessing time-series	62
4.6.3	Normalization of time-series	62
4.6.4	Smoothing time-series	63
4.6.5	Window size of time-series	63
5	Quantifying Human-Image Imitation Activities	65
5.1	Introduction	65
5.2	Time series	65
5.3	Minimum Embedding Parameters	68
5.3.1	Average minimum embedding parameters	70
5.4	Reconstructed state spaces with UTDE	70
5.5	Recurrences Plots	76
5.6	Recurrence Quantification Analysis	82
5.7	Weaknesses and strengths of RQA	86
5.7.1	Sensors and activities	88
5.7.2	Window size	94

Table of contents

5.7.3	Smoothness	94
5.7.4	Participants	97
5.7.5	Final remarks	97
6	Quantifying Human-Humanoid Imitation Activities	99
6.1	Introduction	99
6.2	Time series	100
6.3	Minimum Embedding Parameters	101
6.3.1	Average minimum embedding parameters	103
6.4	Reconstructed state spaces with UTDE	103
6.5	Recurrences Plots	107
6.6	Recurrence Quantification Analysis	110
6.7	Weaknesses and strengths of RQA	113
6.7.1	Sensors and activities	115
6.7.2	Window size	115
6.7.3	Smoothness	119
6.7.4	Participants	119
6.7.5	Final remarks	161 122
7	Conclusions and future work	123
7.1	Conclusions	123
7.2	Future work	126
Appendix A	Examples of Uniform Time-Delay Embedding	131
A.1	20 sample length vector.	131
A.2	Time series for horizontal movement of a triaxial accelerometer.	133
Appendix B	Equipment	137

Table of contents

B.1	NeMEMsi IMU sensors	137
B.2	Time-series preprocessing	139
B.2.1	Organising Data in Multidimensional Arrays	139
B.2.2	Data Synchronisation	140
B.2.3	Time Alignment	140
B.2.4	Issues with IMUs	141
B.3	NAO – humanoid robot	142
Appendix C	Experiment Design	143
C.1	Experiment Check List	143
C.2	Information Sheet	143
Appendix D	Additional Results for HII experiment	149
D.1	Time Series	149
D.2	Embedding parameters	156
D.2.1	Minimum dimension embedding values	156
D.2.2	Minimum delay embedding values	161
D.3	RSSs	166
D.4	RPs	175
D.5	RQAs	180
D.5.1	REC values	180
D.5.2	DET values	183
D.5.3	RATIO values	186
D.5.4	ENTR values	189
Appendix E	Additional results for HHI experiment	193
E.1	Time Series	193
E.2	Embedding parameters	200

Table of contents

E.2.1	Minimum dimension embedding values	200
E.2.2	Minimum delay embedding values	203
E.3	RSSs	206
E.4	RPs	211
E.5	RQAs	216
E.5.1	REC values	216
E.5.2	DET values	217
E.5.3	RATIO values	219
E.5.4	ENTR values	220
References		223

List of figures

1.1	Thesis outline	16
3.1	State space reconstruction methodology	36
3.2	Uniform time-delay embedding	38
3.3	Minimum dimension embedding values with Cao's method	41
3.4	Minimum delay embedding values with AMI's method	43
3.5	Recurrence Plots	46
3.6	Patterns in Recurrence Plots	48
4.1	Human-image imitation (HII) activities	57
4.2	Time series for horizontal and vertical arm movements	58
4.3	Human-humanoid imitation activities	59
4.4	Time series duration of horizontal and vertical arm movements	61
5.1	Time series for horizontal arm movements	66
5.2	Time series for vertical arm movements	67
5.3	Box plots for minimum embedding dimensions	69
5.4	Box plots for 1st minimum AMI	69
5.5	RSSs for horizontal arm movements (no beat)	72
5.6	RSSs for horizontal arm movements (with beat)	73
5.7	RSSs for vertical arm movements (no beat)	74

List of figures

5.8 RSSs for vertical arm movements (with beat)	75
5.9 RPs for horizontal arm movements (no beat)	78
5.10 RPs for horizontal arm movements (with beat)	79
5.11 RPs for vertical arm movements (no beat)	80
5.12 RPs for vertical arm movements (with beat)	81
5.13 Box plots of RQA values for horizontal arm movements	84
5.14 Box plots for RQA values for vertical arm movements	85
5.15 3D surfaces of RQA metrics	87
5.16 3D surfaces of RQA metrics for horizontal arm movements with HS01 . .	90
5.17 3D surfaces of RQA metrics for horizontal arm movements with HS02 . .	91
5.18 3D surfaces of RQA metrics for vertical arm movements with HS01 . .	92
5.19 3D surfaces of RQA metrics for vertical arm movements with HS02 . .	93
5.20 3D surfaces of RQA metrics for different window size lengths	95
5.21 3D surfaces of RQA metrics with three levels of smoothness	96
5.22 3D surfaces of RQA metrics with three participants	98
6.1 Time series for horizontal arm movements	100
6.2 Time series for vertical arm movements	101
6.3 Box plots of minimum embedding parameters	102
6.4 RSSs for horizontal arm movements	105
6.5 RSSs for vertical arm movements	106
6.6 RPs for horizontal arm movements	108
6.7 RPs for vertical arm movements	109
6.8 Box plots for RQA values	112
6.9 3D surfaces for RQA metrics	114
6.10 3D surfaces of RQA metrics for HS01 sensor	116
6.11 3D surfaces of RQA metrics for RS01 sensor	117

List of figures

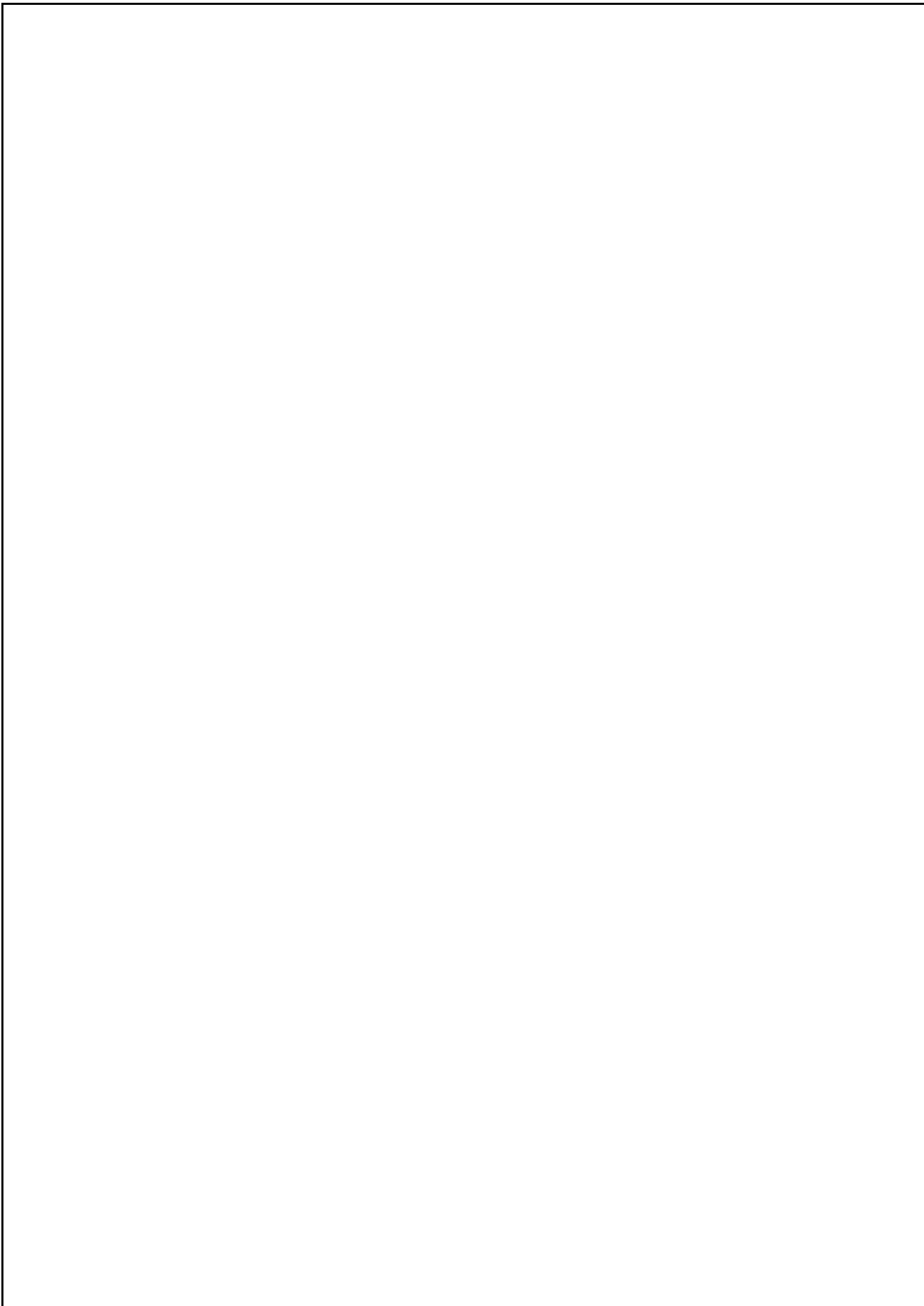
6.12 3D surfaces of RQAs metrics with four window lengths	118
6.13 3D surfaces of RQA metrics with three levels of smoothness	120
6.14 3D surfaces of RQA metrics with three participants	121
A.1 Examples of time series with an IMU	135
B.1 Inertial Measurament Sensor	139
B.2 NAO, humanoid robot from SoftBank	142
C.1 Experiment Check List	144
C.2 Participant Information Sheet (p. 1/4)	145
C.3 Participant Information Sheet (p. 2/4)	146
C.4 Participant Information Sheet (p. 3/4)	147
C.5 Participant Information Sheet (p. 4/4)	148
D.1 Time series for horizontal arm movements (sg0)	150
D.2 Time series for horizontal arm movements (sg1)	151
D.3 Time series for horizontal arm movements (sg2)	152
D.4 Time series for vertical arm movements (sg0)	153
D.5 Time series for vertical arm movements (sg1)	154
D.6 Time series for vertical arm movements (sg2)	155
D.7 Minimum embedding dimensions for horizontal arm movements (no beat)	157
D.8 Minimum embedding dimensions for horizontal arm movements (with beat)	158
D.9 Minimum embedding dimensions for vertical arm movements (no beat) .	159
D.10 Minimum embedding dimensions for vertical arm movements (with beat)	160
D.11 First minimum AMI values for horizontal arm movements (no beat) . .	162
D.12 First minimum AMI values for horizontal arm movements (with beat) .	163
D.13 First minimum AMI values for vertical arm movements (no beat) . . .	164

List of figures

D.14 First minimum AMI values for vertical arm movements (with beat)	165
D.15 RSSs for horizontal normal arm movements (no beat)	167
D.16 RSSs for horizontal normal arm movements (with beat)	168
D.17 RSSs for horizontal faster arm movements (no beat)	169
D.18 RSSs for horizontal faster arm movements (with beat)	170
D.19 RSSs for vertical normal arm movements (no beat)	171
D.20 RSSs for vertical normal arm movements (with beat)	172
D.21 RSSs for vertical faster arm movements (no beat)	173
D.22 RSSs for vertical faster arm movements (with beat)	174
D.23 RPs for horizontal normal arm movements	176
D.24 RPs for horizontal faster arm movements	177
D.25 RPs for vertical normal arm movements	178
D.26 RPs for vertical faster arm movements	179
D.27 REC values for horizontal arm movements	181
D.28 REC values for vertical arm movements	182
D.29 DET values for horizontal arm movements	184
D.30 DET values for vertical arm movements	185
D.31 RATIO values for horizontal arm movements	187
D.32 RATIO values for vertical arm movements	188
D.33 ENTR values for horizontal arm movements	190
D.34 ENTR values for vertical arm movements	191
E.1 Time series for horizontal arm movements (sg0)	194
E.2 Time series for horizontal arm movements (sg1)	195
E.3 Time series for horizontal arm movements (sg2)	196
E.4 Time series for vertical arm movements (sg0)	197
E.5 Time series for vertical arm movements (sg1)	198

List of figures

E.6 Time series for vertical arm movements (sg2)	199
E.7 Minimum embedding dimensions for horizontal arm movements	201
E.8 Minimum embedding dimensions for vertical arm movements	202
E.9 First minimum AMI values for horizontal arm movements	204
E.10 First minimum AMI values for vertical arm movements	205
E.11 RSSs for horizontal normal arm movements	207
E.12 RSSs for horizontal faster arm movements	208
E.13 RSSs for vertical normal arm movements	209
E.14 RSSs for vertical faster arm movements	210
E.15 RPs for horizontal normal arm movements	212
E.16 RPs for horizontal faster arm movements	213
E.17 RPs for vertical normal arm movements	214
E.18 RPs for vertical faster arm movements	215
E.19 REC values for horizontal arm movements	216
E.20 REC values for vertical arm movements	217
E.21 DET values for horizontal arm movements	218
E.22 DET values for vertical arm movements	218
E.23 RATIO values for horizontal arm movements	219
E.24 RATIO values for vertical arm movement	220
E.25 ENTR values for horizontal arm movements	221
E.26 ENTR values for vertical arm movements	221



Chapter 1

Introduction

1.1 Background

Human movement involves not only multiple joints and limbs for a specific task in a determined environment but also external information processed through all of our available senses and our prior experiences. Recent studies in human motion recognition have revealed the possibility of estimating features from lower dimension signals to distinguish differences between styles of movement, such as pedalling (Quintana-Duque, 2012, 2016) or walking (Frank et al., 2010; Samà et al., 2013). Similar approaches have been applied to pattern recognition of physiological signals (speech and heart pathologies or epilepsy) (Gómez-García et al., 2014).

Signals of lower dimension are generally time series of one-dimension in \mathbb{R} which commonly have high nonlinearity, complexity, and non-stationarity (Caballero et al., 2014; Gómez-García et al., 2014; Huffaker et al., 2017). With that in mind, traditional methods in time-domain or frequency-domain generally tend to fail when detecting tiny modulations in frequency or phase (Marwan, 2011). This can mean that subtle signatures of each individual's movement could be missed using traditional methods. However, methods of nonlinear time series analysis can quantify such subtleties in

Introduction

human movement variability (Frank et al., 2010; Gómez-García et al., 2014; Marwan, 2011; Packard et al., 1980; Quintana-Duque, 2012, 2016; Samà et al., 2013; Stergiou and Decker, 2011). Recently, Bradley and Kantz (2015) reviewed methods for nonlinear time series analysis, such as the reconstructed state space (RSS) (Takens, 1981), recurrence plots (RP) (Eckmann et al., 1987) and recurrence quantification analysis (RQA) (Zbilut and Webber, 1992). Such methods are implemented using embedding parameters (m and τ). However, the computation of embedding parameters is still an open problem since there is no general technique to compute the embedding parameters because time series are system-dependent, meaning that defined parameters may only work for one purpose, e.g., prediction, or may not work well for other purposes e.g., computing dynamical invariants (Bradley and Kantz, 2015).

In addition, the quality of the time series signals is reflected on the reliability of the results for nonlinear tools. For instance, methodologies to compute embedding parameters e.g., autocorrelation, mutual information, and nearest neighbour, require data which are well sampled and with little noise (Garland et al., 2016) or need to be purely deterministic signals (Kantz and Schreiber, 2003). Similarly, methods such as RSS, RP and RQA can break down when datasets have different length, different accuracy and precision (Frank et al., 2010), or when data are contaminated with different or unknown sources of noise (Garland et al., 2016). It is surprising that despite these problems, nonlinear dynamics have proven to be helpful to understand and to characterise time series in the context of human movement (Bradley and Kantz, 2015; Frank et al., 2010; Gómez-García et al., 2014; Marwan, 2011; Quintana-Duque, 2012, 2016; Samà et al., 2013; Stergiou and Decker, 2011). Another point to consider when analysing time series analysis using nonlinear dynamics is the appropriate use of post-processing techniques such as interpolation, filtering or normalisation. However,

1.2 Movement Variability

167

there is little research on the effects of post-processing techniques and the interpretation of the results for RSSs, RPs and metrics of RQA.

73

Movement Variability

Variability is inherent within and between all biological systems (Newell and Corcos, 1993). For instance, variability has been studied in electroencephalographic signals in human brains (Klonowski, 2007), in physiological signals like the heart rate variability (Rajendra Acharya et al., 2006; Schumacher, 2004), respiratory patterns of rats (Dhingra et al., 2011), in speech variability where not only the linguistic aspect is investigated but factors like gender, age, social, state of health, emotional state are strongly related to uniqueness of the speaker (Benzeghiba et al., 2007) or even in odor responses based on cultural background and gender (Ferdenzi et al., 2013).

Variability has also been well studied in human body movement, where, for instance, Bernstein (1967) stated that no human movement is repeated exactly with the same trajectory. With that in mind, movement variability has been used as a model of fatigue to prevent chronic musculoskeletal disorders (Mathiassen, 2006; Srinivasan and Mathiassen, 2012). Movement variability has also been considered as an indicator of skilled performance in sport science where, for instance, Wagner et al. (2012) show how movement variability based on statistical analysis varies with skill for three levels 306 of throwing techniques (low-skilled, skilled, and high-skilled). Therefore, Bartlett et al. (2007) concluded that movement variability is ubiquitous across sports (javelin throwing, basketball shooting or running). Another interesting example is that movement variability can be considered as an identifier for personal trait (Sandlund et al., 2017), where many factors of the human body can be considered for identification, such as: age (Krüger et al., 2013; MacDonald et al., 2006; Stergiou et al., 2016; Vaillancourt and Newell, 2003), gender (Svendsen and Madeleine, 2010), pain status (Madeleine et al., 19 148

Introduction

2008; Sandlund et al., 2008), body composition (Chiari et al., 2002), work experience (Madeleine and Madsen, 2009), pace, movement direction or cognitive demands like perception, memory or capacity for introspection (Kanai and Rees, 2011; Srinivasan and Mathiassen, 2012). Additionally, Bartlett et al. (2007) highlighted that movement variability can be interpreted from different theoretical disciplines. For instance, a cognitive control theorist considers variability as undesirable noise and variability is reduced as skill increases, meaning that "becoming dexterous freezes unwanted degrees of freedom in the kinematic chain" (Bartlett et al., 2007, p. 238). In contrast, an ecological motor control specialist considers movement variability either as a functional role in human movement for "coordination change and flexibility to adapt" in different environments (Bartlett et al., 2007, p. 238) or as an exploration and exploitation of body parts in the "perceptual-motor workspace" (Herzfeld and Shadmehr, 2014; Wu et al., 2014).

Stergiou and Decker (2011), in contrast, highlighted that an optimal state of movement variability is associated with healthiness. For instance, motor disabilities may be related to either (i) wide range of behaviours which appear to be random, unfocussed and unpredictable or (ii) narrow range of behaviours which seems to be rigid, inflexible and predictable. Specifically, postural sway variability which is larger for patients with Parkinson disease or the likelihood of falling in elderly individuals which is associated with too little or too much step width variability. This suggest that extremes of movement variability are symptomatic of lower ability to control movement.

1.2.1 Modelling Human Movement Variability

Human movement involves a complex system where many sensorimotor variables such as joints, muscles, nervous system, motor unit and cells are the sources for

1.2 Movement Variability

different types of variability (Newell and Corcos, 1993). Hence, variability encompasses different types, sources and views of variability. For instance, from a biomechanical view, motion variability can be modelled as system of differential equations for the neuro-musculoskeletal control system where motion variations can occur because of "perturbations of initial states of the skeletal system", perturbations of "muscular or neural subsystems ", or "external torques and forces acting on the skeletal system" (Hatze, 1986, p. 13). According to Hatze (1986) motion variability can be caused by (i) direct consequences of adaptive learning process, and (ii) random fluctuations 245 which are the result of stochastic processes in the nervous system. Hence, Hatze (1986) proposed measures of dispersion (e.g. Fourier series and entropy measures) to quantify the deviation of motion from a certain reference. With that, Hatze (1986) pointed out that the combination of deviations from angular coordinates (radians) and linear coordinates (meters) for Fourier series were an unacceptable quantifier as the units are different. Hence, Hatze (1986) proposed the use of entropy as a global quantifier for motion variability and concluded that any movement deviation of a body joint may be the result of deterministic and stochastic causes.

Another approach to model variability has been proposed by Müller and Sternad (2004), who decompose variability into exploration of task tolerance(T), noise reduction(N), and covariation(C). Hence, the quality of performance in goal-oriented tasks, e.g. hitting a target, is defined "by the accuracy and replicability of the results" (deviations from the target) "over repeated attempts of execution" (configuration of joint angles with its velocity, angles and position) (Müller and Sternad, 2004, p. 229). For the experiment, Müller and Sternad (2004) considered table skittles, where participants 34 throw a ball on a string that swings around a center post with the objective of knocking down the skittle at the opposite site. Then, Müller and Sternad (2004) proposed D as the absolute average of distance to the targets in n trials and used this as a measure 10.

Introduction

of the collective performance that combines a function for movement based on the execution vector with a function for the minimum ¹⁰ distance from the target d . Therefore, ³⁴ the overall difference in performance D is decomposed into three unequal contributions ¹⁰ of covariation C , noise reduction N and task tolerance T . Considering a 2-D task space that spanned the release angle α and absolute velocity v , the components of contributions of variability were calculated from five data sets (A , A_0 , A_{shift} , B and B_0): (i) the component of covariation where sets A and A_0 and B and B_0 have the same means and variances, (ii) the component of tolerance where sets A and A_{shift} differ only ¹⁰ on their location in the task space, and (iii) the component of noise where sets A_{shift} and B_0 have the same means but different variances (see Fig. 6 in Müller and Sternad ¹⁰ (2004) for further details). With that in mind, Müller and Sternad (2004) conducted an experiment with forty-two participants for five different locations of the target skittle where for each target a ¹⁰ participant performed 320 trials which is a total of 1600 trials ³⁴ and therefore presented statistical confirmation of the contributions of T , N and C using ANOVA. Hence, Müller and Sternad (2004) concluded that T and N contribute more to improvement of a performance of a task than C for initial practice, meaning that a new combination of angles and velocities explore a large region of solution space (hitting the target). However, for later practice T diminishes, ³⁴ and N and C started to be more relevant. Also, Müller and Sternad (2004) showed in various experiments of throwing actions that variability in the movement results (deviations from the target) is generally smaller than variability in the execution (variables or release angles and ¹⁰ velocities) for which it is concluded that covariation between execution variables is another component of variability. With that in mind, Müller and Sternad (2004) concluded that task space exploration is an essential contribution to the improvement of movement performances which is an explanation to the increase of noise in early practice phases.

1.2 Movement Variability

Seifert et al. (2011) investigated coordination profiles for recreational and competitive breaststroke swimmers and proposed an hourglass model of variability that illustrates the amount of variability as a function of expertise. Hence, Seifert et al. 2011, p. 551 stated recreational swimmers show a considerable amount of intra-variability "as they seek an individually appropriate coordination pattern to accommodate the novel constraints of locomotion in water", whereas experts swimmers, after a considerable practice, will still explore new environments to optimise their technique that create another secondary blooming of variability which is the result of "the environment exploration to optimise their technique with their individual strengths (e.g. physical, anatomical, mental, etc.) and to gain an advantage over competitive swimmers". To test the hourglass model of variability, Seifert et al. (2011) considered the continuous relative phase (CRP) between the elbow phase angle and knee phase angle, therefore CRP is used as an indicator on how swimmers synchronise arm recovery (elbow extension) and leg recovery (knee flexion). Seifert et al. (2011) analysed inter-individual variability of swimmers with the shape of the curves of CRP which provide an indication of the inter-limb coordination, applied statistical measures such as hierarchical clustering using eleven variables of CRP to classify the recreational swimmers into three cluster of coordination (intermediate, most-variable and in-phase) and used Fisher information to test which CRP variables were significantly differentiated the clusters. With that, Seifert et al. (2011) concluded that inter-individual coordination variability for recreational swimmers could be the result of (i) different state of process learning, (ii) environmental constraints (different perception of the aquatic resistance), or (iii) different perception of the task constrains (floating instead of swimming).

Preatoni (2007) and Preatoni et al. (2010, 2013) report that inter-trial variability is defined as combination of functional changes associated with the nonlinear properties of the neuro-musculo-skeletal system (V_{nl}) and random fluctuations in the neuro-motor-

Introduction

skeletal system (V_e). Additionally, Preatoni et al. 2013, p. 72 stated that the random fluctuations in movement variability can be composed by $V_e = V_{eb} + V_{ee} + V_{em}$, where V_{eb} relates to the behavior and is the "error in the sensory information and in the motor output commands", V_{ee} is the "changes in the environmental conditions" and V_{em} is the "changes in measuring and data processing procedures". Therefore, similar as Hatze (1986), Preatoni et al. 2013, p. 77 pointed out that V_{nl} "may be interpreted as the flexibility of the system to explore different strategies to find the most effective strategy among the many available". Hence, Preatoni et al. 2010, p. 1328 concluded that the total variability represents the changes of contributions for V_e and V_{nl} and it is defined as $V_{tot} = V_e + V_{nl}$, where V_{tot} "may reveal the effects of adaptation, pathologies and skills learning". Also, Preatoni et al. (2013) noted that their work only investigate error from biological variability (e.g. V_{eb}) which does not consider non-biological noise resulting from measuring instruments or data post-processing techniques, such non-biological noise has high frequency components that are usually removed. Therefore, the work of Preatoni et al. (2010) and Preatoni et al. (2013) do not consider an overall index to quantify movement variability but the combination of both V_{eb} and V_{nl} . With that in mind, Preatoni (2007) analysed the influences of V_{eb} and V_{nl} for movement repeatability by comparing entropy measures (e.g. ApEn and SampEn) with values of their surrogate counterparts.

Generally, the previous approaches reported different models for movement variability which then are quantified with different tools. For instance, Hatze (1986) and Preatoni et al. (2010, 2013) use entropy measures as the authors consider that the origin of the signals in the human body is the result of deterministic and stochastic processes, whereas Müller and Sternad (2004) and Seifert et al. (2011) reported measures of magnitude that limited the evaluation of the whole trajectories as structures of movement variability in human body activities. Therefore, for this thesis, it is

1.2 Movement Variability

important to note that even with the proposed models for movement variability (Hatze, 13 Müller and Sternad, 2004; Preatoni et al., 2010, 2013; Seifert et al., 2011) which have been quantified with statistical or nonlinear tools, little has been investigated with regards to the reliability of the nonlinear tools when using real-world data that is commonly noisy, deterministic, stochastic or nonstationary (Newell and Slifkin, 1998). A further review of nonlinear analyses is presented in Chapter 2.

1.2.2 Movement Variability in Human-Humanoid Interaction

153 Movement variability in the context of human-humanoid interaction has been investigated for exercising, rehabilitation and dancing purposes in the last six years (Görer 201 et al., 2013; Guneysu et al., 2015, 2014; Peng et al., 2015; Tsuchida et al., 2013).

For instance, Görer et al. (2013) conducted an experiment of a robotic fitness coach where eight elderly participants performed five gestures: three for arm related exercises and two for leg strength exercises. Hence, Görer et al. (2013) with only graphical visualisation of joint angles trajectories extracted from the pose estimation of a kinect sensor, stated that only one subject out of eight fail to imitate the gestures correctly. Additionally, Görer et al. (2013) surveyed participants using a 5-point Likert scale about the positive and negative effect, flow, immersion and challenge of the human-robot interaction activity, concluding that their system is easy to use based on the high scores for immersion and positive effect and low scores for challenge and negative effect. However, the small sample size and somewhat naive analysis of data in the study makes it difficult to generalise these findings.

152 Another example is the work of Guneysu et al. (2014) who conducted experiments with children for upper arm rehabilitation using a play-like child robot interaction. Hence, Guneysu et al. (2014), using a Kinect sensor to get data of joint angles of the participants' skeleton, performed an automatic evaluation of three upper body actions

Introduction

(shoulder abduction, shoulder vertical flexion and extension, and elbow flexion) of eight healthy children who mimicked an humanoid robot. To evaluate motion imitation, Guneyasu et al. 2014, p. 202 considered similarity error using Dynamic Time Warping (DTW) that penalise large angle errors over ten percent in the area range of the motion type and applied recall measure as a representation of "how much of angular area of the baseline motion from the humanoid robot is also covered by the child's motion". Then, Guneyasu et al. (2014) presented the evaluation of five physiotherapists using Intraclass correlation coefficient (ICC) which is a metric for reliability of ratings for motion types, and reported that for the first motion, which consists of only one joint, the metric and physiotherapist evaluations showed high agreement, whereas for the second and third motions, which motions were more complicated consisting of more joint values, the evaluation between the metrics and physiotherapist ratings differed. Guneyasu et al. 2014, p. 203 stated that during the evaluation of complicated movements, children misperceived the actions for which "therapists compensated such misunderstanding by giving high scores to the children while the proposed system only considered angles". This suggests that it is also possible that the physiotherapist' ratings differed from these data because they were considering aspects which could have been incidental to the movements. With that in mind, it is interesting to note that similarity error and recall measures with the ICC metric are not completely reliable since they did not model well complex movements. Recently, Guneyasu et al. (2015) presented an improvement of their previous research where less complex movements, from four physiotherapists performing five actions, were analysed: opening a door with a key, touching the opposite shoulder with hand, taking an object from back to neck, taking an object from the back and reaching an object above the head. Then, Guneyasu et al. (2015) applied traditional statistics (e.g. sample mean and sample variance) to characterise the five actions. For instance, the initial positions of arms changed from

1.2 Movement Variability

person to person, specially for the key turning action which variation were affected by the sample mean, while performances of turning the amplitude of the arm were associated with the standard deviation of the data. However, such statistical differences cannot capture the structure of the time series from each of the participants which performed the movements at different frequencies and therefore with different data length (see Fig. 10 in Guneysu et al. (2015) for further details).

Movement variability in the context of human-humanoid interaction has also been investigated in robotic dance activities. For example, Tsuchida et al. (2013) explored four dance formations which were performed three times by nine participants who had three years of experience: dancing with a robot, dancing alone, dancing with a self-propelled robot and dancing with a projected video. To visualise dance movements, Tsuchida et al. (2013) presented two participant's movement positions with twelve trajectories each (four dance activities times three trials) of z and x directions obtained with a Kinect sensor. Although, the dance experiment was rich in terms of movement variability for both participants and dance activities, only distance between each of the conditions in the dance formation was considered. With that, Tsuchida et al. (2013) concluded that the sense of dancing with a projected video of a person were the closest to dance with a real person and the trajectory of dance with a self-propelled robot were the closest to the trajectory of a dancer. Additionally, Tsuchida et al. (2013) only applied traditional statistics (e.g. ANOVA) to characterise dance movements.

Another aspect of movement variability in the context of human-humanoid interaction is the generation of robotic dance. Recently, Peng et al. (2015) reviewed an hierarchical taxonomy of four categories of robotic dance (cooperative human-robot dance, imitation of human dance motions, synchronisation for music and creation of robotic choreography). Peng et al. (2015) pointed out that the creation of robotic dances is still an open research question because dance motions should generally be

Introduction

both interesting and exciting for users. According to Peng et al. (2015), the creation of robotic dances can be accomplished with any of the following methodologies: (i) random generation: where robots can be programmed with series of predefined algorithms that can be chosen randomly, (ii) mapping rule: where robots can react, and therefore dance, to different factors such as colours, sounds, speech, temperature or human activity, (iii) chaotic dynamics: which are sensitive to initial conditions and can create various dance styles from periodic and couple to rhythm to jumping styles, resulting in innovative and consistent dance patterns, (iv) interactive reinforcement learning: where the robot can automatically choose motions based on rewards of participants' preferences of graceful motions, (v) evolutionary computation: in which multiple iterations of generations of dance motions can create graceful robotic dance motions, and finally (vi) using a ³⁰² Markov chain model, a discrete time stochastic chain, where each sequence of dance motions is considered as a state in the Markov chain producing dance that synchronise with music and emotions. Therefore, while the research questions of this thesis are not fully related to the creation of good robotic dances (e.g, being innovative or having accordance with human aesthetics) (Peng et al., 2015), it is important to note that one of the methodologies to create robotic dance motions is the use of chaotic dynamics which consider initial conditions to generate movements that are neither deterministic nor stochastic.

Although, movement variability in the context of human-humanoid interaction has not been directly investigated in recent years, it can be noted that movement variability is indeed applied in exercise, rehabilitation or dance. Hence, it can be noted that previous work that has analysed gestures, movements or dance activities with only traditional statistics, for which (i) it is not clear how Görer et al. (2013) performed the evaluation of synchronisation for gestures between participants and the humanoid nor what were the methods of evaluation, apart from the visual which had been applied to

1.3 Research questions

classify correct gestures trajectories, and (ii) little has been investigated with regards to the differences in movement of the invited physiotherapists in the work of Guneysu et al. (2014) and Guneysu et al. (2015), (iii) it is not clear, in the results of Tsuchida et al. (2013), why the distribution of trajectories for subject 1 were more uniform than the trajectories of subject 2, and (iv) even though, the robot movements for the experiments of this thesis are simple and pre-programmed, Peng et al. (2015) noted that generation of robotic dance movements can be done with chaotic dynamics.

Therefore, it is suggested that applying nonlinear analyses instead of traditional statistics in the context of human-humanoid interaction might provide a better quantification and understanding of human movements since these are generally both deterministic and stochastic. Similarly, little research has been done in this context with regards to the reliability of nonlinear tools when using real-world time series (e.g. window length, post-processing techniques, noise contamination, nonstationarity, chaotic deterministic, etc).

1.3 Research questions

A number of questions regarding movement variability (MV) have been investigated in the last decade: how is variability controlled while learning a new skill? (Bartlett et al., 2007; Seifert et al., 2011; Wagner et al., 2012), is variability associated with disease or health? (Stergiou and Decker, 2011; Stergiou et al., 2006), what are the sources of variability and how do they interact in the production of observed variation of movement? (Preatoni, 2007; Preatoni et al., 2010, 2013). Nonetheless, little has been investigated regarding to the reliability of nonlinear tools to quantify movement variability (Iwanski and Bradley, 1998; Yao and Lin, 2017) when dealing with real-world data (Bradley and Kantz, 2015; Caballero et al., 2014). Therefore, this thesis explores the effects on three nonlinear tools (e.g. Reconstructed State Space (RSS), Recurrence

Introduction

Plots (RP) and Recurrence Quantification Analysis (RQA)) with different features of time series such as structure, levels of smoothness and window lengths. To perform such exploration, two experiments were conducted with twenty right-handed healthy participants: one for human-image imitation activities and another in the context of human-humanoid imitation activities. For the experiments, participants were asked to imitate simple arm movements and participants and humanoid robot worn inertial sensors that collected time series. Hence, three research questions are investigated in this thesis.

- What are the effects on RSSs, RPs, and RQA metrics of different embedding parameters, different recurrence thresholds and different characteristics of time series (window length size, smoothness and structure)?
- Additionally, what are the weaknesses and strengths of RQA metrics when quantifying MV?
- How the smoothing of raw time series affects the nonlinear analyses when quantifying MV?

1.4 Outline of the thesis

This thesis is organised as shown in Fig. 1.1. Chapter 1 presents a background of quantification of Movement Variability(MV), state-of-the-art for modelling human MV, MV in the context of human-humanoid interaction and research questions are stated. Chapter 2 presents an introduction to fundamentals of time series analysis in terms of: (i) what to measure in Movement Variability(MV)? and (ii) which nonlinear tools are appropriate to measure MV?, including a review of the state-of-the-art literature of nonlinear analyse with real-word data. It is then presented in Chapter 3 a review of state space reconstruction method that entails an explanation for uniform time delay embedding (UTDE) and a description of the techniques to estimate of minimum embedding parameters (e.g. false nearest neighbour and average mutual information), an introduction to Recurrence Plots (RPs), structures of RPs and different metrics to perform Recurrence Quantification Analysis (RQA) as well as the weakness and strengthens of RPs and RQAs. In Chapter 4, the experiments for human-image imitation and human-humanoid imitation are presented describing aims, participants, activities in the experiments, equipment, ethics and preparations of the time series. Chapter 5 and 6 present the results with regards to two experiments (human-image imitation and human-humanoid imitation) for minimum embedding parameters, reconstructed state space using uniform time-delay embedding, recurrence plots, recurrence quantification analysis(RQA) metrics and 3D surfaces of RQA metrics to show the weaknesses and strengths of RQA. Finally, Chapter 7 presents conclusions, the answers for the research questions, the contribution to knowledge and future work for this thesis.

Introduction

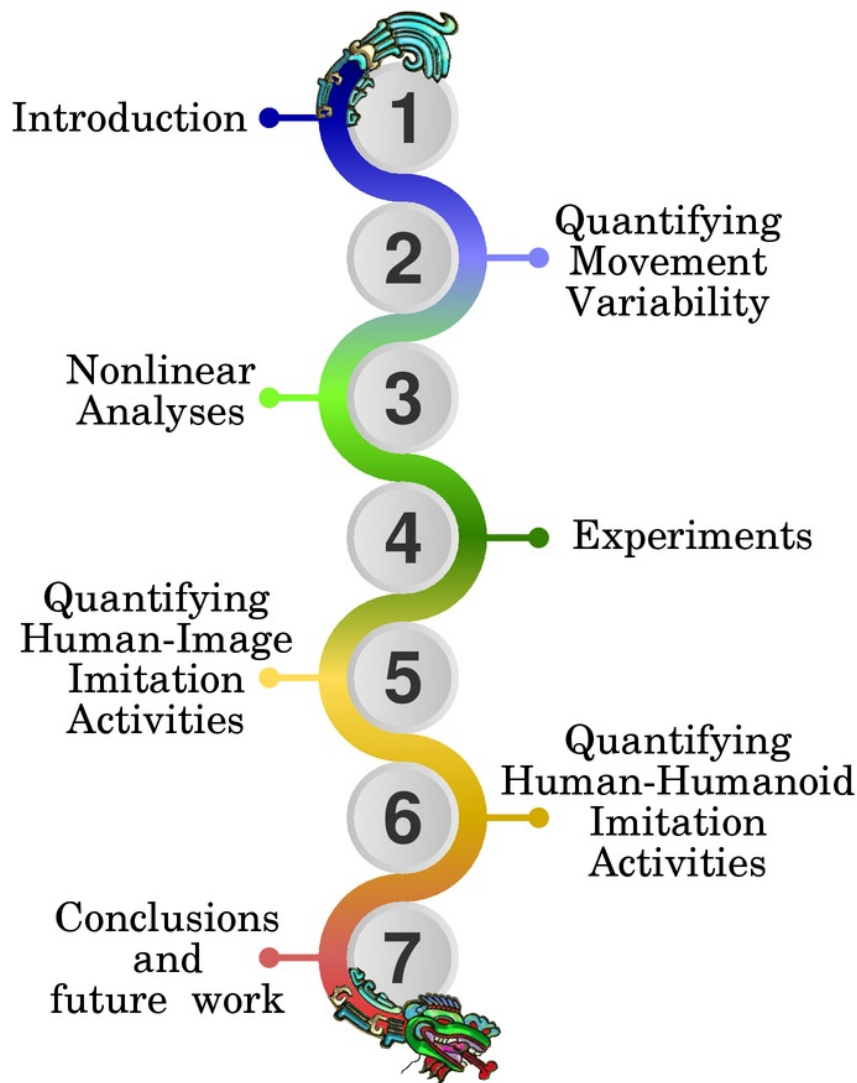


Fig. 1.1 Thesis outline. Chapter numbers with its titles. N.B. Quetzalcoatl is flowing between chapters. "To the Aztecs, Quetzalcoatl, a feathered serpent, was a boundary-maker (and transgressor) between earth and sky". See <https://en.wikipedia.org/wiki/Quetzalcoatl>.

1.5 Publications

1.5 Publications

Partial work of ²⁹⁸ this thesis has been presented in the following four peer-reviewed conferences and has also been submitted to arXiv as a preprint for its submission to PLOS One. Author contributions of Miguel Xochicale (MX), Chris Baber (CB) and Mourad Oussalah (MO) are as follow: Conceptualisation: MX, CB, MO; ¹⁹³ Data Curation: MX; Formal Analysis: MX; Funding Acquisition: MX, CB; Investigation: MX; Methodology: MX; Project Administration: MX; Resources: CB; Software: MX; ⁴³ Supervision: CB; Validation: MX; Verification: MX; Writing - Original Draft Preparation: MX; Writing - Review: CB, MO; and Writing - Editing: MX.

- Xochicale M, Baber C, and Oussalah M. Understanding Movement Variability of Simplistic Gestures Using an Inertial Sensor. *in Proceedings of the 5th ACM International Symposium on Pervasive Displays*, Oulu, Finland, June 2016, pages 239–240. <https://github.com/mxochicale/perdis2016>
- Xochicale M, Baber C, and Oussalah M. ²⁰⁹ Analysis of the Movement Variability in Dance Activities Using Wearable Sensors. *in Wearable Robotics: Challenges and Trends*, Segovia, Spain, October 2016, pages 149–154.
<https://github.com/mxochicale/werob2016>
- Xochicale M, Baber C, and Oussalah M. ²¹ Towards the Quantification of Human-Robot Imitation Using Wearable Inertial Sensors. *in Proceedings of the Companion of the 2017 ACM/IEEE International Conference on Human-Robot Interaction*, Vienna, Austria, March 2017, pages 327–328.
<https://github.com/mxochicale/hri2017>
- Xochicale M, and Baber C. ²¹ Towards the Analysis of Movement Variability in Human-Humanoid Imitation Activities. *in Proceedings of the 5th International* ²⁰⁸

Introduction

Conference on Human Agent Interaction, Bielefeld, Germany, October 2017,
pages 371–374. <https://github.com/mxochicale/hai2017>.

- Kochicale M, and Baber C. Strengths and Weaknesses of Recurrent Quantification Analysis in the context of Human-Humanoid Interaction, *in ArXiv e-prints*, October 2018. <https://arxiv.org/abs/1810.09249>

Chapter 2

Quantifying Movement Variability

2.1 Introduction

It has been stated in Chapter 1 that movement variability can be modelled and quantified using nonlinear tools mainly because the structures of the human physiology (lungs, neurons, etc.) suggest that many of their dynamics are controlled by nonlinear dynamics (Goldberger et al., 1990) and data from human movement is essentially chaotic deterministic, meaning that it is neither deterministic nor stochastic (Hatzé, 1986; Preatoni et al., 2010, 2013; Stergiou et al., 2006). Additionally, data from the human body is noisy, deterministic, stochastic or nonstationary (Caballero et al., 2014; Newell and Slifkin, 1998; Preatoni et al., 2010, 2013; Stergiou and Decker, 2011). Therefore, in this chapter fundamentals of time series, nonlinear tools and nonlinear tools with real-world data will be reviewed.

2.2 Fundamentals of time-series analysis

Biosignals from living systems can typically be nonstationary, nonlinear, deterministic chaotic and noisy (Caballero et al., 2014; Gómez-García et al., 2014; Harbourne and

Quantifying Movement Variability

Stergiou, 2009; Hatze, 1986; Klonowski, 2007; Newell and Slifkin, 1998; Stergiou and Decker, 2011; Stergiou et al., 2006; Wijnants et al., 2009). Therefore, it is important to provide fundamental definitions of time series which will be used through the thesis.

2.2.1 Linear and nonlinear systems

Linear systems are proportional or additive. For example, the interaction between variables of a linear system are negligible whereas for a nonlinear system such interaction of variables can produce emergent properties arising from the initial conditions of the system (Klonowski, 2007).

2.2.2 Stationary and nonstationary signals

Stationary signals have the same mean and variance as time progress (e.g. a sinusoidal signal), however such stationary signal can also be changeable (e.g. alternative sinusoidal signal). In contrast, when statistics of the time series change with time then such a signal is known as nonstationary signal. Nonstationary signals are therefore characterised by transients and drift over time. Examples of nonstationary signals are the time series of seasonal trends and changes (Kitagawa and Gersch, 1984) or Electroencephalography (EEG) signals which present different and changeable intensity over time (Klonowski, 2007).

2.2.3 Deterministic and stochastic systems

A deterministic system is predictable. Deterministic systems have a small number of variables of importance. Deterministic systems are hence modelled with linear ordinary differential equations and their initial conditions and constants. In contrast, stochastic systems are nonpredictable and therefore have more variables of equal importance and are modelled with probability theory (Klonowski, 2007).

2.3 Quantifying Movement Variability with Nonlinear Dynamics

2.2.4 Deterministic chaotic time series

Deterministic signals can dramatically change with a slight change of initial conditions and then after a long time-scale, the signal can appear to be stochastic (Amato, 1992). Similarly, Klonowski 2007, p. 11 pointed out that "chaotic systems behave like they were stochastic but they are also deterministic", meaning that chaotic systems are predictable for a short time-scale but nonpredictable in a long time-scale because of the initial conditions of the systems. Then, Preatoni et al. 2013, p. 78, in experiments in sport science, mentioned that "variability is likely to have both deterministic and a stochastic origin". Therefore, it can be concluded that time series for human body movement are neither independent nor stochastic but deterministic chaotic (Harbourne and Stergiou, 2009; Stergiou and Decker, 2011; Stergiou et al., 2006).

2.3 Quantifying Movement Variability with Non-linear Dynamics

2.3.1 Introduction

Previous studies have shown that movement variability is not considered as a undesired factor that creates errors but a signature for assessment of healthiness (associated with unhealthy pathological states) or skillfulness (associated with the functionality of movement) (Stergiou and Decker, 2011). Fundamentally, movement variability can be either quantified based on magnitude of the variability or the dynamics and complexity of the variability (Caballero et al., 2014). However, finding the right tools to quantify movement variability is still an open problem.

For instance, Preatoni et al. (2010, 2013) point out that conventional statistics (e.g. standard deviation, coefficient of variation, intra-class correlation coefficient)

Quantifying Movement Variability

only quantify the overall variability. Also, Stergiou and Decker (2011) stated that statistical tools (e.g. mean, standard deviation and range) are a measure of centrality, meaning such metrics are compared around a central point. Similarly, Coffey et al. (2011) pointed out that the use of means and standard deviations led to reduction of data and information is therefore discarded.

Additionally, one can apply frequency-domain tools to quantify movement variability. For example, Hatze (1986) proposed a measure of dispersion to quantify the deviation of motion from a certain reference using the Fourier series. However, deviations of motion are from angular coordinates (radians) and linear coordinates (meters) which made them an unacceptable fusion of variables. Vaillancourt et al. (2001) pointed out that it is rare for frequency and amplitude to differ in postural tremor of patients with Parkinson's disease but differences in time-dependent structures are apparent, and associated with a change of regularity of postural tremor. Klonowski (2002, 2007, 2009) stated that frequency-domain tools require stationary data, otherwise using other type of data might create misleading results.

Therefore, applying either statistical tools or frequency-domain tools to quantify movement variability might create misleading results, specially when dealing with signals that are deterministic chaotic (Amato, 1992; Dingwell and Cusumano, 2000; Dingwell and Kang, 2007; Miller et al., 2006), considering that the subtle changes in the neuromuscular-skeletal system are caused by influences of environmental changes, training or latent pathologies (Preatoni et al., 2010, 2013) and that movement variability involves evolution of human movement and the exploratory nature of movement (Caballero et al., 2014; Stergiou and Decker, 2011). Hence, Caballero et al. (2014); Preatoni et al. (2010); Stergiou and Decker (2011) highlighted that movement variability can be better described and quantified with different nonlinear dynamics tools such as: largest Lyapunov exponent (Bruijn et al., 2009; Donker et al., 2007; Kurz et al., 2010; Yang and

2.3 Quantifying Movement Variability with Nonlinear Dynamics

Wu, 2011), fractal analysis (Delignières et al., 2003), entropy rate (Cavanaugh et al., 2010), Sample Entropy (SampEn) (Donker et al., 2007; Liao et al., 2008; Richman and Moorman, 2000; Stins et al., 2009; Vaillancourt et al., 2004), Approximate Entropy (ApEn) (Cavanaugh et al., 2010; Kurz and Hou, 2010; Pincus, 1991; Sosnoff et al., 2006; Sosnoff and Voudrie, 2009), Fuzzy Entropy (FuzzyEn) (Chen et al., 2007), Multiscale Entropy (MSE) (Costa et al., 2002), Permutation Entropy (PE) (Bandt and Pompe, 2002; Vakharia et al., 2015), Quadratic Sample Entropy (QSampEn) (Lake and Moorman, 2011), Amplitude-aware permutation entropy (AAPE) (Azami and Escudero, 2016), Detrended Fluctuation Analysis (DFA) (Gates and Dingwell, 2007, 2008; Hausdorff, 2009) and Recurrence Quantification Analysis (RQA) (Marwan, 2008; Trulla et al., 1996; Zbilut and Webber, 1992).

Having so many nonlinear tools to measure movement variability (MV) led Caballero et al. 2014, p. 67 to raise the following question: "Is there a best tool to measure variability?" which leads us to ask two questions: (i) what to quantify in MV? and (ii) which tools are appropriate to quantify MV?

2.3.2 What to quantify in MV?

Vaillancourt and Newell (2002, 2003) stated that there is no universal increase or decrease in complexity for MV as a function of age or disease but a dependency with the task dynamics. For example, in a constant-force task (where the task dynamics is of low dimension), older adults present less complexity due their inability to introduce additional degrees of freedom in the neuromuscular system. However, there is an increase of complexity in older adults or unhealthy adults when the task dynamic is oscillatory because these type of adults have more difficulty to reduce the dimension output to a lower dimension which are the intrinsic dynamics of their resting state.

Quantifying Movement Variability

In contrast, inspired by Tononi et al. (1998) who modelled complexity in neural networks considering complexity versus regularity, Stergiou et al. (2006) proposed a model of complexity versus predictability variables for optimal human movement variability. The model of Stergiou et al. (2006) stated that higher complex movements are associated with rich behaviour of movements while lower complex movements are associated with poor behaviours of movements being too rigid or too unstable. Hence, higher complexity of movements are characterised by chaotic systems, while lesser complexity of movement is characterised either as noisy systems or periodic systems (having either low amounts of predictability or hight amounts of predictability) (Stergiou et al., 2006).

Therefore, with the works of Vaillancourt and Newell (2002, 2003) and Stergiou et al. (2006), one can quantify movement variablity based on the complexity and predictability of human movement.

2.3.3 Which nonlinear tools are appropriate to quantify MV?

Considering the model of Stergiou et al. (2006) for movement variability, where complexity and predictability variables of a system can characterise and quantify movement variability, it is important to find, to understand and to apply the right tools that measure such variables.

Originally, Pincus (1995, ²²⁴ 1991) proposed Approximate Entropy (ApEn) to quantify regularity of time series. Then, Richman and Moorman (2000) due to self-matching found that the algorithm of ApEn could evoke the occurrence of $\ln(0)$ which made ApEn dependant on the available data for which Sample Entropy (SampEn) were proposed as an algorithm that does not consider self-matching. Hence, SampEn values ³¹ are independent of the length of time series and its algorithm is simpler than ApEn. Then, instead of using single statistics, ³²² Costa et al. (2002) proposed Multiscale Entropy

2.3 Quantifying Movement Variability with Nonlinear Dynamics

(MSE) which computes SampEn of consecutive coarse-grained time series of the original time series defined by the scale factor, τ . With MSE algorithm, (Costa et al., 2002) noted that pathology dynamics for time series of heartbeat intervals are associated with reduction of complexity. Therefore, Costa et al. 2002, p. 3 concluded that physiological complexity is associated with the adaptive capacity of the organism, disease states and aging which "may be defined by a sustained breakdown of long-term correlations and loss of information". Essentially, entropy measures (AppEn and SampEn), quantify regularity and complexity of time series (Preatoni et al., 2013). However, Goldberger (1996) mentioned that the increase of irregularity in time series is not synonymous of increase with physiological complexity. Similarly, an increase of ApEn or SampEn, "implying increase of irregularity and decrease in predictability" (Goldberger et al., 2002, p. 25), is not synonymous with an increase of dynamical complexity when analysing physiology signals (Costa et al., 2002). Hence, Goldberger et al. (2002) demonstrated that ApEn as a regularity statistic is not a direct index of physiological complexity where, for example, a randomised time series of a healthy heartbeat with multi-scale and complex patterns of variability show a higher value of ApEn even though the time series is less complex. Therefore, Goldberger et al. 2002, p. 24 concluded that the loss of physiological complexity can be "better assessed using other measures which can detect and quantify the presence of long-range correlations in nonstationary series." Hence, Costa et al. (2002); Goldberger et al. (2002); Vaillancourt and Newell (2002) concluded that ApEn and SampEn do not necessarily show the right representation of what they intend to measure.

Therefore, considering the previous cons of ApEn, SampEn and MSE, Detrended Fluctuation Analysis (DFA), which is based on analysing fractal features, can quantify long-term correlations of time series (Peng et al., 1995). DFA is calculated as the root mean square fluctuation of an integrated and detrended time series and it is

Quantifying Movement Variability

represented by a scaling exponent, α , which is an indicator for roughness of time series, e.g. "the larger the value of α , the smoother the time series (Peng et al., 1995, p. 83). However, DFA can result in a false conclusion for long term correlations in the time series (Rangarajan and Ding, 2000, p. 5001), therefore DFA "can falsely classify certain type of time series as fractals" (Wijnants et al., 2009, p. 80). With that in mind, Wijnants et al. (2009) proposed the use of RQA as a technique that does not present any constraints with regards to length size, stationary or statistical distribution of the time series. Wijnants et al. (2009) highlighted that SampEn index is calculated over the sequential values of the time series, whereas Shannon entropy in RQA which is computed over the distribution of deterministic lines in the Recurrence Plots (RP) (Marwan, 2008; Trulla et al., 1996; Zbilut and Webber, 1992). Similarly, Rhea et al. (2011) highlighted that algorithms to compute entropy measures are different since ApEn and SampEn are approximations of the Kolmogorov-Sinai Entropy computing the likelihood that a template pattern repeats in the time series while RQAEn is derived from Shannon entropy and is computing number of line segments of varying length in the RP. Even with those differences in the algorithms, smaller values of recurrence percentage of the RQA show the increase of practice of movement dynamics, concluding that such recurrence percentage indicate an increase of system stability (Wijnants et al., 2009).

Another tool to measure variability is the largest Lyapunov exponent (LyE) which is used to "quantify the rate at which nearby trajectories converge or diverge" (Stergiou, 2016, p. 85). For instance, "LyE from a stable system with little to no divergence will be zero (e.g. sine wave)" and "LyE for an unstable system that has highest amount of divergence will be positive and relative hight in value (e.g. 0.469 for random noise)" and for chaotic systems like the Lorenz system, LyE is in between the two of the

2.4 Nonlinear analyses with real-world data

previous extremes ($LyE \approx 0.1$) (Miller et al., 2006, p. 2874). However, LyE requires to be validated using surrogation (Dingwell and Cusumano, 2000; Miller et al., 2006).

Measuring human movement variability requires a combination of the pros and cons of many of the previous tools that analyse either (i) the dynamic complexity or (ii) the degree of regularity, stability or predictability in a system (Goldberger et al., 2002;
Harbourne and Stergiou, 2009; Stergiou and Decker, 2011). For instance, Rangarajan and Ding (2000) stated the use of both spectral analysis and random walk analysis, the base of DFA, is a better approach than only using one tool which can lead to false conclusion for long term correlations in the time series. Similarly, Wijnants et al. (2009) selected different tools (spectral analysis, standard dispersion analysis, DFA, RQA and SampEn) to quantify movement variability that can complement the strengths of some of them and also compensate the weakness of others. Recently, Caballero et al. (2014) proposed the unification of different tools to address every aspect of the dynamics of a systems and the characterisation of the variability.

Although, there is no best tool to measure movement variability and an unification of tools to quantify human movement variability is still an open question, finding the right tool to measure movement variability for a specific problem, and knowing its strengths and weakness of such tool is one of the research questions for this thesis.

2.4 Nonlinear analyses with real-world data

Recently, Huffaker et al. (2017) pointed out that one of the caveats when applying nonlinear time series analysis tools is its unreliability when the estimated metrics come from real-world data which is generally short, noisy and nonstationary. Similarly, Preatoni et al. (2013) mentioned the limitations of nonlinear analyses in sport activities where data required to be large (e.g. number of trials, duration of the experiment and sampling frequency). Caballero et al. (2014) argued that there are weaknesses

Quantifying Movement Variability

of different nonlinear tools regarding the characteristics of the time series such as nonstationarity, length data size, noise, sampling rate. However, in the work of Huffaker et al. (2017), Preatoni et al. (2013) and Caballero et al. (2014) no further exploration of the metrics of nonlinear analyses with real-world data is presented.

2.4.1 Nonsationarity

Nonstationarity of time series signals might create spurious increase or decrease in the metrics of nonlinear tools. For instance, Costa et al. (2007) noted that nonstationarity in the signals might alter the increase of irregularity of signals for the shortest scales when applying MSE. Also, Dingwell and Cusumano (2000) reported nonstationary in time series when using LyE, which required to be validated using surrogation to ensure the robustness of the metric. Hence, Caballero et al. (2014) reported three options when dealing with nonstaionary data: (i) remove nonsatiornary data, (ii) use empirical mode decomposition (EMD), and (iii) apply nonlinear tools, such as DFT and RQA, which are less sensitive to nonstationary data.

To remove nonstationary data, for example, Carroll and Freedman (1993) suggested to remove the trends or to eliminate the initial data (first 20 seconds of samples) to ignore the trend of time series. Hence, van Dieën et al. (2010), in experiments with center of pressure movements in seated balancing, discarded the first 5 seconds of the time series in the start of the measurement.

Also, nonstatioinary time series can be treated with Empirical Mode Decomposition (EMD) method which decompose nonlinear, nonstatioanry signals into their intrinsic frequency components (Huang et al., 1998; Wu and Huang, 2004, 2009). Hence, Costa et al. (2007); Flandrin et al. (2004) tested whether EMD is a robust method for detrending and denoising time series and noted that EMD does not require selection of input parameters. However, the reliability of EMD methods is still an open problem.

2.4 Nonlinear analyses with real-world data

For instance, an extension of EMD called ¹¹³ Multivariate Empirical Mode Decomposition (MEMD) has been proposed ²¹⁹ to analyse multiple time series (Mandic et al., 2013; Rehman and Mandic, 2010). See (Bonnet et al., 2014; Costa et al., 2007; Daubechies et al., 2011; Mert and Akan, 2018; Wu and Hu, 2006) for applications of EMD.

Finally, one can use nonlinear tools that are unaffected by nonstationarity of time series such as Detrended Fluctuation Analys (DFA) (Hausdorff et al., 1995) and ⁷⁶ Recurrence Quantification Analysis (RQA) (Marwan, 2008; Trulla et al., 1996; Zbilut and Webber, 1992). However, Bryce and Sprague (2012) reported negatives of DFA such as the introduction of uncontrolled bias, computational expensiveness and highlight that DFA cannot provide a generic protection against the nonstationarities of the signals.

2.4.2 Data length

²⁹² Many of the nonlinear tools are sensitive to time series length (Caballero et al., 2014). For example, given that Multiscale Entropy (MSE) is considered as statistical measure, the data lengths are recommended to be larger (up to the scale of 6×10^3 data points) to ensure enough samples for the analysis (Costa et al., 2007). Also, LyE (²⁹¹ Wolf et al., 1985) and DFA (Peng et al., 1995) metrics are sensitive to data length, while SampEn (² Rhea et al., 2011) and FuzzyEn (Chen et al., 2007; Richman and Moorman, 2000), the metrics of RQA (¹⁴⁷ Riley et al., 1999; Webber and Zbilut, 1994; Wijnants et al., 2009) and PeEn (Zunino et al., 2009) are less sensitive to time series length.

2.4.3 Sampling rate

One solution when dealing with data length problems is to increase or decrease of sampling rate (Caballero et al., 2014). However, Duarte and Sternad 2008, p. 267 stated "the increase of sampling rate frequency would only increase artificially the data

Quantifying Movement Variability

points without adding information" which therefore raises the problem of oversampling signals. Then, Rhea et al. (2011) investigated the influence of sampling rate in three entropy measures (ApEn, SampEn and RQAEn) concluding that Ap and RQAEn were robust across to the increase of sampling frequency, while SampEn presented significant difference across all sampling frequencies. Rhea et al. (2011) noted that SampEn is more sensitive to coliniarities than Ap and RQAEn at higher frequencies which lead to a decrease of SampEn. Hence, Rhea et al. (2011) concluded that signals at higher frequencies appear to be more regular due to the increase of data, therefore producing erroneous entropy results. Caballero et al. (2013) showed the robustness of SampEn and DFA tools when using different sampling rate frequencies, stating that frequencies near the dynamics of the activity create a more reliable analysis of the dynamics using DFA values and tested the statement of Duarte and Sternad (2008) that increasing the sampling rate do not increase the gain of information. Caballero et al. (2013) also stated that the decrease of sampling rate frequency is recommended because it presents less consumption of computational power.

2.4.4 Noise

Another point to consider is the noise in the signals and how such noise affects nonlinear tools metrics (Caballero et al., 2014). For instance, Rosenstein et al. (1993) tested the robustness of LyE against three levels of noise (lowest, moderate and highest) noting the unreliability of LyE exponents in hight-noise environments. However, such cases of unreliability of LyE is unreal as the reported values of signal-to-noise ratios are substantially lower than the used at the experiments of Rosenstein et al. (1993).

Another example is the work of Chen et al. (2009) who compared the robustness of FuzzEn, ApEn and SampEn metrics against different levels of noise, concluding that for a large value of the parameter r of ApEn and SampEn, these two metrics can work

2.4 Nonlinear analyses with real-world data

well with high level of noise, however when noise increases, ApEn and SampEn fail to distinguish time series with different level of noise, whereas FuzzEn is robust to such highest levels of noise. Also, Bandt and Pompe (2002) by proposing Permutation Entropy (PeEn) to be robust against observational and dynamical noise.

Regardless of the source of noise which can be either mechanical (due to recording equipment) or physiological (due to different neural noise), Rhea et al. (2011) highlighted the importance of the effects on noise in three entropy measures (ApEn, SampEn and RQAEn) which resulted in different results. For instance, values for AnEn and SampEn tended to increase as noise was added to the signals, while RQAEn showed an inverse effect, e.g. RQAEn values decreased as noise in the signal was increased. Similar results for synthetic data were also reported by Pellecchia and Shockley (2015) where RQAEn values decreased from ($RQAEn \approx 5$) for Lorenz system to a ($RQAEn \approx 2$) for a periodic signal with a further decrease ($RQAEn \approx 0.3$) for a sinusoid signal with superimposed noise. Therefore, RQA can also be affected by noise (Rhea et al., 2011). However, the effects of noise and nonstationarity can be mitigated with the selection of the right parameters to perform RQA, particularly, using embedding dimensions from 10 to 20 (Webber and Zbilut, 2005).

Another solution to deal with noisy time series is the use of traditional filtering methods. However, the attenuation of all frequencies of the signal along with the noise, given a cutoff frequency, can cut out information that might be useful for nonlinear time-series. Another option is apply DFA, which additionally to the remove of local trends, it also reduces the noise of the signal (Hausdorff et al., 1995). Alternatively, filtering strategies for nonlinear time-series data can be applied which tailor in a more effective way the properties of nonlinear dynamics (see Bradley and Kantz 2015 and references therein).

Quantifying Movement Variability

2.5 Final remarks

Having reviewed works regarding the questions of: (i) what to quantify in Movement Variability and (ii) which nonlinear tools are appropriate to quantify MV and the strengths and weaknesses of nonlinear analyses with real-world data, it can then be

²⁴⁰ concluded that little research has been done on the effects with Reconstructed State

²⁰ Spaces (RSSs), Recurrent Plots (RPs), and Recurrence Quantification Analysis (RQA)

metrics for different embedding parameters, different recurrence thresholds and different characteristics of time series (window length size, smoothness and structure). Hence, nonlinear analyses such as estimation of embedding parameters, RSSs, RPs, and RQAs are reviewed in the following chapter.

Chapter 3

Nonlinear Analyses

3.1 Introduction

The method of state space reconstruction was originally proposed by Packard et al. (1980) and formalised by Takens (1981). Since then, various investigations and disciplines relative to nonlinear time series analysis have benefited from it (Aguirre and Letellier, 2009; Frank et al., 2010; Samà et al., 2013; Stergiou and Decker, 2011). The method of reconstructed state space (RSS) is based on uniform time-delay embedding (UTDE) which is a simple matrix implementation considering the embedding parameters (m and τ), therefore, matrix represents the reconstruction of an unknown d -dimensional manifold M from a scalar time series (e.g. one-dimensional time series in \mathbb{R}). A manifold, in this context, is a multidimensional curved surface within a space (e.g. a saddle) (Guastello and Gregson, 2011). Henceforth, the method of state space reconstruction using a scalar time series can preserve dynamic invariants such as correlation dimension, fractal dimension, Lyapunov exponents or Kolmogorov-Sinai entropy (Bradley and Kantz, 2015; Krakovská et al., 2015; Quintana-Duque and Saupe, 2013; Quintana-Duque, 2012, 2016). However, there are still many challenging research questions to be answered with regards to the selection of appropriate embedding

Nonlinear Analyses

parameters that preserve the dynamics of a system for the computation of nonlinear tools such as RSS, RPs and RQAs. With that in mind, in the following subsections, we describe in more detail the state space reconstruction theorem (RSSs), uniform time-delay embedding theorem (UTDE), the methods to compute embedding parameters: false nearest neighbours (FNN) and average mutual information (AMI). We also introduce the fundamentals of Recurrence plots (RPs) and Recurrence quantification analysis (RQA).

3.2 State Space Reconstruction Theorem

Following the notation employed in Casdagli et al. (1991); Garland et al. (2016); Gibson et al. (1992); Takens (1981); Uzal et al. (2011); Uzal and Verdes (2010), the method of state space reconstruction is defined by:

$$s(t) = f^t[s(0)], \quad (3.1)$$

where $s, s : A \rightarrow M$ given that $A \subseteq \mathbb{R}$ and $M \subseteq \mathbb{R}^d$, represents a trajectory which evolves in an unknown d -dimensional manifold M , $f : M \rightarrow M$ is an evolution function and f^t , with time evolution $t \in \mathbb{N}$, is the t -th iteration of f that corresponds to an initial position $s(0) \in M$ (Takens, 1981). Then, a point of a scalar time series $x(t)$ in \mathbb{R} , can be obtained with

$$x(t) = h[s(t)], \quad (3.2)$$

where h is a function, $h : M \rightarrow \mathbb{R}$, defined on the trajectory $s(t)$.

Reconstructed state space can then be described as an n -dimensional state space defined by $y(t) = \Psi[\mathbf{X}(t)]$ where $\mathbf{X}(t) = \{x(t), x(t-\tau), \dots, x(t-(m-1)\tau)\}$ is the

3.3 Uniform Time-Delay Embedding (UTDE)

uniform time-delay embedding with a dimension embedding m and delay embedding τ and $\Psi : \mathbb{R}^m \rightarrow \mathbb{R}^n$ is a further transformation of dimensionality (e.g. Principal Component Analysis, Singular Value Decomposition, etc) being $n \leq m$. With that in mind, uniform time-delay embedding, $\mathbf{X}(t)$, defines a map $\Phi : M \rightarrow \mathbb{R}^m$ such that $\mathbf{X}(t) = \Phi(s(t))$, where Φ is a diffeomorphic map (Takens, 1981) whenever $\tau > 0$ and $m > 2d_{box}$ and d_{box} is the box-counting dimension of M (Garland et al., 2016). Then, if Φ is an embedding of an attractor (i.e. evolving trajectories) in the reconstructed state space, a composition of functions represented with F^t is induced on the reconstructed state space:

$$\mathbf{X}(t) = F^t[\mathbf{X}(0)] = \Phi \circ f^t \circ \Phi^{-1}[\mathbf{X}(0)]. \quad (3.3)$$

Hence, an embedding is defined as "a smooth one-to-one coordinate transformation with a smooth inverse" (Casdagli et al., 1991, p. 54). Figure 3.1 illustrates the state space reconstruction.

3.3 Uniform Time-Delay Embedding (UTDE)

Frank et al. (2010) and Samà et al. (2013) refer to the state space reconstruction outlined in 3.2 as "time-delay embeddings" or "delay coordinates", respectively. However, we consider the term "uniform time-delay embedding" as more descriptive and appropriate terminology for this thesis.

The uniform time-delay embedding is represented as a matrix of uniform delayed copies of the time series $\{\mathbf{x}_n\}_{n=1}^N$ where N is the sample length of $\{\mathbf{x}_n\}$ and n is index for the samples of $\{\mathbf{x}_n\}$. $\{\mathbf{x}_n\}_{n=1}^N$ has a sample rate of T . The delayed copies of $\{\mathbf{x}_n\}$ are uniformly separated by τ and represented as $\{\tilde{\mathbf{x}}_{n-i\tau}\}$ where i goes from $0, 1, \dots, (m-1)$ (Fig 3.2). $\{\tilde{\mathbf{x}}_{n-i\tau}\}$ contains information of unobserved state variables and encapsulates the information of the delayed copies of the available time series in

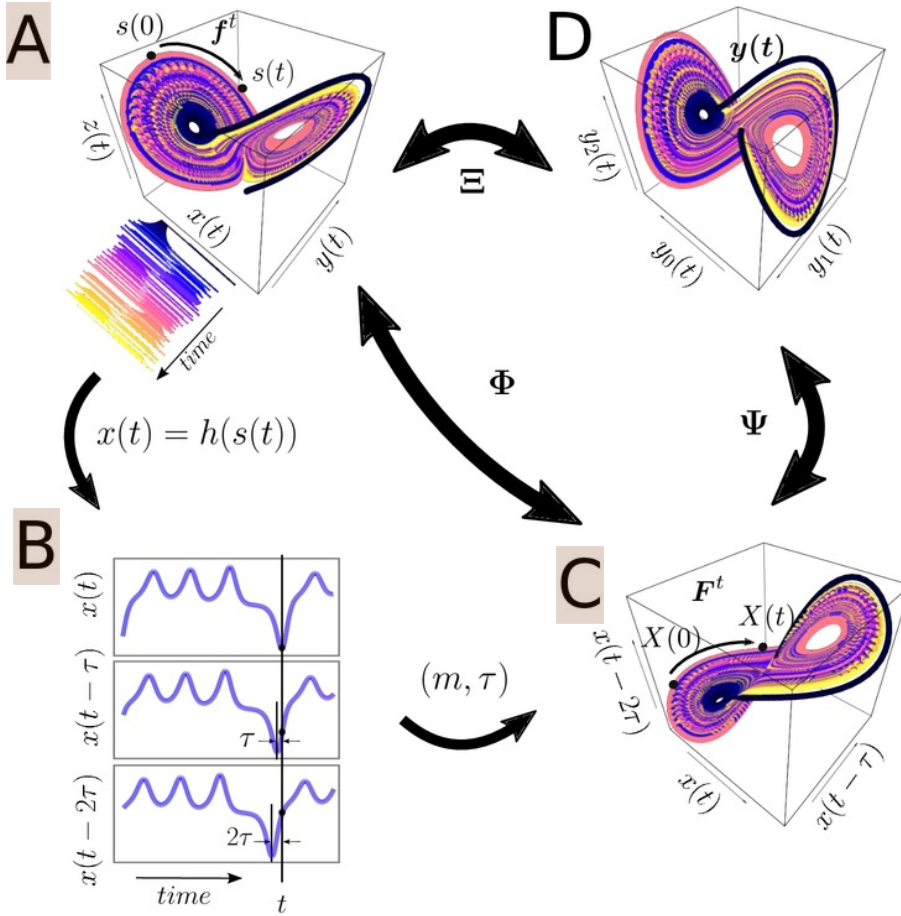


Fig. 3.1 State space reconstruction methodology. State space reconstruction is based on $x(t) = h[s(t)] = h[f^t[s(0)]]$ where h is a function $h : M \rightarrow \mathbb{R}$, defined on the trajectory $s(t)$. f is the true dynamical system, $f : M \rightarrow M$, defined as evolution function and f^t , with time evolution $t \in \mathbb{N}$ which is the t -th iteration of f that corresponds to an initial position $s(0) \in M$. The time-delay embedding represented as the Φ , maps the original d -dimensional state $s(t)$ into the m -dimensional uniform time-delay embedding matrix $X(t)$. The transformation map Ψ maps $X(t)$ into a new state $y(t)$ of dimensions $n < m$. (A) M -dimensional state space (e.g. Lorenz system); (B) Delayed copies of 1-dimensional $x(t)$ from the Lorenz system; (C) m -dimensional reconstructed state space with m and τ , and (D) $y(t)$ is the n -dimensional reconstructed state space. The total reconstruction map is represented as $\Xi = \Psi \circ \Phi$ where Φ is the delay reconstruction map and Ψ is the coordinate transformation map. This figure is adapted from the work of Casdagli et al. (1991); Quintana-Duque (2012); Uzal et al. (2011) and R code to reproduce the figure is available from Xochicale (2018).

285 3.4 Estimation of Embedding Parameters

the uniform time-delay embedding matrix \mathbf{X}_τ^m , $\mathbf{X}_\tau^m \in \mathbb{R}^{m \times m}$, defined as 7

$$\mathbf{X}_\tau^m = \begin{pmatrix} \tilde{\mathbf{x}}_n \\ \tilde{\mathbf{x}}_{n-\tau} \\ \tilde{\mathbf{x}}_{n-2\tau} \\ \vdots \\ \tilde{\mathbf{x}}_{n-(m-1)\tau} \end{pmatrix}^\top, \quad (3.4)$$

where m is the embedding dimension, τ is the embedding delay and $^\top$ denotes the transpose. 65 m and τ are known as embedding parameters. The matrix dimension of 64 \mathbf{X}_τ^m is defined by $N - (m - 1)\tau$ rows and m columns and $N - (m - 1)\tau$ defines the length of each delayed copy of $\{\tilde{\mathbf{x}}_n\}$ in \mathbf{X}_τ^m . A graphical representation of uniform time-delay embedding is shown in Figure 3.2. For further details and explicit examples 284 of uniform time-delay embedding methodology, we refer the reader to the appendix A.

3.4 Estimation of Embedding Parameters

238 The estimation of the embedding parameters (m and τ) is an essential step for the state space reconstruction 151 in order to apply the method of uniform time-delay embedding (UTDE). Hence, we review two of the most common algorithms, which will be used in 1 this thesis, to compute the embedding parameters: the false nearest neighbour (FNN) and the average mutual information (AMI).

3.4.1 13 False Nearest Neighbours (FNN)

To select the minimum embedding dimension m_0 , Kennel et al. (1992) 146 used the method of false neighbours which can be understood as follows: on one hand, when the 105 embedding dimension is too small to unfold the attractor (i.e. evolving trajectories in

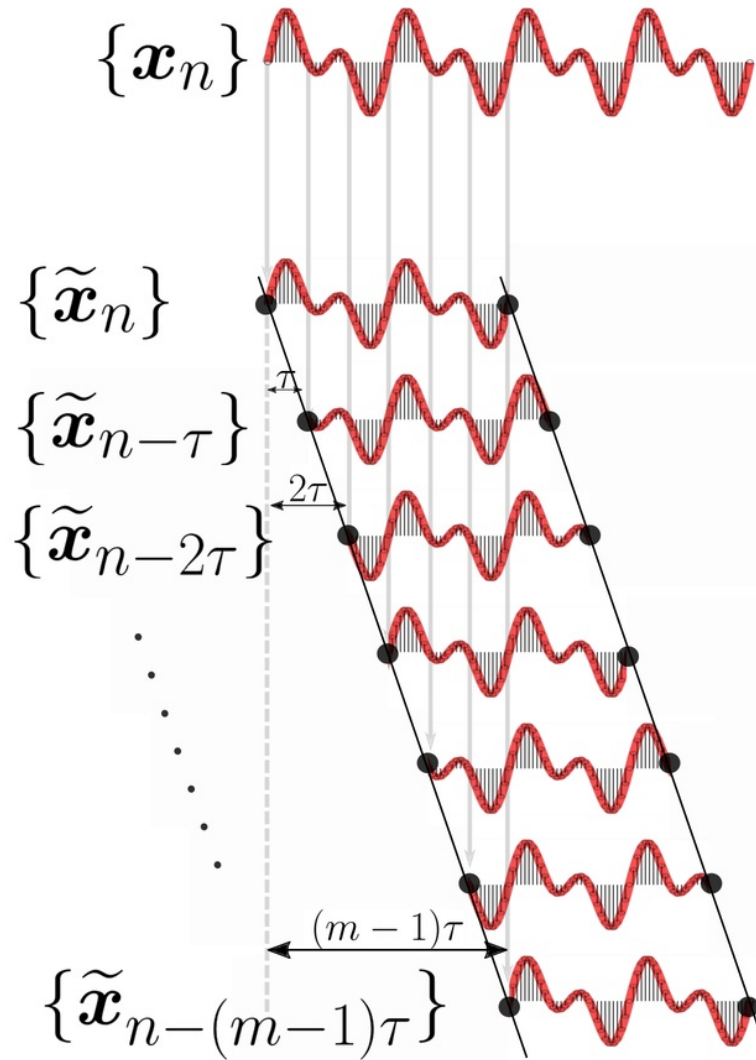


Fig. 3.2 **Uniform time-delay embedding.** UTDE is illustrated as $m - 1$ delayed copies of $\{x_n\}$ which is uniformly separated by τ . UTDE is represented as $\{\tilde{x}_n, \dots, \tilde{x}_{n-(m-1)\tau}\}$ (Eq. 3.4). R code to reproduce the figure is available Xochicale (2018).

3.4 Estimation of Embedding Parameters

a state space) "not all points that lie close to each other will be neighbours and some points appear as neighbours as a result of the attractor being projected down into a smaller space", on the other hand, when increasing the embedding dimension "points that are near to each other in the sufficient embedding dimension should remain close as the dimension increase from m to $m + 1$ " (Krakovská et al., 2015, p. 3).

283 From a mathematical point of view, state space reconstruction is done when the attractor is unfolded with either the minimum embedding dimension, m_0 , or any other embedding dimension value where $m \geq m_0$ (Kennel et al., 1992). In contrast, any large value of m_0 leads to excessive computations (Bradley and Kantz, 2015). Hence, Cao (1997) proposed an algorithm based on the false neighbour method where only the time-series and one delay embedding value are necessary to select 319 the minimum embedding dimension. Cao's algorithm is based on $E(m)$, which is the mean value of all $a(i, m)$, and defined as:

$$\begin{aligned} E(m) &= \frac{1}{N - m\tau} \sum_{i=1}^{N-m\tau} a(i, m) \\ &= \frac{1}{N - m\tau} \sum_{i=1}^{N-m\tau} \frac{\|\mathbf{X}_i(m+1) - \mathbf{X}_{n(i,m)}(m+1)\|}{\|\mathbf{X}_i(m) - \mathbf{X}_{n(i,m)}(m)\|} \end{aligned} \quad (3.5)$$

where $\mathbf{X}_i(m)$ and $\mathbf{X}_{n(i,m)}(m)$ are the time-delay embeddings with $i = 1, 2, \dots, N - (m - 1)\tau$ and $n(i, m) = 1 \leq n(i, m) \leq N - m\tau$. From Eq. 3.5 $E(m)$ is only dependent on m and τ for which $E_1(m)$ is defined as

$$E_1(m) = \frac{E(m+1)}{E(m)}. \quad (3.6)$$

$E_1(m)$ is therefore proposed to describe the variation from m to $m + 1$ in order to find the minimum embedding dimension m_0 (Eq. 3.6). As Cao 1997, p. 44 described: " $E_1(m)$ stops changing when m is greater than some m_0 , if the time series comes from a multidimensional state space then $m_0 + 1$ is the minimum dimension". Additionally,

Nonlinear Analyses

Cao (1997) proposed $E_2(m)$ ²⁸² to distinguish deterministic signals from stochastic signals.

$E_2(m)$ is defined as

$$\overset{43}{E}_2(m) = \frac{E^*(m+1)}{E^*(m)}, \quad (3.7)$$

where

$$\overset{17}{E}^*(m) = \frac{1}{N - m\tau} \sum_{i=1}^{N-m\tau} |\mathbf{X}_i(m+1) - \mathbf{X}_{n(i,m)}(m+1)|. \quad (3.8)$$

For instance, when the signal comes from random noise (values that are independent from each other), all $E_2(m)$ values are approximately equal to 1 (e.g. $E_2(m) \approx 1$). However, for deterministic data $E_2(m)$ is not constant for all m (e.g. $E_2(m) \neq 1$).

As an example of the use of $E_1(m)$ and $E_2(m)$ values, we consider two time series: the solution for the x variable of the chaotic deterministic Lorenz system (Figure 3.3E), and a Gaussian noise time series with zero mean and a variance of one (Figure 3.3F).

We then compute $E_1(m)$ and $E_2(m)$ values for each time series. The $E_1(m)$ values for the chaotic time series appear to be constant after the dimension is equal to six. The determination of six is given that any value of m can be used as $E_1(m)$ values are within the threshold of 1 ± 0.05 (Fig 3.3A). Although the $E_2(m)$ values for the chaotic time series tend to be closer to one as m increases, these are different to one (Fig 3.3C), for which, it can be concluded that the chaotic time series comes from a chaotic deterministic signal. With regard to the noise time series, $E_1(m)$ values appeared to be constant when m is close to thirteen which is defined by the same threshold of 1 ± 0.05 (Figure 3.3B). Then, contrary to the $E_2(m)$ values for a chaotic Lorenz time series, all values of $E_2(m)$ for a noise time series are approximately equal to one (Figure 3.3D). Hence, $E_1(m)$ values then indicate the minimum embedding dimension of the noisy time series is thirteen, however all of the $E_2(m)$ values are approximately equal to one (Figure 3.3D) for which it can be concluded that noise time series is a stochastic signal.

3.4 Estimation of Embedding Parameters

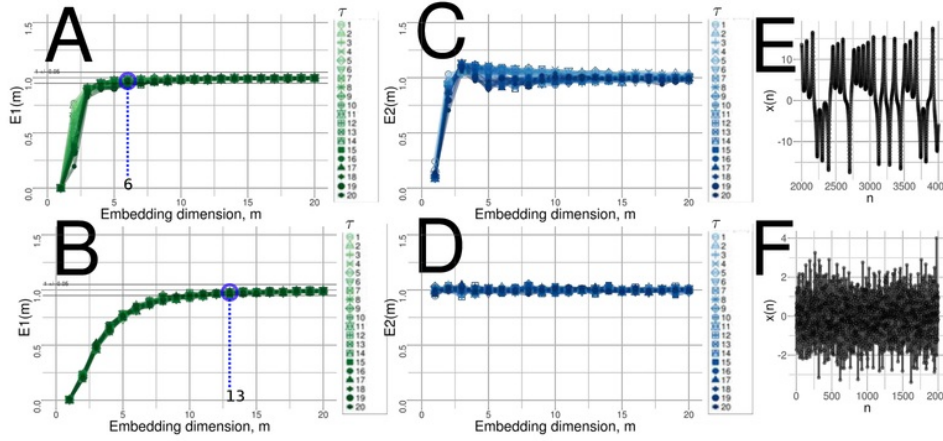


Fig. 3.3 Minimum dimension embedding values with Cao's method. (A, B) $E_1(m)$ values and (C, D) $E_2(m)$ values with variations of τ values from one to twenty for (E) chaotic and (F) random time series. R code to reproduce the figure is available from Xochicale (2018).

167 It is important to note that for this thesis not only the values for $E_1(m)$ and $E_2(m)$ are computed but also a variation of τ from 1 to 20 (Figure 3.3 (A,B,C,D)) has been explored. The purpose of using variations for τ is to show its independence with regard to the $E_1(m)$ (Fig. 3.3(A,B)) and $E_2(m)$ (Fig. 3.3(C,D)). Although Cao (1997) mentioned that no parameters are required to find the minimum embedding dimension, 13 we found that it is necessary to define a threshold for which $E_1(m)$ values appear to be constant. Hence, for the given examples and the reported results for this thesis, we defined a threshold to be 0.05 (see Fig. 3.3(A) with the parallel lines of the threshold near to one 1 ± 0.05).

3.4.2 Average Mutual Information (AMI)

When selecting the delay dimension parameter, τ , one can consider the following two cases: (i) when τ is too small, the elements of time-delay embedding will be along the bisectrix of the phase space and the reconstruction is generally not satisfactory, (ii)

Nonlinear Analyses

when τ is too large the elements of the uniform time-delay embedding will become spread and uncorrelated which makes recovering the underlying attractor (i.e. evolving trajectories in a state space) difficult if not impossible (Casdagli et al., 1991; Emrani et al., 2014; Garcia and Almeida, 2005).

There are many approaches to compute the embedding parameters (Bradley and Kantz, 2015), for instance, geometry-based methodologies where the amount of space filled in the reconstructed state is the metric to compute the delay embedding (Rosenstein et al., 1994) or theoretical approaches to estimate an optimal parameter for τ Casdagli et al. (1991). However, the autocorrelation function and the average mutual information (AMI) are the two most commonly used algorithms to compute the minimum delay embedding parameter τ_0 . Emrani et al. (2014) used the autocorrelation function in which the first zero crossing is considered as the minimum delay embedding parameter. ²⁷⁷ However, the autocorrelation function is a linear statistic whereas AMI considers the nonlinear dynamical correlations (Fraser and Swinney, 1986; Krakovská et al., 2015). With that in mind, the AMI algorithm is described below to estimate the minimum delay embedding parameter, τ_0 .

To compute the AMI, an histogram of $x(n)$ using n bins is calculated and then a probability distribution of data is computed (Kantz and Schreiber, 2003). AMI is therefore denoted by $I(\tau)$ which is the average mutual information between the original time series, $x(n)$, and the delayed time series, $x(n - \tau)$, delayed by τ (Kabiraj et al., 2012). AMI is defined by

$$I(\tau) = \sum_{i,j}^N p_{ij} \log_2 \frac{p_{ij}}{p_i p_j}. \quad (3.9)$$

Probabilities are defined as follows: p_i is the probability that $x(n)$ has a value inside the i -th bin of the histogram, p_j is the probability that $x(n + \tau)$ has a value inside the j -th bin of the histogram and $p_{ij}(\tau)$ is the probability that $x(n)$ is in bin i and $x(n + \tau)$ is in bin j . The AMI is measured in bits (base 2, also called shannons) (Garcia and

3.4 Estimation of Embedding Parameters

Sawitzki, 2016; Kantz and Schreiber, 2003). For small τ ($\tau < 3$), AMI will be large ($I(\tau) > 6$) and as m increase AMI will then decrease rapidly. Hence, as τ increase and goes to a large limit, $x(n)$ and $x(n + \tau)$ have nothing to do with each other and $p(ij)$ is factorised as $p_i p_j$ for which AMI is close to zero. Then, in order to obtain τ_0 , "it has to be found in the first minimum of $I(\tau)$ where $x(n + \tau)$ adds maximal information to the knowledge from $x(n)$ " meaning that the redundancy between $x(n + \tau)$ and $x(n)$ is the least (Kantz and Schreiber, 2003, p. 151).

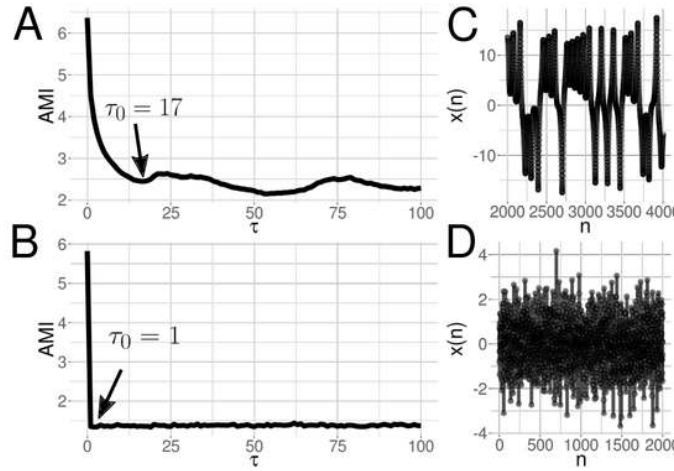


Fig. 3.4 Minimum delay embedding values with AMI's method. (A, B) AMI values where its first minimum value in the curve is the minimum time delay embedding (τ_0), for (C) a chaotic and (D) noise time series. R code to reproduce the figure is available from Xochicale (2018).

For example, we compute the AMI for two time series: (i) the x solution of the deterministic chaotic Lorenz system, and (ii) a noise time series using a normal distribution with mean zero and standard deviation equal to one. The AMI plots are shown in Figure 3.4, where the minimum delay embedding parameter for the chaotic time series is $\tau_0 = 17$ and for the noise time series is $\tau_0 = 1$. Hence, it can be concluded that the amount of knowledge for any noise time series is zero for which the first minimum embedding parameter is equal to one. On the contrary, the first minimum of

Nonlinear Analyses

the AMI for the chaotic time series is $\tau_0 = 17$ which is the value that maximize the independence in the reconstructed state space (Bradley and Kantz, 2015).

3.4.3 Overall minimum embedding parameters

The method to select minimum embedding parameters (m_0 and τ_0) for this thesis is firstly to compute m_0 with FNN algorithm (considering a threshold of 0.05 for $E_1(m)$ values) and secondly to compute τ_0 (with AMI which does not need any extra parameters). Hence, from the previous example of the chaotic deterministic Lorenz system, Fig 3.3(A) is used, for instance, to determine the minimum dimension embedding ($m_0 = 6$) and Fig 3.4(A) is used to determine the minimum delay embedding (276 $\tau_0 = 17$). Therefore with the selection of the minimum embedding parameters, the reconstructed attractor is created in order to ensure with τ_0 the maximum independence between $x(t)$ and $x(t + \tau_0)$ and with m_0 allowing the trajectories in the reconstructed state space to be unfolded.

For N time series, we use a sample mean for an overall value of embedding minimum embedding parameters ($\bar{m}_0, \bar{\tau}_0$) in which minimum values (m_{0_i}, τ_{0_i}) are averaged over N which is the total number of minimum embedding values:

$$\bar{m}_0 = \frac{1}{N} \sum_{i=1}^N m_{0_i}, \quad (3.10)$$

$$\bar{\tau}_0 = \frac{1}{N} \sum_{i=1}^N \tau_{0_i}. \quad (3.11)$$

3.5 Reconstructed State Space with UTDE

(275) Given a time series $x(n)$, the UTDE matrix is computed with its minimum embedding parameters and then PCA is applied in order to select the first three axis of the rotated

3.6 Recurrence Plots (RP)

data to create the reconstructed state spaces (Frank et al., 2010; Samà et al., 2013). See Fig. 3.1 that illustrates and describes the method of reconstructed state space with UTDE.

3.6 Recurrence Plots (RP)

Henri Poincaré in 1890 ²⁷⁴ introduced the concept of recurrences in conservative systems, however the discovery was not put into practice until the development of faster computers (²⁷³Marwan et al., 2007), for which Eckmann et al. (1987) introduced a method ⁶ where recurrences in the dynamics of a system can be visualised. The intention of ²⁷²Eckmann et al. (1987) was to propose a tool, called Recurrence Plot (RP), that provides ⁶insights into high-dimensional dynamical systems where trajectories are very difficult to visualise. Hence, "RP is a tool that helps us to investigate the m -dimensional phase space trajectories through a two-dimensional representation of its recurrences" (Marwan and Webber, 2015, p. 7). Similarly, Marwan and Webber (2015) pointed out that in ²⁷¹addition to the methodologies of the state space reconstruction and other dynamic invariants (e.g. Lyapunov exponent, Kolmogorov-Sinai entropy), the recurrences of the trajectories in the phase space can provide important clues to characterise the underlying process for periodicities (as Milankovitch cycles) or irregular cycles (as El Niño Southern Oscillation). Such recurrences can not only be visualised using Recurrence Plots (RP) but also be quantified with Recurrence Quantification Analysis (RQA) metrics, which leads to applications of these tools in various areas such as Economics, Physiology, Neuroscience, Earth Science, Astrophysics and Engineering ⁵⁸(Marwan et al., 2007).

A recurrence plot based on time series $\{\mathbf{x}_n\}$ is computed from the state space ¹⁸⁶reconstruction with uniform time-delay embedding method ¹³ $X(i) = \{\tilde{\mathbf{x}}_n, \dots, \tilde{\mathbf{x}}_{n-(m-1)\tau}\}$ ²⁰where $i = 1, \dots, N$, N is the number of considered states of $X(i)$ and $X(i) \in \mathbb{R}^m$

Nonlinear Analyses

(²³⁴ Eckmann et al., 1987). The recurrence plot is therefore a two-dimensional ⁸ $N \times N$ square matrix, \mathbf{R} , where a black dot is placed at (i, j) whenever $X(i)$ is sufficiently close to $X(j)$:

$$\mathbf{R}_{i,j}^m(\epsilon) = \Theta(\epsilon_i - \|X(i) - X(j)\|), \quad X(i) \in \mathbb{R}^m, \quad i, j = 1, \dots, N, \quad (3.12)$$

where N is the number of considered states of $X(i)$, ϵ is a threshold distance, $\|\cdot\|$ a norm, and $\Theta(\cdot)$ is the Heaviside function (i.e. $\Theta(x) = 0$, if $x < 0$, and $\Theta(x) = 1$ otherwise) (¹⁵⁸ Fig 3.5) (Eckmann et al., 1987; Marwan et al., 2007; Marwan and Webber, 2015). RP is also characterised with a line of identity (LOI) which is a black main diagonal line due to $R_{i,j} = 1$ ($i, j = 1, \dots, N$). ²³³

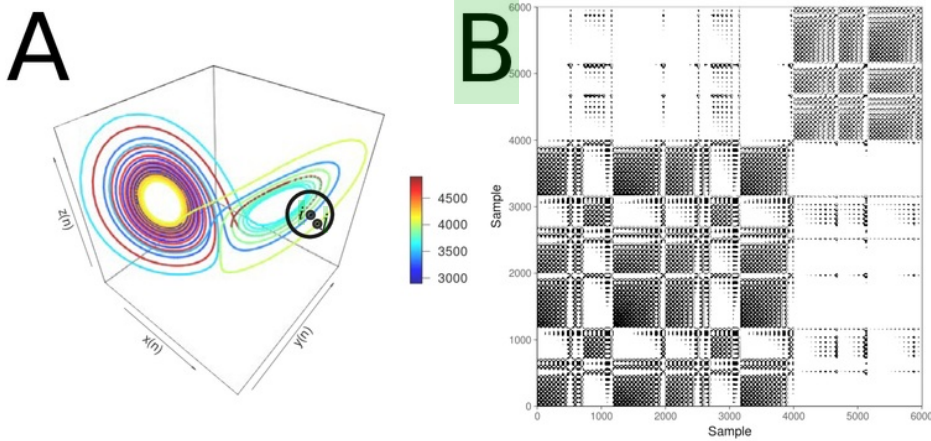


Fig. 3.5 Recurrence Plots. (A) State space of the Lorenz system with ⁷² controlling parameters ($\rho = 28, \sigma = 10, \beta = 8/3$). A point, j , in trajectory $X()$ which falls into the neighborhood ⁵⁸ (black circle) of a given point at i is a recurrent point and is represented as a black dot in the recurrence plot at location (i, j) or white otherwise. (B) Recurrence plot using the three components of the Lorenz system and the RP with no embeddings and threshold $\epsilon = 5$. This figure is adapted from Marwan and Webber (2015) and R code to reproduce it is available from Xochicale (2018).

3.6 Recurrence Plots (RP)

3.6.1 Structures of Recurrence Plots

Pattern formations in RPs can be designated either as topology for large-scale patterns or texture for small-scale patterns. In the case of topology, the following pattern formations are presented: (i) homogeneous where uniform recurrence points are spread in the RP e.g., uniformly distributed noise (Figure 3.6A), (ii) periodic and quasi-periodic systems where diagonal lines and checkerboard structures represent oscillating systems, e.g., sinusoidal signals (Figure 3.6B), (iii) drift where paling or darkening recurrence points away from the LOI is caused by drifting systems, e.g., logistic map (Figure 3.6C), and (iv) disrupted where recurrence points are presented white areas or bands that indicate abrupt changes in the dynamics, e.g. Brownian motion (Figure 3.6D) (Eckmann et al., 1987; Marwan and Webber, 2015). Texture, for small-scale patterns, can be categorised as: (i) single or isolated recurrence points that represent rare occurring states, do not persist for any time or fluctuate heavily, (ii) dots forming diagonal lines where the length of the small-scale parallel lines in the diagonal are related to the ratio of determinism or predictability in the dynamics of the system, and (iii) dots forming vertical and horizontal lines where the length of the lines represent a time length where a state does not change or change very slowly and the patterns formation represent discontinuities in the signal, and (iv) dots clustering to inscribe rectangular regions which are by related to laminar states or singularities (Marwan and Webber, 2015).

Although, each of the previous pattern descriptions of the structures in the RP offer an idea of the characteristics of dynamical systems from time-series, these descriptions might be misinterpreted and conclusions might tend to be subjective as these require the interpretation of a researcher(s). Because of that, recurrence quantification analysis (RQA) offer objective metrics to quantify the visual characteristics of recurrent pattern structures in the RP (Zbilut and Webber, 1992).

Nonlinear Analyses

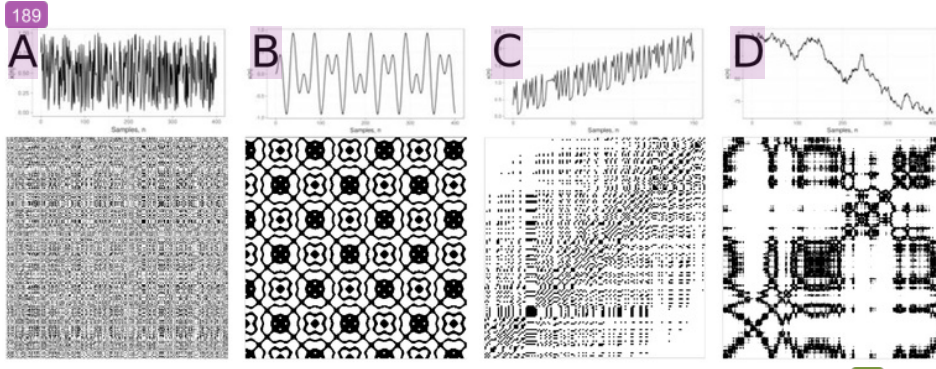


Fig. 3.6 Patterns in Recurrence Plots. Time-series with its respective recurrence plots for: (A) uniformly distributed noise, (B) super-positioned harmonic oscillation ($\sin(\frac{1}{5} * t) * \sin(\frac{5}{100} * t)$), (C) drift logistic map ($x_{i+1} = 4x_i(1 - x_i)$) corrupted with a linearly increase term ($0.01 * i$), and (D) disrupted brownian motion ($x_{i+1} = x_i + 2 * rnorm(1)$). Figure is adapted from Marwan and Webber (2015) and R code to reproduce the figure is available from Xochicale (2018).

3.7 Recurrence Quantifications Analysis (RQA)

Zbilut and Webber (1992) proposed metrics to investigate the density of recurrence points in RPs, then histograms of lengths for diagonal lines in RPs were studied by Trulla et al. (1996), then Marwan (2008) introduced the term Recurrence Quantification Analysis (RQA). RQA metrics are percentage of recurrence, percentage of determinism, ratio, Shannon entropy of the frequency distributions of the line lengths, maximal line length and divergence, trend and laminarity (Marwan et al., 2007; Marwan and Webber, 2015).

3.7.1 Measures of RP based on the recurrence density

The percentage of recurrence (REC) or recurrence rate (RR) is defined as

$$REC(\epsilon, N) = \frac{1}{N^2 - N} \sum_{i,j=1}^N R_{i,j}^m(\epsilon), \quad (3.13)$$

3.7 Recurrence Quantifications Analysis (RQA)

which enumerates the black dots in the RP excluding the line of identity. RR is a measure of the relative density of recurrence points in the sparse matrix (Marwan and Webber, 2015).

3.7.2 Measures of RP based on diagonal lines

The percent determinism (DET) is defined as the fraction of recurrence points that form diagonal lines and it is determined by

$$DET = \frac{\sum_{l=d_{min}}^N l H_D l}{\sum_{i,j=1}^N R_{i,j}(\epsilon)}, \quad (3.14)$$

where

$$H_D(l) = \sum_{i,j=1}^N (1 - R_{i-1,j-1}(\epsilon))(1 - R_{i+l,j+l}(\epsilon)) \prod_{k=0}^{l-1} R_{i+k,j+k}(\epsilon) \quad (3.15)$$

is the histogram of the lengths of the diagonal structures in the RP. DET can be interpreted as the predictability of the system for periodic signals which, in essence, have longer diagonal lines for chaotic signals shorter or absent diagonal lines for stochastic signals (Marwan et al., 2007; Marwan and Webber, 2015). Similarly, DET is considered as a measurement for the organisation of points in RPs (Iwanski and Bradley, 1998).

RATIO is defined as the ratio between DET and REC and it is calculated from the frequency distributions of the lengths of the diagonal lines. RATIO is useful to discover dynamic transitions (Marwan and Webber, 2015).

ENT is the Shannon entropy of the frequency distribution of the diagonal line lengths and it is defined as

$$ENT = - \sum_{l=d_{min}}^N p(l) \ln p(l) \quad \text{with} \quad p(l) = \frac{H_D(l)}{\sum_{l=d_{min}}^N H_D(l)}. \quad (3.16)$$

Nonlinear Analyses

ENT ⁵⁸ reflects the complexity of the deterministic structure in the system. For instance, ⁹⁷ for uncorrelated noise or oscillations, the value of ENT is rather small and indicates low complexity of the system, therefore "the higher the ENT is the more complex the dynamics are" (Marwan and Webber, 2015, p. 15).

3.7.3 Some weaknesses and strengths of RP and RQA.

²³¹ One of the main advantages of the use of RP is their capacity to detect small modulations in frequency or phase that are not detectable using standard methods e.g. spectral or wavelet analysis (Marwan, 2011). Nonetheless, RP is a very young field in nonlinear dynamics and many questions are still open, for instance, different parameters for window length size of the time series, embedding parameters or recurrence threshold can generate different results in RQA metrics (Eckmann et al., 1987; Marwan, 2011). Additionally, the selection of recurrence threshold, ϵ , can depend on the system that is analysed. For instance, when studying dynamical invariants ϵ require to be very small, for trajectory reconstruction ϵ requires to have a large thresholds or when studying dynamical transition there is little importance about the selection of the threshold ¹⁸² (Marwan, 2011). Other criteria for the selection of ϵ is that the recurrence threshold should be five times larger than the standard deviation of the observational noise or ²⁵ the use of diagonal structures within the RP is suggested in order to find the optimal recurrence threshold for (quasi-)periodic process (Marwan, 2011).

Similarly, Iwanski and Bradley (1998) highlighted the importance of choosing the right embedding parameters to perform RQA for which many experiments have to be performed using different parameters ⁴⁷ in order to have a better intuition of the nature of the time series and how this is represented by using RQA. In the same investigation, Iwanski and Bradley (1998) pointed out that RQA metrics are quantitatively and qualitatively independent of embedding dimension. However, with an example, Iwanski

3.7 Recurrence Quantifications Analysis (RQA)

and Bradley (1998) showed that two dissimilar RPs one from the Rössler system and the other from a sine-wave signal of varying period have got equal values of REC (2.1%) and have approximately equal values of DET (42.9%, 45.8%, respectively). Also, Iwanski and Bradley (1998) pointed out the importance of choosing the right parameters to perform RQA, since many experiments must be performed with different parameters to have a better intuition of the nature of the time series and how this is represented using RQA. Other example to determine embedding parameters for the RQA is the method of Zbilut and Webber (1992) in which 3D surfaces are created with an increase of embedding parameters (m and τ), then, for instance, Zbilut and Webber (1992) explored fluctuations and gradual changes in the 3D surfaces that provide information about the embeddings parameters. Recently, Marwan and Webber (2015) created 3D surfaces for visual selection of not only embedding parameters but also recurrence thresholds.

With that, therefore, it can be stated for this thesis that little has been investigated with regards to: (i) the strengthens and weaknesses of different nonlinear tools when using real-world data which is nonstationarity, noisy and has different sampling rate and length (Section 2.4), (ii) different models for movement variability where, for instance, not only the model of Stergiou et al. (2006) where complexity and predictability variables can characterise movement variability but also it can take into account the dependencies of the task dynamics (Vaillancourt and Newell, 2002, 2003) (Section 2.3.2), and (iii) the selection and application the right tools in order to quantify MV (Section 2.3.3). We, therefore, explore, in this thesis, the weaknesses and strengths of the window size of time series, embedding parameters for RSS with UTDE and recurrence threshold for RP and RQA in order to gain a better insight into the underlying time series collected from inertial sensors in the context of human-humanoid imitation activities.

3.8 Final remarks

In this chapter, we introduced fundamentals of nonlinear analyses such as RSS with UTDE, estimation of embedding parameters with FNN and AMI, RP, and four RQA metrics (REC, DET, RATIO, and ENTR). It is important to note that this thesis is only focused on traditional methods (FNN and AMI) to compute embedding parameters, as the computation of embedding parameters ²⁶⁹ is still an open challenge (Gómez-García et al., 2014; Uzal et al., 2011). We also pointed out some weaknesses and strengths of RP and RQA metrics which will be explored in two experiments (see Chapter 4), taking into account some of the issues of real-world time series data analysis, and present results for embedding parameters, RPs, RQAs and 3D surfaces of RQAs, as one of our contribution to knowledge in this thesis, that increment not only embedding parameters (Iwanski and Bradley, 1998) but also recurrence thresholds (see Chapters 5 and 6).

Chapter 4

Experiments

4.1 Aims

We design two experiments for human-image interaction (HII) and human-humanoid interaction (HHI) where participants perform simple arm movements repetitions. The aims of the experiments is not only to investigate the weaknesses and robustness of RSS, UTDE, embedding parameters, RP and RQA metrics regarding different conditions presented in real-world time series data (noise, nonstationarity, smoothness, window size lengths and structures), but also to present experimental scenarios where one can observe how the variables that model movement variability (e.g. complexity, predictability and activity type) (Stergiou et al., 2006; Vaillancourt and Newell, 2002, 2003) affect nonlinear analyses.

4.2 Participants

Twenty-three participants, from now on defined as pN where N is the number of participant, were invited for two experiments of simple arm movements. However, it is important to note that although the same number of participants performed the

Experiments

experiments, different number of participants were take into account for each of the experiments due to either technical problems with the sensors or the instructions of the experiments were mistakenly given.

4.2.1 Human-Image Imitation Activities

Only six participants ($p01, p04, p05, p10, p11, p15$) were considered for the experiment of Human-Image Imitation (HII) activities due to problems with the inertial sensors such as bluetooth disconnections and drifting of time synchronisation (Section B.2.4).

Hence, the six participants were male right-handed healthy participants and have a
85 mean and standard deviation (SD) age of mean=19.5 (SD=0.83) years.

4.2.2 Human-Humanoid Imitation Activities

For the experiment of Human-Humanoid Imitation (HHI) activities, data for only twenty participants were analysed since the instructions for $p01$, who was the only left-handed, were mistakenly given in a way that movements were differently performed from what had been planned, and for participants $p13$ and $p16$ data were corrupted because of bluetooth communications problems with the sensors (Section B.2.4). With that in mind, all of the 20 participants were right-handed healthy participants, being four females and sixteen males, with a mean and standard deviation (SD) age of mean=19.8 (SD=1.39) years.

4.3 Equipment

During the experiments, time series were collected with four neMEMSi Inertial Measurement Units (IMUs) using a sampling rate of 50Hz (Comotti et al., 2014). neMEMSi sensors provide tri-axial time series from the accelerometer, gyroscope and magnetome-

4.4 Ethics

ter sensors and quaternions. See Appendix B.1 for further technical information of NeMEMSi IMU sensors.

With regard to the human-humanoid imitation activities, NAO, a humanoid robot from Aldebaran (Gouaillier et al., 2009), were programmed with choreographer to perform horizontal and vertical arm movements. See Appendix B.3 for further technical information regarding NAO and the code of NAO's movements.

4.4 Ethics

The experiments of this thesis were conducted in November 2016 and participants confirmed reading and understanding the participant information sheet of the experiments
204 and were able to withdraw from the experiment at any time without giving any reason.

The design of the experiments is adhered to University of Birmingham regulations,
data were anonymised and videos were stored only a personal computer in accordance
9 with the Data Protection Act 1998. Refer to Appendix C for further information about
268 the ethics, online participation information sheets and experiment check list.

4.5 Experiments

4.5.1 Human-Image Imitation Activities

In the experiment of human-image imitation (HHI), four wearable IMUs sensors were used and attached to the right hand of the participant (Figure 4.1 A,D). Then, participants performed two experiments: (i) an unconstrained arm movement imitation activity where participants only receive instructions and look at images of the arm movements, and (ii) a constrained experiment where participants hear a beat to synchronise their arm movements.

Experiments

Arm movements following an image while not hearing a beat

Participants received instructions to perform unconstrained upper arm movements while only looking at an image for

- ten repetitions of horizontal arm movement at their comfortable velocity (Fig. 4.1(A, B, C)),
- ten repetitions of vertical arm movement at their comfortable velocity (Fig. 4.1(D, F, E)),
- ten repetitions of horizontal arm movement at a faster velocity than the comfortable velocity but not at their fastest velocity (Fig. 4.1(A, B, C)), and
- ten repetitions of vertical arm movement at a faster velocity than the comfortable velocity but not at their fastest velocity (Fig. 4.1(D, F, E)).

Arm movements following an image while hearing a beat

Participants received instructions to perform constrained upper arm movements while listening a beat to constraint their movements.

- ten repetitions of horizontal arm movement at normal velocity (Fig. 4.1(A, B, C)),
- ten repetitions of vertical arm movement at normal velocity (Fig. 4.1(D, F, E)),
- ten repetitions of horizontal arm movement at faster velocity and (Fig. 4.1(A, B, C)), and
- ten repetitions of vertical arm movement at faster velocity (Fig. 4.1(D, F, E)).

To visualise the time series of the previous activities, Figs 4.2 show time series using smoothed gyroscope of Y and Z for the sensor HS01 of participant 01.

4.5 Experiments

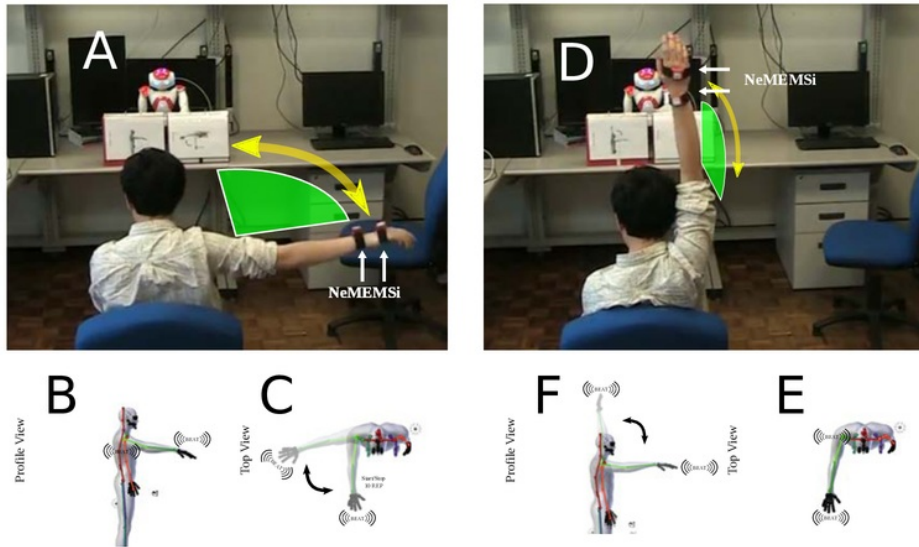


Fig. 4.1 Human-image imitation (HII) activities. (A) HII of horizontal arm movement, (B) image of the profile view for horizontal arm movement, (C) image of the top view for horizontal arm movement, (D) HII of vertical arm movement, (E) image of the profile view for vertical arm movement, and (F) image of the top view for vertical arm movement. (B, C, F and E) show '(((BEAT)))' to indicate the participants arm movements synchronisation when hearing a beat.

Experiments

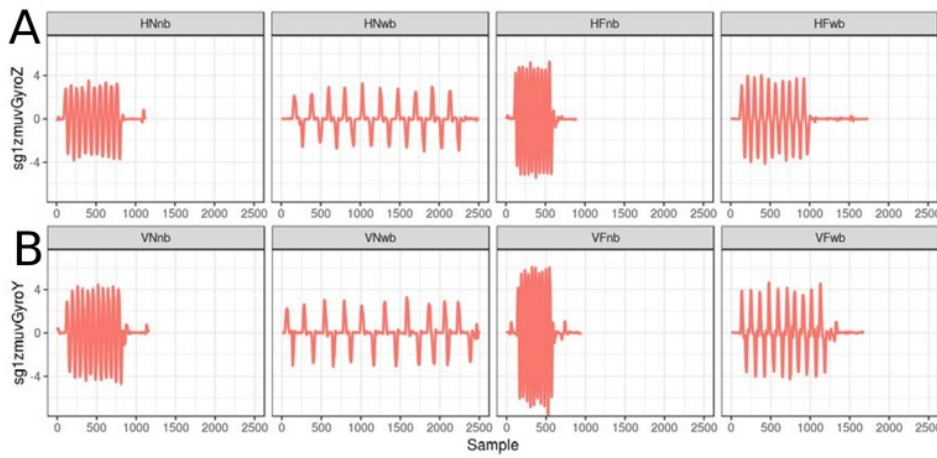


Fig. 4.2 Time series for horizontal and vertical arm movements. Time series of smoothed data from gyroscope sensor ($sg1zmuvGyroZ$ and $sg1zmuvGyroY$) of participant 01 with sensor HS01 for different velocity arm movements: (A) Horizontal Normal with no beat (HNnb), Horizontal Normal with beat (HNwb), Horizontal Faster with no beat (HFnb) and Horizontal Faster with beat (HFwb), and (B) Vertical Normal with no beat (VNnb), Vertical Normal with beat (VNwb), Vertical Faster with no beat (VFnb) and Vertical Faster with beat (VFwb). R code to reproduce the figure is available Xochicale (2018).

4.5 Experiments

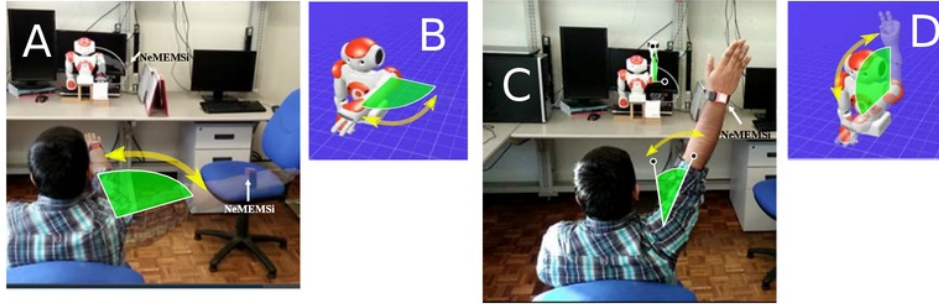


Fig. 4.3 **Human-humanoid imitation activities.** Face-to-face human-humanoid imitation (HHI) activities for (A) HHI of horizontal arm movement, (B) Humanoid horizontal arm movement, (C) HHI of vertical arm movement, and (D) Humanoid vertical arm movement.

4.5.2 Human-Humanoid Imitation Activities

For the human-humanoid imitation (HHI) experiment four wearable IMUs sensors were used in which two sensors were attached to the right hand of the participant and two sensors were attached to the left hand of the humanoid robot (Figure 4.3 A,C). Then, in the face-to-face imitation activity, each participant was asked to imitate repetitions of simple horizontal and vertical arm movements performed by the humanoid robot in the following conditions:

- ten repetitions of horizontal arm movement at normal (HN) and faster (HF) velocity (Fi. 4.3 A), and
- ten repetitions of vertical arm movement at normal (VN) and faster (VF) velocity (Fig. 4.3 C).

The normal and faster velocity of arm movements is defined by the duration in number of samples of one repetition of NAO's arm movements. We select NAO's arm movements duration to distinguish between normal and faster arm movements as the movements from the humanoid robot have less variation between repetition to repetition. The duration for one repetition of the horizontal arm movement at normal velocity, HN,

Experiments

is about 5 seconds considering that each repetition last around 250 samples. For horizontal arm movement at faster velocity, HF, each repetition were performed in around 2 seconds which correspond to 90 samples of data. The vertical arm movement at normal velocity, VN, were performed in 6 seconds which is around 300 samples of data. For vertical arm movement at faster velocity, VF, each repetition lasts about 2.4 seconds which correspond to 120 samples of data. To visualise the distinction between normal and faster velocity for horizontal and vertical arm movements, Fig 4.4 shows smoothed time series for axes Z and Y of the gyroscope sensors with four window lengths: 2-sec (100-samples), 5-sec (250-samples), 10-sec (500-samples) and 15-sec (750-samples).

4.6 Processing of time series

4.6.1 Raw time-series

Considering the work of Shoaib et al. (2016) which provided evidence of an improvement in recognition activities when combining data from accelerometer and gyroscope, analysis for time series, in this thesis, uses only the accelerometer and gyroscope of the IMU sensors which leaves magnetometer and quaternions for future investigations because of their possible variations with regard to magnetic disturbances.

Time series from the accelerometer are defined by triaxial time series $A_x(n)$, $A_y(n)$, $A_z(n)$ which forms the matrix \mathbf{A} (Eq. 4.1), and the same for data from the gyroscope which is defined by triaxial time-series of $G_x(n)$, $G_y(n)$, $G_z(n)$ representing the matrix \mathbf{G} (Eq. 4.2). Both triaxial time series of each sensor, a and g , are denoted with its respective axes subscripts x, y, z , where n is the sample index and N is the same maximum length of all axes for the time series. Matrices \mathbf{A} and \mathbf{G} are represented as

4.6 Processing of time series

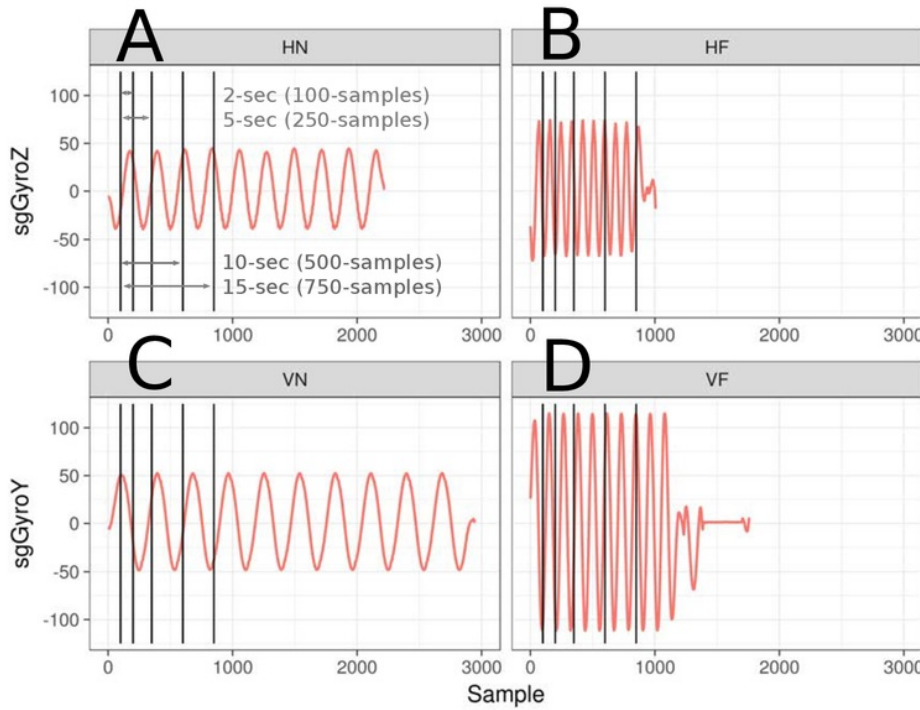


Fig. 4.4 Time series duration of horizontal and vertical arm movements. Time series of smoothed data from gyroscope sensor for different velocity arm movements performed by NAO: (A) Horizontal Normal arm movement, HN, (B) Horizontal Faster arm movement, HF, (C) Vertical Normal arm movement, VN, and (D) Vertical Faster arm movement, VF. Additionally, (A) shows window sizes for 2-seconds (100 samples), 5-seconds (250 samples), 10-seconds (500 samples) and 15-seconds (750 samples) which are also presented in (B), (C) and (D). R code to reproduce the figure is available Xochicale (2018).

Experiments

follow

$$\mathbf{A} = \begin{pmatrix} A_x(n) \\ A_y(n) \\ A_z(n) \end{pmatrix} = \begin{pmatrix} \textcolor{blue}{188} \\ a_x(1), a_x(2), \dots, a_x(N) \\ a_y(1), a_y(2), \dots, a_y(N) \\ a_z(1), a_z(2), \dots, a_z(N) \end{pmatrix}, \quad (4.1)$$

$$\mathbf{G} = \begin{pmatrix} G_x(n) \\ G_y(\textcolor{red}{n}) \\ G_z(\textcolor{brown}{n}) \end{pmatrix} = \begin{pmatrix} \textcolor{red}{181} \\ g_x(1), g_x(2), \dots, g_x(N) \\ g_y(1), g_y(2), \dots, g_y(N) \\ \textcolor{brown}{318} \\ g_z(1), g_z(2), \dots, g_z(N) \end{pmatrix}, \quad (4.2)$$

134 where n is the sample index and N is the same maximum length of all axes for the time series.

4.6.2 Postprocessing time-series

After the collection of raw time-series from four NeMEMSi sensors, time synchronisation alignment and interpolation were performed 267 in order to create time series with the same length and synchronised time. We refer the reader to Appendix B for technical information about the time synchronisation process and IMU sensors.

4.6.3 Normalization of time-series

164 Tim series are normalised to have zero mean and unit variance using sample mean and sample standard deviation (Ioffe and Szegedy, 2015). 311 The sample mean and sample standard deviation using $x(n)$ is given by

$$\mu_{x(n)} = \frac{1}{N} \left(\sum_{i=1}^N x(i) \right), \quad \sigma_{x(n)} = \sqrt{\frac{\sum_{i=1}^N (x(i) - \mu_{x(n)})^2}{N-1}}, \quad (4.3)$$

7 then the normalised data, $\hat{x}(n)$, is computed as follows

$$\hat{x}(n) = \frac{x(n) - \mu_{x(n)}}{\sigma_{x(n)}}. \quad (4.4)$$

4.6.4 Smoothing time-series

Using a low-pass filter is the common way to either capture the low frequencies (below 15 Hz) that represent %99 of the human body energy or to get the gravitational and body motion components of accelerations (below 0.3 Hz) (Anguita et al., 2013). However, for this thesis the main focus is on the conservation of the structure of the time series in terms of the width and heights where, for instance, a Savitzky-Golay filter can help to accomplish such task (Press et al., 1992). Savitzky-Golay filter is based on the principle of moving window average which preserves the area under the curve (the zeroth moment) and its mean position in time (the first moment) but the line width (the second moment) is violated and that results, for example, in the case of spectrometric data where a narrow spectral line is presented with reduced height and width. The aim of Savitzky-Golay filtering is hence to find the filter coefficients c_n that preserve higher momentums which are based on local least-square polynomial approximations (Press et al., 1992; Savitzky and Golay, 1964; Schafer, 2011). Therefore, Savitzky-Golay coefficients are computed using an R function `sgolay(p,n,m)` where p is the filter order, n is the filter length (must be odd) and m is the m -th derivative of the filter coefficients (signal R developers, 2014). Smoothed signal is represented with a tilde over the original signal: $\tilde{x}(n)$.

4.6.5 Window size of time-series

With regard to the window size, Shoaib et al. (2016) compared seven window lengths (2, 5, 10, 15, 20, 25, 30 seconds) and combination of inertial sensors (accelerometer, gyroscope and linear acceleration sensor) in activity recognition performance for repetitive activities (walking, jogging and biking) and less repetitive activities (smoking, eating, giving a talk or drinking a coffee). Similarly, Shoaib et al. (2016) experimented with different window size effect to conclude that the increase of window size improved

Experiments

the recognition of complex activities because these required a large window to learn the repetitive motion patterns. Also, Shoaib et al. (2016) concluded that the use of large window size improve the recognition performance of less repetitive activities which mainly involve random hand gestures.

For the activities in this thesis which are mainly repetitive, we selected only four window sizes: 2-s window (100 samples), 5-s window (250 samples), 10-s (500 samples) and 15-s window (750 samples) (Figure 4.4).

Chapter 5

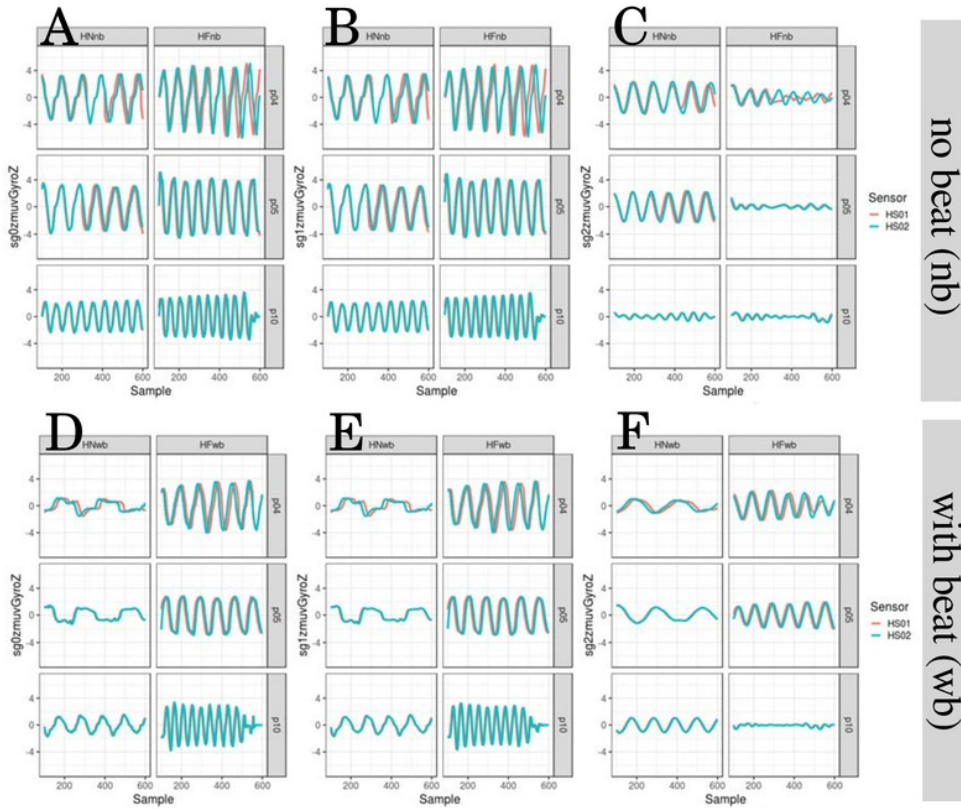
Quantifying Human-Image Imitation Activities

5.1 ¹¹¹ Introduction

In this chapter, we present the results of the experiments of human-image imitation activities, described in Section 4.5.1, which include time series, minimum embedding parameters, RSS with UTDE, RPs, RQAs and weaknesses and strengthens of RQA.

5.2 Time series

To make the visual comparison easier, we consider time series for only three participants ($p04$, $p05$, $p10$) with a window length of 500 samples. Hence, Figs 5.1 and 5.2 show the time series for horizontal and vertical arm movements of participants following an image while not hearing a beat (nb) and hearing a beat (wb). Also, three levels of smoothness of normalised time series are presented (sg0, sg1 and sg2). The remained time series are presented in Appendix D.1.



265

Fig. 5.1 Time series for horizontal arm movements. Time series for (A,D) raw-normalised ($sg0zmuvGyroZ$), (B,E) normalised-smoothed 1 ($sg1zmuvGyroZ$), and (C,F) normalised-smoothed 2 ($sg2zmuvGyroZ$). Time series are for three participants ($p04$, $p05$, and $p10$) for horizontal movements in normal and faster velocity with no beat (HNnb, HFnb) and with beat (HNwb, HFwb) using the normalised GyroZ axis ($zmuvGyroZ$) and two sensors attached to the participant wrist (HS01, HS02). R code to reproduce the figure is available from Xochicale (2018).

5.2 Time series

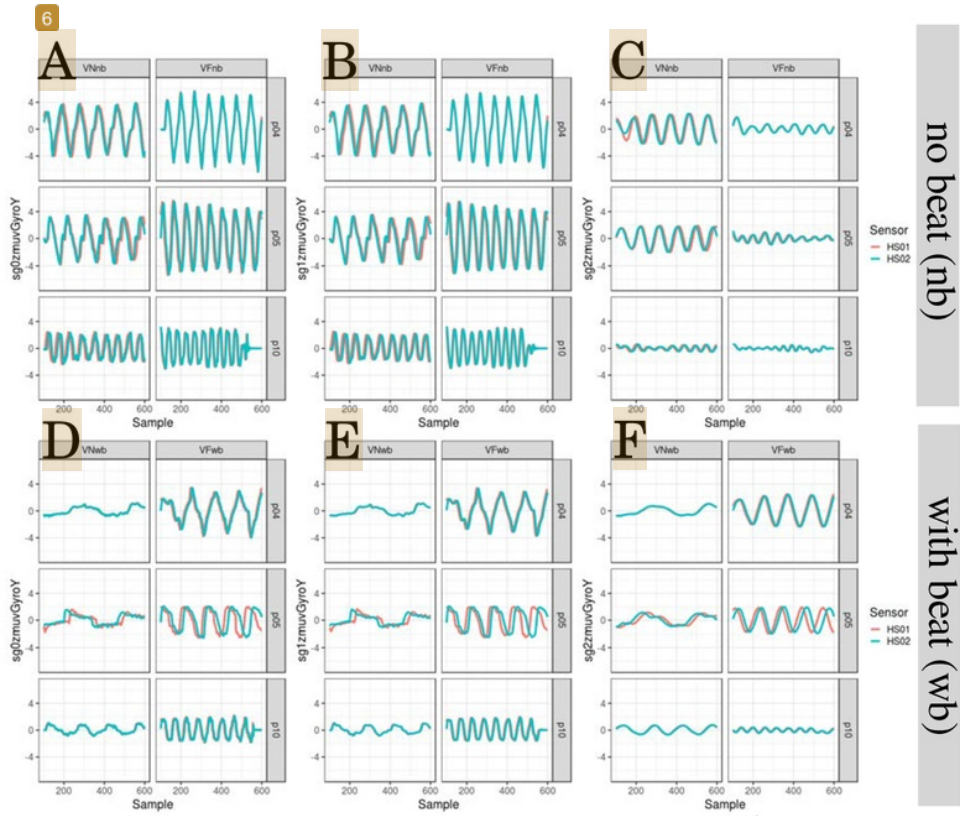


Fig. 5.2 Time series for vertical arm movements. Time series for (A,D) raw-normalised ($sg0zmuvGyroY$), (B,E) normalised-smoothed 1 ($sg1zmuvGyroY$), and (C,F) normalised-smoothed 2 ($sg2zmuvGyroY$). Time series are for three participants ($p04$, $p05$, and $p10$) for vertical movements in normal and faster velocity with no beat (VNnb, VFnb) and with beat (VNwb, VFwb) using the normalised GyroY axis ($zmuvGyroY$) and two sensors attached to the participant wrist (HS01, HS02). R code to reproduce the figure is available from Xochicale (2018).

5.3 Minimum Embedding Parameters

The first step to create Reconstructed State Spaces (RSSs) with the use of Uniform
65 Time-Delay Embedding (UTDE) is to compute the average minimum embedding
65 parameters for all participants, sensors and activities using False Nearest Neighbour
(FNN) and Average Mutual Information (AMI) algorithms.

Hence, Figs. 5.3 illustrate the box plots for minimum embedding dimensions. For horizontal arm movements (Figs. 5.3(A)), one can notice how the interquartile range appear to be near to one independently of the activity or sensor. With regards to the level of smoothness, there is a decrease of sample mean (gray rhombus) as the smoothness increase. Similarly, for vertical arm movements (Figs. 5.3(B)) the interquartile range of activities and sensors appears to be near to one and the increase of smoothness is affected by a decrease in sample means (gray rhombus). For further
215 details of the mimimum dimension values see Figs D.7, D.8, D.9 and D.10 in Appendix D.2.

Figs. 5.4 illustrate the box plots for first minimum AMI. Box plots for horizontal arm movements (Figs. 5.4(A)) for HNwb appear more spread (interquartile range between 10 to 20) while other activities there is a slight variation of values (interquartile range between 5 to 10). Little can be said regardless the sample mean of each axis (gray rhombus) which is not proportionally affected as the smoothed of the time series increase. Box plots for vertical arm movements (Figs. 5.4(B)) show that the interquartile range of each activity is constant except for the activity VFwb which range are between 5 to 10. The increase of smoothness of time series made the sample mean (gray rhombus) to increase of the points. For further details of the mimimum
157 dimension values see Figs D.11, D.12, D.13 and D.14 in Appendix D.2.

5.3 Minimum Embedding Parameters

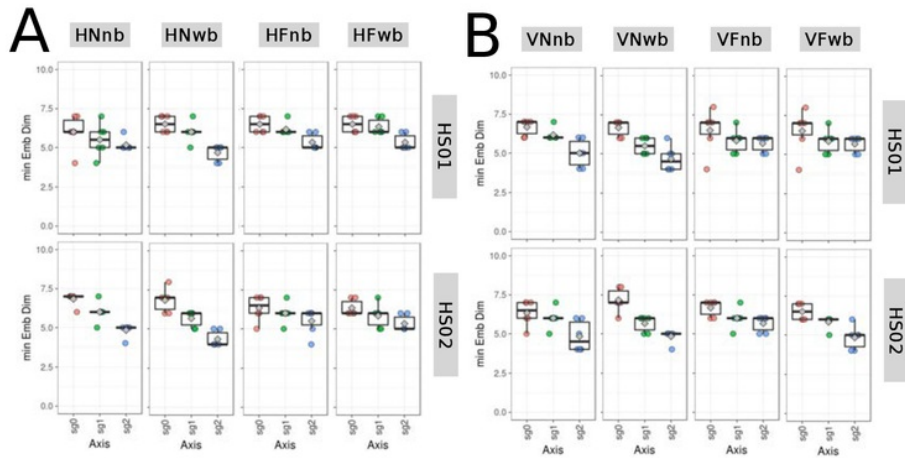


Fig. 5.3 Box plots for minimum embedding dimensions. Box plots of minimum embedding dimensions for (A) horizontal and (B) vertical arm movements for normal and faster velocity (N/F) with no beat (nb) and with beat (wb) movements using sensors 01 and 02 attached to the wrist of the participant (HS01, HS02). Minimum embedding dimensions are for six participants ($p_01, p_04, p_05, p_{10}, p_{11}, p_{15}$) with three smoothed signals (sg0, sg1 and sg2) and window lenght of 10-sec (500 samples). R code to reproduce the figure is available from Xochicale (2018).

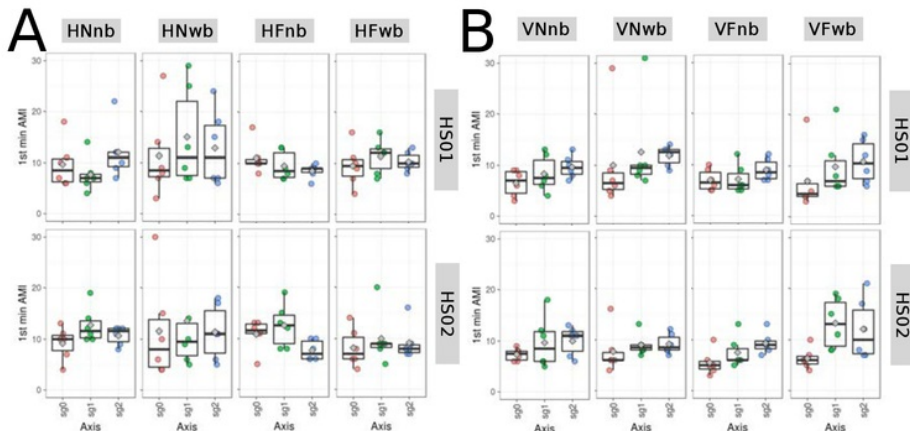


Fig. 5.4 Box plots for 1st minimum AMI. Box plots of the 1st minimum AMI values for (A) horizontal and (B) vertical arm movements for normal and faster velocity (N/F) with no beat (nb) and with beat (wb) movements using sensors 01 and 02 attached to the wrist of the participant (HS01, HS02). First minimum AMI values are for six participants ($p_01, p_04, p_05, p_{10}, p_{11}, p_{15}$) with three smoothed signals (sg0, sg1 and sg2) and window lenght of 10-sec (500 samples). R code to reproduce the figure is available from Xochicale (2018).

5.3.1 Average minimum embedding parameters

Although the implementation of Uniform Time-Delay Embedding (UTDE) is simple, the main challenge is the selection of appropriate embedding parameters to reconstruct the state spaces of each time series as these are unique in terms of its structure (modulation of amplitude, frequency and phase) (Bradley and Kantz, 2015; Frank et al., 2010; Samà et al., 2013). With that in mind, one problem we faced in this thesis is the selection of embedded parameters that can represent all time series. Our solution to that problem was to compute a sample mean over all values for all participants, activities and sensors (Section 3.4.3). Hence, the average minimum embedding parameters is computed with a sample mean of $\bar{m}_0 = 9$ from the minimum values of $E_1(m)$ in Figs 5.3 and a sample mean of $\bar{\tau}_0 = 6$ from minimum values of AMIs in Figs 5.4. Hence, Reconstructed State Spaces (RSSs), Recurrence Plots (RPs) and Recurrence Quantification Analysis (RQA) metrics are computed with the average minimum embedding parameters ($\bar{m}_0 = 9$, $\bar{\tau}_0 = 6$).

5.4 Reconstructed state spaces with UTDE

Reconstructed state spaces for horizontal normal and horizontal faster arm movements with no beat are shown in Fig 5.5. The smoothness of the time series show a slight change of smoothed trajectories in the RSSs for sg0zmuvGyroZ and sg1zmuvGyroZ, while the RSSs trajectories for sg2zmuvGyroZ appear to be distorted (Fig 5.5). One can see slightly differences in the RSSs trajectories when comparing sensors HS01 and HS02 for horizontal normal arm movement with no beat (Fig 5.5(A, B)) and horizontal faster arm movements with no beat (Fig 5.5(C, D)). With regards to the type of movement, the RSSs trajectories appear to change little when comparing horizontal normal with faster arm movements (Fig 5.5).

5.4 Reconstructed state spaces with UTDE

Fig 5.6 shows trajectories of the reconstructed state space for horizontal normal and horizontal faster arm movements while beat sounds. Hence, as in Fig 5.5, it can also be noted in Fig 5.6 that the smoothness of sg0zmuvGyroZ and sg1zmuvGyroZ appear to affect little the RSSs trajectories, while RSSs trajectories for sg2zmuvGyroZ substantially change so as to show different patterns. However, the trajectories in the RSS appear to change little when comparing the differences between the type of sensors HS01 and HS02 (Fig 5.6). For the type of movements, trajectories show differences for horizontal normal and horizontal faster arm movements (Fig 5.6).

Fig 5.7 show trajectories for reconstructed state spaces of vertical normal and vertical faster arm movements with no beat. Smoothness of the RSSs trajectories is slightly noticed for sg0zmuvGyroY and sg1zmuvGyroY, whereas RSSs trajectories for sg2zmuvGyroY are evidently different (Fig 5.7). When comparing the RSSs trajectories from sensors HS01 and HS02, it can be noted little change, whereas the comparison from type of movement, the trajectories difference is more notable (Fig 5.7).

Fig 5.8 show trajectories for reconstructed state space of vertical normal and vertical faster arm movements for participants hearing a beat. Smoothness of RSSs trajectories appear to show slightly differences between sg0zmuvGyroY and sg1zmuvGyroY, however RSSs trajectories for sg2zmuvGyroY are different (Fig 5.8). With regards to the type of sensor HS01 and HS02, RSSs trajectories appear to change little, whereas for type of activity of normal and faster arm movements, RSSs trajectories show evidently differences (Fig 5.8).

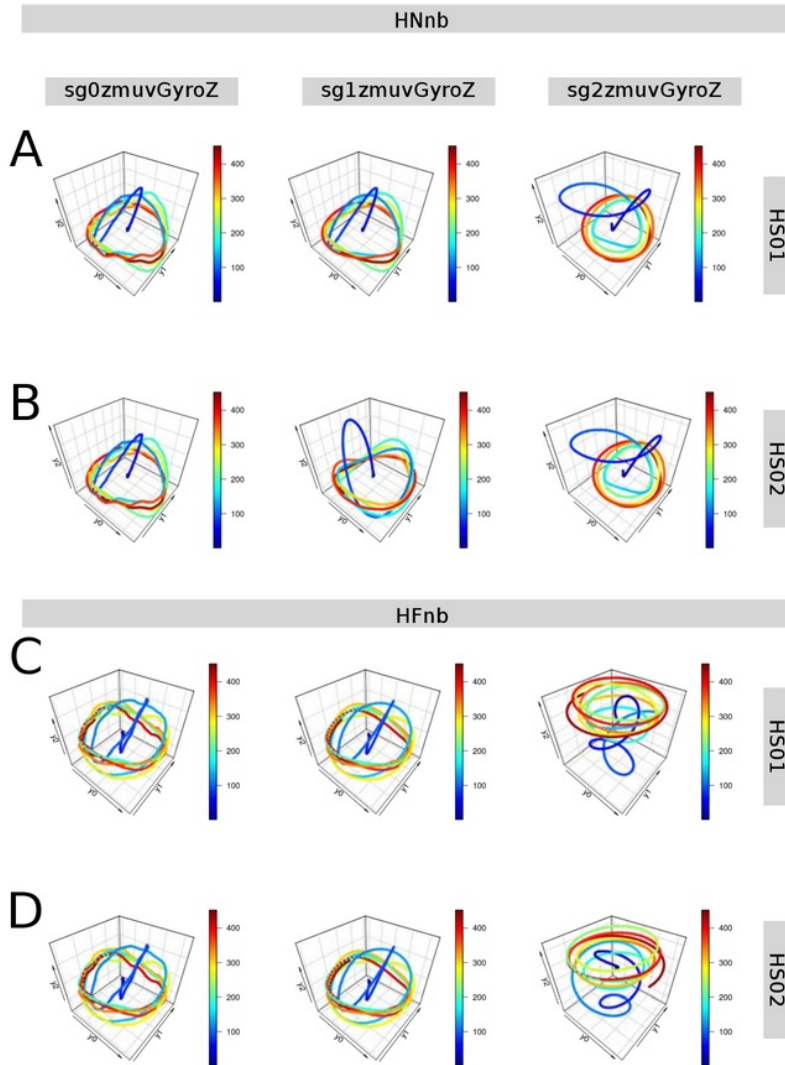


Fig. 5.5 RSSs for horizontal arm movements (no beat). Reconstructed state spaces of participant p01 for (A, B) horizontal normal movements with no beat (HNnb) and (C, D) horizontal faster velocity with no beat (HFnb). Time series for raw-normalised ($sg0zmuvGyroZ$), normalised-smoothed 1 ($sg1zmuvGyroZ$) and normalised-smoothed 2 ($sg2zmuvGyroZ$) with (A, C) sensor attached to the participant (HS01), and (B, D) sensor attached to the participant (HS02). Reconstructed state spaces were computed with embedding parameters $m = 9$, $\tau = 6$. R code to reproduce the figure is available from Xochicale (2018).

5.4 Reconstructed state spaces with UTDE

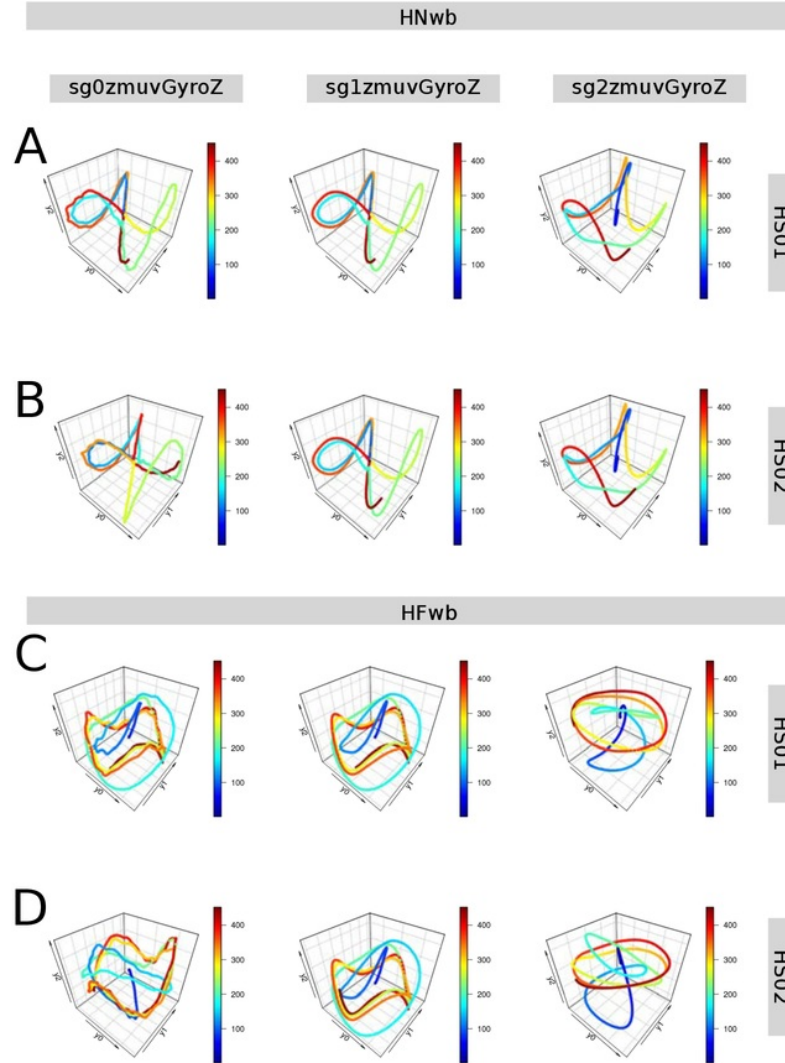


Fig. 5.6 Reconstructed state spaces of participant p01 for (A, B) horizontal normal movements with beat (HNwb) and (C, D) horizontal faster velocity with beat (HFwb). Time series for raw-normalised ($sg0zmuvGyroZ$), normalised-smoothed 1 ($sg1zmuvGyroZ$) and normalised-smoothed 2 ($sg2zmuvGyroZ$) with (A, C) sensor attached to the participant (HS01), and (B, D) sensor attached to the participant (HS02). Reconstructed state spaces were computed with embedding parameters $m = 9$, $\tau = 6$. R code to reproduce the figure is available from Xochicale (2018).

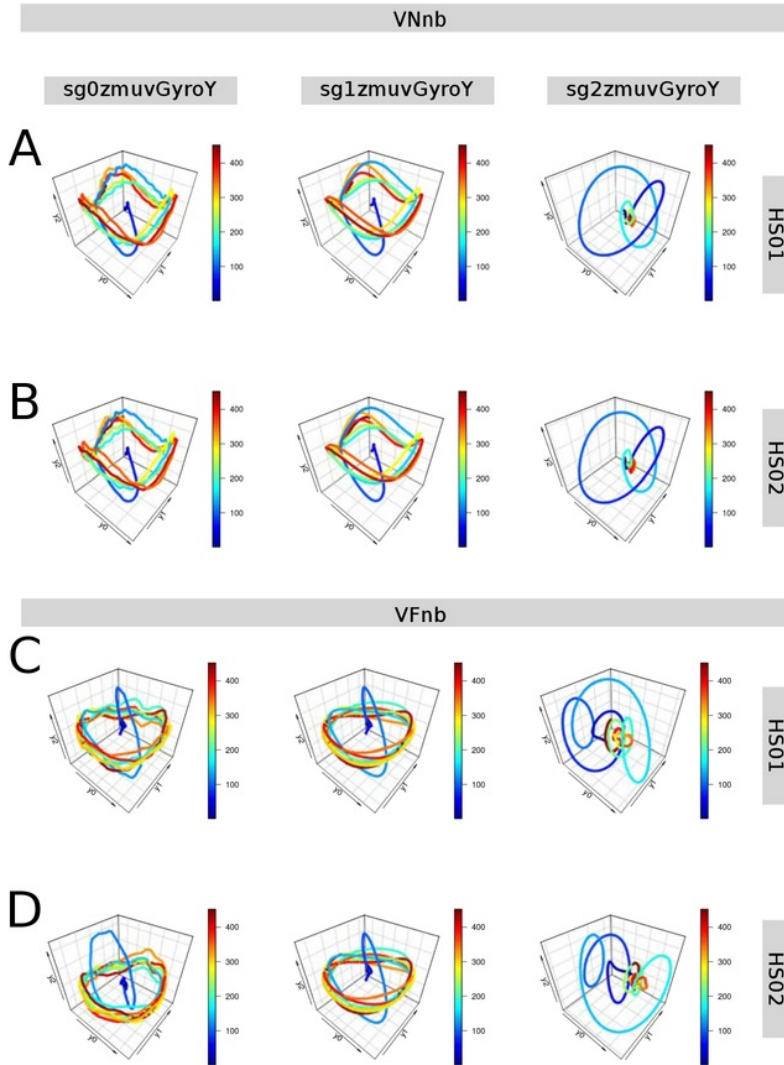


Fig. 5.7 Reconstructed state spaces of participant p01 for (A, B) vertical normal movements with no beat (VNnb) and (C, D) vertical faster velocity with no beat (VFnb). Time series for raw-normalised ($sg0zmuvGyroY$), normalised-smoothed 1 ($sg1zmuvGyroY$) and normalised-smoothed 2 ($sg2zmuvGyroY$) with (A, C) sensor attached to the participant (HS01), and (B, D) sensor attached to the participant (HS02). Reconstructed state spaces were computed with embedding parameters $m = 9$, $\tau = 6$. R code to reproduce the figure is available from Xochicale (2018).

5.4 Reconstructed state spaces with UTDE

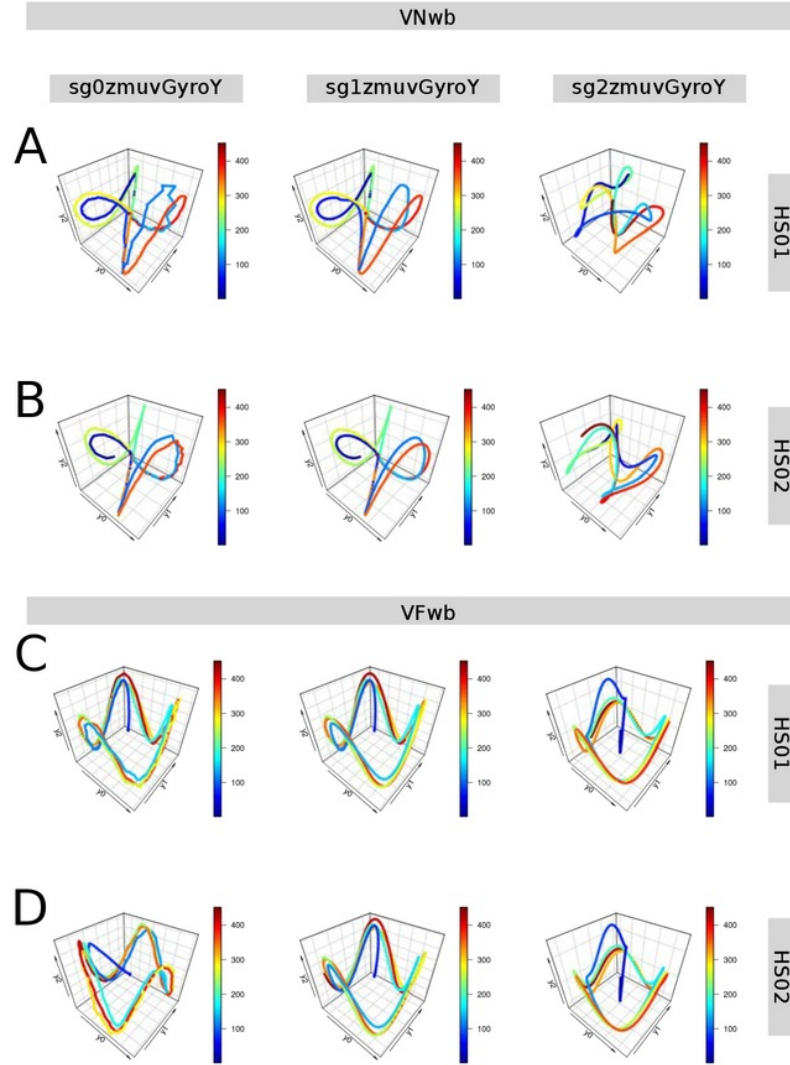


Fig. 5.8 Reconstructed state spaces of participant p01 for (A, B) vertical normal movements with beat (VNwb) and (C, D) vertical faster velocity with beat (VFwb). Time series for raw-normalised ($sg0zmuvGyroY$), normalised-smoothed 1 ($sg1zmuvGyroY$) and normalised-smoothed 2 ($sg2zmuvGyroY$) with (A, C) sensor attached to the participant (HS01), and (B, D) sensor attached to the participant (HS02). Reconstructed state spaces were computed with embedding parameters $m = 9$, $\tau = 6$. R code to reproduce the figure is available from Xochicale (2018).

5.5 Recurrences Plots

In this section it is described the patterns of recurrence plots (RPs), computed with ¹ embedding parameters $m = 9$, $\tau = 6$ and a recurrence threshold $\epsilon = 1$, of participant p01 for horizontal and vertical arm movements in normal and faster velocity with beat and no beat sound (Figs 5.9, 5.10, 5.11 and 5.12).

Figs 5.9 show recurrence plots for horizontal normal and horizontal faster arm movements with no beat sound. For horizontal normal arm movements with no beat, patterns in RPs for sg0zmuvGyroZ and sg1zmuvGyroZ look similar, however patterns in RPs for sg2zmuvGyroZ are different, such behavior of RPs patterns is similar with regards to the smoothness presented in horizontal and faster arm movements with beat (Fig 5.10). With regards to the type of sensor, there is little visual differences in RPs patterns, while patterns of RPs for different activities present diagonal lines that appear to be closer and more dense for horizontal faster arm movement than horizontal normal arm movements (Fig 5.9).

Figs 5.10 show patterns of RPs for horizontal normal and faster arm movements while participants listen to a beat. For these patterns in the RPs, the type activities for normal and faster arm movements can be easily noticed in the patterns, as well as the change of smoothness between sg0zmuvGyroZ and sg1zmuvGyroZ with the patterns for sg2zmuvGyroZ. It can also be noted that there is little visual differences between the RP patterns for sensor HS01 and HS02.

Figs 5.11 show patterns of RPs for vertical normal and faster arm movements while no hearing a beat. One can note the the evidently differences of patterns between the levels of smoothness where, for instance, patterns of RPs from sg0zmuvGyroY and sg1zmuvGyroY looks similar while RPs for sg2zmuvGyroY are completely black. Similarly, one can see little visual changes when comparing RPs patterns between

5.5 Recurrences Plots

sensors HS01 and HS02. However, the RPs patterns create a more dense presence of diagonal lines for faster arm movements than for normal arm movements.

Figs 5.12 show RPs patterns for vertical normal and faster arm movements for participants hearing a beat. Patterns of RP for vertical normal and vertical faster arm movements are visually noticeable as well as RPs patterns for changes in the increase of smoothness between sg0zmuvGyroY and sg1zmuvGyroY and with sg2zmuvGyroY. Once can also note that there is little visual changes of RPs patterns from different sensors.

Quantifying Human-Image Imitation Activities

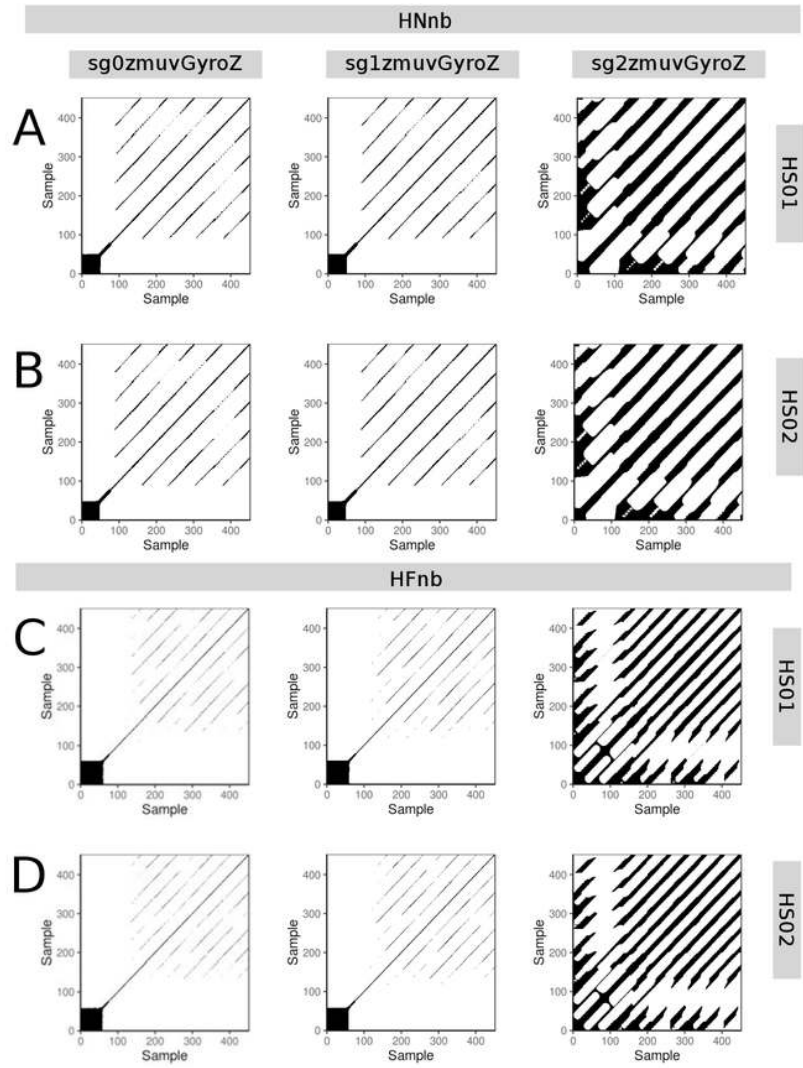


Fig. 5.9 RPs for horizontal arm movements (no beat). Recurrence plots of participant p01 for (A, B) horizontal normal movements with no beat (HNnb) and (C, D) horizontal faster movements with no beat (HFnb). Time series for raw-normalised ($sg0zmuvGyroZ$), normalised-smoothed 1 ($sg1zmuvGyroZ$) and normalised-smoothed 2 ($sg2zmuvGyroZ$) with (A, C) sensor 01 attached to the participant (HS01), and (B, D) sensor 02 attached to the participant (HS02). Recurrence plots were computed with embedding parameters $m = 9$, $\tau = 6$ and recurrence threshold $\epsilon = 1$. R code to reproduce the figure is available from Xochicale (2018).

5.5 Recurrences Plots

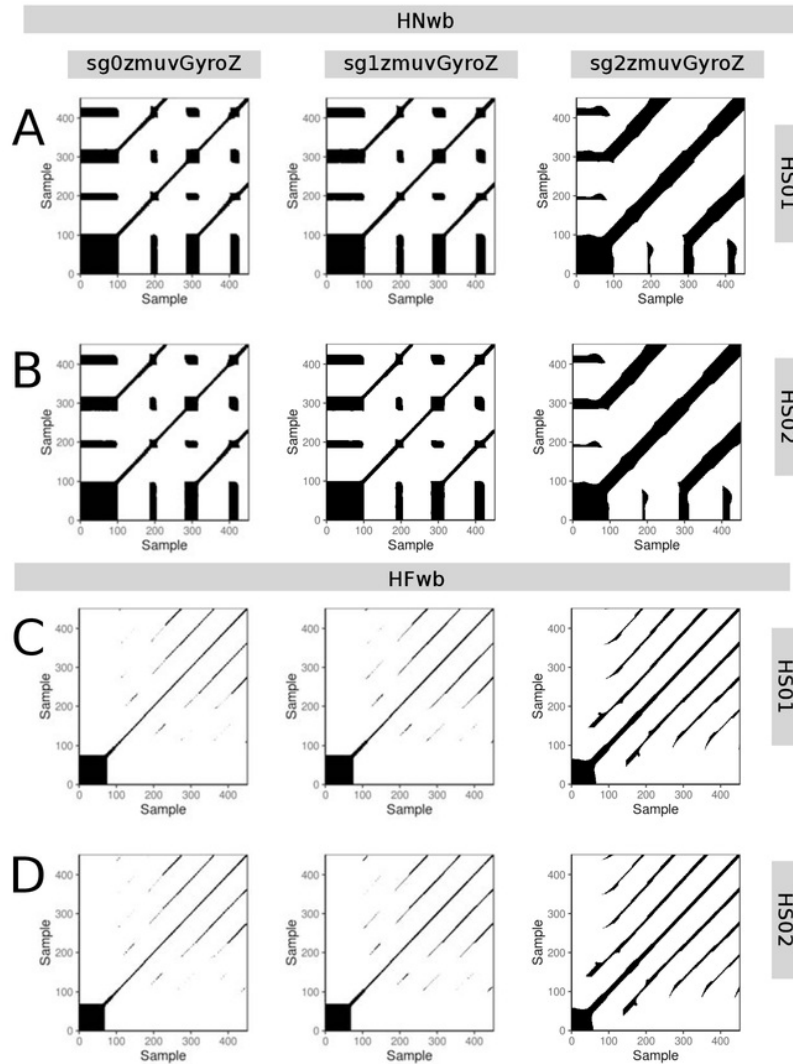


Fig. 5.10 RPs for horizontal arm movements (with beat). Recurrence plots of participant p01 for (A, B) horizontal normal movements with beat (HNwb) and (C, D) horizontal faster movements with beat (HFwb). Time series for raw-normalised ($sg0zmuvGyroZ$), normalised-smoothed 1 ($sg1zmuvGyroZ$) and normalised-smoothed 2 ($sg2zmuvGyroZ$) with (A, C) sensor 01 attached to the participant (HS01), and (B, D) sensor 02 attached to the participant (HS02). Recurrence plots were computed with embedding parameters $m = 9$, $\tau = 6$ and recurrence threshold $\epsilon = 1$. R code to reproduce the figure is available from Xochicale (2018).

Quantifying Human-Image Imitation Activities

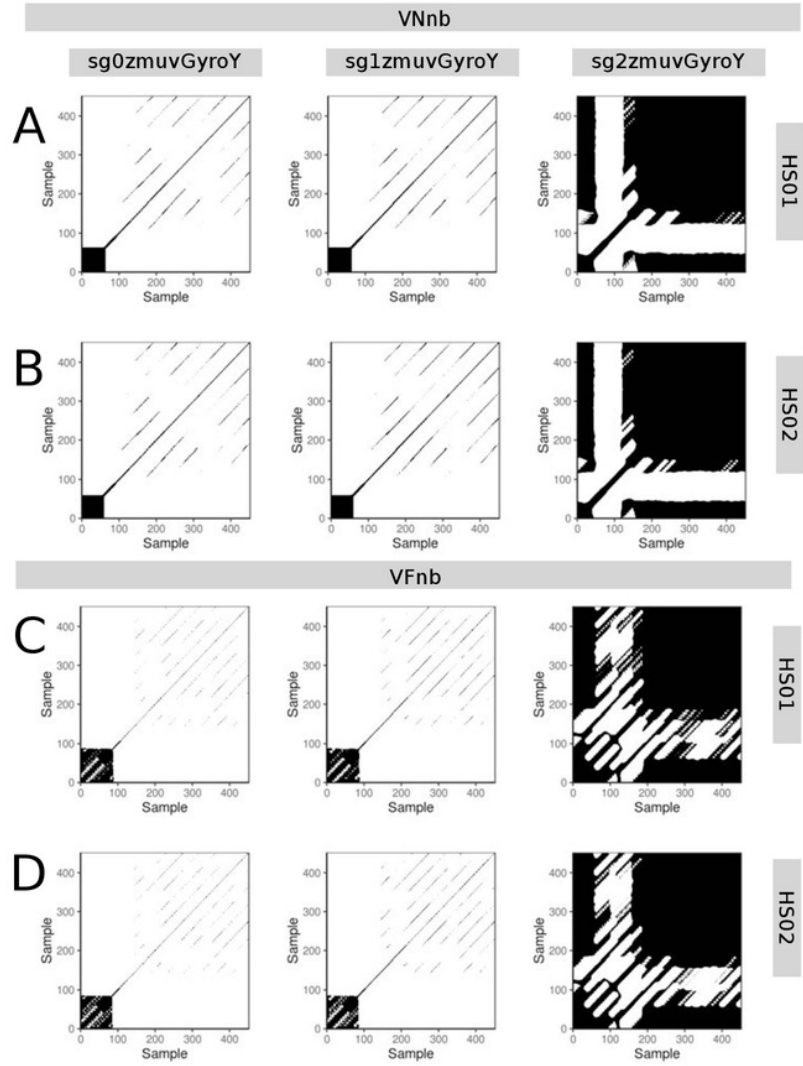


Fig. 5.11 RPs for vertical arm movements (no beat). Recurrence plots of participant p01 for (A, B) vertical normal movements with no beat (VNnb) and (C, D) vertical faster movements with no beat (VFnb). Time series for raw-normalised ($sg0zmuvGyroY$), normalised-smoothed 1 ($sg1zmuvGyroY$) and normalised-smoothed 2 ($sg2zmuvGyroY$) with (A, C) sensor 01 attached to the participant (HS01), and (B, D) sensor 02 attached to the participant (HS02). Recurrence plots were computed with embedding parameters $m = 9$, $\tau = 6$ and recurrence threshold $\epsilon = 1$. R code to reproduce the figure is available from Xochicale (2018).

5.5 Recurrences Plots

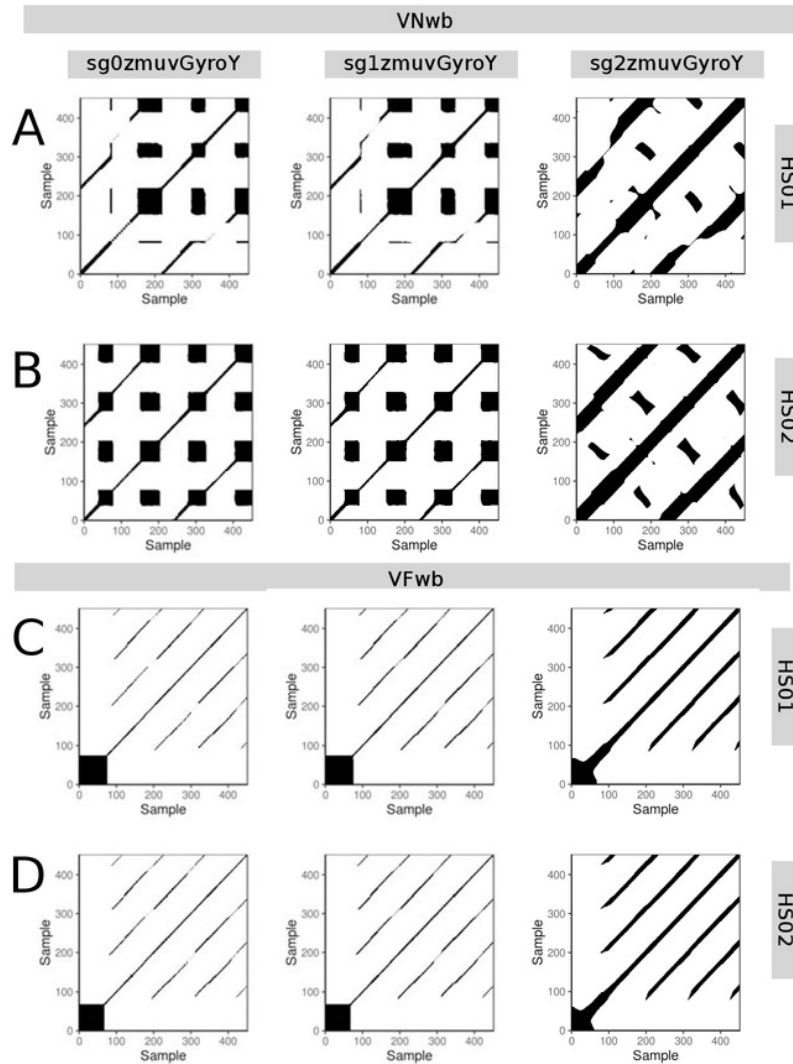


Fig. 5.12 **RPs for vertical arm movements (with beat).** Recurrence plots of participant p01 for (A, B) vertical normal movements with beat (VNwb) and (C, D) vertical faster movements with beat (VFwb). Time series for raw-normalised ($sg0zmuvGyroY$), normalised-smoothed 1 ($sg1zmuvGyroY$) and normalised-smoothed 2 ($sg2zmuvGyroY$) with (A, C) sensor 01 attached to the participant (HS01), and (B, D) sensor 02 attached to the participant (HS02). Recurrence plots were computed with embedding parameters $m = 9$, $\tau = 6$ and recurrence threshold $\epsilon = 1$. R code to reproduce the figure is available from Xochicale (2018).

5.6 Recurrence Quantification Analysis

In this section is shown Recurrence Quantification Analysis (RQA) metrics (REC, DET, RATIO and ENTR) of six participants ($p01, p04, p05, p10, p11, p15$) for horizontal arm movements (HNnb, HNwb, HFnb, HFwb) and vertical arm movements (VNnb, VNwb, VFnb, VFwb) with sensors HS01 and HS02, and three smoothed time series (sg0zmuvGyro, sg1zmuvGyro and sg2zmuvGyro).

REC values

Figs 5.13(A) and 5.14(A) show box plots of REC values, representing % of black dots in the RPs, for horizontal arm movements and vertical arm movements. In figs 5.13(A) can be noted that the interquartile range for sg2 is greater than the sg0 and sg1 for activities HNnb and HFnb, while REC values for activities HNwb and HFwb appear to increase its sample mean (gray rhombus) as the smoothness increase. Similarly, in figs 5.14(A) can be seen that there is a large interquartile range for sg2 in activities with no beat (VNnb, VFnb), while activities with beat (VNwb and VFwb) appear to be increase its sample mean (gray rhombus) as the smoothness of the time series increase. REC values from sensors HS01 and HS02 appear to differ little for both horizontal and vertical arm movements. For further details of individual REC values of participants, see Figs D.27 and D.28 in Section D.5.

DET values

DET values, representing predictability and organisation of the RPs, appear to be constant regardless of the source of time series (Figs 5.13(B) and 5.14(B)). However, it can be noted a slight increase of DET values as the smoothness increase. For further details of individual DET values of participants, see Figs D.29, D.30 in Section D.5.

5.6 Recurrence Quantification Analysis

RATIO values

RATIO values, representing dynamics transitions, for horizontal and vertical arm movements are shown in Figs 5.13(C) and 5.14(C). In Figs 5.13(C), for vertical arm movements, can be noted that HNwb activity present the less interquartile range while other seem to have similar interquartile range. Also, the increase of smoothness makes RATIO values to decrease (see gray rhombus). Similarly, in Figs 5.14(C), for vertical arm movements, is shown that VNwb has the less interquartile range as well as sg2 for VFnb and VFwb activities. The increase of smoothness of time series affect in way that sample mean values of RATIO values (gray rhombus) decrease. For further details of individual DET values of participants, see Figs D.31, D.32 in Section D.5.

ENTR values

Figs 5.13(D) and 5.14(D) show ENTR values, representing the complexity of the structure of time series, for horizontal and vertical arm movements. Generally, figs 5.13(D) and 5.14(D) illustrate that the increase of smoothness affects the increase of sample mean (gray rhombus) of ENTR values in each of the activities and sensors. For both vertical and horizontal ENTR values for Nwb seems to be a bit higher than Nnb, while Fnb and Fwb appear to be have similar values. Also, there is little changes between HS01 and HS02 sensors. For further details of individual ENTR values of participants, see Figs D.33, D.34 in Section D.5.

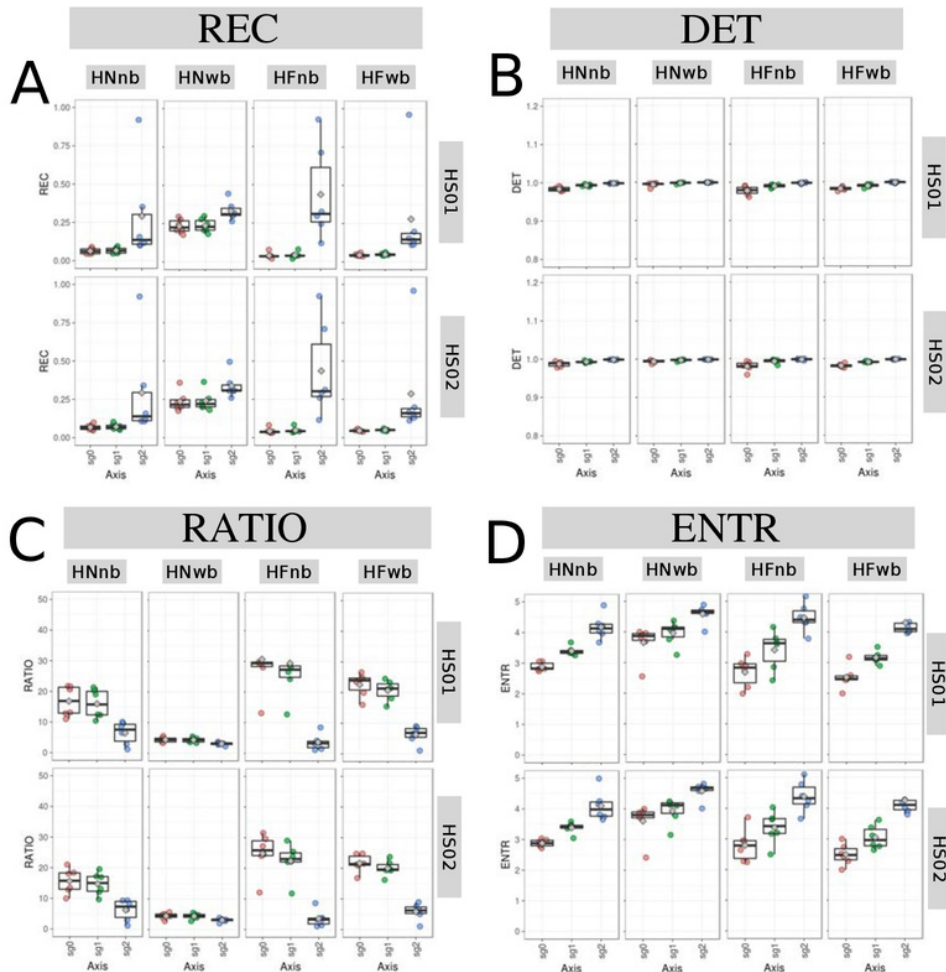


Fig. 5.13 Box plots of RQA values for horizontal arm movements. Box plots of (A) REC, (B) DET, (C) RATIO, and (D) ENTR values for 6 participants performing HNnb, HNwb, HFnb and HFwb movements with sensors HS01, HS02 and three nooothed-normalised time series (sg0, sg1 and sg2). RQA values were computed with embedding parameters $m = 9$, $\tau = 6$ and recurrence threshold $\epsilon = 1$. R code to reproduce the figure is available from Xochicale (2018).

5.6 Recurrence Quantification Analysis

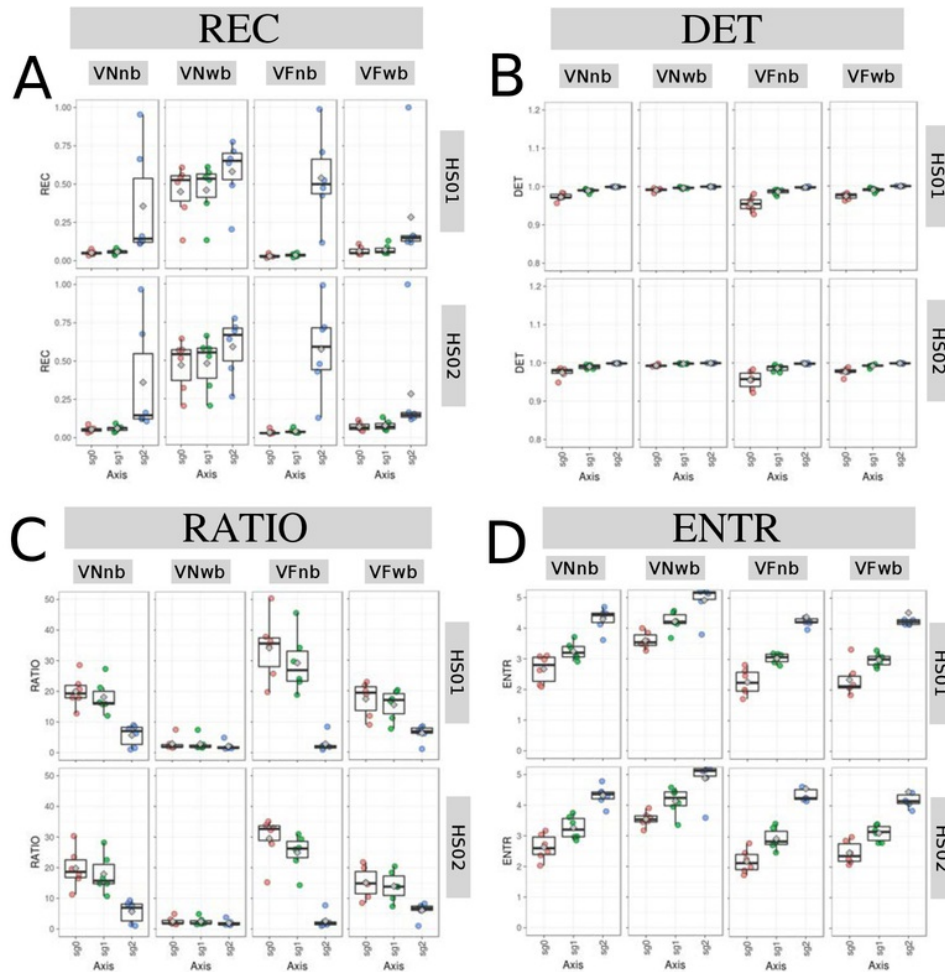


Fig. 5.14 Box plots for RQA values for vertical arm movements. Box plots of (A) REC, (B) DET, (C) RATIO, and (D) ENTR values for 6 participants performing VNnb, VNwb, VFnb and VFwb movements with sensors HS01, HS02 and three smoothed-normalised time series (sg0, sg1 and sg2). RQA values were computed with embedding parameters $m = 9$, $\tau = 6$ and recurrence threshold $\epsilon = 1$. R code to reproduce the figure is available from Xochicale (2018).

5.7 Weaknesses and strengths of RQA

Surfaces for RQA metrics (REC, DET, RATIO, ENTR) are computed with the variation of embedding values by an increase of one ($0 \leq m \leq 10$, $0 \leq \tau \leq 10$) and recurrence thresholds by an increase of 0.1 ($0.2 \leq \epsilon \leq 3$). Hence, we show different characteristics of 3D surfaces of RQA considering different activities, sensors, window size lengths and level of smoothness and participants.

Figs 5.15 show the surfaces for RQA metrics (REC, DET, RATIO, ENTR) using time series of participant *p01*, sensor HS01, activity HNnb, sg0zmuvGyroZ axis and a 500 window size length. The 3D surface for REC values, representing the % of recurrence dots in the RP, show highest values of REC when embedding values are near to 1 and the recurrence threshold is at the maximum ($\epsilon = 3$ for this surfaces). Similarly, it can be seen a decrease of REC values as the embedding dimension and embedding delay values increase, however there is an increase of REC values as the recurrence threshold is increasing (Fig 5.15(A)). Regarding the 3D surface for DET values, representing predictability and organisation of the RPs, Fig 5.15(B) show slightly uniform values when varying both embedding parameters and recurrence threshold with the exception of embedding parameters near to 1 and recurrence thresholds near to 0.2 where the DET values are smaller. 3D surface for RATIO values, representing dynamic transitions, show a plateau with low values recurrence threshold values greater than 1.0. However, there is a fluctuated increase of RATIO values as the embedding values increase given that the recurrence threshold is lower than 1 (Fig 5.15(C)). For ENTR values, representing the complexity of the structure of the time series, Fig 5.15(D) show a maximum value of ENTR when embedding parameters are near to 1 and recurrence threshold values are near to 3.0. It can also be noted fluctuations in the 3D surface when ENTR values are greater than 2.5 (red surface) for embedding dimensions between 3 to 9 and a decrease of ENTR values per each embedding dimension for

5.7 Weaknesses and strengths of RQA

delay embedding values (yellow surface). Additionally, ENTR values decrease as the embedding dimension and delay embedding decrease.

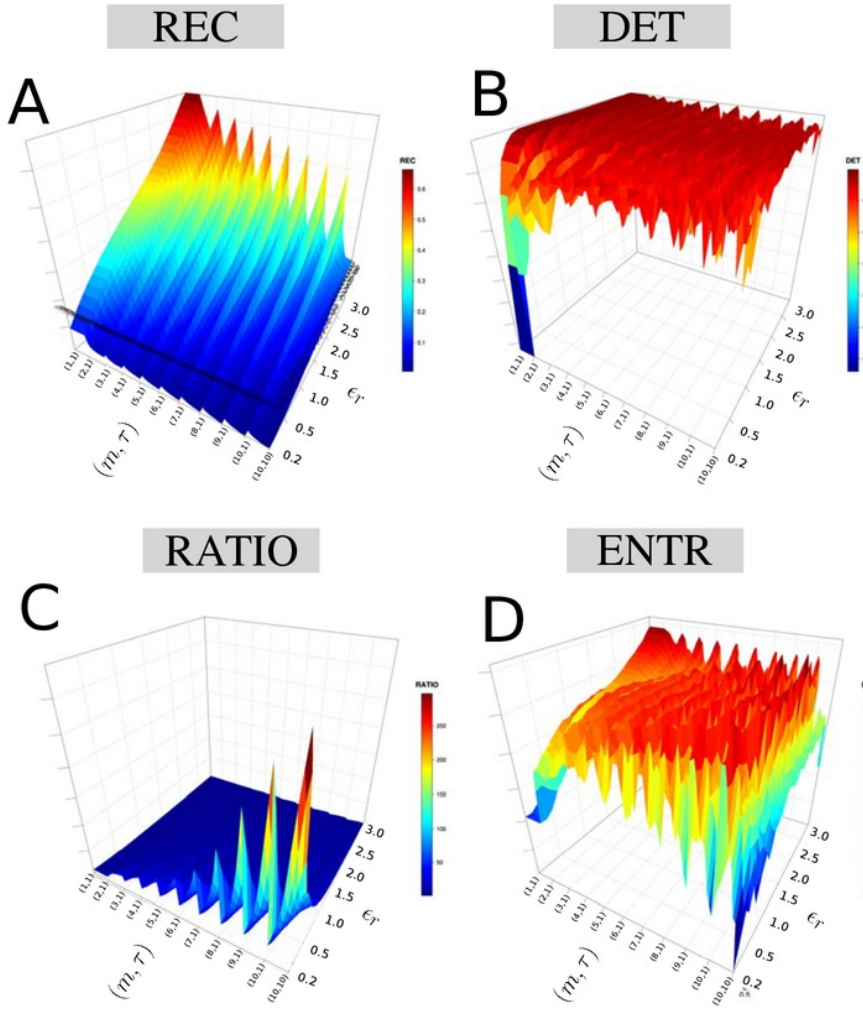


Fig. 5.15 **3D surfaces of RQA metrics.** 3D surfaces for RQA values (A) REC, (B) DET, (C) RATIO and (D) ENTR with an increasing pair of embedding parameters ($0 \leq m \leq 10$, $0 \geq \tau \leq 10$) and recurrence thresholds ($0.2 \geq \epsilon \leq 3$). RQA metrics are computed with the time series of participant p01 using HS01 sensor, HNb activity, sg0zmuvGyroZ axis and 500 samples for window size length. R code to reproduce the figure is available from Xochicale (2018).

4

5.7.1 Sensors and activities

Figs 5.16 and 5.17 show 3D surfaces of RQA metrics (REC, DET, RATIO, ENTR) for horizontal arm movements (HNnb, HNwb, HFnb, HFwb) using sensor HS01 and HS02 for participant *p01* with sg0zmuvGyroZ axis and 500 window size lenght. Hence, Figs 5.16 present 3D surfaces of RQA metrics for HS01, where 3D surfaces for REC values (Fig 5.16(A)) appear to be similar across the activities (HNnb, HFnb, HFwb) with the exception of HNwb which decrease of REC values is mainly affected by the increase of recurrence threshold and slightly affected to the increase of embedding dimension parameters. For DET values, 3D surfaces in Figs 5.16(B) appear to show values near to 1.0 (red colour surface), however HNwb shown fluctuations of DET values as the embedding dimension increase, it can also be noted a decrease of DET values for certain values of recurrence threshold (2.6 for HNwb, 0.3 for HFnb, and 0.3 for HFwb). For Fig 5.16(C)), 3D surfaces for RATIO values appear to be similar, showing a plateau for values between 0 to 50 (blue surface) and the increase of peaks is different for each of the activities. For Fig 5.16(D), ENTR values present different surface formations, for instance, HNnb show fluctuated higher values of ENTR (red colour surface), whereas for activity HNwb the ENTR values are higher (red colour surface) for recurrence threshold near to 3.0, ENTR values for HFnb appear to be higher when embedding dimension is near to 10, while higher values for ENTR values for HFwb appear to be when the recurrence threshold is near to 0.2.

Then, looking and comparing visually one by one of the surfaces for sensors HS01 and HS02 in Figs 5.16 and 5.17, one can notice little differences in the shape of the surfaces. Similarly, there is little variations in the surfaces for vertical arm movements with the sensors HS01 and HS02 (Figs 5.18 and 5.19).

With regards to horizontal and vertical movements, 3D surfaces appear to be similar for REC, DET and RATIO values with sensor HS01 (Figs 5.16 and 5.18) and sensor

5.7 Weaknesses and strengths of RQA

HS02 (Figs 5.17 and 5.19), however 3D surfaces for ENTR values in each of the arm movements presents distinguishable variations in the surfaces, see Figs 5.16(D) and 5.18(D) for horizontal and vertical arm movements with sensor HS01 and Figs 5.17(D) and 5.19(D) for horizontal and vertical arm movements with sensor HS02.

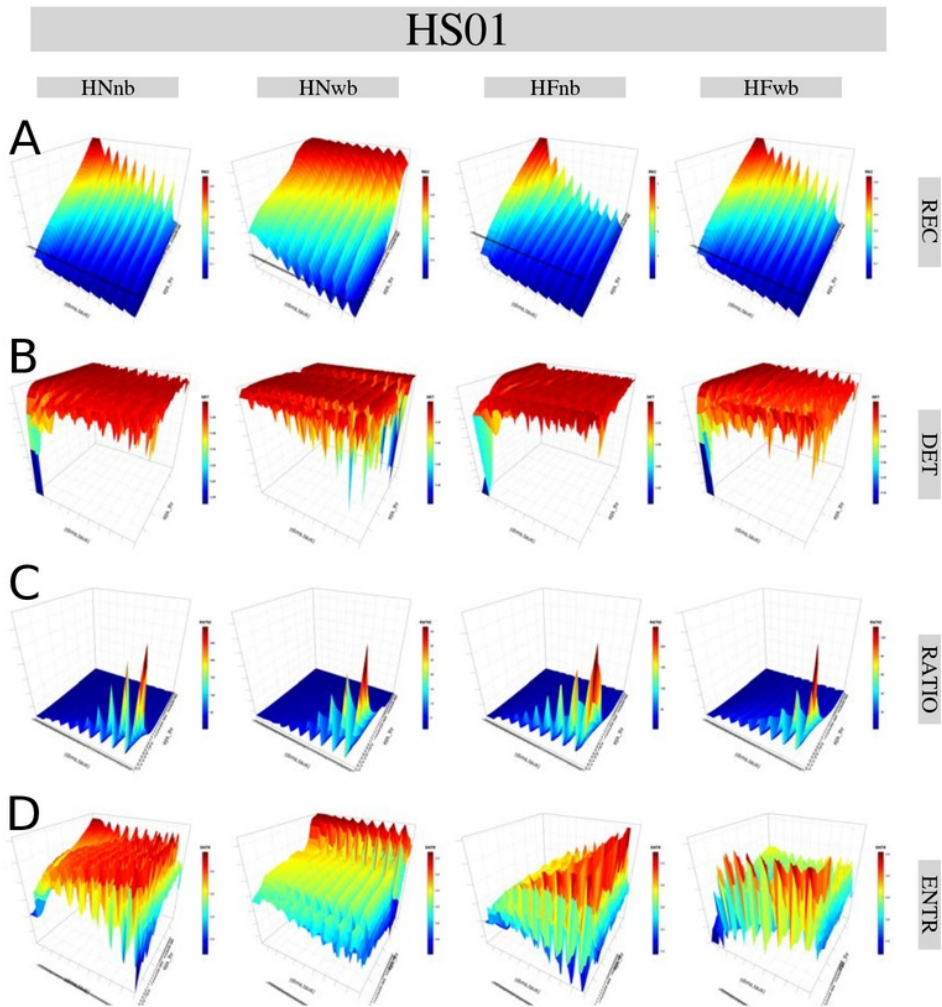


Fig. 5.16 3D surfaces of RQA metrics for horizontal arm movements with HS01. 3D surfaces for (A) REC, (B) DET, (C) RATIO and (D) ENTR values with increasing pair of embedding parameters ($0 \leq m \leq 10$, $0 \geq \tau \leq 10$) and recurrence thresholds ($0.2 \geq \epsilon \leq 3$). RQA metrics are computed with the time series of participant p01 for sensors HS01, horizontal arm movement activities (HNnb, HNwb, HFnb, HFwb) and sg0zmuvGyroZ axis with 500 samples window size length. R code to reproduce the figure is available from Xochicale (2018).

5.7 Weaknesses and strengths of RQA

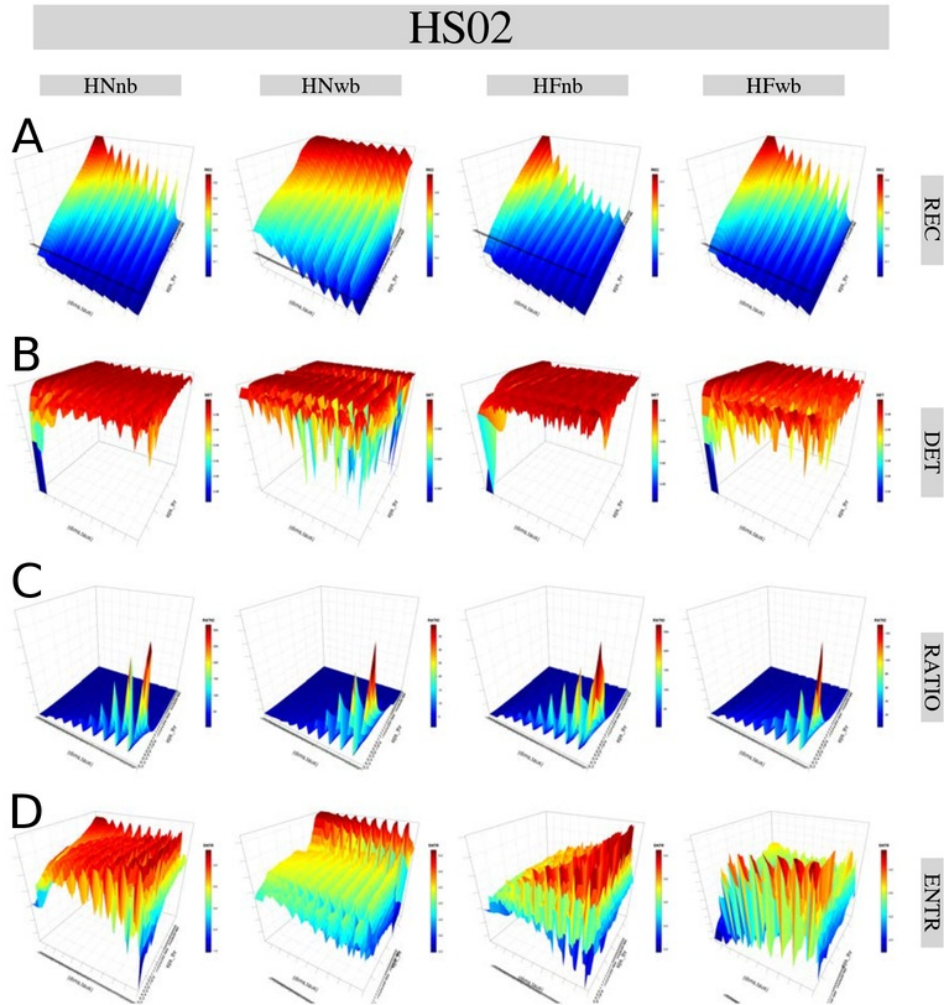


Fig. 5.17 3D surfaces of RQA metrics for horizontal arm movements with **HS02**. 3D surfaces for (A) REC, (B) DET, (C) RATIO and (D) ENTR values with increasing pair of embedding parameters ($0 \geq m \leq 10$, $0 \geq \tau \leq 10$) and recurrence thresholds ($0.2 \geq \epsilon \leq 3$). RQA metrics are computed with the time series of participant p01 for sensors HS02, horizontal arm movement activities (HNnb, HNwb, HFnb, HFwb) and sg0zmuvGyroZ axis with 500 samples window size length. R code to reproduce the figure is available from Xochicale (2018).

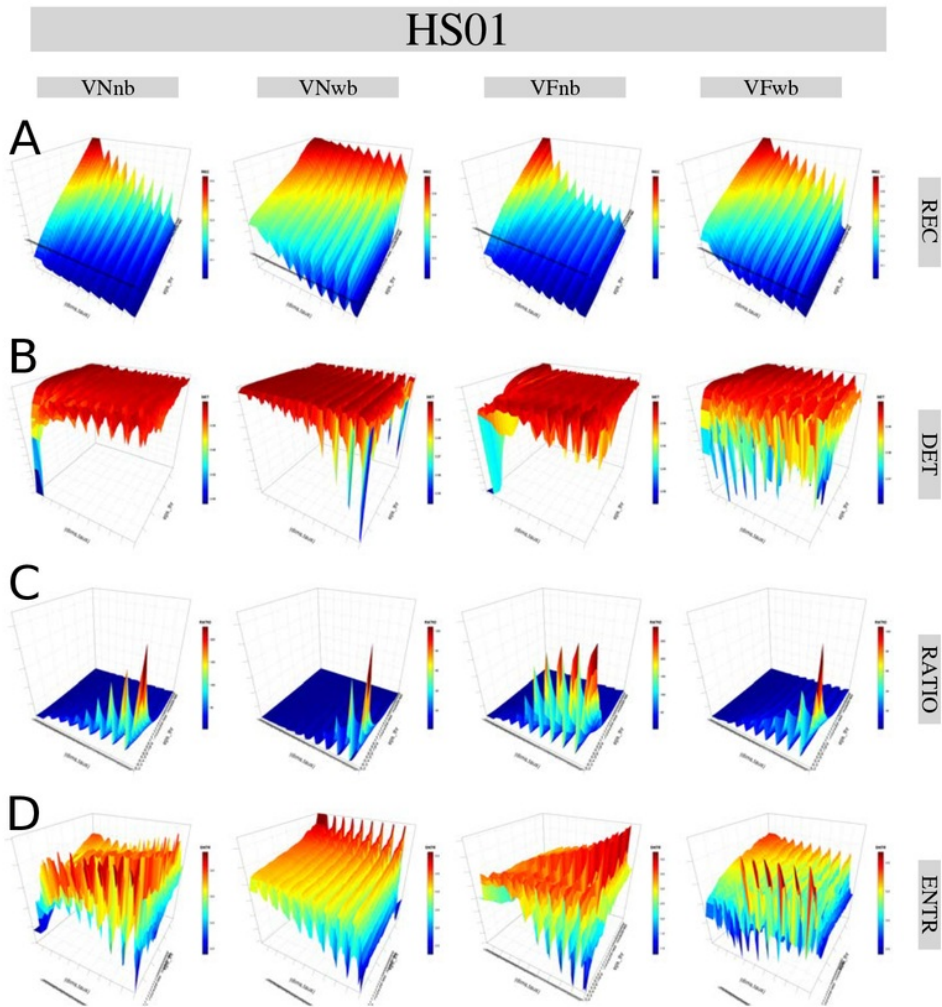


Fig. 5.18 3D surfaces of RQA metrics for vertical arm movements with HS01. 3D surfaces for (A) REC, (B) DET, (C) RATIO and (D) ENTR values with increasing pair of embedding parameters ($0 \geq m \leq 10$, $0 \geq \tau \leq 10$) and recurrence thresholds ($0.2 \geq \epsilon \leq 3$). RQA metrics are computed with the time series of participant p01 for sensors HS01, vertical arm movements activities (VNnb, VNwb, VFnb, VFwb) and sg0zmuvGyroY axis with 500 samples window size length. R code to reproduce the figure is available from Xochicale (2018).

5.7 Weaknesses and strengths of RQA

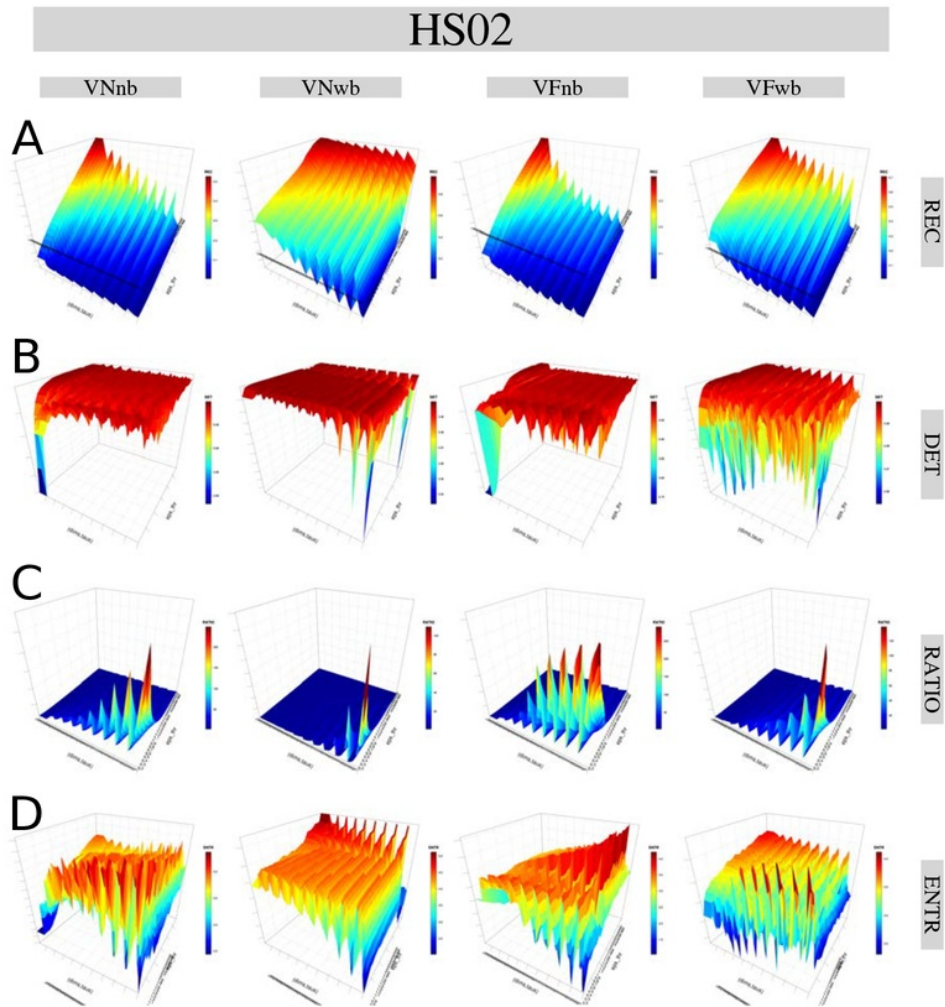


Fig. 5.19 3D surfaces of RQA metrics for vertical arm movements with HS02.
 3D surfaces for (A) REC, (B) DET, (C) RATIO and (D) ENTR values with increasing pair of embedding parameters ($0 \geq m \leq 10$, $0 \geq \tau \leq 10$) and recurrence thresholds ($0.2 \geq \epsilon \leq 3$). RQA metrics are computed with the time series of participant p01 for sensors HS02, vertical arm movements activities (VNnb, VNwb, VFnb, VFwb) and sg0zmuvGyroY axis with 500 samples window size length. R code to reproduce the figure is available from Xochicale (2018).

5.7.2 Window size

3D surfaces of REC values with a short window length (100 samples) can affect the shape of 3D surface, however for window size of 250, 500, and 700 samples, the 3D surfaces appear to show little changes (Figs 5.20(A)). For instance, one can see 3D surfaces of DET values with a window of 100 size length is slightly different to other surfaces but keeping the plateau (red surface) in each of the surfaces (Figs 5.20(B)). Similarly, the 3D surfaces of RATIO values preserve the same plateau (blue surface) with little variations in the surfaces as window size length increase (Figs 5.20(C)). 3D surfaces for ENTR values appear to have similar aspects as the fluctuations of the curves keeps the same values (red and yellow colours). It can also be noted that the smoothness of 3D surfaces decrease as the embedding dimension parameters increase and such smoothness is also affected by the window length (see Figs 5.20(D)).

5.7.3 Smoothness

Figs 5.21 show the effects of three levels of smoothness (sg0zmuvGyroZ, sg1zmuvGyroZ and sg2zmuvGyroZ) in the RQA metrics. Generally, 3D surfaces from sg2zmuvGyroZ are affected by the smoothness. It can also be noted that REC values and ENTR values present a slightly different surfaces (see Figs 5.21(A, D)), while DET and RATIO values appear to be similar which is mainly reflected in the colour of the curves (see Figs 5.21(B, C)). In Figs 5.21(A), 3D surfaces for REC values tend be smoothed as the ²⁶³ smoothness of the time series increase to the point where the increase of recurrence threshold affects the shape of the surfaces. Similarly, in Figs 5.21(C), 3D surface for ENTR values is ¹⁶⁴ affected by the smoothness of the time series to the point that the fluctuations in the surface does change drastically the shape by showing only an increase of ENTR values as the recurrence threshold increase.

5.7 Weaknesses and strengths of RQA

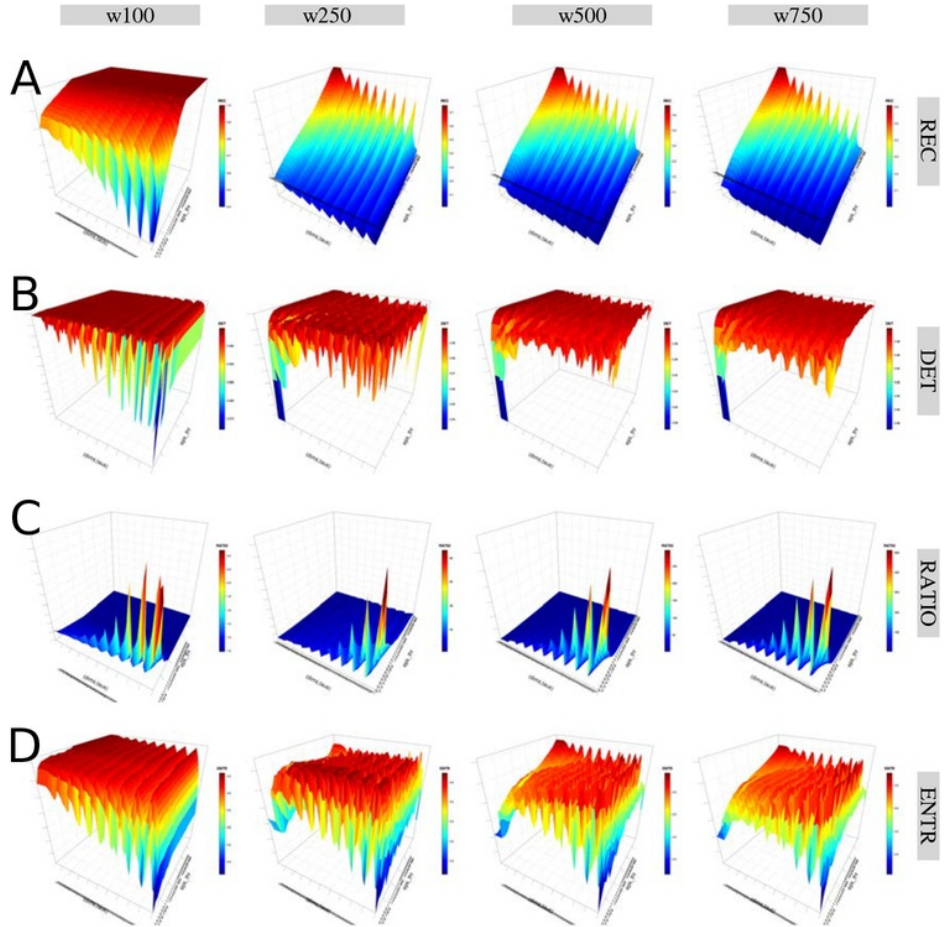


Fig. 5.20 3D surfaces of RQA metrics for different window size lengths. 3D surfaces of RQA metrics ((A) REC, (B) DET, (C) RATIO, and (D) ENTR) with increasing embedding parameters and recurrence thresholds for four window lengths (w100, w250, w500 and w750). RQA metrics values are for time series of participant p01 using HS01 sensor, HNb activity and sg0zmuvGyroZ axis. R code to reproduce the figure is available from Xochicale (2018).

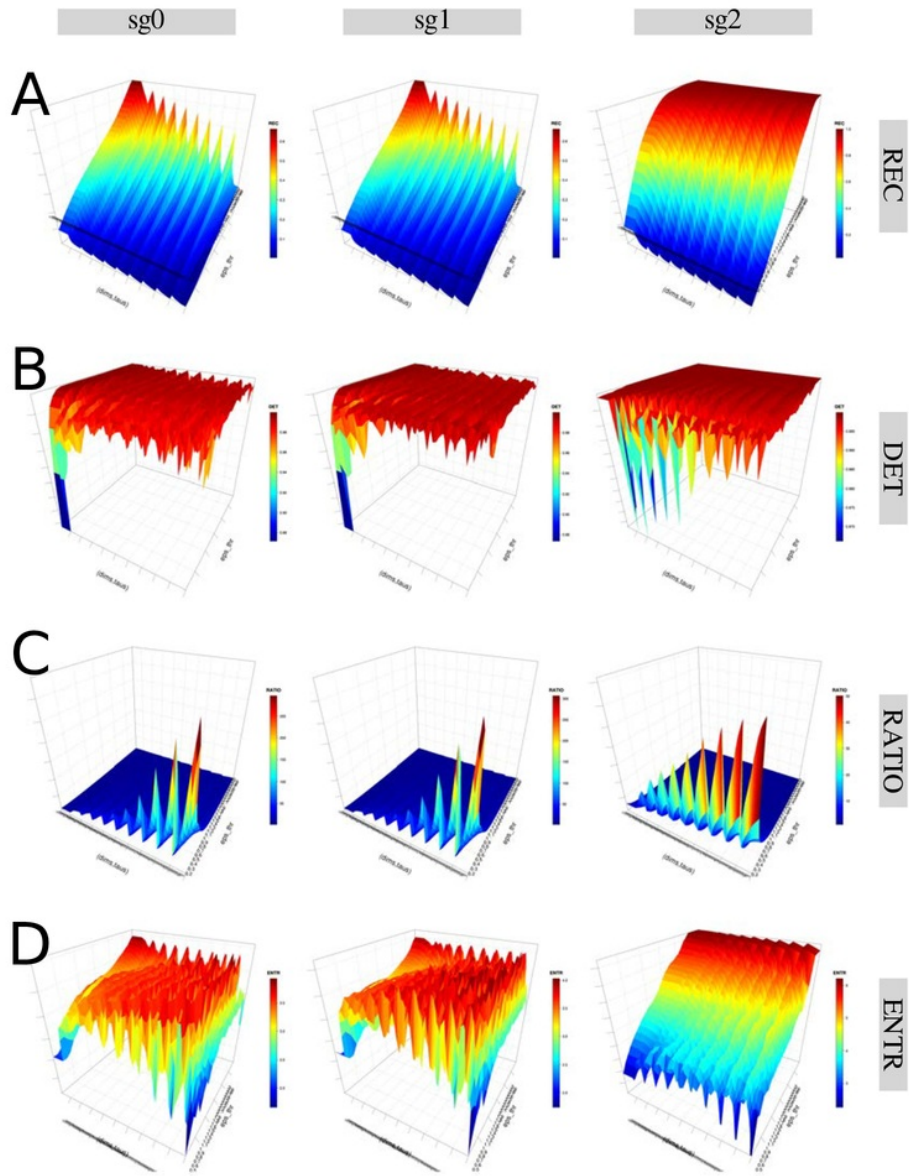


Fig. 5.21 3D surfaces of RQA metrics with three levels of smoothness. 3D surfaces of RQA metrics ((A) REC, (B) DET, (C) RATIO, and (D) ENTR) with increasing embedding parameters and recurrence thresholds for three levels of smoothness (sg0zmuvGyroZ, sg1zmuvGyroZ, and sg2zmuvGyroZ). RQA metrics are computed from time series of participant p01 using HS01 sensor, HNb activity and 500 samples window length. R code to reproduce the figure is available from Kochicale (2018).

5.7.4 Participants

The shape of 3D surfaces of RQA metrics is also affected when using time series from different participants (Figs 5.22). For instance, 3D surface of DET values show slightly but noticeable differences in the fluctuations when embedding dimension and recurrence threshold increase (Figs 5.22(B)) which is similar for ENTR values where the fluctuations of the 3D surfaces changes for each of the participants (Figs 5.22(D)). However, the shape of 3D surfaces for RET values and RATIO values is little affected with the change of participants (Figs 5.22(A, C)).

5.7.5 Final remarks

Having different sources of time series (participants, sensors, activities, window size length or level of smoothness) produces different results in nonlinear analyses tools (FNN, AMI, RSSs with UTDE, RPs and RQAs) and these results can also be sensitive to perform nonlinear analyses with different parameters (minimum dimension threshold, embedding parameters or recurrence thresholds). Hence, we created 3D surfaces of RQA metrics with the variation of embedding parameters and recurrence thresholds, such surfaces appear to be helpful to understand the dynamics of any kind of time series with little parametrization of nonlinear tools. For instance, 3D surfaces of ENTR values, with only the selection of variation of range of parameters, show clearly differences in the shape of 3D surfaces regardless of the source of the time series. Hence making 3D surfaces of ENTR values a robust metric which helps us to understand the dynamics of human movement variability from different time series data.

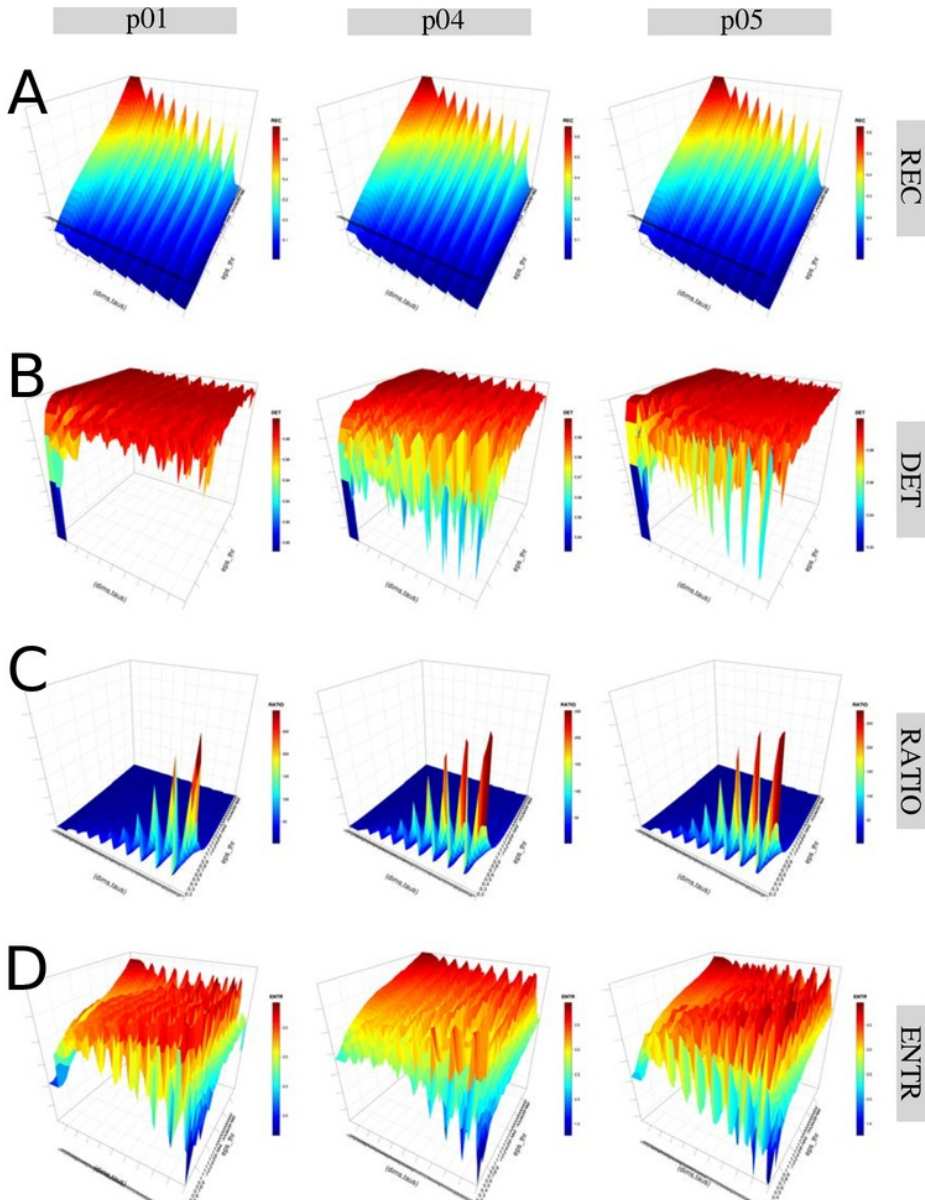


Fig. 5.22 3D surfaces of RQA metrics with three participants. 3D surfaces of RQA metrics ((A) REC, (B) DET, (C) RATIO, and (D) ENTR) for participants $p01$, $p04$ and $p05$ with increasing embedding parameters and recurrence thresholds. RQA metrics values are for time series of HS01 sensor, HNb activity and 500 samples window length. R code to reproduce the figure is available from Xochicale (2018).

Chapter 6

Quantifying Human-Humanoid Imitation Activities

6.1 Introduction

Considering the experiment of Human-Humanoid Imitation Activities (Section 4.5.2), we investigated the robustness and weaknesses of the reconstructed state spaces (RSSs) using the uniform time-delay embedding technique (UTDE) and ²⁰ recurrence plots (RPs) for recurrent quantification analysis (RQA) methodologies for the following conditions of time series data:

- Three levels of smoothness for the normalised data (`sg0zmuv`, `sg1zmuv` and `sg2zmuv`), computed from two different filter lengths (29 and 159) with the same polynomial degree of 5 using the function `sgolay(p,n,m)` (signal R developers, 2014),
- Four velocities of arm movement activity: horizontal normal (HN), horizontal faster (HF), vertical normal (VN) and vertical faster (VF), and

Quantifying Human-Humanoid Imitation Activities

- Four window length size: 2-sec (100 samples), 5-sec (250 samples), 10-sec (500 samples) and 15-sec (750 samples).

Further details about the processing of time series are presented in Section 4.6.

6.2 Time series

To make visual comparison easier, we only present a 10-sec (500 samples) window length time series for three participants ($p01$, $p02$ and $p03$) performing horizontal arm movements using axis GyroZ (Figs. 6.1) and vertical arm movements using axis GyroY (Figs. 6.2). Other data are presented in Appendix D. We consider different levels of smoothness of the normalised data with two different Savitzky-Golay filter lengths (29 and 159) with the same polynomial degree of 5 using `sgolay(p,n,m)` (signal R developers, 2014).

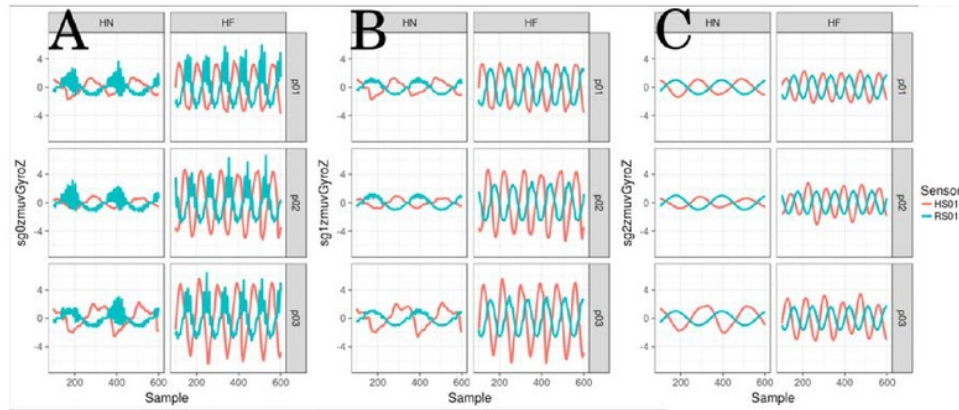


Fig. 6.1 Time series for horizontal arm movements. (A) raw-normalised ($sg0zmuvGyroZ$), (B) normalised-smoothed 1 ($sg1zmuvGyroZ$) and (C) normalised-smoothed 2 ($sg2zmuvGyroZ$). Time series are only for three participants ($p01$, $p02$, and $p03$) for horizontal movements in normal and faster velocity (HN, HF) with the normalised GyroZ axis ($zmuvGyroZ$) and with one sensor attached to the participant (HS01) and other sensor attached to the robot (RS01). R code to reproduce the figure is available from Kochicale (2018).

6.3 Minimum Embedding Parameters

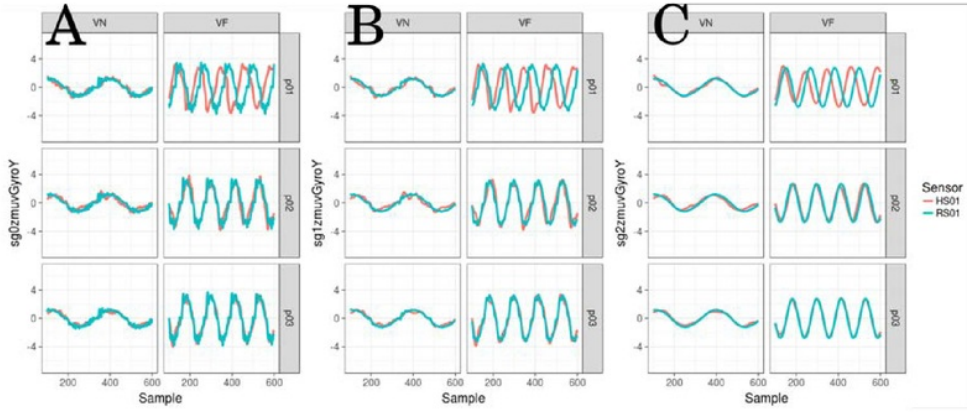


Fig. 6.2 Time series for vertical arm movements. (A) raw-normalised ($sg0zmuvGyroY$), (B) normalised-smoothed 1 ($sg1zmuvGyroY$) and (C) normalised-smoothed 2 ($sg2zmuvGyroY$). Time series are only for three participants ($p01$, $p02$, and $p03$) for vertical movements in normal and faster velocity (VN, VF) with the normalised GyroY axis ($zmuvGyroY$) and with one sensor attached to the participant (HS01) and other sensor attached to the robot (RS01). R code to reproduce the figure is available from Xochicale (2018).

6.3 Minimum Embedding Parameters

As mentioned in Section 5.3 in Chapter 5, we computed minimum embedding parameters using FNN and AMI algorithms for time series of this section.

Hence, Figs 6.3(A) show box plots of the minimum embedding dimensions of twenty participants performing horizontal and vertical arm movements at normal and faster velocities (HN, HF, VN and VF) with attached sensors to participants (HS01) and to the robot (RS01). Generally, Figs 6.3(A) show that minimum embedding values appear to be constant for sensor RS01 as their interquartile range in the box plots are near to 0.1 with the exception of two axis. Minimum embedding values for sensor HS01 appear to show more variations as their interquartile range of the box plots are near to 1 with four exceptions. Additionally, it can be seen in Figs 6.3(A) that there is a decrease of mean values (rhombus) in the box plots as smoothness of time series increase. See

Quantifying Human-Humanoid Imitation Activities

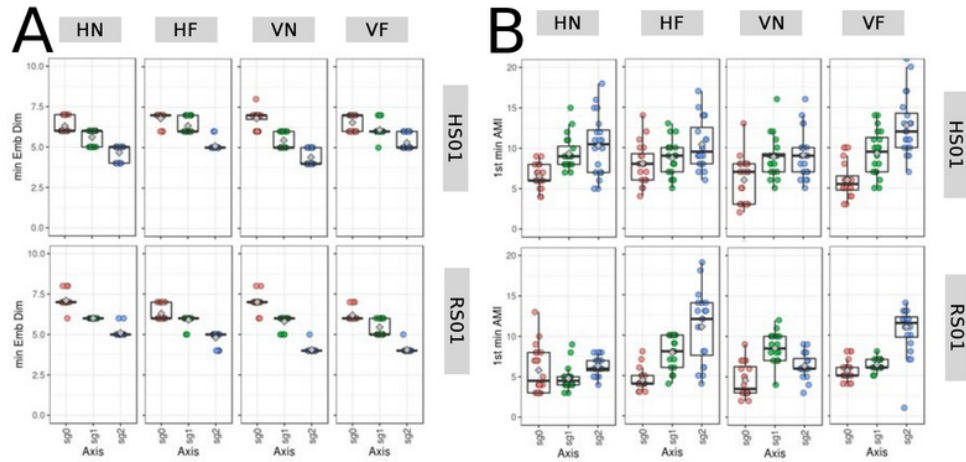


Fig. 6.3 Box plots of minimum embedding parameters. Box plots of (A) minimum embedding dimensions and (B) first minimum AMI values for Horizontal Normal (HN), Horizontal Faster (HF), Vertical Normal (VN) and Vertical Faster (VF) with sensors attached to participants (HS01) and sensor attached to robot (RS01). Minimum embedding dimensions are for twenty participants (p_{01} to p_{20}) with three smoothed signals ($sg_0zmuvGyroZ$ (sg_0), $sg_1zmuvGyroZ$ (sg_1) and $sg_2zmuvGyroZ$ (sg_2)) and window length of 10-sec (500 samples). R code to reproduce the figure is available from Xochicale (2018).

Figs. E.7 and E.8 in appendix E.2 for detailed values of embedding dimensions for each participant.

Similarly, the first minimum values of AMI values for participants (p_{01} to p_{20}), activities (HN, HF, VN, and VF) and sensors (HS01, RS01) are shown in the box plots of Figs 6.3(B). It can be seen that values for HS01 tend to be more spread as the smoothness of the time series is increasing (see the increase of both mean (rhombus) and interquartile range). However, AMI values for RS01 do not show such increase in relation with the increase of smoothness excepting for HF and VF (see the increase of both mean (rhombus) and interquartile range) (Figs 6.3(B)). See Figs. E.9 and E.10 in appendix E.2 for more details about AMI values for each participant.

214

6.4 Reconstructed state spaces with UTDE

6.3.1 Average minimum embedding parameters

Following the Section 3.4.3 to compute the overall average of minimum embedding parameters, the sample mean for the minimum values of $E_1(m)$ from Figs 6.3(A) is $\bar{m}_0 = 6$ and the sample mean for minimum values of AMIs from Figs 6.3(B) is $\bar{\tau}_0 = 8$, for which the overall average minimum embedding parameters is ($\bar{m}_0 = 6$, $\bar{\tau}_0 = 8$). Hence, we use the average minimum embedding parameters ($\bar{m}_0 = 6$, $\bar{\tau}_0 = 8$) to compute Reconstructed State Spaces (RSSs), ²⁰ Recurrence Plots (RPs) and Recurrence Quantification Analysis (RQA) metrics for human-humanoid activities.

6.4 Reconstructed state spaces with UTDE

Considering Section 3.5 and time series for participant *p01* (Figs 6.1, 6.2) the reconstructed state spaces for horizontal arm movements (Figs 6.4) and vertical arm movements (Figs 6.5) are computed with $\bar{m}_0 = 6$ and $\bar{\tau}_0 = 8$

The trajectories of the RSSs for horizontal normal and faster from HS01 and RS01 are slightly smoothed as the time-series smoothness increase (Figs 6.4). Although the frequency of the movement increase from normal to faster velocity activities, the trajectories RSSs in Figs 6.4(B) show higher oscillations specially for a maximum values of smoothness (sg2zmuvGyroZ), while the trajectories in the RSS for HF in Figs 6.4(D) show a lower and smoothed oscillations as the smoothness increase. In contrast, the time series for vertical movements are less noisy and well structured (Figs 6.2) for which the trajectories in the RSSs seem to be less organised, specially for Fig 6.5(A,C), while time series for vertical faster movements (VF) which have more periods (Figs 6.2) present trajectories in the RSS with well defined patterns (6.5(C,D)).

⁴³ It is important to note that the smoothness of time series also create an effect on

Quantifying Human-Humanoid Imitation Activities

smoothness in the trajectories of the RSS, being the RS01 more organised and more persistent while trajectories for HS01 are more changeable (Figs. 6.4, 6.5).

Therefore, one can observe by eye the differences in each of the trajectories in the reconstructed state spaces (Figs 6.4, 6.5), however one might be not objective when quantifying those differences since such observations might vary from person to person. With that in mind, in our early experiments, we tried to objectively quantify those differences using euclidean distances between the origin to each of the points in the trajectories in the trajectories of the RSSs, however these created suspicious metrics, specially for trajectories which looked very messy. Hence, we proposed to apply Recurrence Quantification Analyses (RQA) in order to have a more objective quantification of the differences in each of the cases of the time series.

262

6.4 Reconstructed state spaces with UTDE

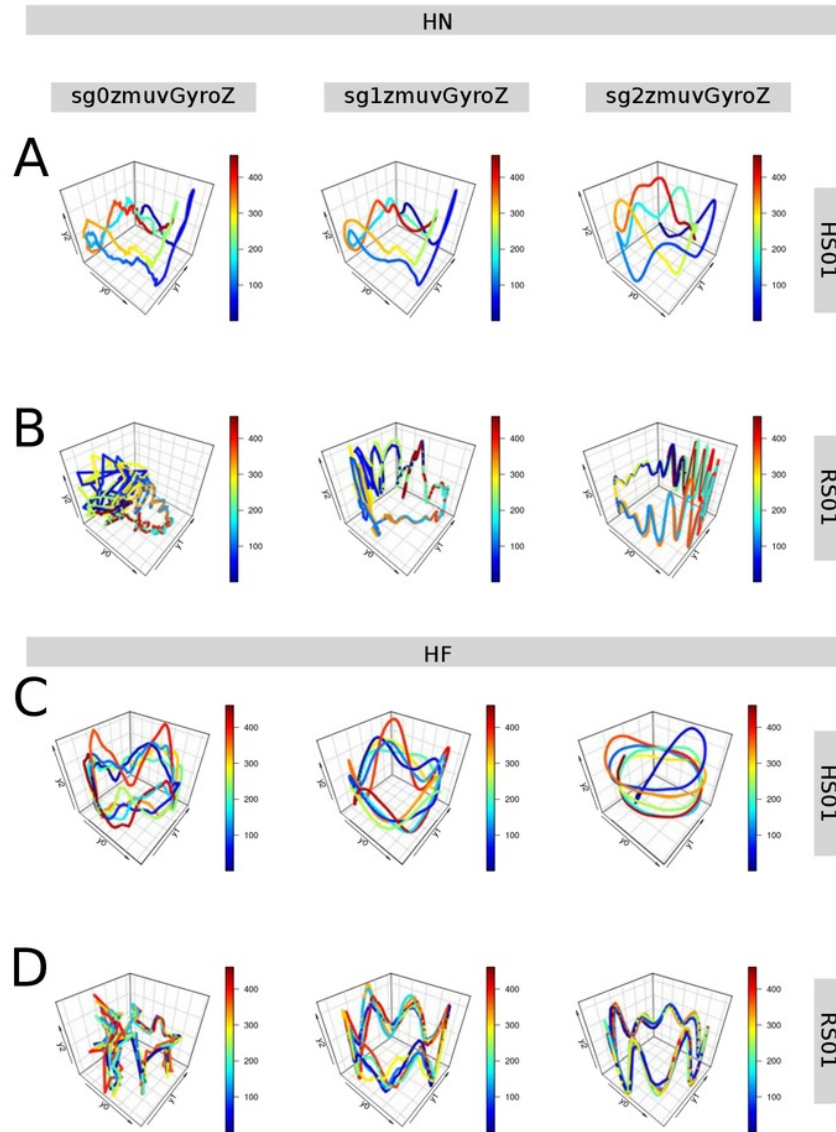


Fig. 6.4 RSSs for horizontal arm movements. Reconstructed state spaces of participant p01 for horizontal movements in normal and faster velocity (HN, HF) with raw-normalised (`sg0zmuvGyroZ`), non-¹⁶normalised-smoothed 1 (`sg1zmuvGyroZ`) and normalised-smoothed 2 (`sg2zmuvGyroZ`) time series of the sensors attached to the participant (HS01) and other sensor attached to the robot (RS01). Reconstructed state spaces were computed with embedding parameters $m = 6$, $\tau = 8$. R code to reproduce the figure is available from Xochicale (2018).

Quantifying Human-Humanoid Imitation Activities

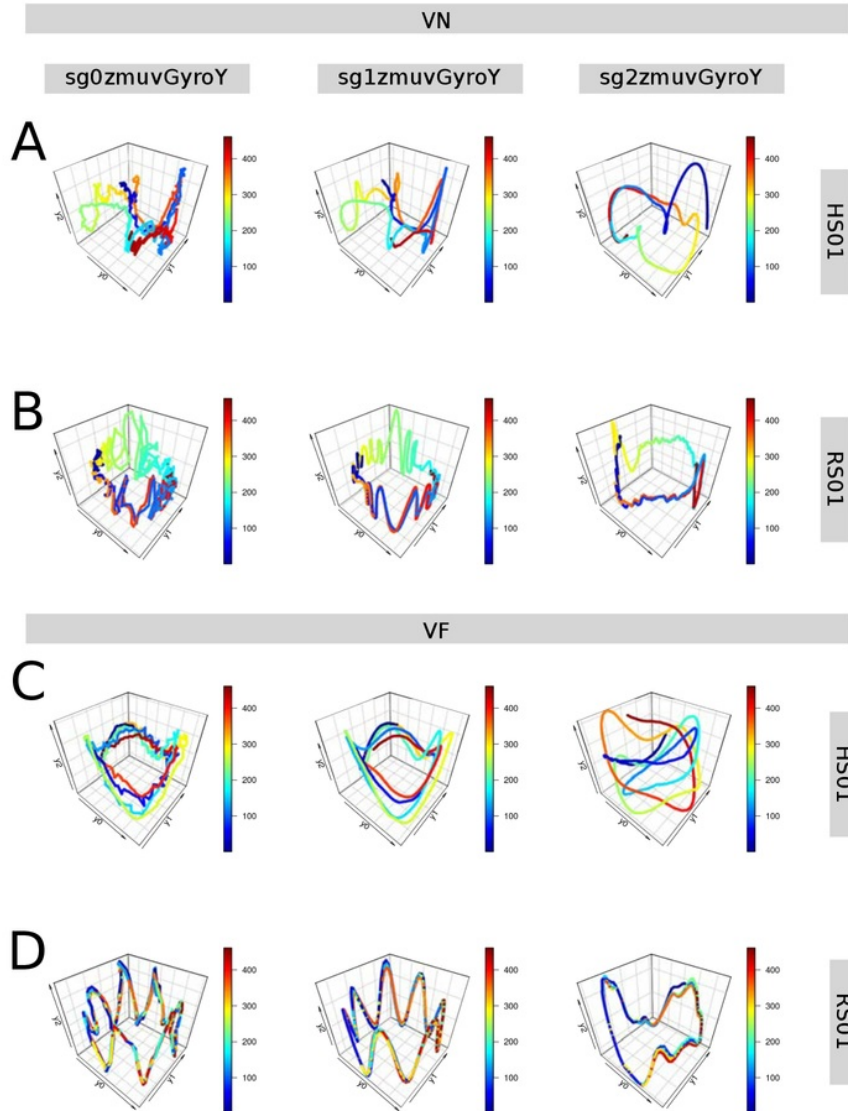


Fig. 6.5 RSSs for vertical arm movements. Reconstructed state spaces of participant p01 for vertical movements in normal and faster velocity (VN, VF) with raw-normalised ($sg0zmuvGyroZ$), n₁₆-normalised-smoothed 1 ($sg1zmuvGyroZ$) and normalised-smoothed 2 ($sg2zmuvGyroZ$) time series of the sensors attached to the participant (HS01) and other sensor attached to the robot (RS01). Reconstructed state spaces were computed with embedding parameters $m = 6$, $\tau = 8$. R code to reproduce the figure is available from Xochicale (2018).

6.5 Recurrences Plots

Considering the time series of Figs 6.1 and 6.2, we computed its Recurrence Plots for horizontal arm movements (Fig 6.6) and vertical arm movements (Fig 6.7) using the average embedding parameters ($m = 6, \tau = 8$)²¹³ and a recurrence threshold of $\epsilon = 1$. For the selection of the recurrence threshold, Marwan (2011) pointed out that choosing an appropriate recurrence threshold is crucial to get meaningful representations in the RPs, however, for this thesis where quantifying movement variability is our aim, we give little importance to the selection of the recurrence threshold for the RPs as long as it is able to represent the dynamical transitions in each of the time series.¹⁵⁶

In general, the increase of smoothness in time series results in thicker and better defined diagonal lines in the RPs (Figs 6.6, 6.7). Additionally, due to the changes in velocities of the movements the patterns in the RPs present an increase of diagonal lines and a decrease of line thickness. Although, the patterns of RPs show consistency with the movements type and velocities changes, it can be noticed that patterns of the RPs for HS01 are not well defined while patterns of the RPs for RS01 shown a more consistent pattern (Fig 6.6, 6.7).

²⁶¹ It is important to note that only RPs for participant 01 are presented in (Fig 6.7, 6.6), however other RPs for all participants are presented in Appendix D.4. With that in mind, we can highlight that, as similar as, the Reconstructed State Spaces (Figs 6.4, 6.5), the patterns in the RPs can be easily noticed by eye for different conditions of the time series (Figs 6.6, Fig 6.7), however these characteristics in the patterns of the RPs are subjective for the person who analysed them and might vary from person to person. That lead us to apply Recurrence Quantification Analysis (RQA) in order to have an objective quantification metric for the movement variability for each of the conditions of the time series.²⁶⁰

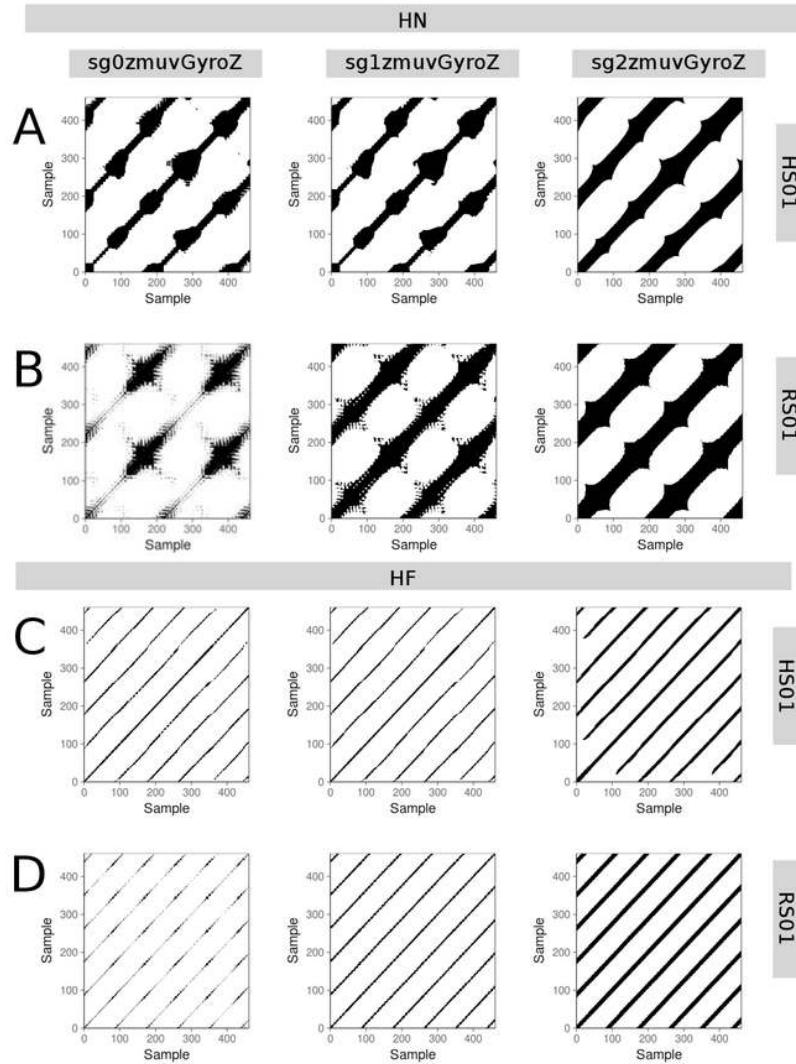


Fig. 6.6 RPs for horizontal arm movements. Recurrence plots of participant p01 for horizontal movements in normal and faster velocity (HN, HF) with time series of raw-normalised ($sg0zmuvGyroZ$), normalised-smoothed 1 ($sg1zmuvGyroZ$) and normalised-smoothed 2 ($sg2zmuvGyroZ$), and sensors attached to the participant (HS01) and to the robot (RS01). Recurrence plots were computed with embedding parameters $m = 6$, $\tau = 8$ and $\epsilon = 1$. R code to reproduce the figure is available from Kochicale (2018).

6.5 Recurrences Plots

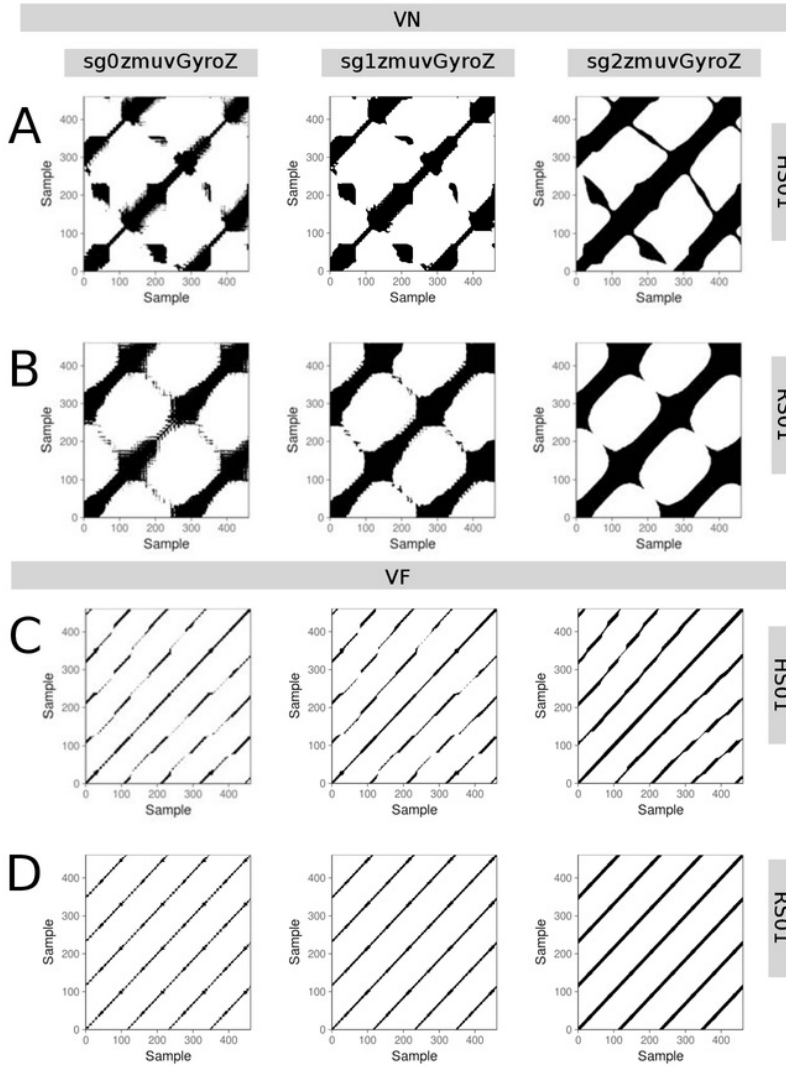


Fig. 6.7 RPs for vertical arm movements. Recurrence plots of participant *p01* for vertical movements in normal and faster velocity (VN, VF) with time series of raw-normalised (*sg0zmuvGyroZ*), normalised-smoothed 1 (*sg1zmuvGyroZ*) and normalised-smoothed 2 (*sg2zmuvGyroZ*), and sensor ₁ attached to the participant (HS01) and to the robot (RS01). Recurrence plots were computed with embedding parameters $m = 6$, $T = 8$ and $\epsilon = 1$. R code to reproduce the figure is available from Xochicale (2018).

6.6 Recurrence Quantification Analysis

Considering the RPs for 20 participants performing four activities (HN, HF, VN and VF) with sensors attached to the human (HS01) and to the humanoid robot (RS01) and with the increase of smoothness of time series (sg0zmuvGyroZ, sg1zmuvGyroZ and sg2zmuvGyroZ), we hence compute four metrics of RQA metrics (REC, DET, RATIO and ENTR) with embedding parameters $m = 6$, $\tau = 8$ and recurrence threshold $\epsilon = 1$.¹

REC values

It can be seen in the box plots of Figs 6.8(A) that REC values, representing the % of black dots in the RPs, are more spread for HN and VN movements (higher interquartile range) than HF and VF movements (lower interquartile range) for HS01 sensor. In contrast, REC values for RS01 sensor present little variation (interquartile range of 0.01). With regard to the increase of smoothness of time series (sg0, sg1 and sg2), REC values present little variation as the smoothness is increasing for time series from HS01 (changes of mean values (rhombus)) while REC values are more affected with the smoothness for data from RS01 (see the incremental changes of mean values (rhombus)). See Figs E.19 and E.20 in appendix E.2 for more details about individual REC values for each participant.

DET values

Figs 6.8(B) illustrate DET values, representing predictability and organisation of the RPs, which change very little (interquartile range is around 0.1) for type of movement, level of smoothness or type of sensor. See Figs E.21 and E.22 in appendix E.2 for more details about individual DET values for each participant.

6.6 Recurrence Quantification Analysis

RATIO values

Figs 6.8(C) present RATIO values, representing dynamic transitions, for horizontal and vertical movements. It can be seen that RATIO values for HS01 sensor vary less for HN movements (interquartile range around 2) than HF movements (interquartile range around 5). It can also be noticed a decrease of variation in RATIO values as the smoothness of the time series is increasing (grey rhombus). See Figs E.23 and E.24 in appendix E.2 for more details about individual RATIO values for each participant.

ENTR values

Fig. 6.8(D) show ENTR values, representing the complexity of the structure the time series, for both horizontal and vertical movements. ENTR values for HS01 sensor show more variation (interquartile range around 0.5) than ENTR values for RS01 sensor which appear to be more constant (interquartile range 0.1). It can also be said that the smoothness of time series affects each of the axis by an increase of mean values (see gray rhombos). See Figs E.25 and E.26 in appendix E.2 for more details about individual ENTR values for each participant.

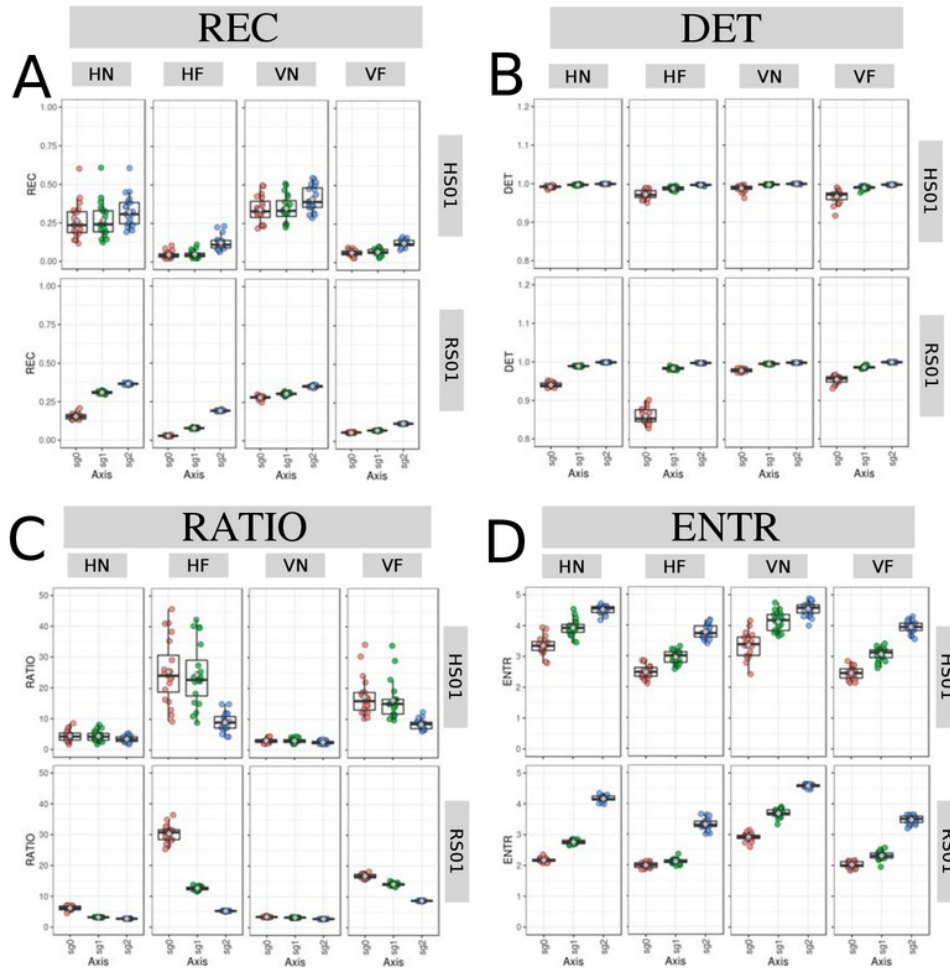


Fig. 6.8 Box plots for RQA values. Box plots of (A) REC, (B) DET, (C) RATIO, and (D) ENTR values for 20 participants performing HN, HF, VN and VF movements with sensors HS01 and RS01 and three smoothed-normalised time series (sg0, sg1 and sg2). RQA values were computed with embedding parameters $m = 6$, $\tau = 8$ and $\epsilon = 1$. R code to reproduce the figure is available from Xochicale (2018).

6.7 Weaknesses and strengths of RQA

Considering the Section 3.7.3 regarding the weaknesses and strengths of RQA, we computed RQA metrics (REC, DET, RATIO and ENTR) and plotted 3D surfaces using an unitary increase of pair embedding parameters ($0 > m \leq 10$, $0 > \tau \leq 10$) and a decimal increase of 0.1 for recurrence thresholds ($0.2 \geq \epsilon \leq 3$) (Fig. 6.9). Hence, Fig. 6.9(A) shows an increase for REC values, the percentage of black dots in the RP, as the recurrence threshold increase, while the variation for embedding parameters creates little decrease of REC values as the embedding dimensions. increase and even a more slighter decrements of REC values for the increase of τ . For the 3D surface of DET values (Fig. 6.9(B)), representing predictability and organisation of the RPs, one can be noted a plateau for DET values near to 1 for embedding dimension parameters of less than 5 and recurrence threshold values of greater than 2 (red surface). It can also be observed that the increases of delay embedding made the DET values increase so as to make an cascade effect in the surface along with the increase of dimension embedding m . For RATIO values, representing dynamic transitions, Fig. 6.9 shows that the 3D surface present a plateau (blue surface) of RATIO values near to zero for recurrence thresholds greater than 1.0, while fluctuations are more evident for recurrence thresholds of less than 1.0, particularly it can also be noted an increase in the fluctuations of RATIO values as the embedding dimension is increasing. For ENTR values in Fig. 6.9(D), representing the complexity of the structures in time series, one can be noted that the increase of recurrence threshold is, not strictly proportional to the increase of ENTR values. It can also be observed in Fig. 6.9(D) that the increase of delay embeddings affects little the ENTR values for embedding dimensions of 1, while for higher values of embedding dimensions there is a decrease of ENTR values, and there is a decrease of ENTR values as delay dimension value is increasing.

259

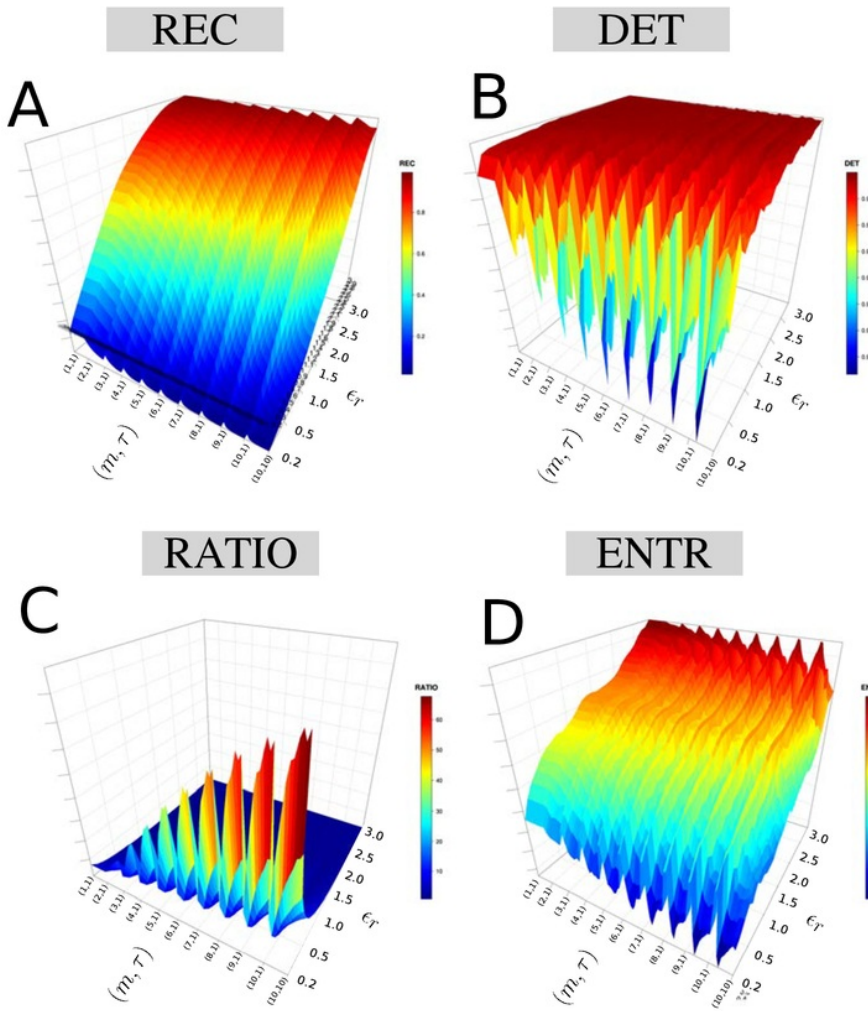


Fig. 6.9 3D surfaces for RQA metrics. 3D surfaces for (A) REC, (B) DET, (C) RATIO and (D) ENTR values with increasing pair of embedding parameters ($0 \leq m \leq 10$, $0 \leq \tau \leq 10$) and recurrence thresholds ($0.2 \geq \epsilon \leq 3$). RQA metrics are computed with the time series of participant p01 using HS01 sensor, HN activity, sg0zmuvGyroZ axis and 500 samples for window size length. R code to reproduce the figure is available from Xochicale (2018). 4

6.7 Weaknesses and strengths of RQA

6.7.1 Sensors and activities

We also computed 3D surfaces of RQA metrics for different sensors and different activities (Figs. 6.10, 6.11), where it can generally be noted similar 3D surface patterns for RQA metrics as the ones in Fig. 6.9.

The 3D surfaces for REC values (Fig. 6.10(A)) show slightly differences with regard to vertical or horizontal activities however there are notable differences for normal and faster velocities, specially for the faster movements where the 3D surfaces shown a maximum REC value for embedding dimension values near to 1 and for recurrence thresholds near to 3. The 3D surfaces for DET values (Fig. 6.10(B)) and RATIO values (Fig. 6.10(C)) show slightly notable variations across the type of activities. For 3D surfaces of ENTR values it can be noted a slightly variation for the surfaces of normal and faster velocities (Fig 6.10(D)).

As similar as Fig 6.10, the 3D surfaces patters for RS01 in Fig 6.11 show the differences between the activities performed at normal and faster velocities specially for REC and ENTR values (Fig 6.10(A, D)), while 3D surfaces for DET and RATIO values show slightly variations (Fig 6.10(B, C)).

6.7.2 Window size

Figs. 6.12 illustrate 3D surfaces for RQA metrics with four window size lengths of 100, 250, 500 and 750 samples. In general, it can be said that the increase of samples in the time series creates 3D surface patterns with better resolution.

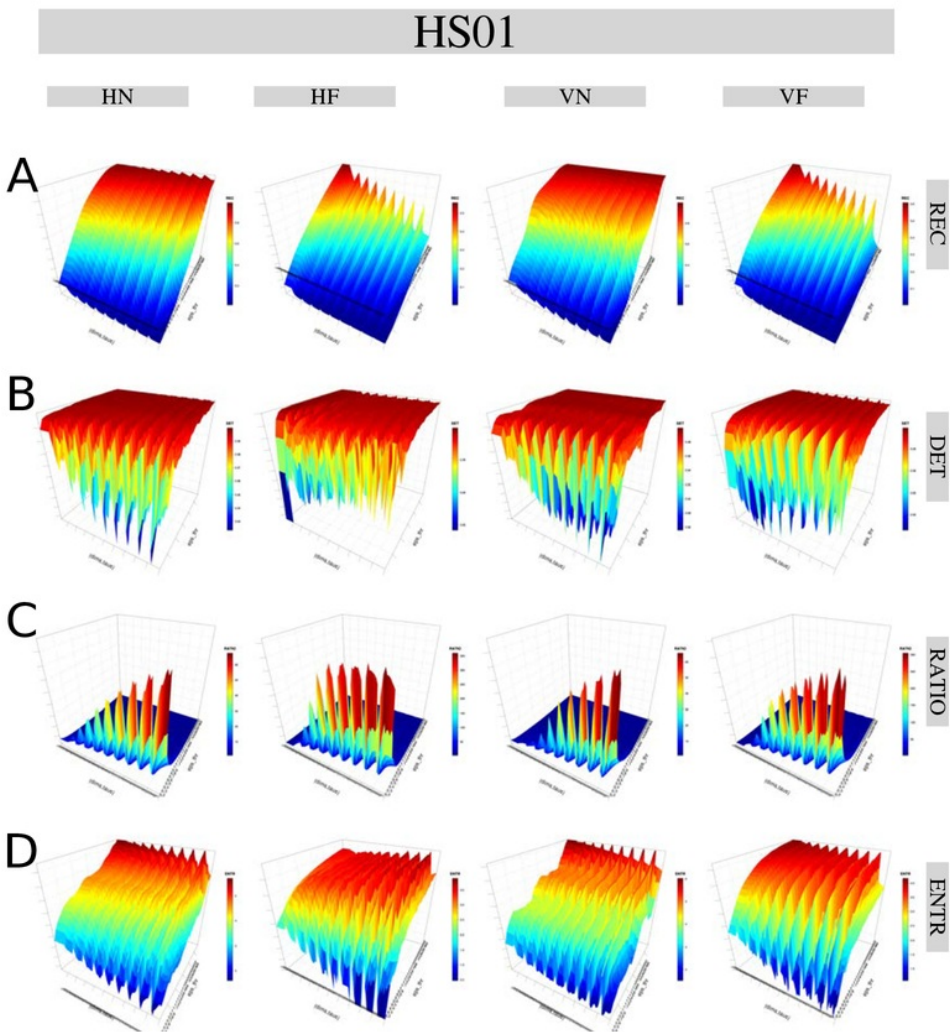


Fig. 6.10 3D surfaces of RQA metrics for HS01 sensor. 3D surfaces of RQA metrics ((A) REC, (B) DET, (C) RATIO, and (D) ENTR) with increasing embedding parameters and recurrence thresholds are for time series of participant *p01* for sensors HS01, activities (HN, HF, VN and VF) and sg0zmuvGyroZ axis with 500 samples window size length. R code to reproduce the figure is available from Xochicale (2018).

6.7 Weaknesses and strengths of RQA

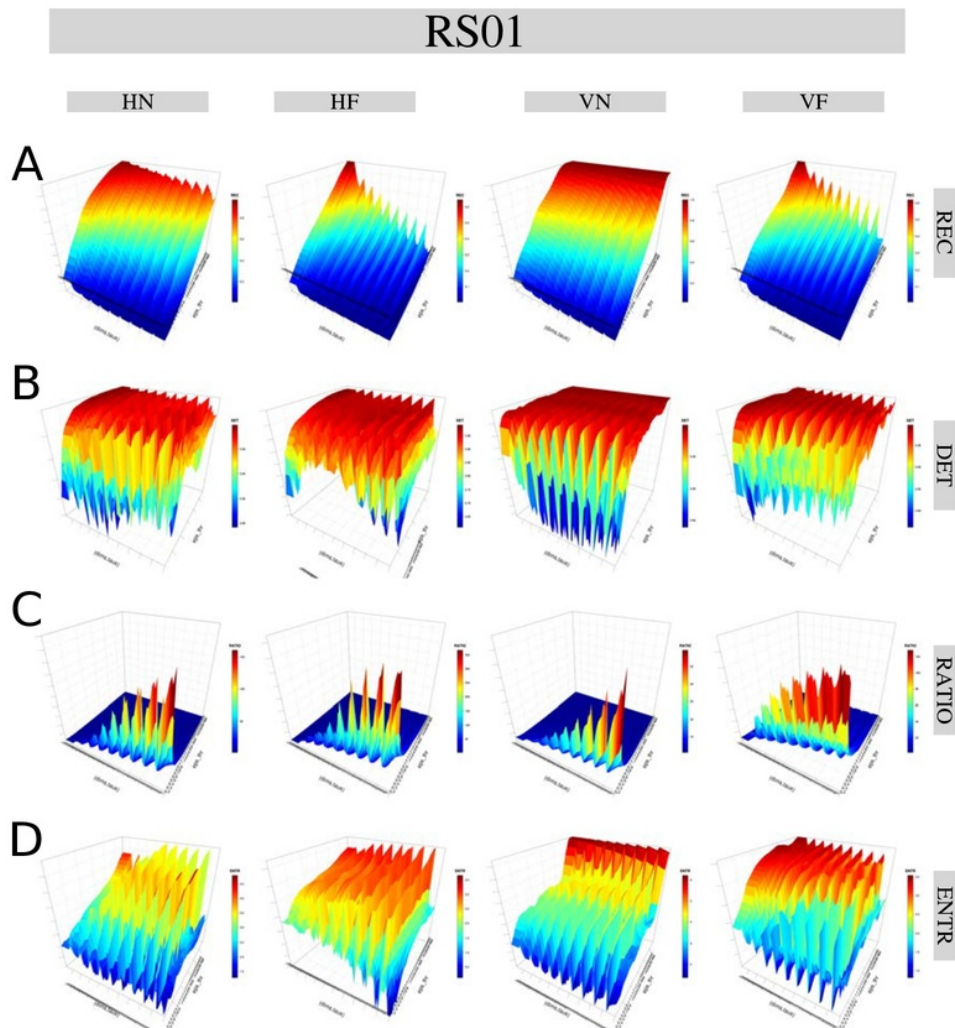


Fig. 6.11 3D surfaces of RQA metrics for RS01 sensor. 3D surfaces of RQA metrics ((A) REC, (B) DET, (C) RATIO and (D) ENTR) with increasing embedding parameters and recurrence thresholds are for time series of humanoid robot for sensors RS01, activities (HN, HF, VN and VF) and sg0zmuvGyroZ axis with 500 samples window size length. R code to reproduce the figure is available from Xochicale (2018).

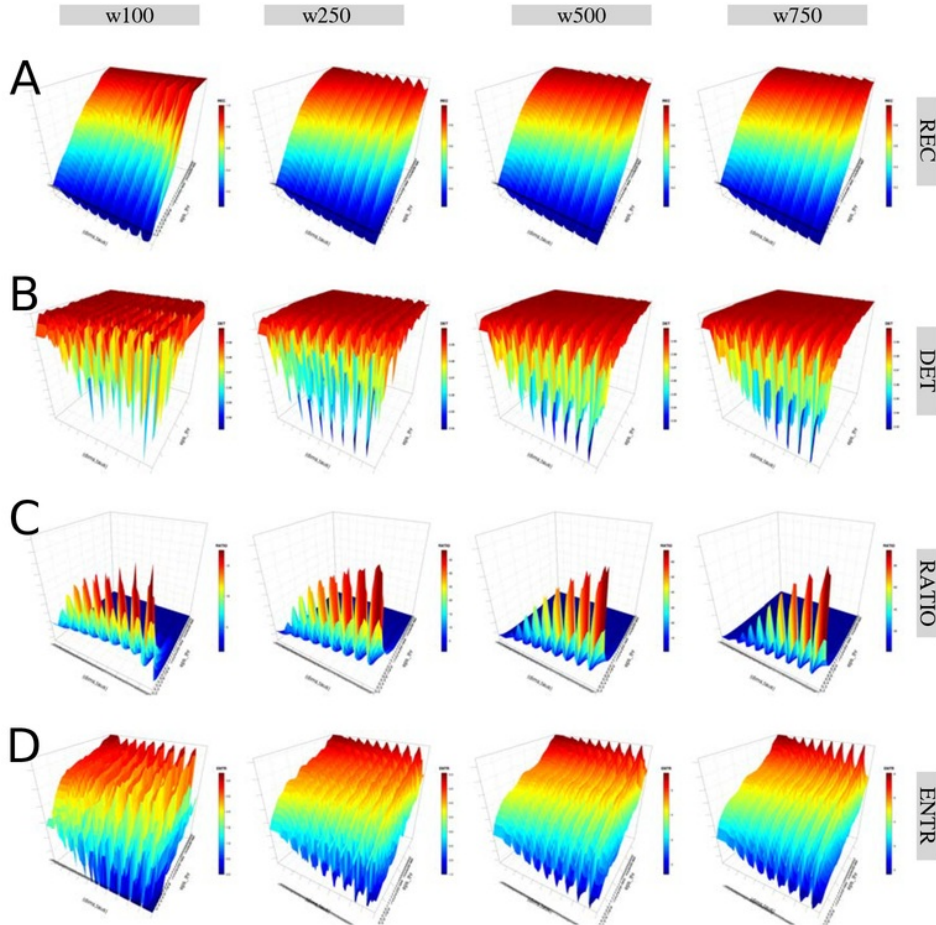


Fig. 6.12 3D surfaces of RQAs metrics with four window lengths. 3D surfaces of RQA metrics ((A) REC, (B) DET, (C) RATIO, and (D) ENTR) with increasing embedding parameters and recurrence thresholds for four window lengths (w100, w250, w500 and w750). RQA metrics values are for time series of participant *p01* using HS01 sensor, HN activity and sg0zmuvGyroZ axis. R code to reproduce the figure is available from Xochicale (2018).

6.7 Weaknesses and strengths of RQA

6.7.3 Smoothness

Figs 6.13 present 3D surfaces of the RQA metrics considering three levels of smoothness of the time series (sg0, sg1, sg2). It can then be noted that such smoothness have a direct effect on the smoothness of the 3D surfaces. Especially for dimension embeddings lower than 2 with in REC and ENTR values (Fig. 6.13(A, D)). The 3D surfaces of DET values are smoothed to a degree that the plateau (red surface) is increase, while RATIO values appear to be less affected to the level of smoothness (Fig. 6.13(C)).

6.7.4 Participants

Figs 6.14 illustrate 3D surfaces of RQA metrics for three participants. It can be noted that differences of the 3D surfaces across participants are more notable with REC (Fig. 6.14(A)) and ENTR values (Fig. 6.14(D)), while minor differences of 3D surfaces across participants are presented in DET (Fig. 6.14B)) and RATIO vales (Fig. 6.14(C)).

Quantifying Human-Humanoid Imitation Activities

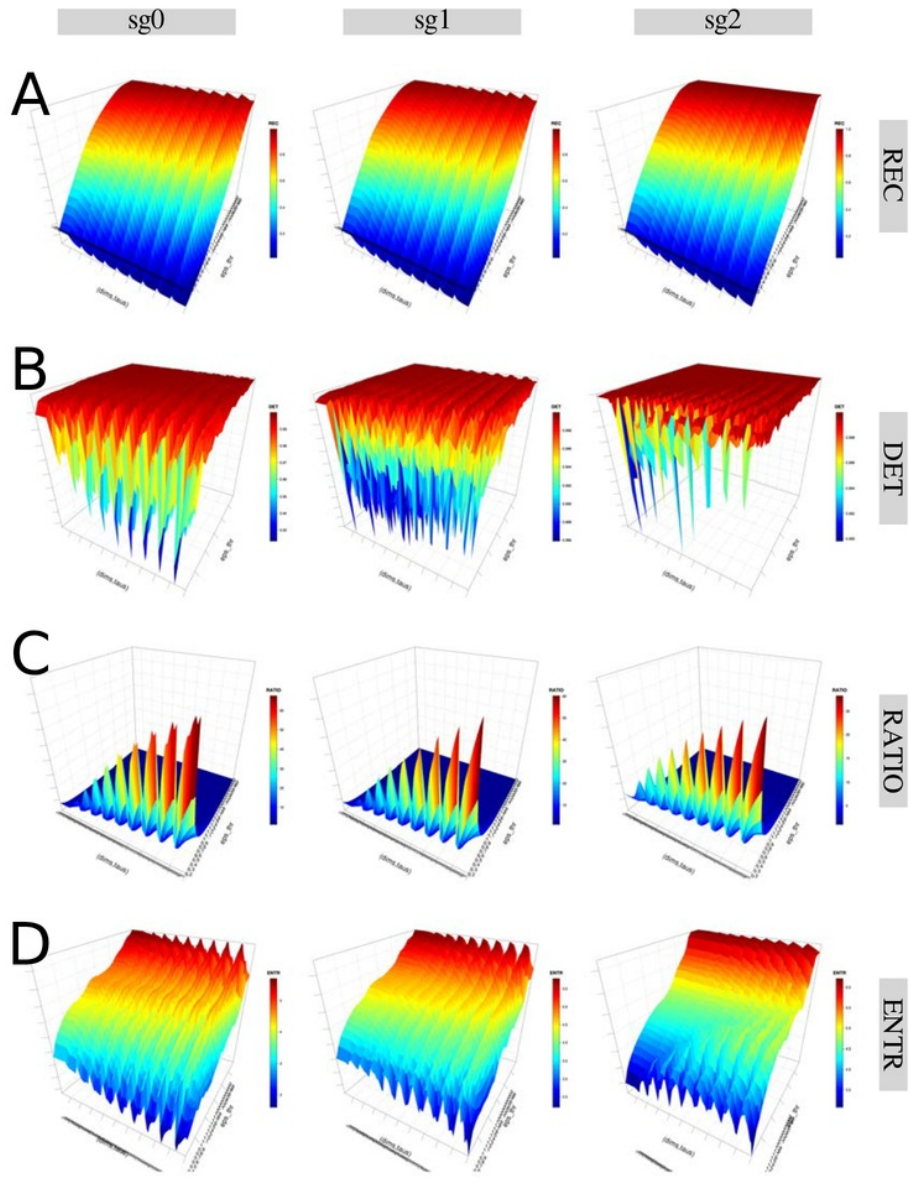


Fig. 6.13 3D surfaces of RQA metrics with three levels of smoothness. 3D surfaces of RQA metrics ((A) REC, (B) DET, (C) RATIO, and (D) ENTR) with increasing embedding parameters and recurrence thresholds for three levels of smoothness (sg0zmuvGyroZ, sg1zmuvGyroZ and sg1zmuvGyroZ). RQA metrics are computed from time series of participant p01 using HS01 sensor, HN activity and 500 samples window length. R code to reproduce the figure is available from Kochicale (2018).

6.7 Weaknesses and strengths of RQA

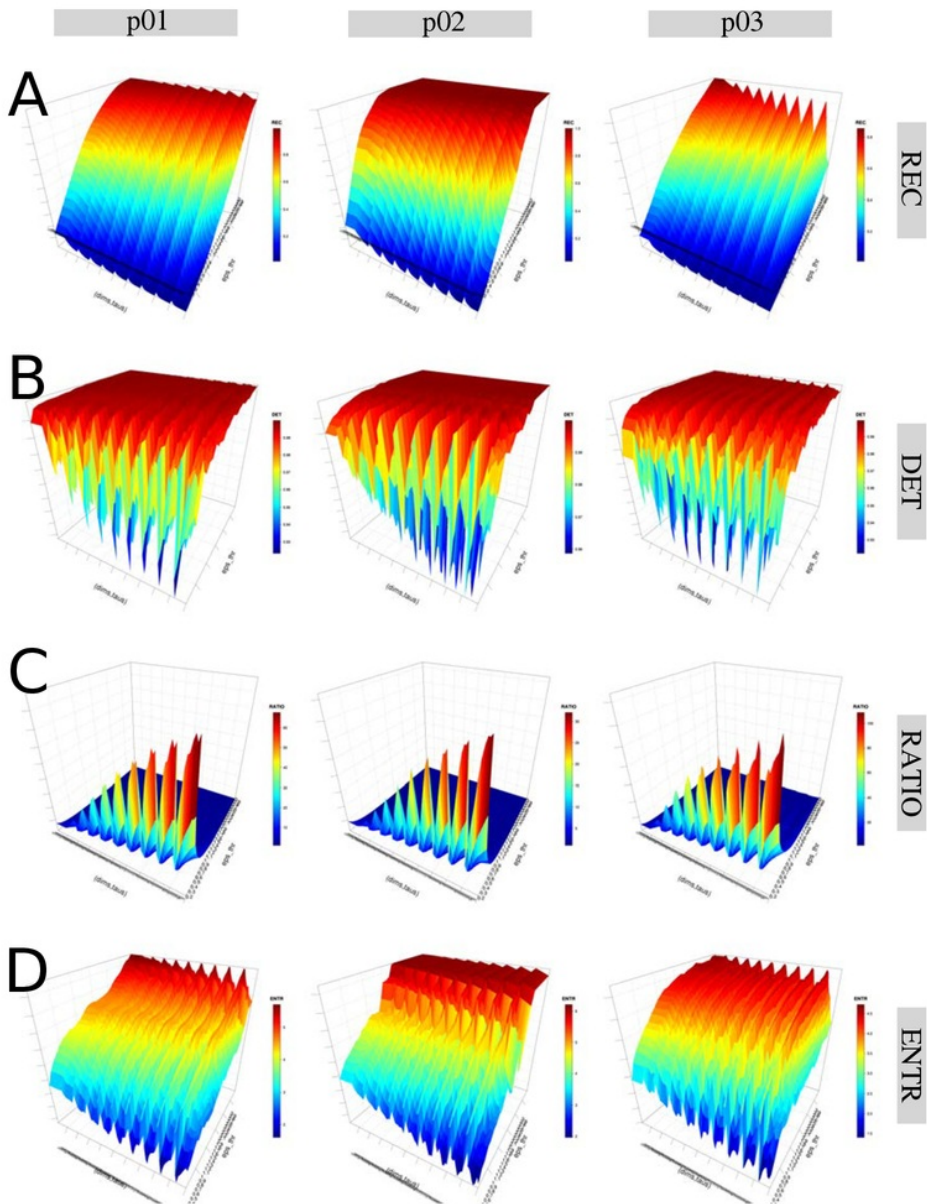


Fig. 6.14 3D surfaces of RQA metrics with three participants. 3D surfaces of RQA metrics ((A) REC, (B) DET, (C) RATIO, and (D) ENTR) for participants $p01$, $p02$ and $p03$ with increasing embedding parameters and recurrence thresholds. RQA metrics values are for time series of HS01 sensor, HN activity and 500 samples window length. R code to reproduce the figure is available from Xochicale (2018).

6.7.5 Final remarks

Generally, it can be noted the changes for RQA metrics are evident with both the increase of embedding dimension parameters and the recurrence threshold for different structures, window size, levels of smoothness of the time series. RATIO values present a plateau (blue colour surface) which is independently to the source of time series, however there are peaks that change differently based on the source of time series for increasing embedding parameters with recurrence threshold less than one. For DET values, 3D surfaces present a fluctuated surface (red colour) which slightly differs with the source of time series. With regards to REC values, 3D surfaces are affected by the velocity of movements, for instance, surfaces for normal velocity presents an increase of REC values as recurrence threshold increase and keeping slightly uniform surface changes for the increase of embedding parameters, however for faster velocity the 3D surface fluctuations decrease as the embedding dimension increase and recurrence thresholds increase. Similar as the human-image activities (see Section 5.7 in Chapter 5), 3D surfaces for ENTR values in human-humanoid interaction present changes for any source of time series, making ENTR values a robust metric to quantify movements variability from different time series in human-humanoid activities.

⁴⁶ Chapter 7

Conclusions and future work

7.1 Conclusions

In this thesis, we went from the use of RRSs with UTDE, RPs to RQA metrics in order to realise that one should compute and then select the appropriate embedding parameters before using any of the tools for nonlinear analyses, however the process of selection for appropriate embedding parameters can be laborious (see Chapter 3) and in addition to that it is still an open problem (Gómez-García et al., 2014). We then found the work of (Iwanski and Bradley, 1998) in which is stated that patterns in RPs and metrics for RQA are independent of embedding dimension parameters. However, that is not the case when using different recurrence thresholds. Hence, embedded parameters and recurrence thresholds were considered to create 3D surfaces of RQA which, I hypothesise, might be a better approach to provide understanding on the dynamics of different characteristic of time series such as window size length, participants, sensors and levels of smoothness (see weaknesses and strengths of RQA in Chapters 5 and 6).

To my knowledge, I can conclude that, no scientific work has been reported regarding nonlinear analyses (e.g. RSSs with UTDE, RPs and RQAs) to quantify movement variability in the context of human-humanoid interaction. Additionally, this thesis

Conclusions and future work

has explored the weaknesses and strengths of RQA using 3D surfaces of the variation of embedding parameters and recurrence thresholds such approach requires little parametrization. We then found that the 3D surfaces for RQA ENTR metric can be used to model any of the effects of movement variability of the activities as well as the post processing of real-world time series data which have different window size length, smoothness and structures (shape, amplitude and phase) of time series that correspond to different activities or different participants (see Sections of weaknesses and strengths of RQA in Chapters 5 and 6). Hence, in the following sections, we will point out the positives and negatives of this thesis by answering the raised research questions in Chapter 1.

What are the effects of different parameters for nonlinear analyses with different characteristics of time series?

It is evident that time series from different sources of time series (e.g. participants, movements, axis type, window size lengths or levels of smoothness) will present differences for not only embedding parameters but also for the patterns in RSSs, RP, RQAs and 3D surfaces of RQA metrics. With that in mind, we conclude that the selection of the appropriate embedding parameters or recurrence threshold is crucial to get meaningful results from nonlinear analyses tools. However, in this thesis we find that the creation of 3D surfaces of RQA metrics is a new approach that is independent of either the type of time series or the selection of parameters.

7.1 Conclusions

What are the weaknesses and strengths of RQA metrics when quantifying MV?

After getting results from our experiments, we can state that the weaknesses of RQA are (i) the requirement of an expert(s) for interpretation and computation of embedding parameters and recurrence thresholds, (ii) the implementation and computation of methods is laborious and algorithms and the computation of those parameters is still an open problem, and (iii) the selection of particular parameters to apply nonlinear analyses does not necessarily give the best representation of the dynamics of the time series.
229

With regards to the strengths of RQA metrics, we realised that varying embedded parameters and recurrence thresholds to create 3D surfaces of RQA might be: (i) a better approach to understand the dynamics of different characteristic of time series and (ii) require little set up of parametrisation.
24

How the smoothing of raw time series affects the nonlinear analyses when quantifying MV?

The answer depends on what to measure, for instance, to avoid erratic changes in the metrics, smoothing raw signals can help to obtain well defined and constant metrics. However, we observed that the increase of level of smoothness of time series created more complex trajectories in the RSSs and added more black dots in Recurrence Plots (see RSSs and RPs sections in Chapters 5 and 6). It is important to mention that some RQA's metrics (e.g. DET and ENTR) are more robust to the effect of smoothness of time series.
257

Also, using raw data, one might create a closer representation of the nature of movement variability. However, we state that further investigation is required to be

done as we think that finding the right balance between smoothness and the raw data to capture movement variability is still a problem.

7.2 Future work

Inertial sensors

To have fundamental understanding of the nature of signals collected through inertial sensor ¹⁵³ in the context of human-robot interaction, future experiments can be conducted considering the application of derivatives to the acceleration data. With that in mind, it can then be explored (i) the jerkiness of movements and therefore the nature of arm movements which typically have minimum jerk (Flash and Hogan, 1985), (ii) the relationship with different body parts, for instance, how rapid or slowly one performs arm and legs movements as we grow up (de Vries et al., 1982; Mori and Kuniyoshi, 2012) or (iii) the application, to real-world time series data, of higher derivatives of displacement with respect time such as jounce, snap, crackle and pop (Eager et al., 2016).

Nonlinear analyses

Optimal embedding parameters

When using the method of False Nearest Neighbour (Cao, 1997), where the values for $E_1(m)$ stop changing to find the minimum embedding dimension, a threshold ⁶ should be defined in order to obtain the minimum embedding dimension m_0 . Hence, ⁶ a further investigation is required for the selection of the threshold in the $E_1(m)$, as the selection of the threshold in this thesis is only based on no particular method but visual inspection of the $E_1(m)$ curves (see Section 3.4.1 in Chapter 3). Similarly, further research is required to be done with regards to the selection of the minimum

7.2 Future work

delay embedding because it is not clear: (i) why the choose of the first minimum of the AMI is the minimum delay embedding parameter (Kantz and Schreiber, 2003) or (ii) why the probability distribution of the AMI function is computed with the use of histograms which depends on a heuristic choice of number of bins for the AMI partitioning (Garcia and Almeida, 2005). Additionally, "the AMI method is proposed for two dimensional reconstructions and extended to be used in a multidimensional case which is not necessarily hold in higher dimensions" (Gómez-García et al., 2014, p. 156).

146 Other methodologies for state space reconstruction.

In addition to the method of Uniform Time-Delay Embedding to reconstruct state spaces, other methods have been investigated stating a better dynamic representations of time series in the reconstructed state spaces: (i) the nonuniform time-delay embedding methodology where the consecutive delayed copies of $\{\mathbf{x}_n\}$ are not equidistant (Pecora et al., 2007; Quintana-Duque and Sause, 2013; Quintana-Duque, 2012, 2016; Uzal et al., 2011), and (ii) uniform 2 time-delay embedding method which takes advantage of finding an embedding window instead of the traditional method of finding the embedding parameters separately (Gómez-García et al., 2014).

RQA parameters

Having presented our results with RQA metrics, we consider that further investigation is required to be done in order to have a better understanding of the RQA metrics and ensure its robustness in many of its applications. For example, Marwan et al. (2007) and Marwan and Webber (2015) reviewed different aspects to compute RPs using different criteria for (i) neighbours, (ii) different norms (L_{1-norm} , L_{2-norm} , or $L_{\infty-norm}$) or (iii) different methods to select the recurrence thresholds such as: using

Conclusions and future work

only certain percentage of the signal ($\sqrt{m_0} \times 10\%$ of the fluctuations of the time series) (Letellier, 2006), selecting a determined amount of noise, and using a factor based on ²¹² the standard deviation of the observational noise Marwan et al. (2007).

Robustness of Entropy measures with RQA

Further investigation is required to be done with regards to the use of Shannon entropy with recurrence plots. For example, Letellier (2006) investigated the robustest of the Shannon entropy based on line segments distributions of recurrence plots S_{RP} against the Shannon entropy based on system dynamics S_{SD} . With that, Letellier (2006) pointed out that Shannon entropy based on recurrence plots has strong dependency with the choice of observable, variable of the dynamical system, while Shannon entropy based on system dynamics is more robust to noise-contaminated signals. Recently, Corso et al. (2017) tackled the quite know problem of ENTR with RQA in a logistic map (Marwan et al., 2007) where ENTR values decrease despite the increase of nonlinearity by introduction the use of microstates. Additionally, Corso et al. (2017) presented the robustness of his method with changes to recurrence thresholds.

Advanced RQA quantifications

In addition to the applied RQA metrics (REC, RATIO, DET and ENTR) for recurrence quantification, I can see different lines of research for this thesis which is the investigation of methods of the RP based on complex networks statics, calculation of dynamic invariants, study of the intermittency in the systems, applying different windowing techniques or the study of bivariate recurrence analysis for ⁶ correlations, couplings, ⁸ coupling directions or synchronisation between dynamical systems (Marwan et al., 2007; Marwan and Webber, 2015).

Variability in perception of velocity

While conducting the experiments with different arm movements velocities (e.g. normal and faster), we realised that participants perceive velocity differently, shedding light for a have better understanding on why each participant perceive body movement velocity differently and how to quantify such variability of perception of movement. For instance, from our experiments we realised that some participants considered a normal velocity movement as a slow velocity movement and some others considered a slow velocity movement as being performed in normal velocity. With that in mind, we hypothesise that the differences in perception of velocities are related to the background of each person, personality traits or even to some kind of movement experience (in music or sports) that make them more aware of their body movements.

A richer dataset of real-world time series

It should also be highlighted that the experiments for this thesis are limited to twenty three healthy right-handed participants of a range age of mean 19.8 and SD=1.39, for which participants of different ages, state of health and anthropomorphic features would create a richer dataset of real-world time series.

Applications

I can foresee many of the published work regarding modeling human movement variability applied to the context of human-humanoid interaction. For instance, implementing nonlinear analyses algorithms in humanoid robots to evaluate the improvement of movement performances (Müller and Sternad, 2004), to quantify and provide feedback of level skillfulness as a function of movement variability (Seifert et al., 2011) or to quantify movement adaptations, pathologies and skill learning (Preatoni, 2007; Preatoni et al., 2010, 2013). More specifically in the context of human-humanoid rehabilitation

Conclusions and future work

where little work has been done (Görer et al., 2013; Guneyşu et al., 2015) with regards to the use of nonlinear analyses and therefore provide adequate metrics to quantify and provide feedback for movement variability.

Appendix A

Examples of Uniform Time-Delay Embedding

Two examples regarding the methodology of uniform time-delay embedding are presented: (A.1) using a 20 sample length vector, and (A.2) using a time series from horizontal movement of a triaxial accelerometer.

A.1 20 sample length vector.

For this example, we propose to work with a vector $\{\mathbf{x}_n\}_{n=1}^{20}$ with a sample length $N = 8$ in order to implement an uniform time-delay embedding matrix, \mathbf{X}_τ^m , with embedding dimension of $m = 5$ and delay dimension of $\tau = 3$ (Eq. (3.4)). The representation of

151

Examples of Uniform Time-Delay Embedding

the uniform time-delay embedding matrix \mathbf{X}_3^5 is as follows 24

$$\mathbf{X}_3^5 = \begin{pmatrix} \tilde{\mathbf{x}}_n \\ \tilde{\mathbf{x}}_{n-3} \\ \tilde{\mathbf{x}}_{n-6} \\ \tilde{\mathbf{x}}_{n-9} \\ \tilde{\mathbf{x}}_{n-12} \end{pmatrix}^\top \quad (\text{A.1})$$

The dimension of the uniform time-delay embedding matrix is defined by $N - (m - 1)\tau$ 65 64 rows and m columns. $N - (m - 1)\tau$ is also the sample length of the delayed copies of \mathbf{x}_n which is equal to eight ($20 - ((5 - 1) * 3) = 8$). Therefore, \mathbf{X}_3^5 can be explicitly represented as

$$\mathbf{X}_3^5 = \begin{pmatrix} x_1 & x_2 & x_3 & x_4 & x_5 & x_6 & x_7 & x_8 \\ x_4 & x_5 & x_6 & x_7 & x_8 & x_9 & x_{10} & x_{11} \\ x_7 & x_8 & x_9 & x_{10} & x_{11} & x_{12} & x_{13} & x_{14} \\ x_{10} & x_{11} & x_{12} & x_{13} & x_{14} & x_{15} & x_{16} & x_{17} \\ x_{13} & x_{14} & x_{15} & x_{16} & x_{17} & x_{18} & x_{19} & x_{20} \end{pmatrix}^\top \quad (\text{A.2})$$

After transposing \mathbf{X}_3^5 , one can see that the ranges of values of the uniform time-delay embedded matrix are between $((m - 1)\tau) + 1$ to N (for this example from 13 to 20):

A.2 Time series for horizontal movement of a triaxial accelerometer.

$$\mathbf{X}_3^5 = \begin{pmatrix} x_1 & x_4 & x_7 & x_{10} & x_{13} \\ x_2 & x_5 & x_8 & x_{11} & x_{14} \\ x_3 & x_6 & x_9 & x_{12} & x_{15} \\ 145 & x_4 & x_7 & x_{10} & x_{13} & x_{16} \\ x_5 & x_8 & x_{11} & x_{14} & x_{17} \\ x_6 & x_9 & x_{12} & x_{15} & x_{18} \\ x_7 & x_{10} & x_{13} & x_{16} & x_{19} \\ x_8 & x_{11} & x_{14} & x_{17} & x_{20} \end{pmatrix} = \begin{pmatrix} 173 \\ \mathbf{X}[13] \\ \mathbf{X}[14] \\ \mathbf{X}[15] \\ \mathbf{X}[16] \\ \mathbf{X}[17] \\ \mathbf{X}[18] \\ \mathbf{X}[19] \\ \mathbf{X}[20] \end{pmatrix}. \quad (\text{A.3})$$

A.2 Time series for horizontal movement of a triaxial accelerometer.

In this example, it is considered a time series of a triaxial accelerometer (Figure A.1(C)), captured from repetitions of a horizontal trajectory (Figure A.1(A)) performed by user (Figure A.1(B)). From Figure A.1(C) is evidently that the $A_y(n)$ is the most affected axis of the accelerometer due to the movement's characteristics in the horizontal trajectory. With that in mind, we select $A_y(n)$ as the input time series for the uniform time-delay embedding theorem.

Considering that the sample rate of the data is 50 Hz, we propose to work with a vector of sample length of $N = 1000$ which corresponds to 20 seconds of data. Then, with minimum embedding parameters $m = 7$ and $\tau = 11$, the dimensions of the uniform time-delay embedding matrix, \mathbf{A}_{y11}^7 , are 934 ($N - (m - 1)\tau$) rows and 7 (m) columns.

⁴⁷

Examples of Uniform Time-Delay Embedding

$\mathbf{A}_{y_{11}}^7$ is therefore represented as follows:

$$\mathbf{A}_{y_{11}}^7 = \begin{pmatrix} A_y(n) \\ A_y(n-11) \\ A_y(n-22) \\ A_y(n-33) \\ A_y(n-44) \\ A_y(n-55) \\ A_y(n-66) \end{pmatrix}^\top = \begin{pmatrix} a_y(1) & \dots & a_y(934) \\ a_y(12) & \dots & a_y(945) \\ a_y(23) & \dots & a_y(956) \\ a_y(34) & \dots & a_y(967) \\ a_y(45) & \dots & a_y(978) \\ a_y(56) & \dots & a_y(989) \\ a_y(67) & \dots & a_y(1000) \end{pmatrix}^\top \quad (\text{A.4})$$

$$\mathbf{A}_{y_{11}}^7 = \begin{pmatrix} a_y(1) & a_y(12) & a_y(23) & a_y(34) & a_y(45) & a_y(56) & a_y(67) \\ \vdots & \vdots & \vdots & \vdots & \vdots & \vdots & \vdots \\ a_y(934) & a_y(945) & a_y(956) & a_y(967) & a_y(978) & a_y(989) & a_y(1000) \end{pmatrix} \quad (\text{A.5})$$

$$\mathbf{A}_{y_{11}}^7 = \begin{pmatrix} \mathbf{A}_{y_{11}}^7[67] \\ \vdots \\ \mathbf{A}_{y_{11}}^7[1000] \end{pmatrix}. \quad (\text{A.6})$$

A.2 Time series for horizontal movement of a triaxial accelerometer.

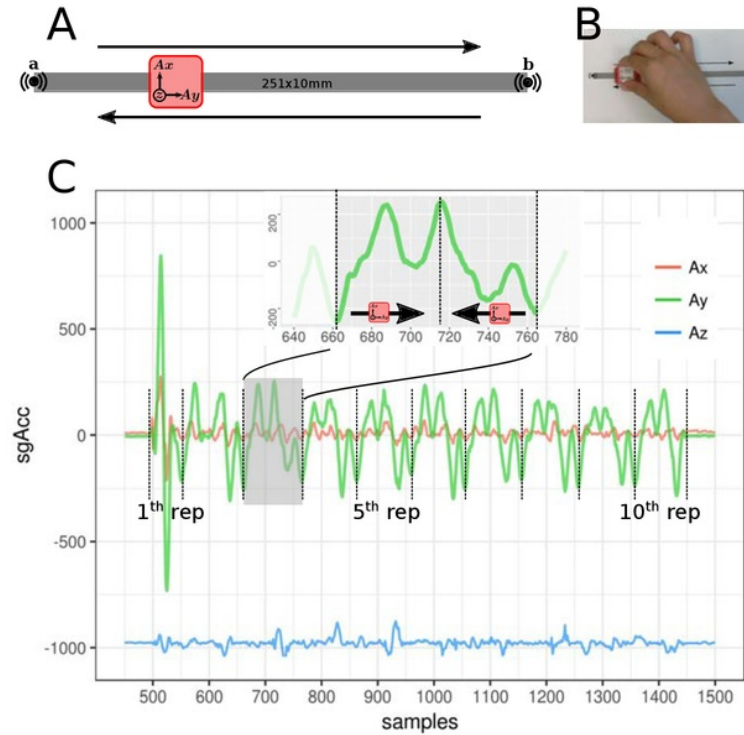


Fig. A.1 Example of time series with an IMU (A). Triaxial accelerometer (in red) is moved repetitively across a line of 251 mm from point **a** to **b** and then from **b** to **a**. The points **a** and **b** indicate when a click sound is produced. (B). Person's hand holding the sensor horizontally across the line. (C). Time series for the triaxial accelerometer ($A_x(n)$, $A_y(n)$, $A_z(n)$) for ten repetitive horizontal movements across a line. The top time series only shows A_y axis which corresponds to one cycle of the horizontal movement and the black arrows represent the movement's direction of the accelerometer with respect to the produced time series.



Appendix B

Equipment

B.1 NeMEMSi IMU sensors

For this work, data were collected using NeMEMSi sensors Comotti et al. (2014) that provide 3D accelerometer, 3D magnetometer, 3D gyroscope and quaternions (Figure B.1). It is important to note that NeMEMSi sensors were tested against the state-of-the-art device MTi-30 IMU from xsense. The comparison values between NeMEMSi and MTi-30 in terms of standard deviation of the noise of each component of the Euler angles at a static state are lower than 0.1 degrees. Additionally, the NeMEMSi provide not only to have a lower-power consumption but also the smaller dimensions against other state-of-the-art brands of IMUs. In the following sections, some features of the IMU are presented, however, we refer the readers to check Comotti et al. (2014) for further details.

Equipment

Sample rate and power consumption

Data streaming can be set up to be streamed at 25 Hz, 50 Hz and 100Hz which affects the power consumption from 29mAh, 32mAh and 35mAh, respectively. For this work, the sample rate were set up to 50 Hz.

Sensors

The outputs of the NeMEMSi sensor include:

Orientation

* Euler angles (Yaw, Pitch and Roll). * Quaternions.

Accelerometer (Linear acceleration)

* Raw and calibrated XYZ measurement from ± 2 / ± 4 / ± 6 / ± 8 / ± 16

Gyroscope (Rate of turn)

* Raw and calibrated XYZ measurement from ± 245 / ± 500 / ± 2000 degrees per second.

Magnetometer (Magnetic field)

* Raw and calibrated XYZ measurement from ± 4 / ± 8 / ± 12 / ± 16 gauss.

Microprocessor

* Architecture: ARM 32-bit Cortex M4 CPU with FPU and DSP instructions *
Max.frequency: 100MHz * Memory Size: 512 Kbytes * RAM: 128 Kbytes SRAM

B.2 Time-series preprocessing

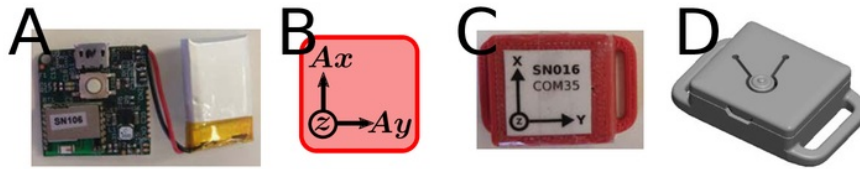


Fig. B.1 Inertial Measurement Sensor (A) Printed Circuit Board (PCB) with 165mAh battery, (B) axis orientation, (C) real case, and (D) 3D model for the case.

Connectivity

* Bluetooth: Class 2, bluetooth 3.0 * Range: 10 m * Transmission rate: Up to 560 kbps with Service Port to Port * Multipoint: Up to 7 slaves

Form factor

* Electronics physical dimension: 25L x 25W x 4H (mm) * Electronics Weight: 3.3 gr * Dimension with battery and casing: 42L x 28W x 11.5 (mm) * Weight with batter and casing: 15 gr

B.2 Time-series preprocessing

Code and data for the following sections is available in (Xochicale, 2018). However, the documentation and organisation of the repository will be updated in January 2018.

B.2.1 Organising Data in Multidimensional Arrays

Scripts in MATLAB were created to synchronise the data using the clock drift and clock offset values which were provided for each of the NeMEMSi sensors. Then the data from each sensor is aligned in time using `finddelay()` and `alignsignals()` in MATLAB.

Equipment

B.2.2 Data Synchronisation

To find the delay between two sensors that were attached to the same place of the body parts, a function called `finddelayMX()` was created. Such function computes the autocorrelation between two signals using (`xcorr()`) then the maximum value of the autocorrelation function is extracted to create a delay between the values of maximum index in the autocorrelation function and the length of the first signal.

The function `alignsignalsMX()` was used to align two signals based on `finddelayMX()`. The function `alignsignalsMX()` uses six inputs of which `sA` and `sB` are the sensors, then the windowframe of which the information of the signal is extracted from another activities, the MainAxis of which the signal are going to be extracted, the truncate delay that is created to synchronise the signals adding an extra delay that is based on the length of previous signals and tuning delay that can be useful to tune the delay in the case of the delay is not appropriate when the signals are too noisy. Then, it is used the `aligntwosignals()` to align only two signals. The inputs of `aligntwosignals()` are `X` and `Y` for the input vectors, truncate delay for the previous delay of two signals and tuning delay in case that signals are too noisy and the `xcorr` fail to find an appropriate delay.

B.2.3 Time Alignment

Given four vectors of time t_1, t_2, t_3, t_4 , it is extracted the minimum and maximum values of the start of the four sequence of time, it was also extracted the minimum and maximum values to the end of the four sequence of time. However, after aligning the vectors it has been noticed that there were different values of length across vectors i.e.: 1880, 1986, 1987, 1988 Therefore the length for the second vector was used as the primary length because is the one that is present the minimum value of the three maximum lengths. Then `interp1(x,v,vq,'phchip')` was used to interpolate the

B.2 Time-series preprocessing

length of each of the vectors such as the length of all vectors is: 1986, 1986, 1986, 1986. It has been chosen the `phchip` since the interpolation present values for each of the points which were different for the NA values from what it has been got when using `linear`.

B.2.4 Issues with IMUs

For the experiment of human-image imitation activities where eight activities were performed per participant, we observed that time synchronisation had issues because of the drift in time, also some disconnection because of the bluetooth module. In contrast, for the human-humanoid imitation activities where only four activities were performed by participant, the data collection of time series did have little issues with regard to the drift in time and bluetooth data streaming.

Equipment

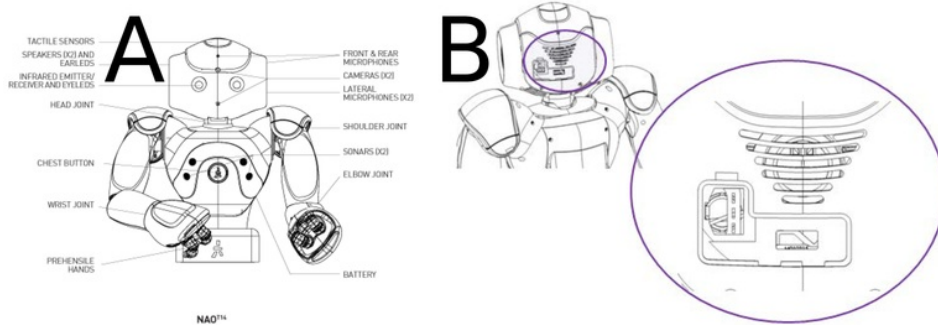


Fig. B.2 **NAO, humanoid robot from SoftBank.** (A) NAO body type T4 with its parts, and (B) back design of NAO version 04.

B.3 NAO – humanoid robot

For the human-humanoid interaction experiments of this thesis, we used a NAO humanoid robot version 04 from SoftBank (Fig .B.2). NAO were programmed for simple horizontal and vertical arm movements using Choregraphe, an API to program NAO, and then exported interpolated values to python code.

Appendix C

Experiment Design

C.1 Experiment Check List

Fig. C.1 show the experiment check list for the experiments which consist of 1. Participant Information, 2. Setting up sensors, 3. Experiments, 4. Stop sensors, and 5. Extra notes

C.2 Information Sheet

²¹⁰
Figs. C.2, C.3, C.4 and C.5 show the Online Participation Sheet which were made as a google Form.

Experiment Design

Experiment Check List. Participant: p---

Human-Humanoid Imitation Activities

1. Information

- 1.1 Participant Information Sheet 1.2 Anthropometric Data
 1.3 Sitting the participant on the Chair
 1.4 Start Recording Video 1.5 Show participant p-- to the camera

2. Setting Up Sensors

Status	Description	Status
HII		HRI
<input type="checkbox"/>	Create Data Path	<input type="checkbox"/>
<input type="checkbox"/>	Open Muse Applications	<input type="checkbox"/>
<input type="checkbox"/>	Turn ON the sensors	<input type="checkbox"/>
<input type="checkbox"/>	Pair the sensor [sensor number and port number]	<input type="checkbox"/>
<input type="checkbox"/>	Set the sampling rate to 50 Hz	<input type="checkbox"/>
<input type="checkbox"/>	Open settings for Time Sync parameters	<input type="checkbox"/>
<input type="checkbox"/>	Compute the Time Sync parameters	<input type="checkbox"/>
<input type="checkbox"/>	PrintScreen the Time Sync parameters and Save Capture	<input type="checkbox"/>
<input type="checkbox"/>	Close settings and set parameters	<input type="checkbox"/>
<input type="checkbox"/>	Start Recording data	<input type="checkbox"/>
<input type="checkbox"/>	Shake all sensors	<input type="checkbox"/>

- 2.1.a Attach Sensors to the Participant
(check sensor orientation)
 2.1.b Attach Sensors to the Robot
(check sensor orientation)
 2.1.a Attach Sensors to the Participant
(check sensor orientation)
 2.2.b Attach Sensors to the Participant
(check sensor orientation)

3. Experiment

- 3.1.a Human-Image Int [NO BEAT]

Status	Description
<input type="checkbox"/>	Hor Normal
<input type="checkbox"/>	Ver Normal
<input type="checkbox"/>	Hor Fast
<input type="checkbox"/>	Ver Fast

- 3.2.b Human-Robot Int [BEAT]

Status	Description
<input type="checkbox"/>	./HN.sh p--
<input type="checkbox"/>	./VN.sh p--
<input type="checkbox"/>	./HF.sh p--
<input type="checkbox"/>	./VF.sh p--

- 3.2.a Human-Image Int [BEAT]

Status	Description
<input type="checkbox"/>	aplay HN_beat.wav
<input type="checkbox"/>	aplay VN_beat.wav
<input type="checkbox"/>	aplay HF_beat.wav
<input type="checkbox"/>	aplay VF_beat.wav

4. Stop

- 4.1.a Stop Sensor Recording 4.1.b Stop Sensor Recording
 4.2.a Save Data 4.2.b Save Data
 4.3.a Disconnect Sensors 4.3.b Disconnect Sensors
 4.4 Stop Video Recording

5. Notes

Fig. C.1 Experiment Check List.

C.2 Information Sheet

25/10/2018

21

A Study of Movement Variability in Human-Humanoid Interaction Activities

A Study of Movement Variability in Human-Humanoid Interaction Activities

*Required

Introduction

The aim of this study is to explore how participant's performance of simple movements affects the movement variability in the following conditions: a) following an image while not hearing a beat and while hearing a beat; and b) following a humanoid-robot while not hearing a beat and while hearing a beat.

The estimated time for the study is between 40 to 45 minutes.

Miguel P. Xochicale [<http://mxochicale.github.io/>]
Doctoral Researcher in Human-Robot Interaction
School of Electronic, Electrical and System Engineering
University of Birmingham, UK

1. Online Participant Information Sheet

Who will conduct the research?

The study is conducted by Miguel P. Xochicale as part of his PhD degree in Electronic, Electrical and System Engineering at the University of Birmingham. The research is supervised by Professor Chris Barber and Professor Martin Russell in the Electronic, Electrical and System Engineering department at the University of Birmingham.

What is the purpose of the research?

The aim of this study is to explore how participant's performance of simple movements affects the movement variability in the following conditions: a) following an image while not hearing a beat and while hearing a beat; and b) following a humanoid-robot while not hearing a beat and while hearing a beat.

What will happen during the experiment?

During the experiment you will be asked to wear two inertial sensors in your right hand and you will perform 10 repetitions for horizontal and vertical arm movements in six conditions:

Condition 1. Following an image while NOT hearing a beat
Condition 2. Following an image while hearing a slow beat rate
Condition 3. Following an image while hearing a fast beat rate

(a 5 minutes break will be given at this point)

Condition 4. Following a humanoid-robot while NOT hearing a beat
Condition 5. Following a humanoid-robot while hearing a slow beat rate
Condition 6. Following an image while hearing a fast beat rate.

30

https://docs.google.com/forms/d/1dPN6D_53CRg4pkDYplfDg6fSh6FaQ4Z7M0xI_11Fq4/edit

1/4

Fig. C.2 Participant Information Sheet (p. 1/4)

Experiment Design

25/10/2018

A Study of Movement Variability in Human-Humanoid Interaction Activities

What type of data will be collected during the experiment?

Three types of data will be collected:
i) Data from inertial sensors will be collected. Each inertial sensor has a accelerometer, magnetometer, gyroscope.
ii) Audio from a microphone to record the movements of the humanoid-robot.
iii) A video will be recorded for visualisation and demonstration purposes (let me know if you are uncomfortable with the video recording).

What happens to the data collected?

The data will be analysed in order to explore how participant's performance of simple movements affects the movement variability in the previous six conditions of movement.

140

How Is Confidentiality Maintained in the experiment?

The law called the Data Protection Act (1998) tells us how to keep your information secure.

17

Your data will be treated as confidential and you will be assigned a unique identifying code which will be used to identify your data. If you have decided to provide your name and email address, it will remain confidential and we will not give your details to anyone else. No other personal data will be recorded about participants (no ethnicity, address, telephone number, etc.)

What is the duration of the experiment?

The estimated time for the study is between 40 to 45 minutes.

Where the experiment will be conducted?

The experiment will be conducted in room N310 which is in third floor at Gisbert Kapp Building (G8), University of Birmingham.

Will the results of this research be published?

Data collected will be used for conference and journal publications and the PhD thesis results.

Will there be compensation for participating?

You are invited to participate in this study but will receive no compensation.

Can I withdrawal from the experiment after given my consent?

Yes, you can withdrawal from the experiment at any time after given your consent which might be either before the start of your experiment session, during the session, or after finishing the session. In case of withdrawal, all your data will be discarded and will not be used anywhere in the study.

30

https://docs.google.com/forms/d/1dPN6D_53CRg4pkDYplfDg6fSnh6FaQ4Z7M0xI_11Fq4/edit

2/4

Fig. C.3 Participant Information Sheet (p. 2/4)

C.2 Information Sheet

25/10/2011

253

A Study of Movement Variability in Human-Humanoid Interaction Activities

Contact Details

If you have any questions about the project, you can contact Miguel by e-mail or telephone, using the details provided below:

7

Doctoral Researcher: Miguel P. Kochicale [mmp479@bham.ac.uk].
Department: School of Electronic Electrical and Systems Engineering

7

Primary Supervisor: Professor Chirs Baber [c.baber@bham.ac.uk]
Department: School of Electronic Electrical and Systems Engineering

7

Secondary Supervisor: Professor Martin Russell [m.j.russell@bham.ac.uk]
Department: School of Electronic Electrical and Systems Engineering

1. Statement of understanding/consent *

Tick all that apply.

9

I confirm that I have read and understand the participant information online sheet for this study. I have had the opportunity to ask questions if necessary and have had these answered satisfactorily.

9

I understand that I am able to withdraw from the experiment at any time without giving any reason. If I withdraw my data will be removed from the study and will be destroyed.

I understand that my personal data will be processed for the purposes detailed above, in accordance with the Data Protection Act 1998.

Based upon the above, I agree to take part in this study.

2. Your Name *

3. Email *

2. Antropometric Data

4. Participant Number (e.g. p11) *

30

5. What is your gender? *

Mark only one oval.

Male

Female

30

6. What is your age in years? *

7. What is your handeness? *

Mark only one oval.

30

Right

https://docs.google.com/forms/d/1dPN6D_53CRg4pkDYplfDg6fSh6FaQ4Z7M0xI_11Fq4/edit

3/4

Fig. C.4 Participant Information Sheet (p. 3/4)

Experiment Design

25/10/2018

A Study of Movement Variability in Human-Humanoid Interaction Activities

8. Have you received formal music training? *

Mark only one oval.

- No
- Yes (less than 5 years)
- Yes (more than 5 years)

9. What is your arm length in centimetres? *

Mark only one oval.

- Less than 45
- 45
- 46
- 47
- 48
- 49
- 50
- 51
- 52
- 53
- 54
- 55
- 56
- 57
- 58
- 59
- 60
- More than 60

10. What is your height in centimeters? *

11. What is your weight in kilograms? *



https://docs.google.com/forms/d/1dPN6D_53CRg4pkDYplfDg6fSnh6FaQ4Z7M0xI_11Fq4/edit

4/4

Fig. C.5 Participant Information Sheet (p. 4/4)

Appendix D

Additional Results for HII experiment

D.1 Time Series

Time series for horizontal arm movements (Figs D.1, D.2, and D.3) and vertical arm movements (Figs D.4, D.5, D.6). Both time series are only for a window size of 500 samples length. For the remained window size lengths of time series data, we refer the reader to download the data and code at Xochicale (2018).

Additional Results for HII experiment

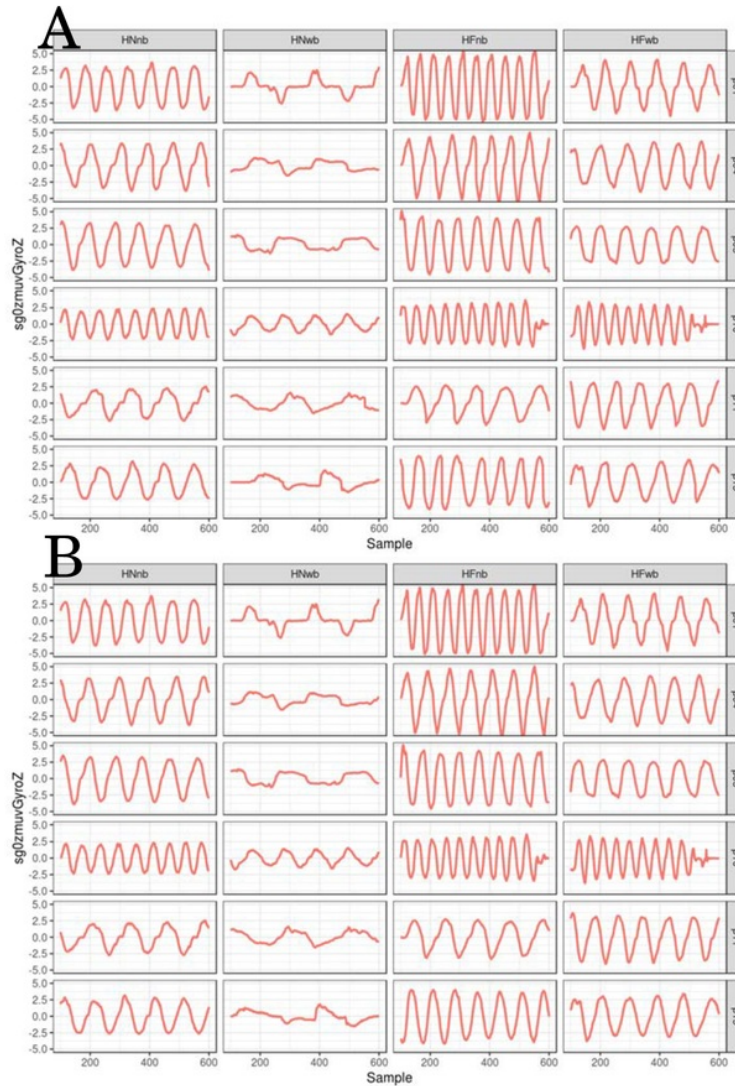


Fig. D.1 Time series for horizontal arm movements (sg0) Time series for sg0GyroZ are for six participants (*p01, p04, p05, p10, p11, p15*) for horizontal movements in normal and faster velocity with no beat (HNnb, HFnb) and with beat (HNwb, HFwb) using the normalised GyroZ axis (zmuvGyroZ) and two sensors attached to the participant wrist (HS01, HS02). R code to reproduce the figure is available from Kochicale (2018).

D.1 Time Series

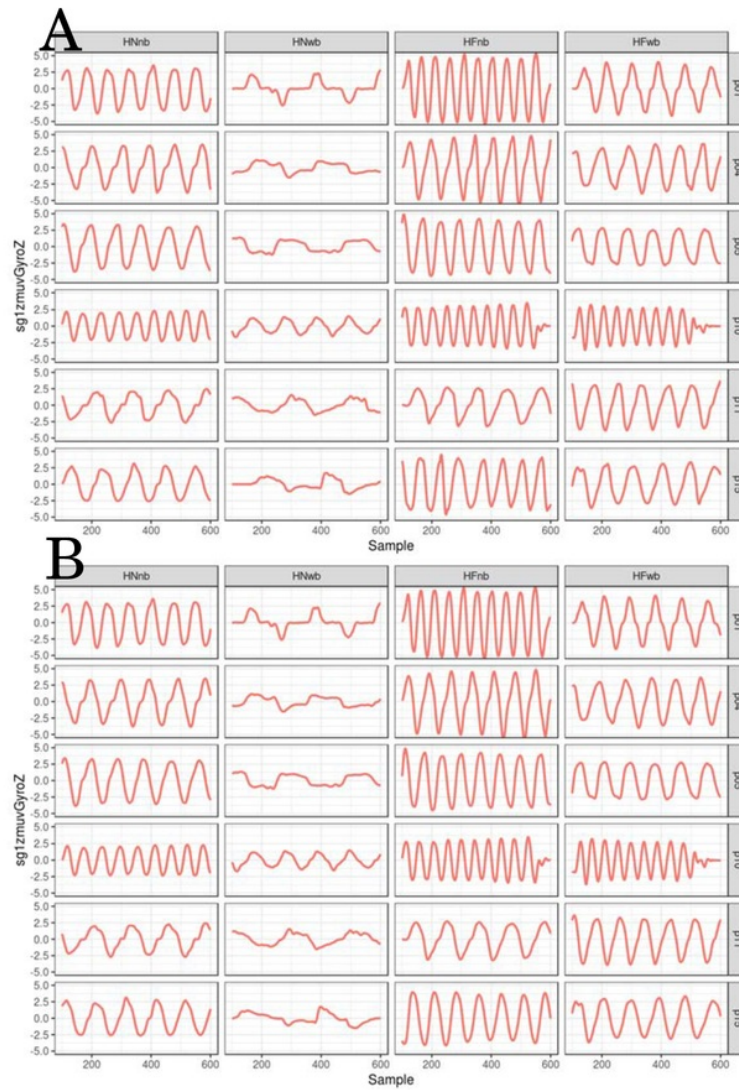


Fig. D.2 Time series for horizontal arm movements (sg1) Time series for sg1GyroZ for six participants (*p01, p04, p05, p10, p11, p15*) for horizontal movements in normal and faster velocity with no beat (HNnb, HFnb) and with beat (HNwb, HFwb) using the normalised GyroZ axis (zmuvGyroZ) and two sensors attached to the participant wrist (HS01, HS02). R code to reproduce the figure is available from Kochicale (2018).

Additional Results for HII experiment

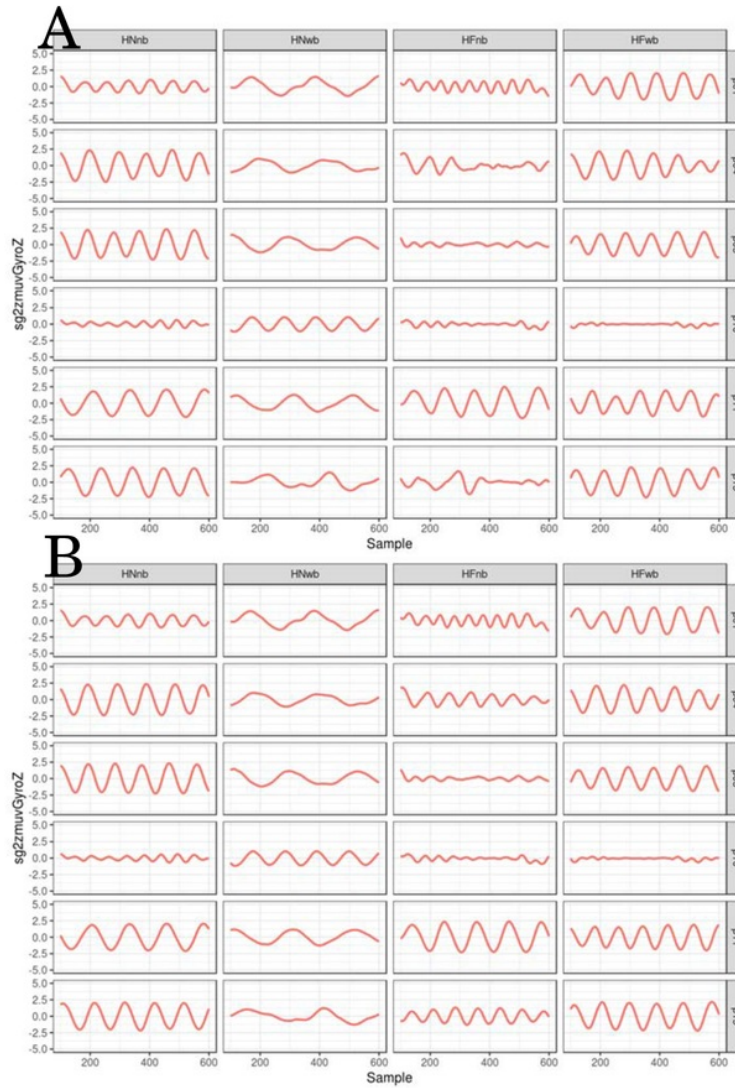


Fig. D.3 Time series for horizontal arm movements (sg2) Time series for sg2GyroZ for six participants (*p01, p04, p05, p10, p11, p15*) for horizontal movements in normal and faster velocity with no beat (HNnb, HFnb) and with beat (HNwb, HFwb) using the normalised GyroZ axis (zmuvGyroZ) and two sensors attached to the participant wrist (HS01, HS02). R code to reproduce the figure is available from Kochicale (2018).

D.1 Time Series

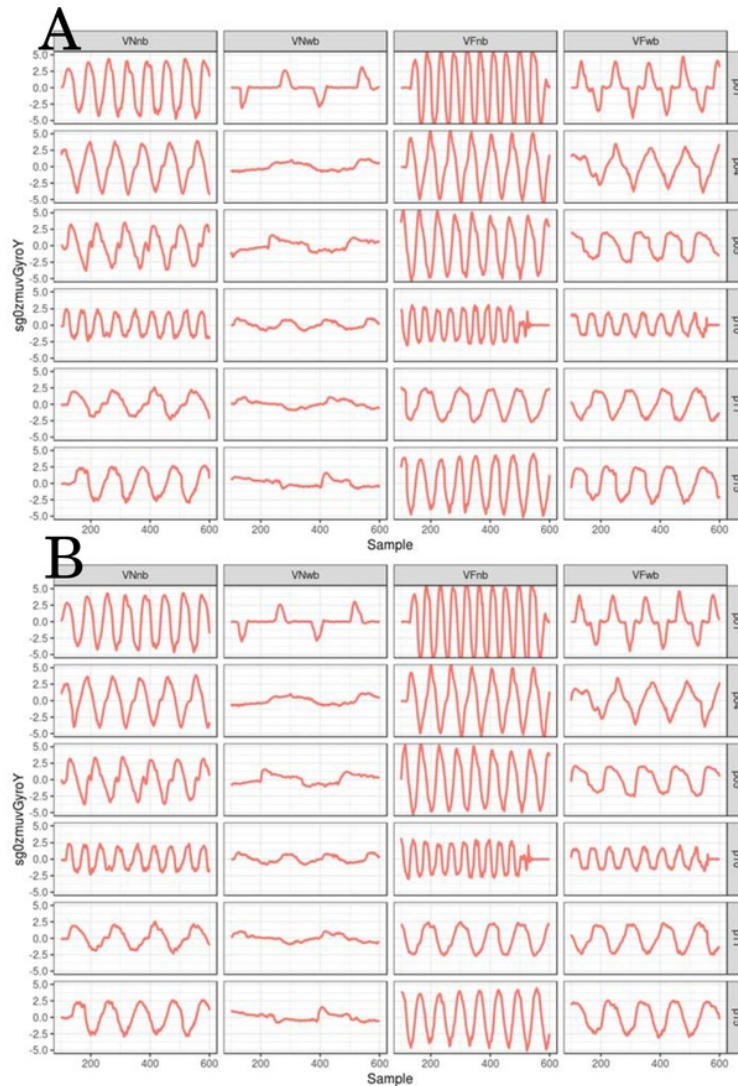


Fig. D.4 Time series for vertical arm movements (sg0) Time series for sg0GyroY are for six participants (*p01, p04, p05, p10, p11, p15*) for vertical movements in normal and faster velocity with no beat (VNnb, VFnb) and with beat (VNwb, VFwb) using the normalised GyroZ axis (zmuvGyroY) and two sensors attached to the participant wrist (HS01, HS02). R code to reproduce the figure is available from Xochicale (2018).

Additional Results for HII experiment

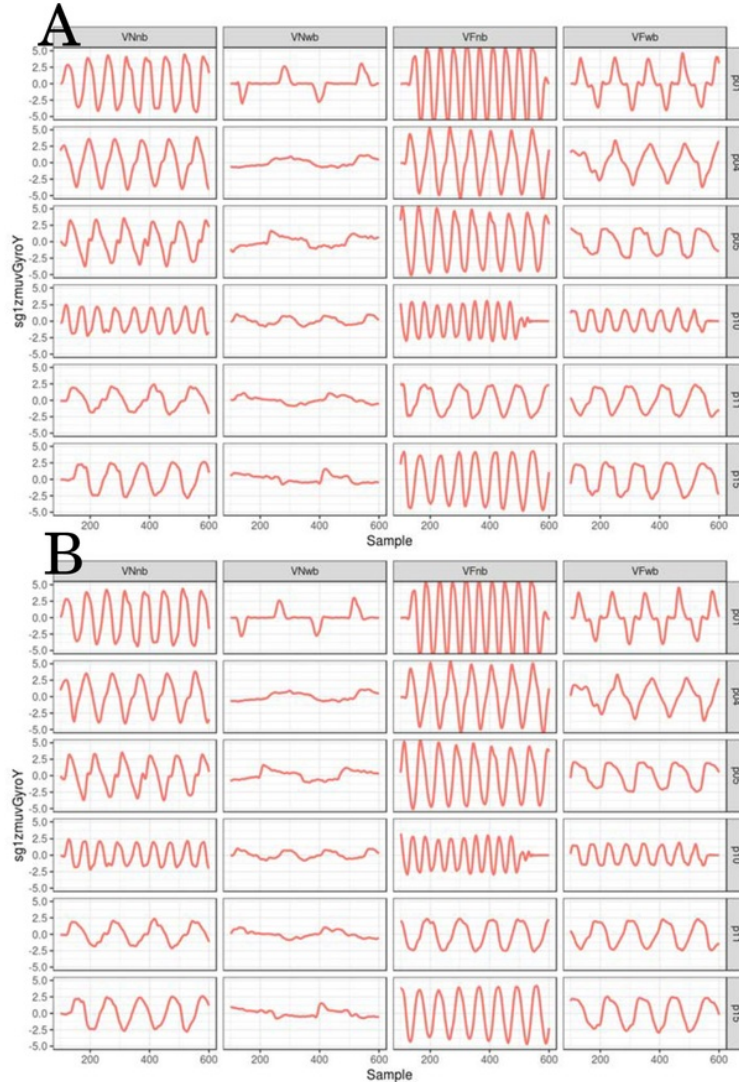


Fig. D.5 Time series for vertical arm movements (sg1) Time series for sg1GyroY for six participants (*p01, p04, p05, p10, p11, p15*) for vertical movements in normal and faster velocity with no beat (VNnb, VFnb) and with beat (VNwb, VFwb) using the normalised GyroZ axis (zmuvGyroY) and two sensors attached to the participant wrist (HS01, HS02). R code to reproduce the figure is available from Xochicale (2018).

D.1 Time Series

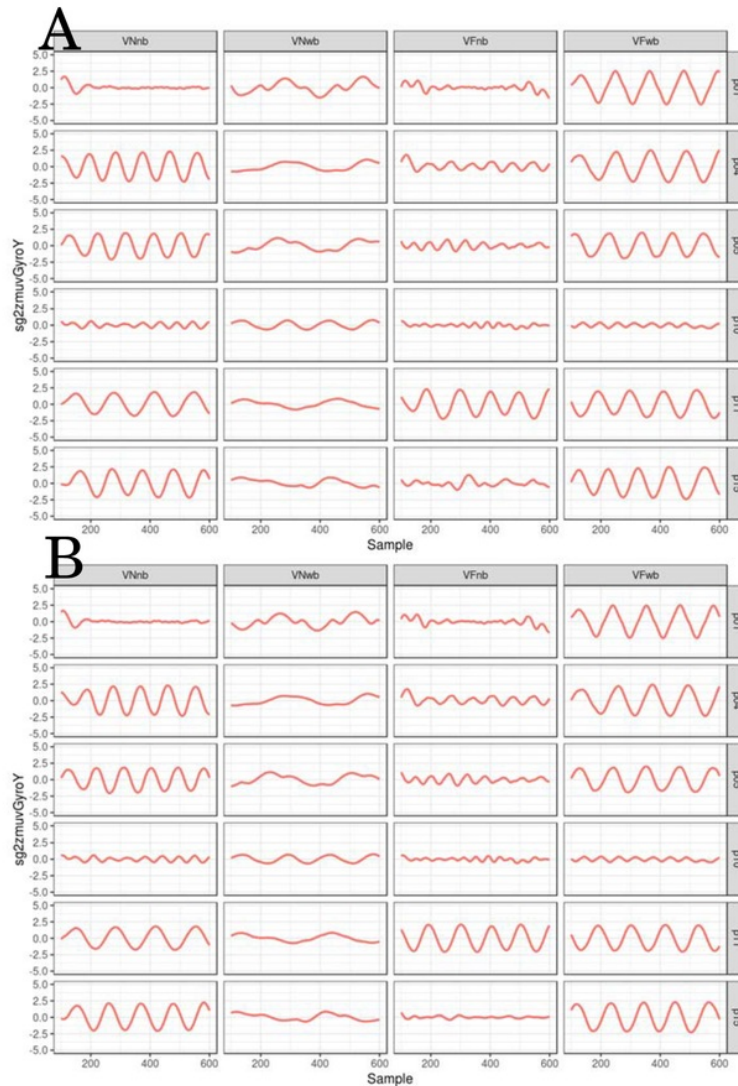


Fig. D.6 Time series for vertical arm movements (sg2) Time series for sg2GyroY for six participants (*p01, p04, p05, p10, p11, p15*) for vertical movements in normal and faster velocity with no beat (VNnb, VFnb) and with beat (VNwb, VFwb) using the normalised GyroY axis (zmuvGyroY) and two sensors attached to the participant wrist (HS01, HS02). R code to reproduce the figure is available from Xochicale (2018).

D.2 Embedding parameters

D.2.1 Minimum dimension embedding values

Values of minimum embedding dimensions for horizontal normal arm movements with no beat (HNnb) and horizontal faster arm movements with no beat (HFnb) are shown in Fig D.7 which values of minimum embedding dimensions present a fluctuation of values between four and seven over six participants. It can also be noted a slightly variation of minimum embedding dimension values over participants when comparing HS01 and HS02 (Fig D.7(A, B)). With regards to the smoothness of the time series, the minimum embedding values are also smoothed showing less variations of values over six participants (Fig D.7).

Values of minimum embedding dimension for horizontal normal arm movements with beat (HNwb) and horizontal faster arm movements with beat (HFwb) are shown in Fig D.8 where is shown a fluctuations of values for minimum embedding dimension between five and seven. Similarly as in Fig D.7, Fig D.8 show changes of minimum embedding dimension between participants and the smoothness of the time series also affects the smoothness of minimum embedding dimension values.

Values of minimum embedding dimension for vertical arm movements with no beat
130 are shown in Figs D.9(A, B) where the smoothness of the time series have little effect
57 on the minimum embedding dimension values, whereas smoothness of time series affects
the smoothness of the minimum embedding values for vertical faster arm movements
130 with no beats (Fig D.9(C, D)).

Fig D.10 shows the variation of minimum embedding values for vertical arm movements with beat where the smoothness of the time series affects both vertical normal and vertical faster movements with a slight decrease on each of the values as the smoothness increase.

D.2 Embedding parameters

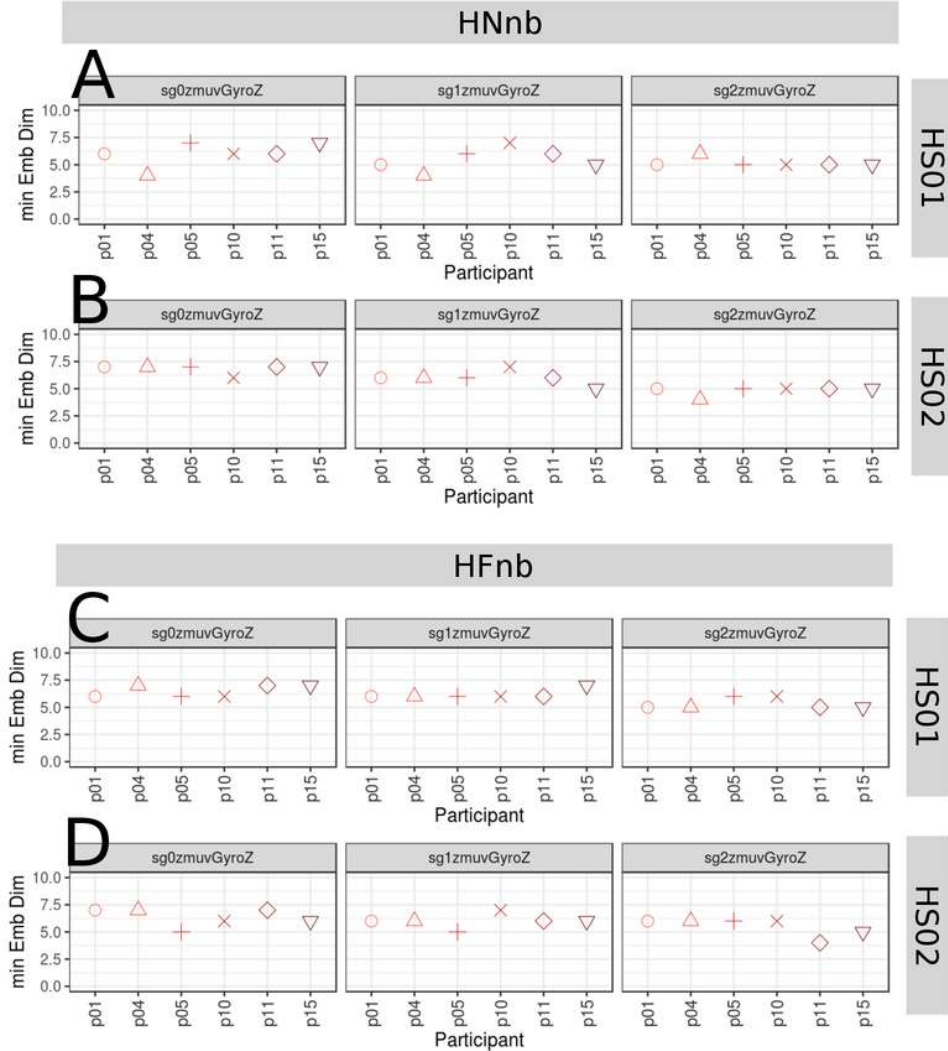


Fig. D.7 Minimum embedding dimensions for horizontal arm movements (no beat). (A, B) Horizontal Normal with no beat (HNnb), and (C, D) Horizontal Faster with no beat (HFnb) movements. (A, C) Sensor 01 attached to the participant (HS01), and (B, D) sensor 02 attached to the participant (HS02). Minimum embedding dimensions are for six participants (p01, p04, p05, p10, p11, p15) with three smoothed signals (sg0zmuvGyroZ, sg1zmuvGyroZ and sg2zmuvGyroZ) and window lenght of 10-sec (500 samples). R code to reproduce the figure is available from Xochicale (2018).

Additional Results for HII experiment

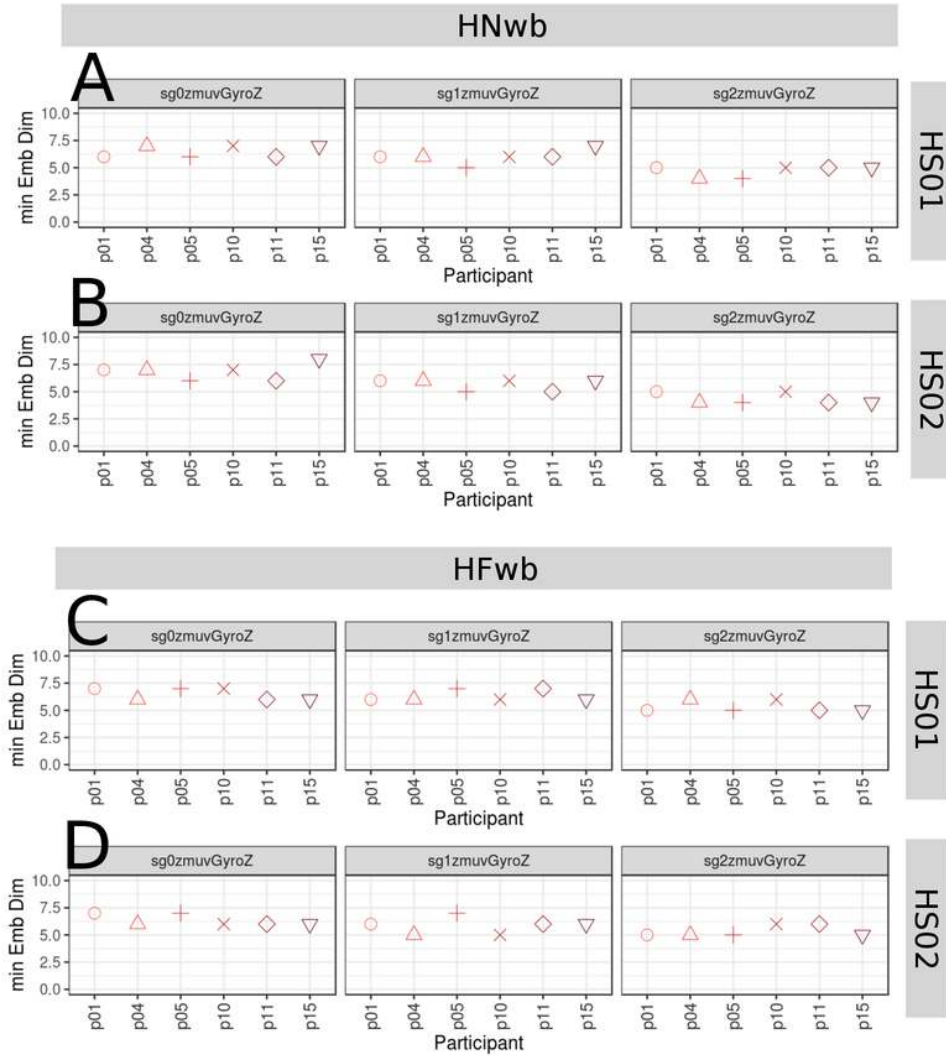


Fig. D.8 Minimum embedding dimensions for horizontal arm movements (with beat). (A, B) Horizontal Normal with beat (HNwb), and (C, D) Horizontal Faster with beat (HFwb) movements. (A, C) Sensor 01 attached to the participant (HS01), and (B, D) sensor 02 attached to the participant (HS02). Minimum embedding dimensions are for six participants (p01, p04, p05, p10, p11, p15) with three smoothed signals (sg0zmuvGyroZ, sg1zmuvGyroZ and sg2zmuvGyroZ) and window lenght of 10-sec (500 samples). R code to reproduce the figure is available from Xochicale (2018).

D.2 Embedding parameters

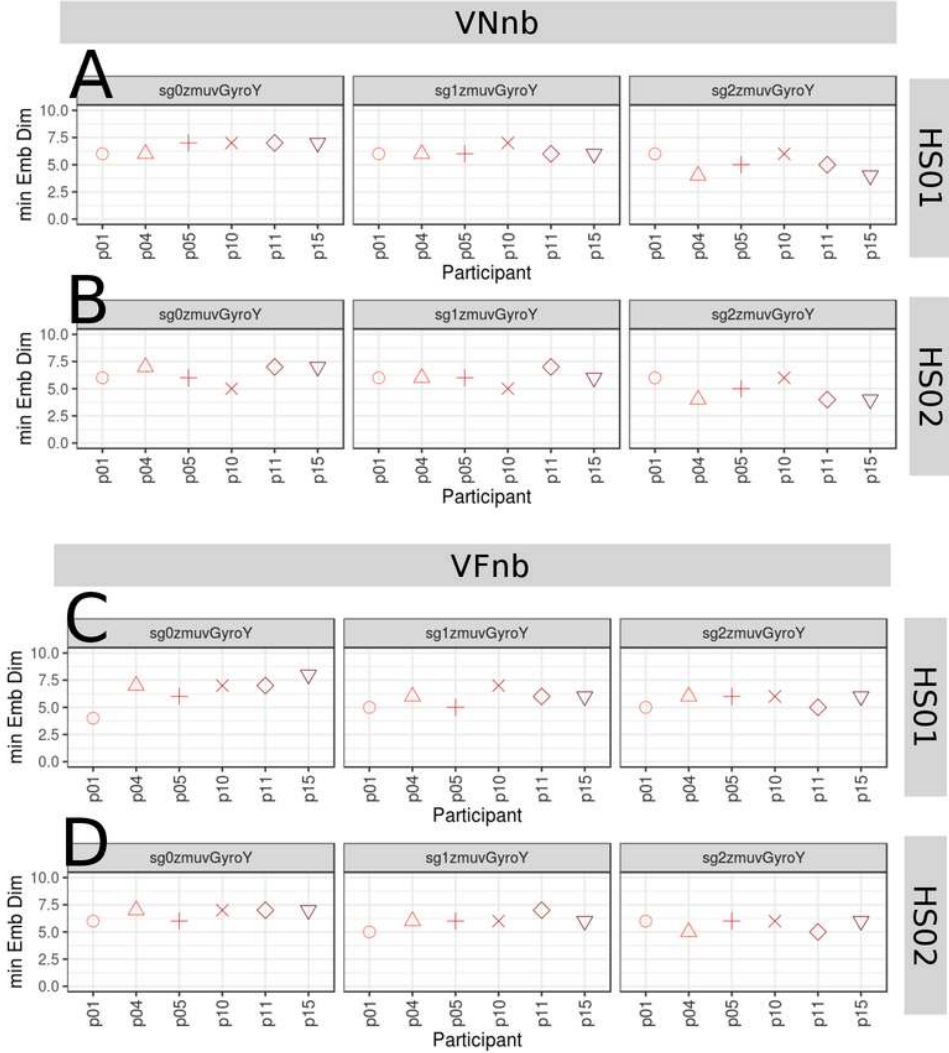


Fig. D.9 Minimum embedding dimensions for vertical arm movements (no beat). (A, B) Vertical Normal with no beat (VNnb), and (C, D) Vertical Faster with no beat (VFnb) movements. (A, C) Sensor 01 attached to the participant (HS01), and (B, D) sensor 02 attached to the participant (HS02). Minimum embedding dimensions are for six participants (p01, p04, p05, p10, p11, p15) with three smoothed signals (sg0zmuvGyroZ, sg1zmuvGyroZ and sg2zmuvGyroZ) and window lenght of 10-sec (500 samples). R code to reproduce the figure is available from Xochicale (2018).

Additional Results for HII experiment

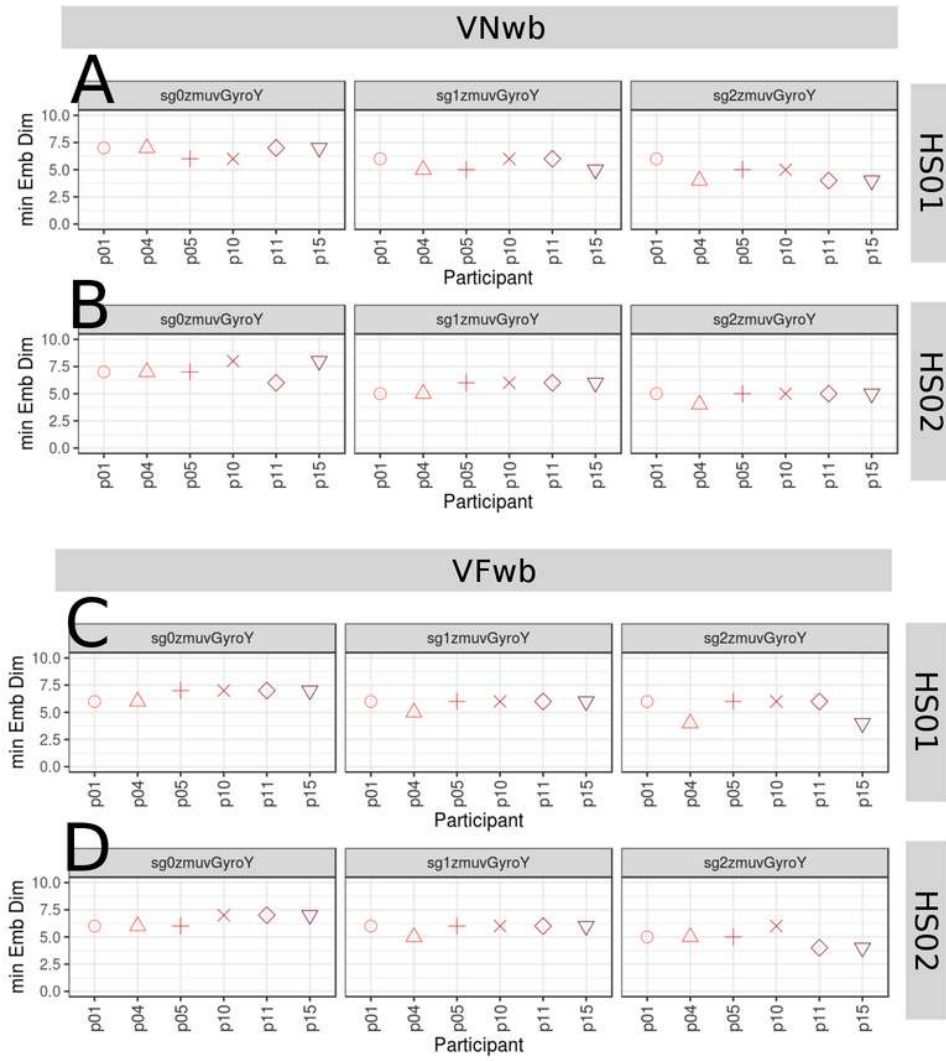


Fig. D.10 Minimum embedding dimensions for vertical arm movements (with beat). (A, B) Vertical Normal with beat (VNwb), and (C, D) Vertical Faster with beat (VFwb) movements. (A, C) Sensor 01 attached to the participant (HS01), and (B, D) sensor 02 attached to the participant (HS02). Minimum embedding dimensions are for six participants (p01, p04, p05, p10, p11, p15) with three smoothed signals (sg0zmuvGyroZ, sg1zmuvGyroZ and sg2zmuvGyroZ) and window lenght of 10-sec (500 samples). R code to reproduce the figure is available from Xochicale (2018).

D.2 Embedding parameters

D.2.2 Minimum delay embedding values

The general behavior for horizontal and vertical arm movements with regards to the smoothness of the time series is that the first minimum AMI values increase as the increase of the smoothness which is due to smoothed AMI curves (Figs D.11, D.12, D.13 and D.14).

Fluctuations of minimum AMI values from sensor HS01 are more evident than for sensor HS02 for horizontal normal arm movements with no beat (Fig D.11(A, B)), whereas fluctuations of minimum AMI values from sensors HS01 and HS02 for horizontal faster arm movements with no beat appear to be similar (Fig D.11(C, D)). Similarly, fluctuations of minimum AMI values are more evidently for horizontal normal arm movements with beat (Fig D.12(A, B)) than horizontal faster arm movements with beat (Fig D.12(C, D)).

As smoothness increase, minimum AMI values for vertical normal arm movements with no beat appear to fluctuate more (Figs D.13(A, B)) than vertical faster arm movements with no beat (Figs D.13(C, D)), whereas for vertical normal and vertical faster arm movements with beat the fluctuation of minimum AMI values is more evidently, specially when comparing vertical normal arm movements (Figs D.14(A, B)) with vertical faster arm movements (Figs D.14(C, D)).

Additional Results for HII experiment

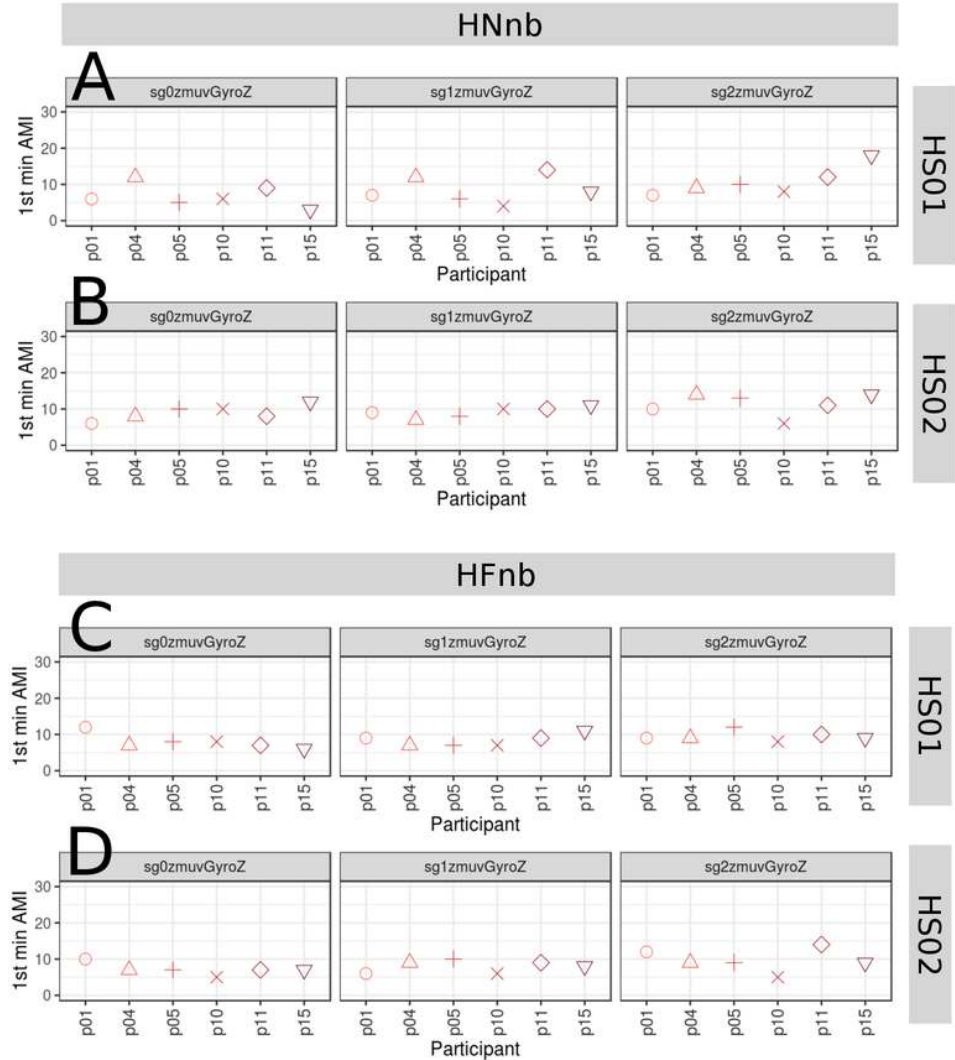


Fig. D.11 First minimum AMI values for horizontal arm movements (no beat). (A, B) Horizontal Normal with no beat (HNnb), and (C, D) Horizontal Faster with no beat (HFnb) movements. (A, C) Sensor attached to the participant (HS01), and (B, D) sensor attached to the participant (HS02). First minimum AMI values are for six participants (p01, p04, p05, p10, p11, p15) with three smoothed signals (sg0zmuvGyroZ, sg1zmuvGyroZ and sg2zmuvGyroZ) and window lenght of 10-sec (500 samples). R code to reproduce the figure is available from Xochicale (2018).

D.2 Embedding parameters

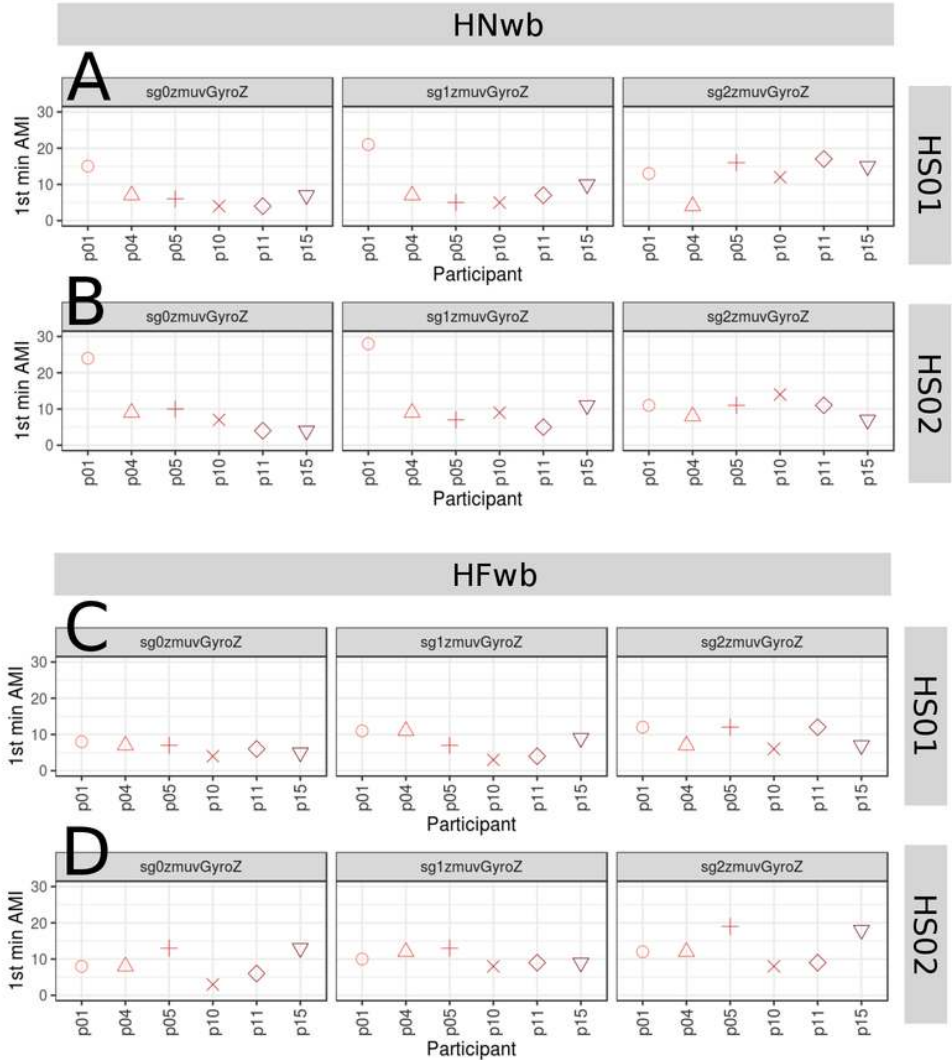


Fig. D.12 First minimum AMI values for horizontal arm movements (with beat). (A, B) Horizontal Normal with beat (HNwb), and (C, D) Horizontal Faster with beat (HFwb) movements. (A, C) Sensor attached to the participant (HS01), and (B, D) sensor attached to the participant (HS02). First minimum AMI values are for six participants (p01, p04, p05, p10, p11, p15) with three smoothed signals (sg0zmuvGyroZ, sg1zmuvGyroZ and sg2zmuvGyroZ) and window lenght of 10-sec (500 samples). R code to reproduce the figure is available from Xochicale (2018).

Additional Results for HII experiment

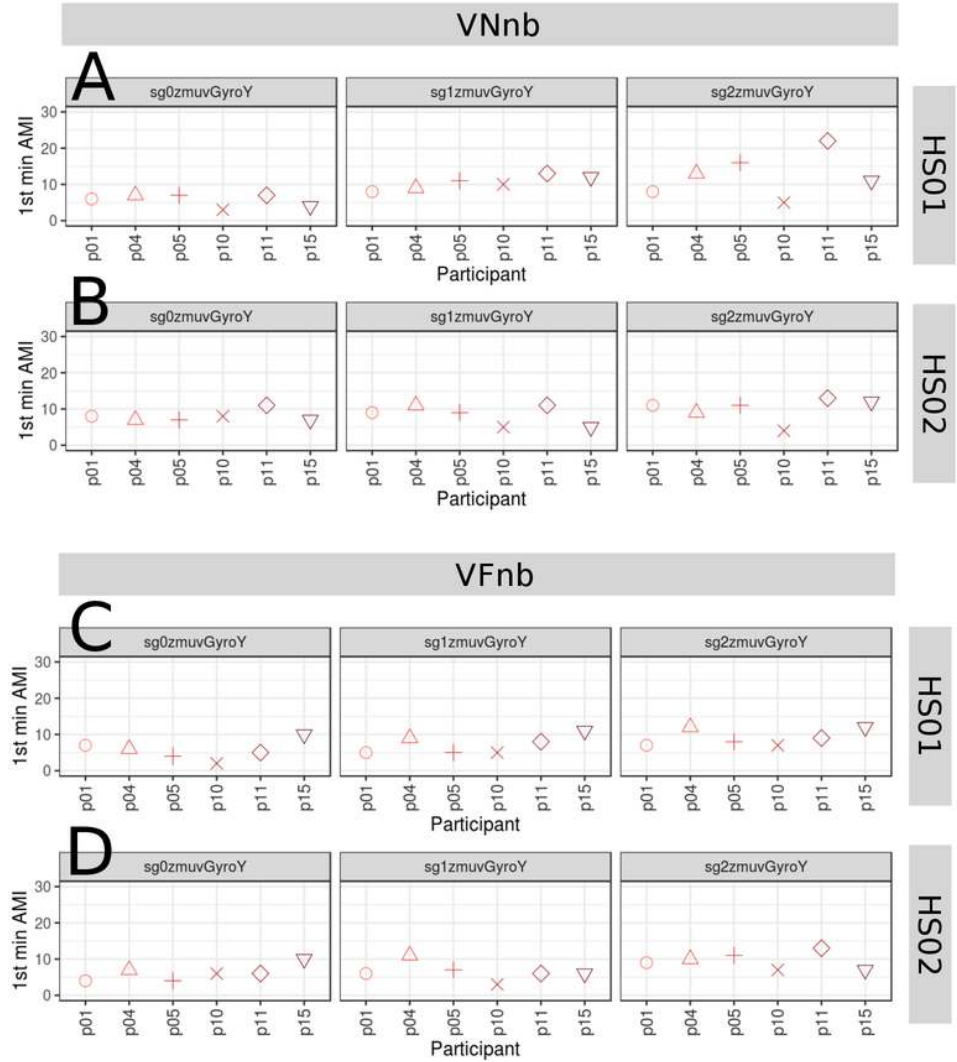


Fig. D.13 First minimum AMI values for vertical arm movements (no beat).
 (A, B) Vertical Normal with no beat (VNb), and (C, D) Vertical Faster with no beat (VFnb) movements. (A, C) Sensor attached to the participant (HS01), and (B, D) sensor attached to the participant (HS02). First minimum AMI values are for six participants (p01, p04, p05, p10, p11, p15) with three smoothed signals (sg0zmuvGyroZ, sg1zmuvGyroZ and sg2zmuvGyroZ) and window lenght of 10-sec (500 samples). R code to reproduce the figure is available from Xochicale (2018).

D.2 Embedding parameters

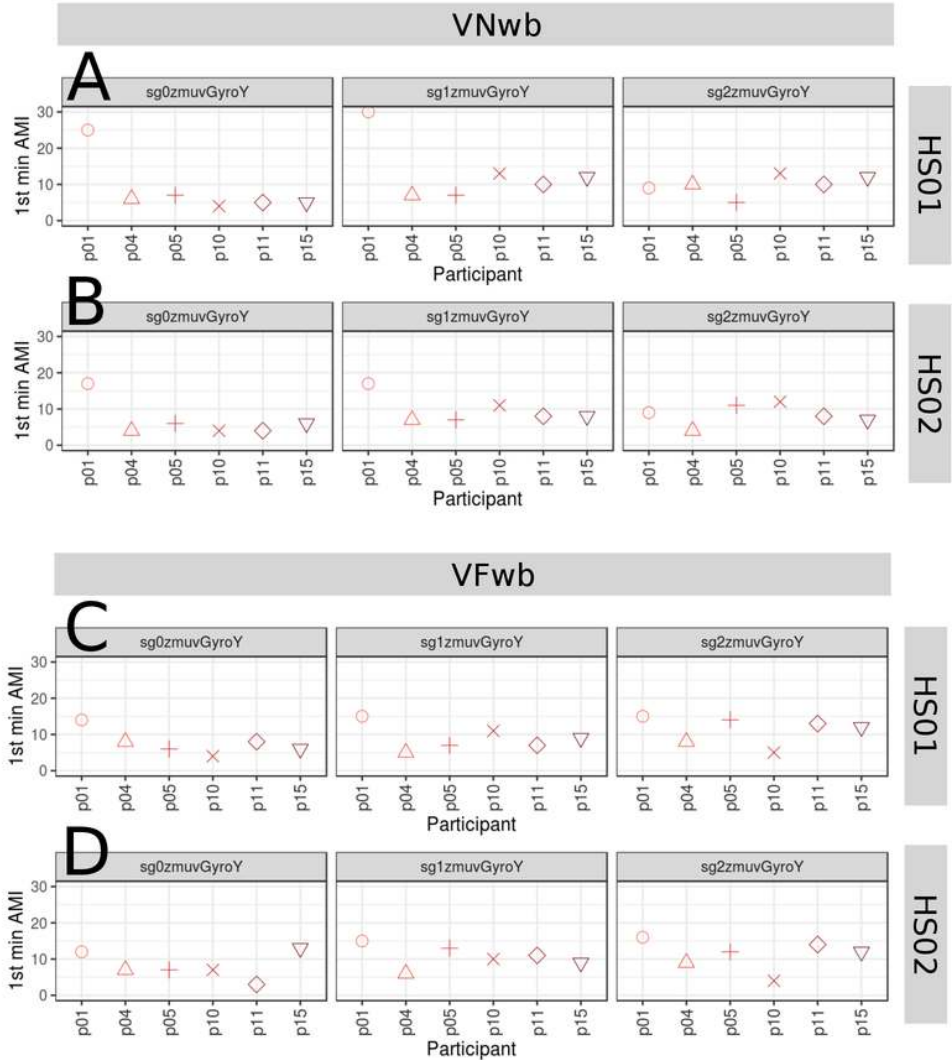


Fig. D.14 First minimum AMI values for vertical arm movements (with beat). (A, B) Vertical Normal with beat (VNwb), and (C, D) Vertical Faster with beat (VFwb) movements. (A, C) Sensor attached to the participant (HS01), and (B, D) sensor attached to the participant (HS02). First minimum AMI values are for six participants (p01, p04, p05, p10, p11, p15) with three smoothed signals (sg0zmuvGyroZ, sg1zmuvGyroZ and sg2zmuvGyroZ) and window lenght of 10-sec (500 samples). R code to reproduce the figure is available from Xochicale (2018).

D.3 RSSs

The following Figs. [D.17](#), [D.18](#), [D.15](#), [D.16](#), [D.21](#), [D.22](#), [D.19](#), [D.20](#) illustrate reconstructed state spaces of participant *p04* with a window length size of 500 samples. We refer the reader to download the data and code at Xochicale (2018) for the remained window size lengths and other participants.

D.3 RSSs

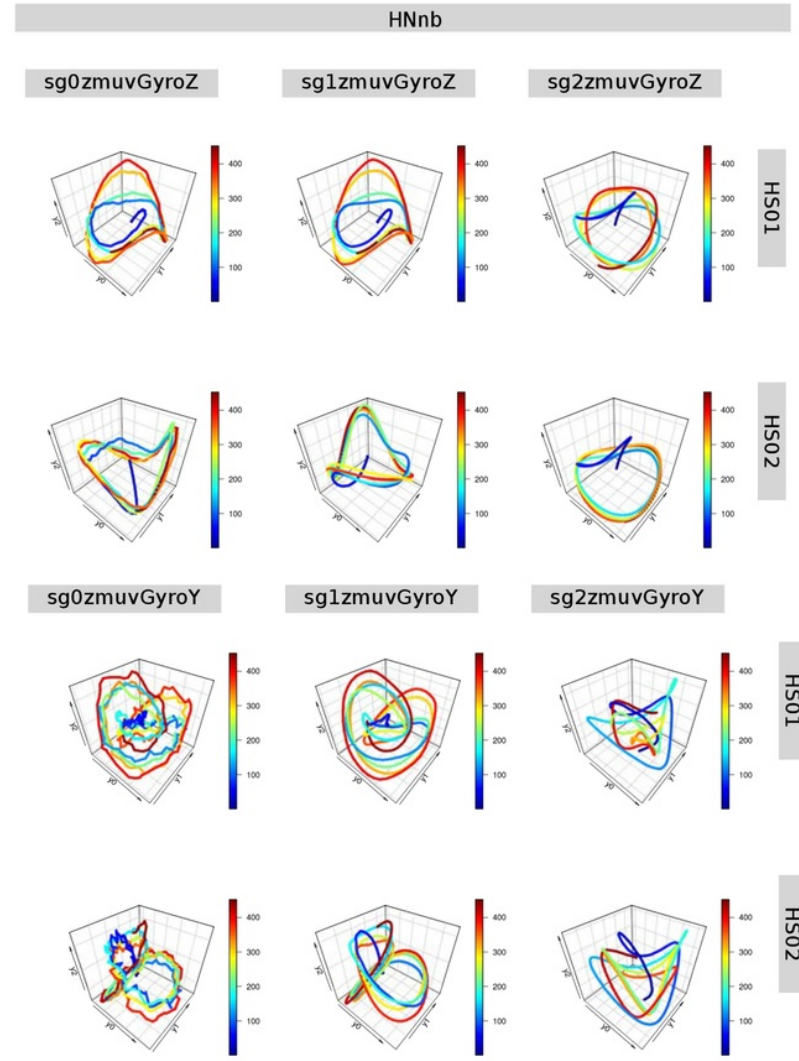


Fig. D.15 RSSs for horizontal normal arm movements (no beat). Reconstructed state spaces of participant $p04$ with time series for raw-normalised (sg0), normalised-smoothed 1 (sg1) and normalised-smoothed 2 (sg2), with sensors attached to the participant (HS01, HS02). Reconstructed state spaces were computed with embedding parameters $m = 9$, $\tau = 6$. R code to reproduce the figure is available from Xochicale (2018).

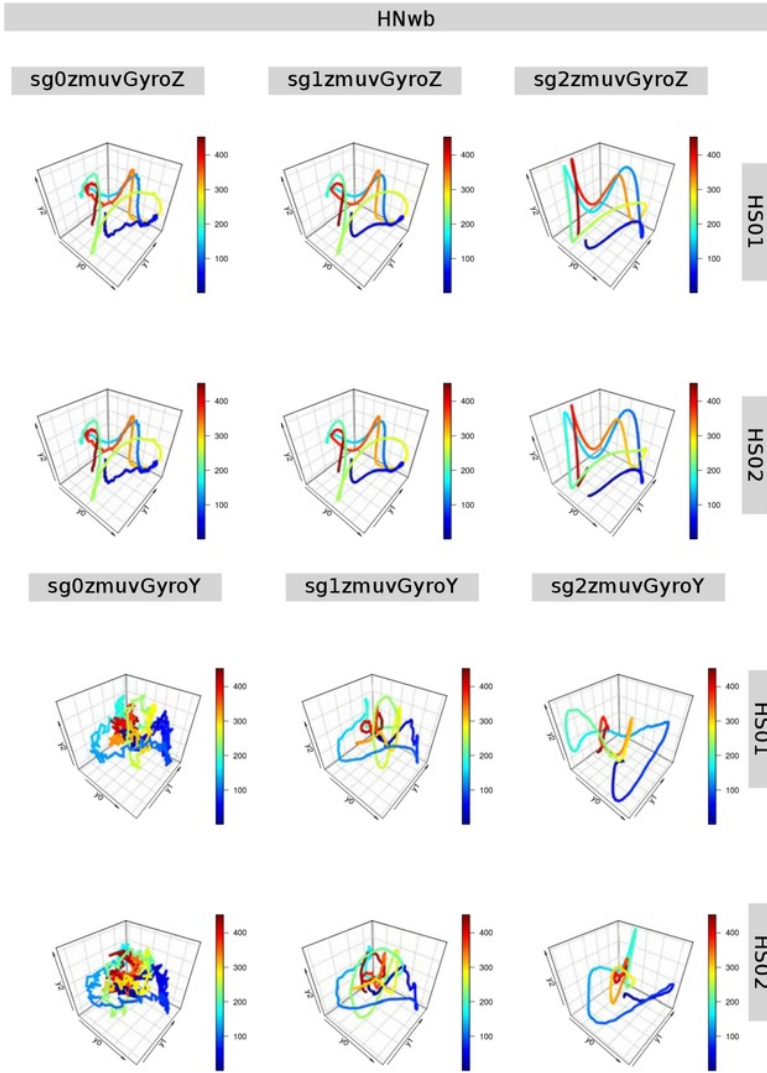


Fig. D.16 RSSs for horizontal normal arm movements (with beat). Reconstructed state spaces of participant $p04$ with time series for raw-normalised (sg0), normalised-smoothed 1 (sg1) and normalised-smoothed 2 (sg2), with sensors attached to the participant (HS01, HS02). Reconstructed state spaces were computed with embedding parameters $m = 9$, $\tau = 6$. R code to reproduce the figure is available from Kochicale (2018).

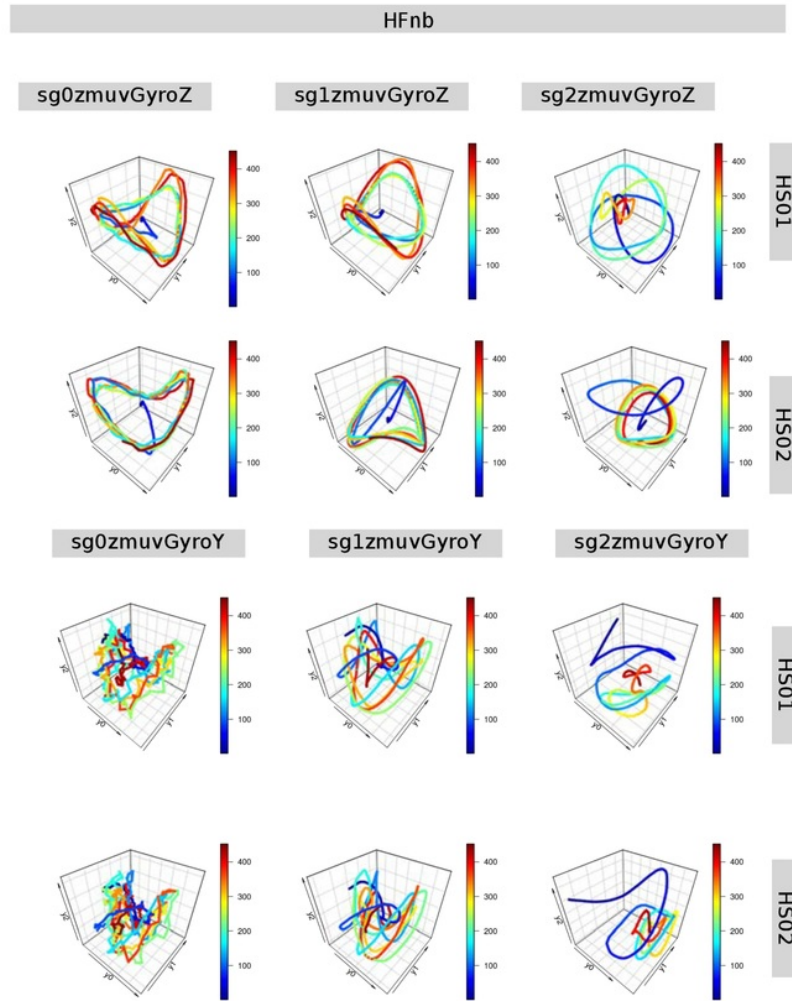


Fig. D.17 RSSs for horizontal faster arm movements (no beat). Reconstructed state spaces of participant $p04$ with time series for raw-normalised (sg0), normalised-smoothed 1 (sg1) and normalised-smoothed 2 (sg2), with sensors attached to the participant (HS01, HS02). Reconstructed state spaces were computed with embedding parameters $m = 9$, $\tau = 6$. R code to reproduce the figure is available from Xochicale (2018).

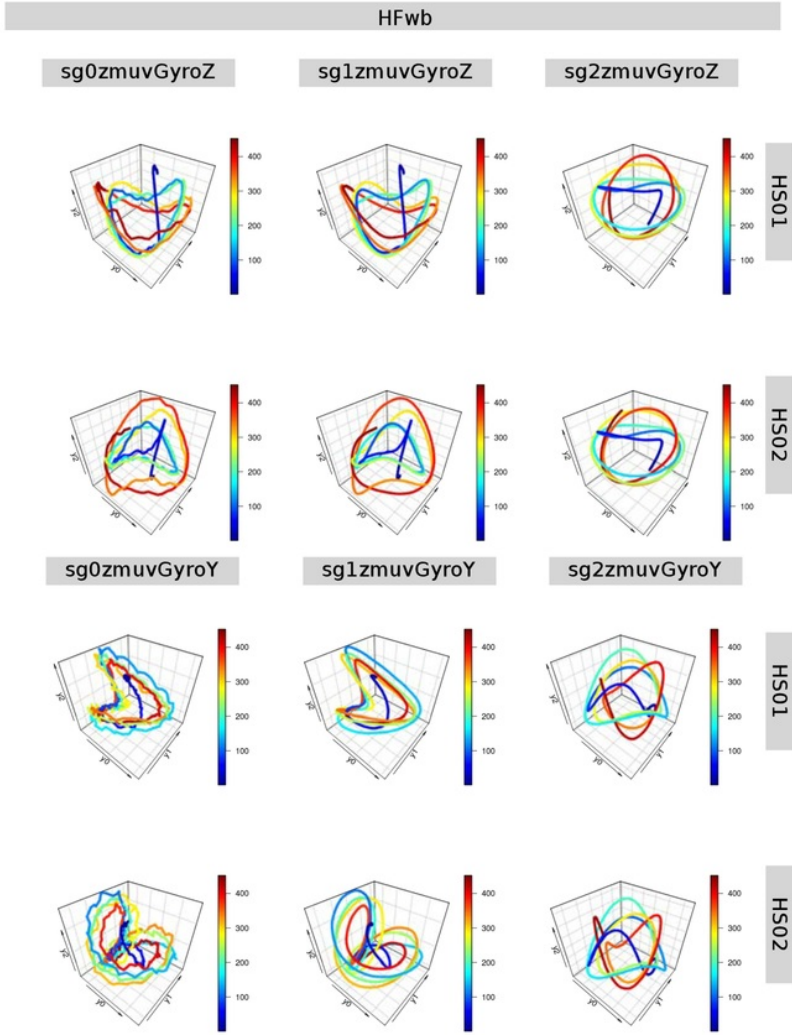


Fig. D.18 RSSs for horizontal faster arm movements (with beat). Reconstructed state spaces of participant $p04$ with time series for raw-normalised (sg0), normalised-smoothed 1 (sg1) and normalised-smoothed 2 (sg2), with sensors attached to the participant (HS01, HS02). Reconstructed state spaces were computed with embedding parameters $m = 9$, $\tau = 6$. R code to reproduce the figure is available from Kochicale (2018).

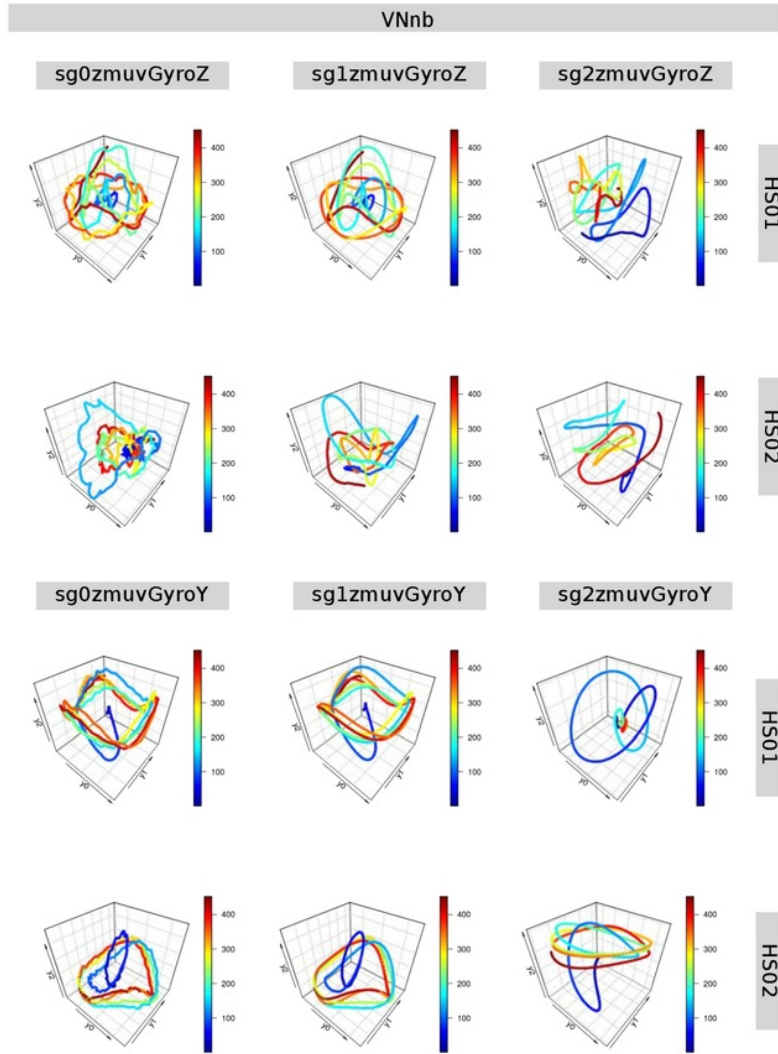


Fig. D.19 RSSs for vertical normal arm movements (no beat). Reconstructed state spaces of participant $p04$ with time series for raw-normalised (sg0), normalised-smoothed 1 (sg1) and normalised-smoothed 2 (sg2), with sensors attached to the participant (HS01, HS02). Reconstructed state spaces were computed with embedding parameters $m = 9$, $\tau = 6$. R code to reproduce the figure is available from Xochicale (2018).

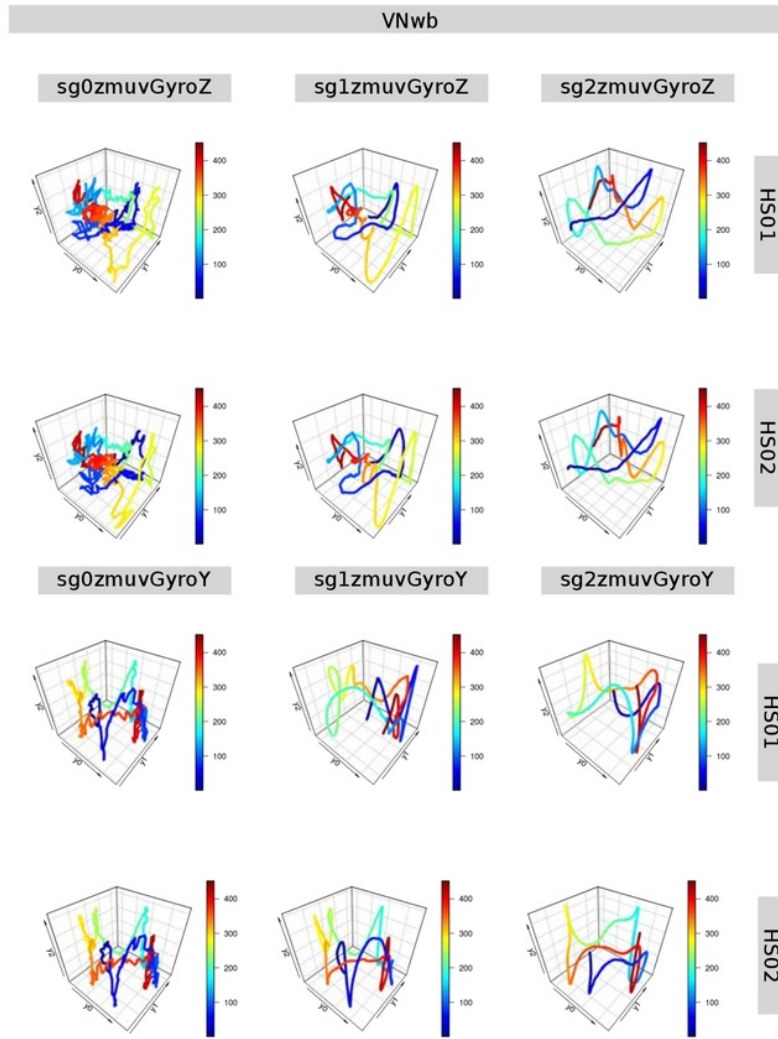


Fig. D.20 **RSSs for vertical normal arm movements (with beat).** Reconstructed state spaces of participant $p04$ with time series for raw-normalised (sg0), normalised-smoothed 1 (sg1) and normalised-smoothed 2 (sg2), with sensors attached to the participant (HS01, HS02). Reconstructed state spaces were computed with embedding parameters $m = 9$, $\tau = 6$. R code to reproduce the figure is available from Xochicale (2018).

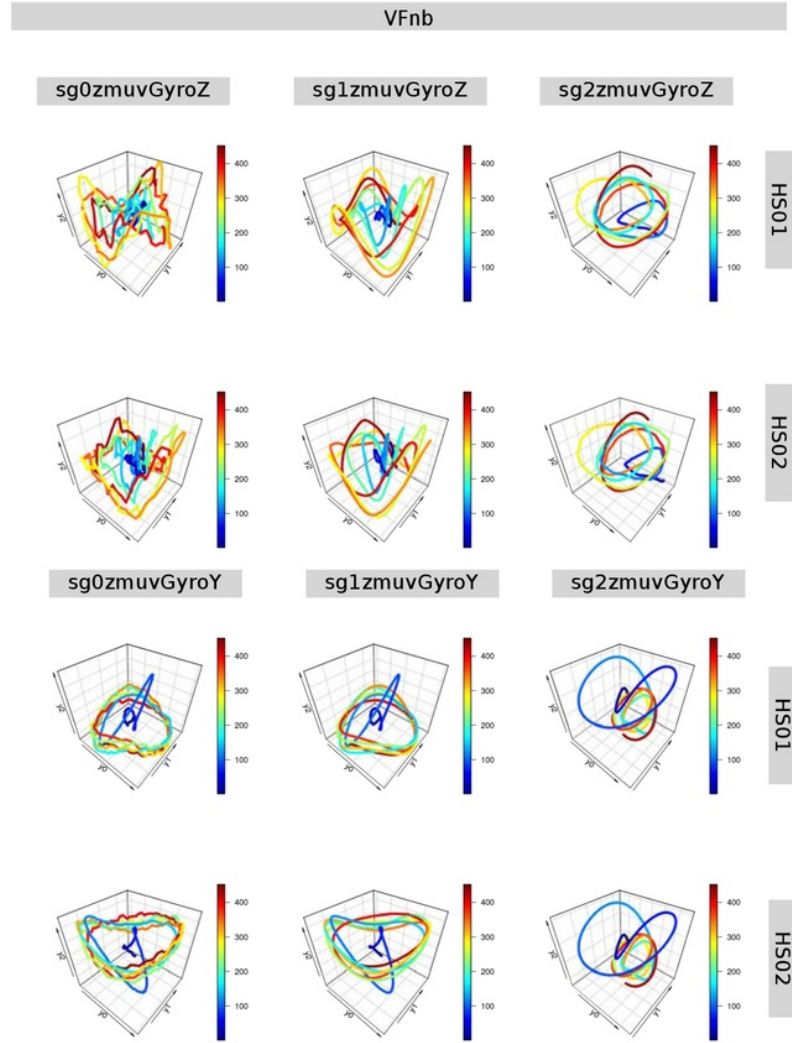


Fig. D.21 RSSs for vertical faster arm movements (no beat). Reconstructed state spaces of participant $p04$ with time series for raw-normalised (sg0), normalised-smoothed 1 (sg1) and normalised-smoothed 2 (sg2), with sensors attached to the participant (HS01, HS02). Reconstructed state spaces were computed with embedding parameters $m = 9$, $\tau = 6$. R code to reproduce the figure is available from Xochicale (2018).

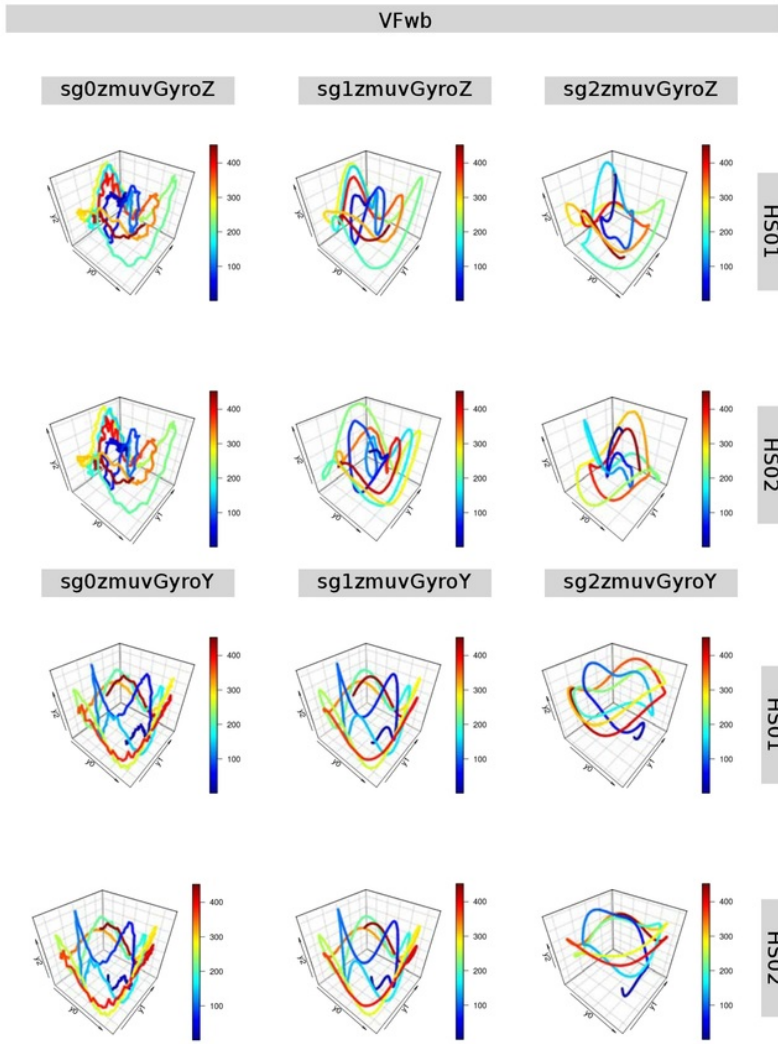


Fig. D.22 RSSs for vertical faster arm movements (with beat). Reconstructed state spaces of participant p04 with time series for raw-normalised (sg0), normalised-smoothed 1 (sg1) and normalised-smoothed 2 (sg2), with sensors attached to the participant (HS01, HS02). Reconstructed state spaces were computed with embedding parameters $m = 9$, $\tau = 6$. R code to reproduce the figure is available from Xochicale (2018).

D.4 RPs

The following Figs. D.24, D.23, D.26, D.25 illustrate reconstructed state spaces of participant $p04$ with a window length size of 500 samples. We refer the reader to download the data and code at Xochicale (2018) for the remained window size lengths and other participants.

Additional Results for HII experiment

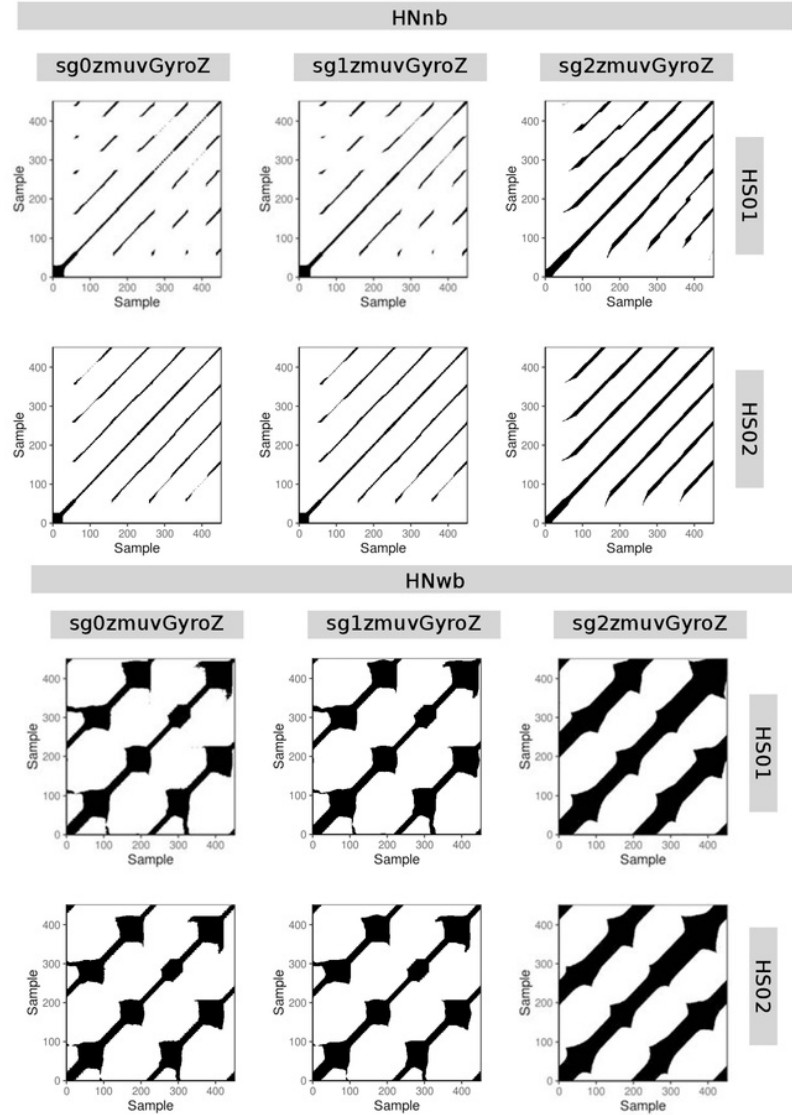


Fig. D.23 RPs for horizontal normal arm movements. Recurrence plots of participant p04 for horizontal normal movements with no beat (HNnb) and horizontal normal movements with beat (HNwb). Time series for raw-normalised (sg0zmuvGyroZ), normalised-smoothed 1 (sg1zmuvGyroZ) and normalised-smoothed 2 (sg2zmuvGyroZ) with HS sensors attached to the participant (HS01, HS02). Recurrence plots were computed with embedding parameters $m = 9$, $\tau = 6$ and recurrence threshold $\epsilon = 1$. R code to reproduce the figure is available from Xochicale (2018).

D.4 RPs

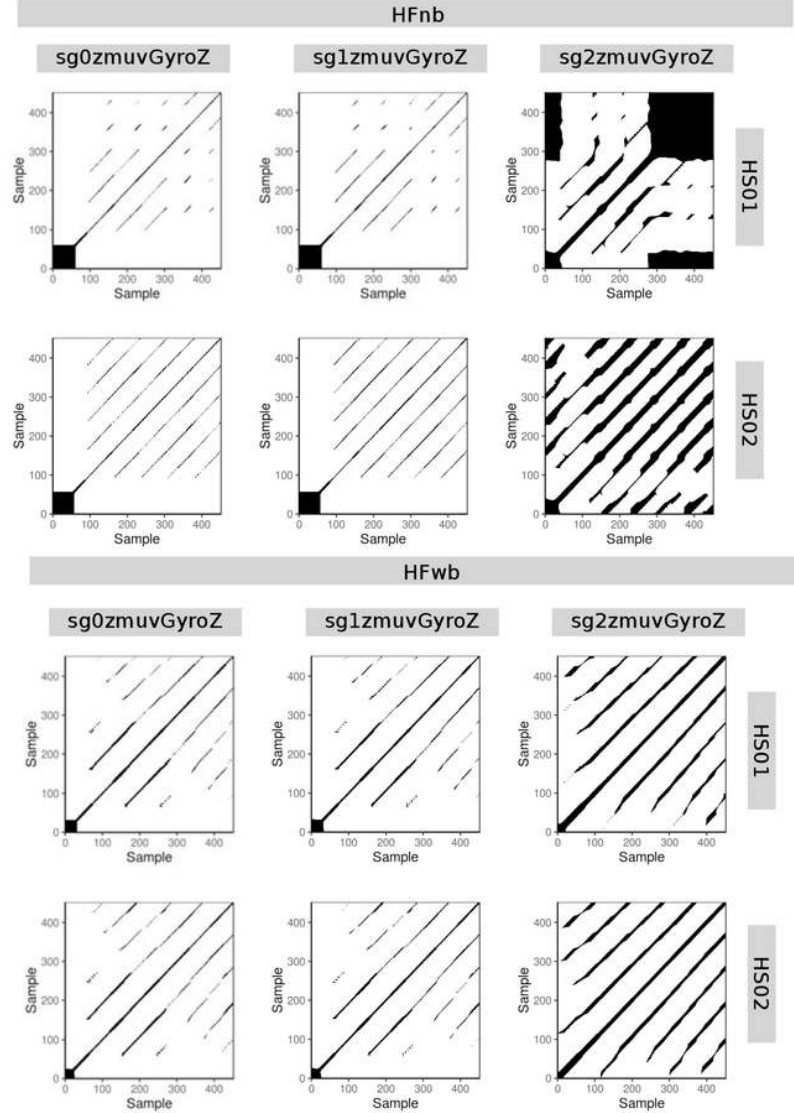


Fig. D.24 RPs for horizontal faster arm movements. Recurrence plots of participant *p04* for horizontal faster movements with no beat (HNnb) and horizontal faster movements with beat (HFwb). Time series for raw-normalised (sg0zmuvGyroZ), normalised-smoothed 1 (sg1zmuvGyroZ) and normalised-smoothed 2 (sg2zmuvGyroZ) with $\textcolor{red}{1}$ sensors attached to the participant (HS01, HS02). Recurrence plots were computed with embedding parameters $m = 9$, $\tau = 6$ and recurrence threshold $\epsilon = 1$. R code to reproduce the figure is available from Xochicale (2018).

Additional Results for HII experiment

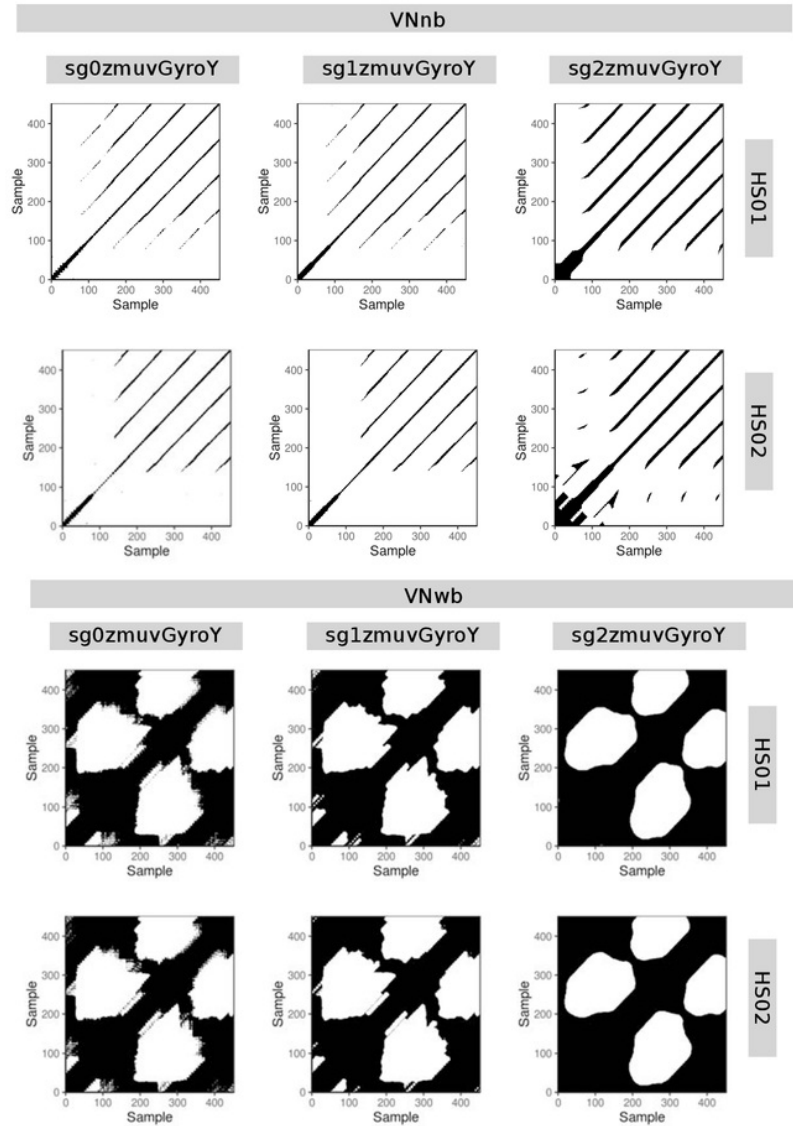


Fig. D.25 RPs for vertical normal arm movements. Recurrence plots of participant $p04$ for horizontal normal movements with no beat (VNnb) and horizontal normal movements with beat (VFwb). Time series for raw-normalised (sg0zmuvGyroY), normalised-smoothed 1 (sg1zmuvGyroY) and normalised-smoothed 2 (sg2zmuvGyroY) with HS sensors attached to the participant (HS01, HS02). Recurrence plots were computed with embedding parameters $m = 9$, $\tau = 6$ and recurrence threshold $\epsilon = 1$. R code to reproduce the figure is available from Xochicale (2018).

D.4 RPs

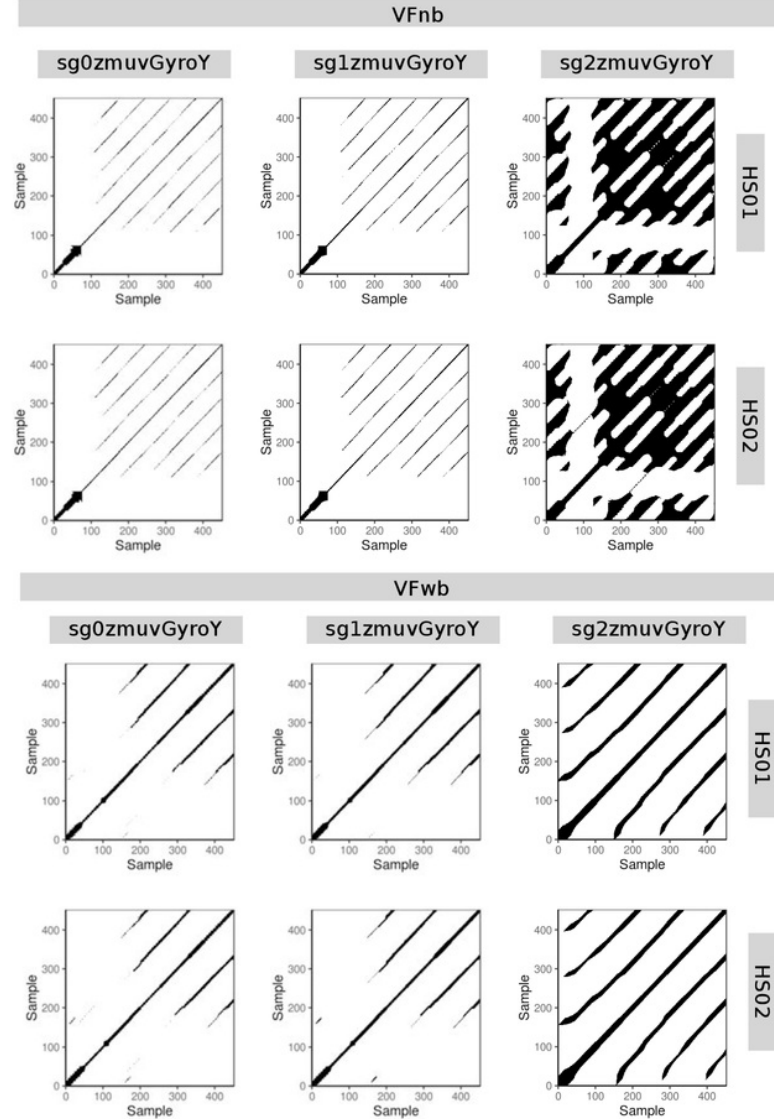


Fig. D.26 RPs for vertical faster arm movements. Recurrence plots of participant *p04* for horizontal faster movements with no beat (VNnb) and horizontal faster movements with beat (VFwb). Time series for raw-normalised (*sg0zmuvGyroY*), normalised-smoothed 1 (*sg1zmuvGyroY*) and normalised-smoothed 2 (*sg2zmuvGyroY*) with *1* sensors attached to the participant (HS01, HS02). Recurrence plots were computed with embedding parameters $m = 9$, $\tau = 6$ and recurrence threshold $\epsilon = 1$. R code to reproduce the figure is available from Xochicale (2018).

D.5 RQAs

D.5.1 REC values

Figs D.27 and D.28 show REC values, representing the % of black dots in the RPs, for vertical and horizontal arm movements.

It can be noted in Fig D.27 that REC values present little differences when comparing sensor HS01 and HS02. Similarly, considering the smoothness of the time series, REC values for participants appear to be similar in each of the activities (HNnb, HNwb, HFnb, HFwb) for sg0zmuvGyroZ and sg1zmuvGyroZ, while REC values for sg2zmuvGyroZ appear to fluctuate a bit more. With regards to the type of activity, horizontal arm movements with beat (HNwb) appear to fluctuate more than other activities (HNnb, HFnb, HFwb). Also RET values appear to fluctuate more and be greater for faster arm movements whereas RET values for normal arm movements appear to be constant (Fig D.27).

Figs D.28 show RET values for vertical arm movements. It can be noted that RET values appear to be similar for sensors HS01 and HS02 and the smoothness effect in REC values is more evident for sg2zmuvGyroY than REC values for sg0zmuvGyroY and sg1zmuvGyroY. RET values appear to fluctuate more for vertical normal arm movements with beat (VNwb) than other activities (VNnb, VFnb, VFwb) and RET values for VNnb, VFnb and VFwb appear to be constant and show little fluctuation between participants.

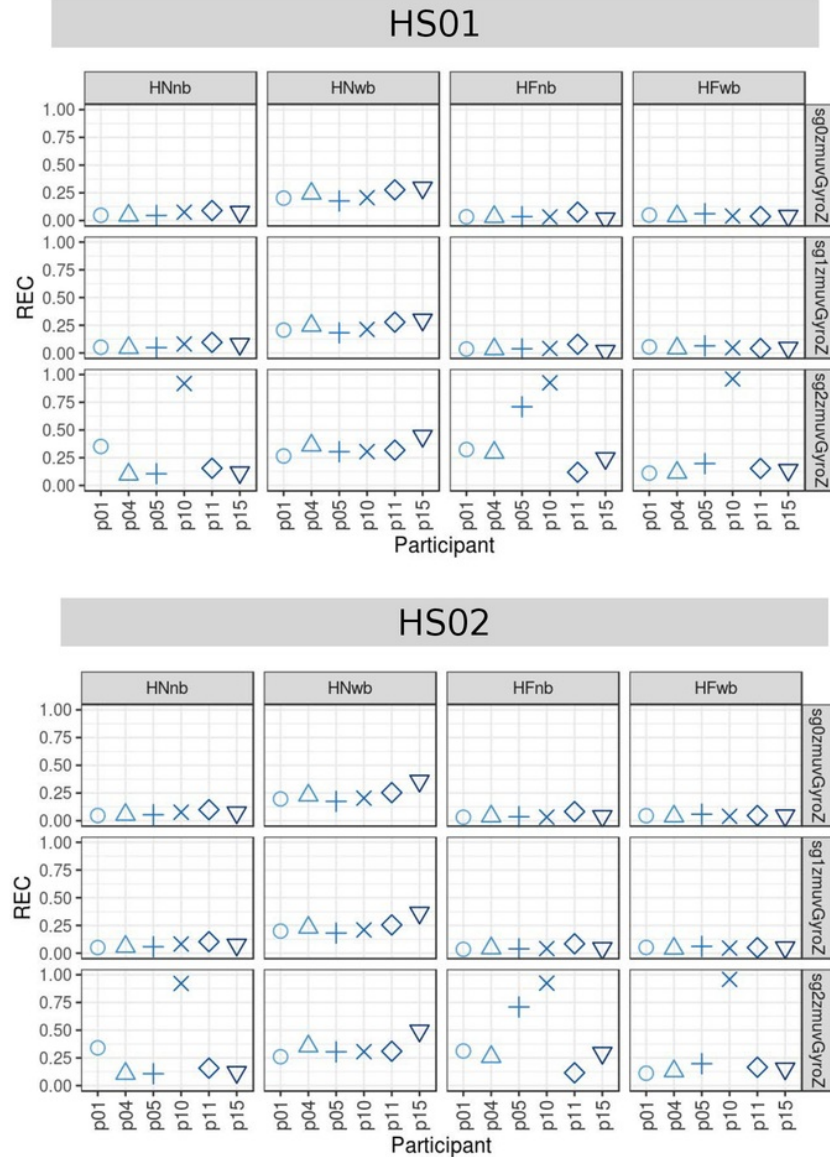


Fig. D.27 REC values for horizontal arm movements. REC values (representing % of black dots in the RPs) for 6 participants performing horizontal arm movements (HNnb, HNwb, HFnb, HFwb) for sensors HS01, HS02 and three smoothed-normalised axis of GyroZ (sg0zmuvGyroZ, sg1zmuvGyroZ and sg2zmuvGyroZ). REC values were computed with embedding parameters $m = 9$, $\tau = 6$ and recurrence threshold $\epsilon = 1$. R code to reproduce the figure is available from Xochicale (2018).

Additional Results for HII experiment

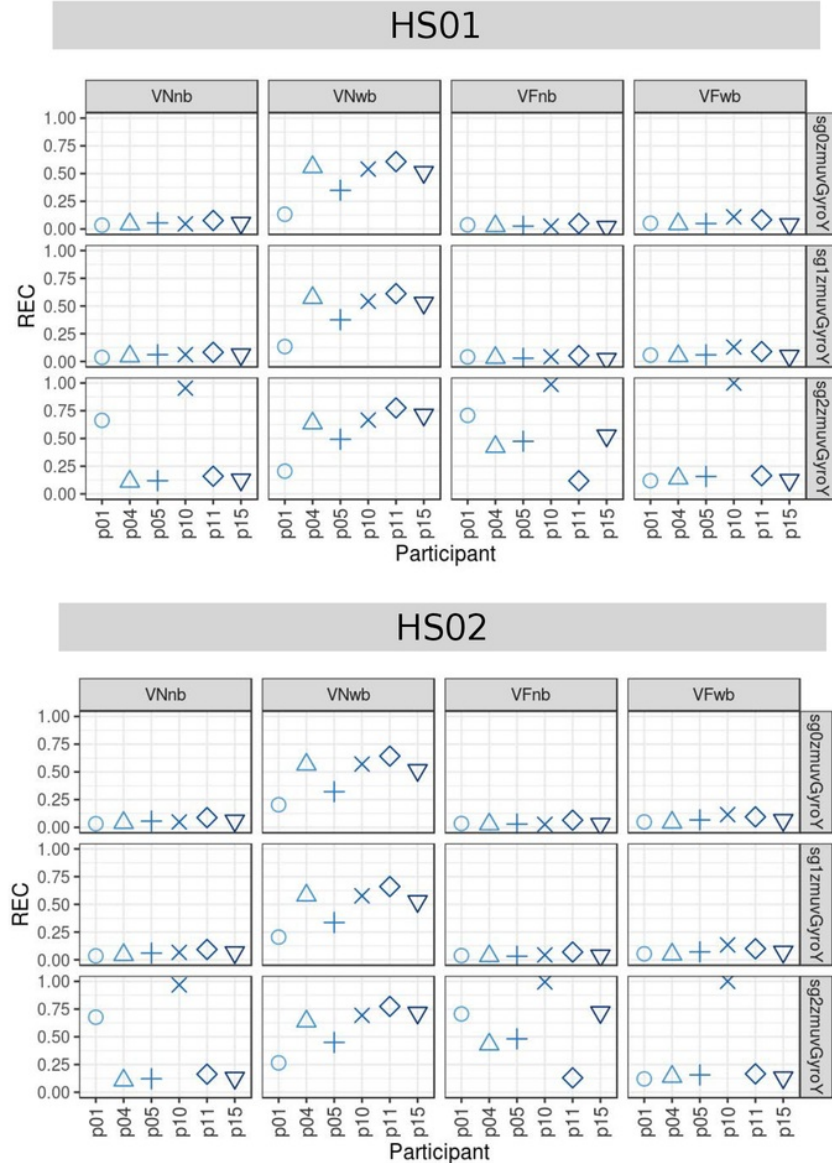


Fig. D.28 **REC values for vertical arm movements.** REC values (representing % of black dots in the RPs) for 6 participants performing vertical arm movements (VNnb, VNwb, VFnb, VFwb) for sensors HS01, HS02 and three smoothed-normalised axis of GyroZ (sg0zmuvGyroZ, sg1zmuvGyroZ and sg2zmuvGyroZ). REC values were computed with embedding parameters $m = 9$, $\tau = 6$ and recurrence threshold $\epsilon = 1$. R code to reproduce the figure is available from Xochicale (2018).

D.5.2 DET values

DET values appear to be constant for any source of time series (Figs D.29 and D.30). For both horizontal and vertical arm movements, the increase of smoothness of time series appear to affect the smoothness of DET values by making them to appear more similar as the smoothness increase. Additionally, it can be noted more fluctuations of DET values for faster activities (HFnb, HFwb) than normal activities (HNnb, HNwb), specifically for sg0zmuvGyroY (Figs D.29, D.30).

Additional Results for HII experiment

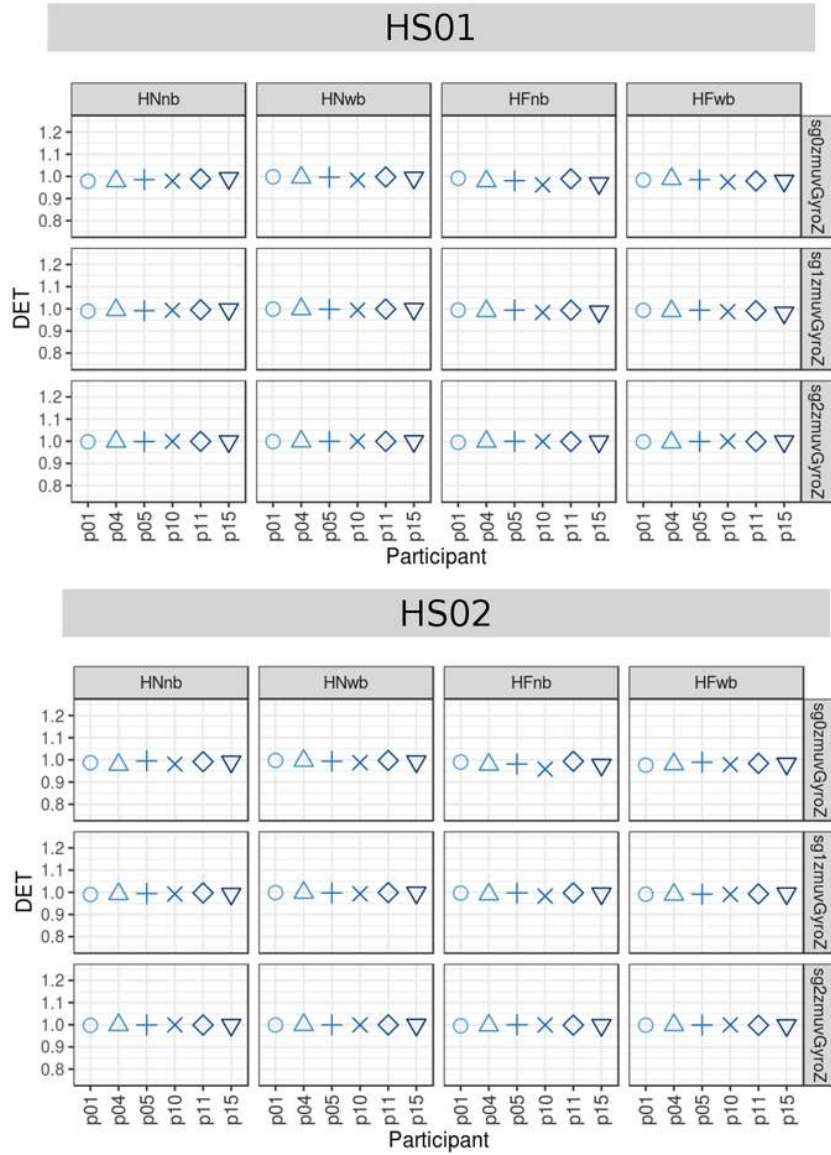


Fig. D.29 DET values for horizontal arm movements. DET values (representing predictability and organisation of the RPs) for 6 participants performing horizontal arm movements (HNnb, HNb, HFnb, HFwb) for sensors HS01, HS02 and three smoothed-normalised axis of GyroZ (sg0zmuvGyroZ, sg1zmuvGyroZ and sg2zmuvGyroZ). DET values were computed with embedding parameters $m = 9$, $\tau = 6$ and recurrence threshold $\epsilon = 1$. R code to reproduce the figure is available from Xochicale (2018).

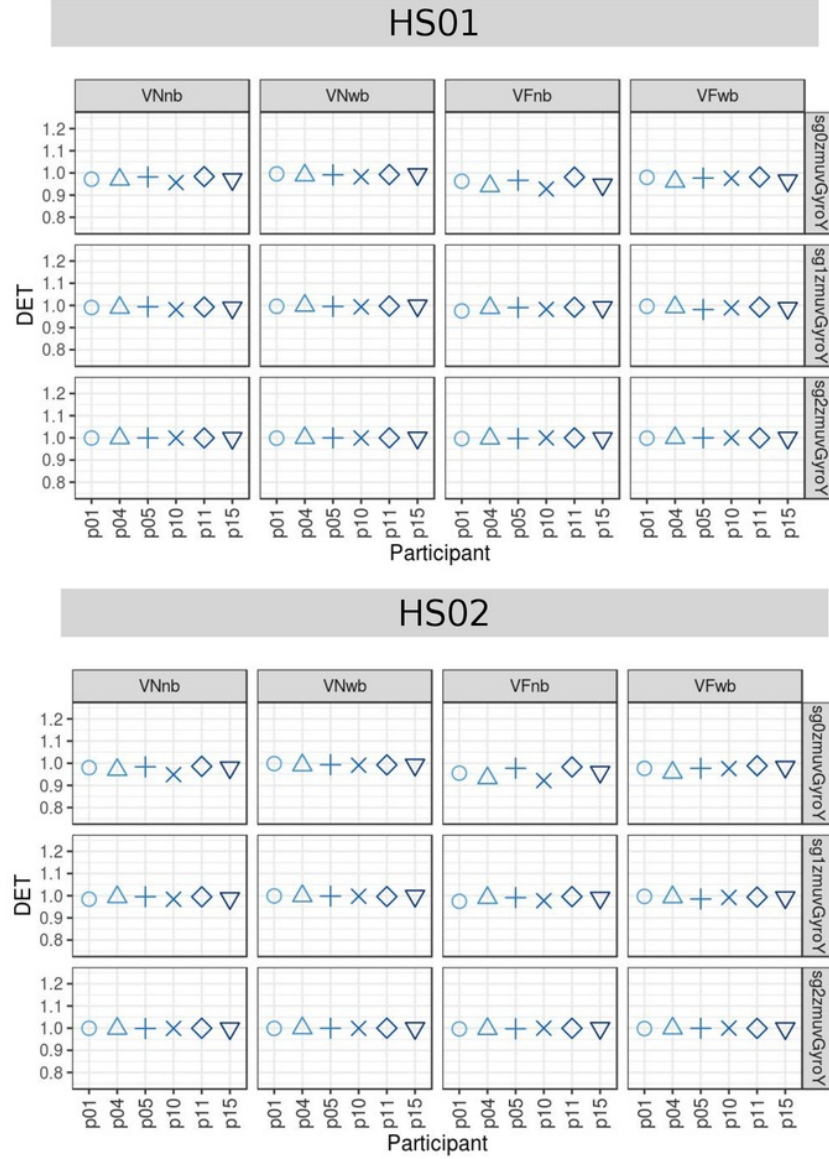


Fig. D.30 DET values for vertical arm movements. DET values (representing predictability and organisation of the RPs) for 6 participants performing vertical arm movements (VNnb, VNwb, VFnb, VFwb) for sensors HS01, HS02 and three smoothed-normalised axis of GyroY (sg04muvGyroY, sg1zmuvGyroY and sg2zmuvGyroY). DET values were computed with embedding parameters $m = 9$, $\tau = 6$ and recurrence threshold $\epsilon = 1$. R code to reproduce the figure is available from Xochicale (2018).

D.5.3 RATIO values

RATIO values for horizontal and vertical arm movements ¹³⁰ are shown in Figs D.31 and D.32.

The fluctuation of RATIO values for horizontal faster arm movements appear to be more notable than RATIO values for horizontal normal arm movements. RATIO values appear to be constant for activity HNwb than other activities (HNnb, HFnb, HFwb). Regarding the smoothness of time series, RATIO values appear to have similar values for sg0zmuvGyroZ and sg1zmuvGyroZ while RATIOS values are more uniform for sg2zmuvGyroZ. With regards to type of sensor, RET values appear to be similar for HS01 and HS02 with the exception of *p*15 in HFnb activity (Figs D.31).

Figs D.32 show RATIO values for vertical arm movements. The fluctuation of RATIO values appears to be constant for the activity VNwb whereas other RATIO values for other activities (VNnb, VFnb, VFwb) appear to fluctuate more. The ²⁵² smoothness of the time series affects only the RATIO values for sg2zmuvGyroY as these appear to be constant, while RET values for sg0zmuvGyroY and sg1zmuvGyroZ appear to have the similar RATIO values. Additionally, RATIO values for type of sensors HS01 and HS02 appear to show similar values as well, with the exception of *p*15 in the VFnb activity.

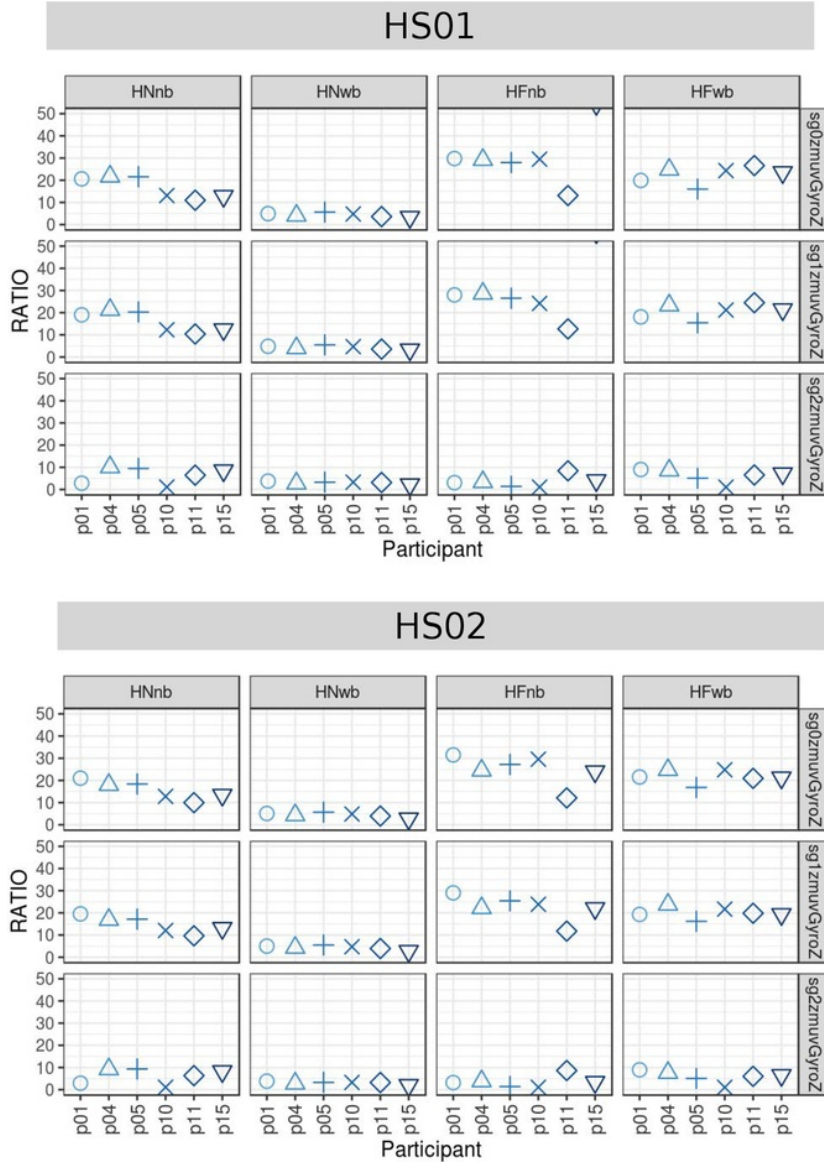


Fig. D.31 RATIO values for horizontal arm movements. RATIO values, representing dynamic transitions, for 6 participants performing horizontal arm movements (HNnb, HNwb, HFnb, HFwb) with sensors HS01, HS02 and three smoothed-normalised axis of GyroZ (sg0zmuvGyroZ, sg1zmuvGyroZ and sg2zmuvGyroZ). RATIO values were computed with embedding parameters $m = 9$, $\tau = 6$ and recurrence threshold $\epsilon = 1$. R code to reproduce the figure is available from Xochicale (2018).

Additional Results for HII experiment

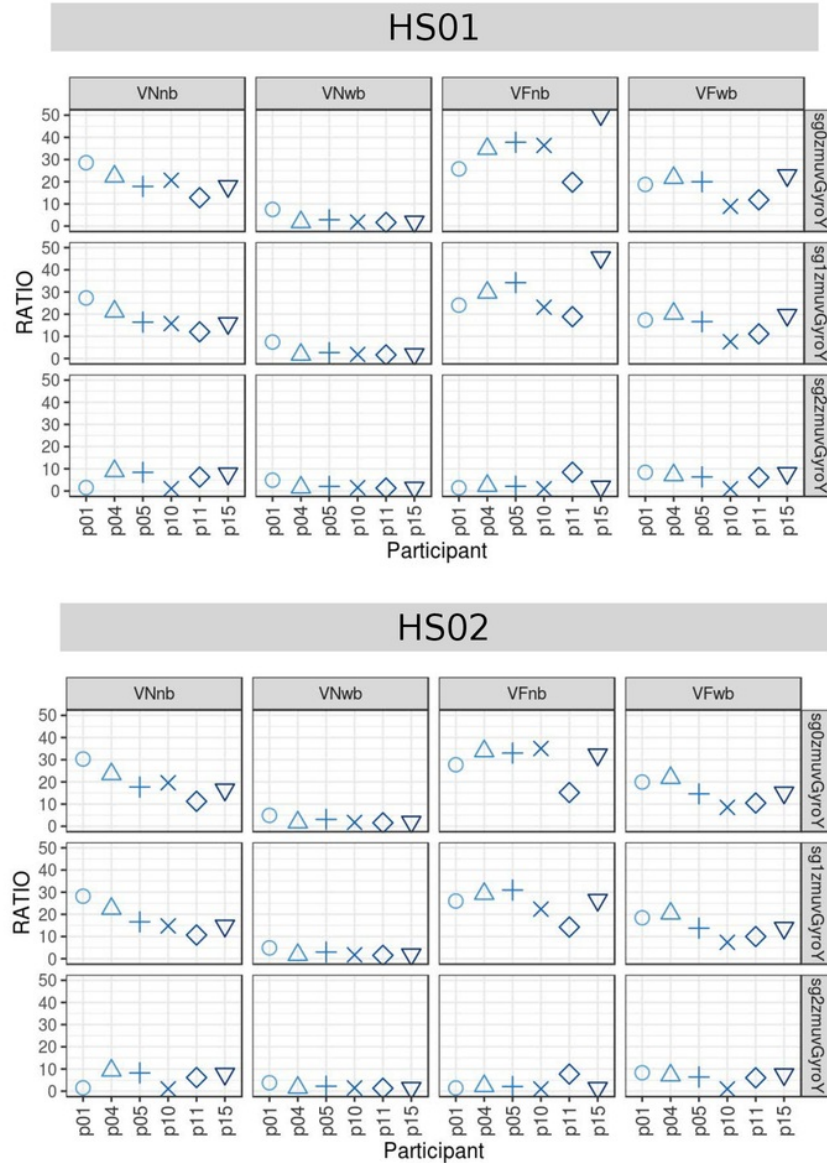


Fig. D.32 **RATIO values for vertical arm movements.** RATIO values, representing dynamic transitions, for 6 participants performing vertical arm movements (VNnb, VNwb, VFnb, VFwb) with sensors HS01, HS02 and three smoothed-normalised axis of GyroY (sg0zmuGyroY, sg1zmuGyroY, sg1zmuvGyroY and sg2zmuvGyroY). RATIO values were computed with embedding parameters $m = 9$, $\tau = 6$ and recurrence threshold $\epsilon = 1$. R code to reproduce the figure is available from Xochicale (2018).

D.5.4 ENTR values

ENTR values for horizontal and vertical arm movements are shown in Figs D.33 and D.34.

Figs D.33 show ENTR values for horizontal arm movements. ENTR values appear to be similar for sg0zmuvGyroZ and sg1zmuvGyroZ and oscillate between 2 to 4, while ENTR values for sg2zmuvGyroZ appear to show similar fluctuations but with higher ENTR values oscillating between 3.5 to 5 with the exception of *p*10 with activities VNnb and VFwb for sg2zmuvGyroY which ENTR values are slightly out of range. ENTR values appear to be similar for sensor HS01 and HS02.

Figs D.34 show ENTR values for vertical arm movements. ENTR values for sg0zmuvGyroY and sg1zmuvGyroY appear to show the same values and oscillate between 2 to 4, while ENTR values appear to oscillate between 3.5 to 5 with the exception of *p*10 with activities VNnb and VFwb for sg2zmuvGyroY which ENTR values are out of range. ENTR values for sensor HS01 and HS02 appear to show the same values.

Additional Results for HII experiment

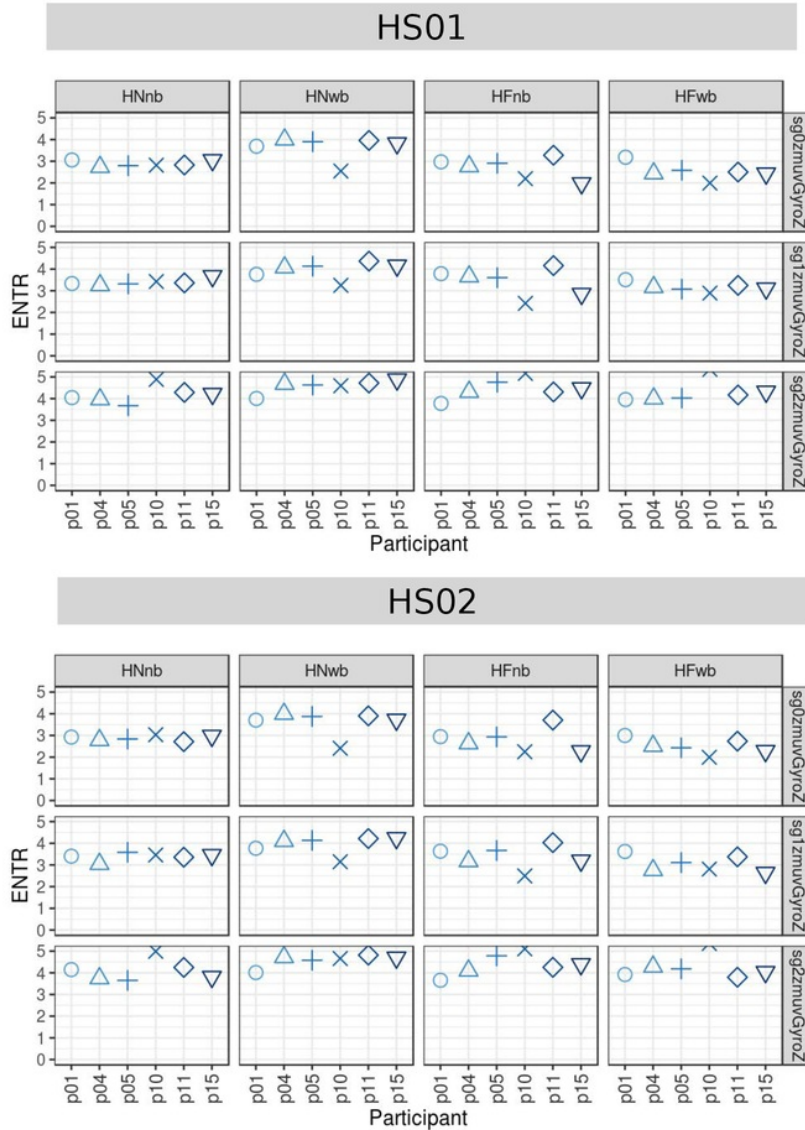


Fig. D.33 **ENTR** values for horizontal arm movements. ENTR values (representing the complexity of the deterministic structure in time series) for 6 participants performing horizontal arm movements (HNnb, HNwb, HFnb, HFwb) for sensors HS01, HS02 and three smoothed-normalised axis of GyroZ (sg0zmuvGyroZ, sg1zmuvGyroZ and sg2zmuvGyroZ). ENTR values were computed with embedding parameters $m = 9$, $\tau = 6$ and recurrence threshold $\epsilon = 1$. R code to reproduce the figure is available from Xochicale (2018).

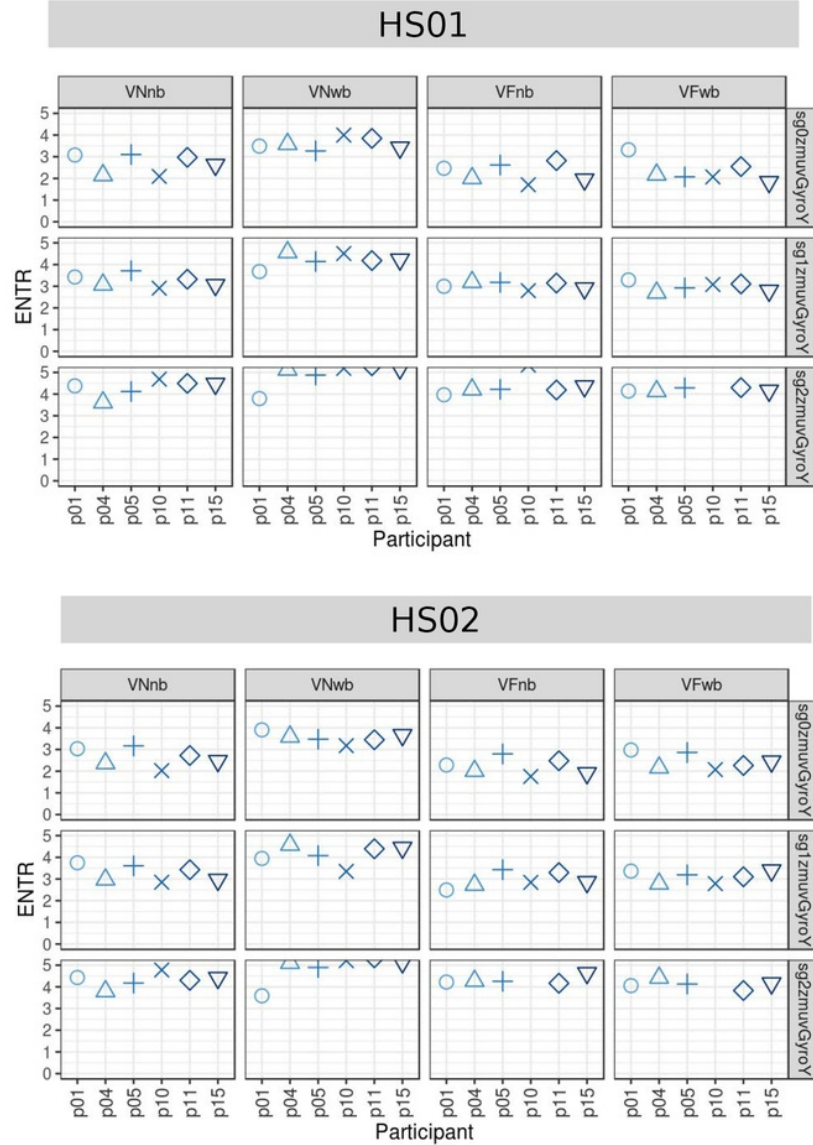


Fig. D.3⁶² ENTR values for vertical arm movements. ENTR values (representing the complexity of the deterministic structure in time series) for 6 participants performing vertical arm movements (VNnb, VNwb, VFnb, VFwb) for sensors HS01, HS02 and three smoothed-normalised axis of GyroY (sg0zmuvgyroY, sg1zmuvgyroY and sg2zmuvgyroY). ENTR values were computed with embedding parameters $m = 9$, $\tau = 6$ and recurrence threshold $\epsilon = 1$. R code to reproduce the figure is available from Xochicale (2018).



Appendix E

Additional results for HHI experiment

E.1 Time Series

Time series for twenty participants with a window length size of 500 samples of horizontal arm movements (Figs. E.1, E.2, E.3) and vertical arm movements (Figs. E.4, E.5, E.6). For the remained window size lengths of time series data, we refer the reader to download the data and code at Xochicale (2018).

Additional results for HHI experiment

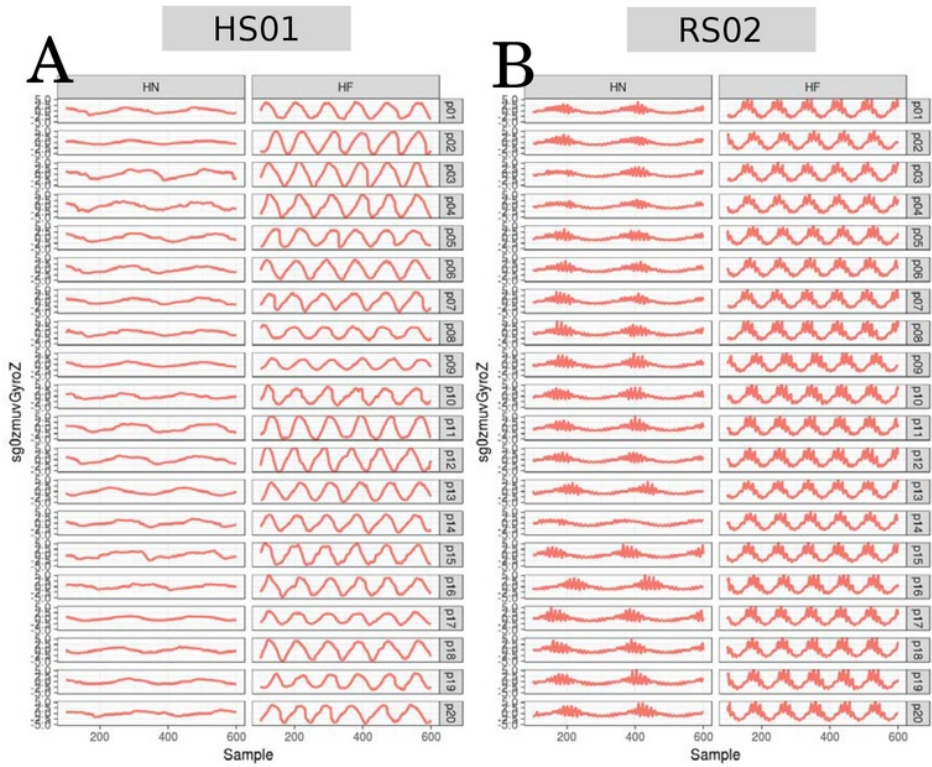


Fig. E.1 Time series for horizontal arm movements (sg0) Time series for sg0zmuvGyroZ for twenty participants ($p01$ to $p20$) for horizontal movements in normal (HN) and horizontal faster (HF) velocity with sensors attached to the participant wrist (HS01) and to the humanoid wrist (RS02). R code to reproduce the figure is available from Xochicale (2018).

E.1 Time Series

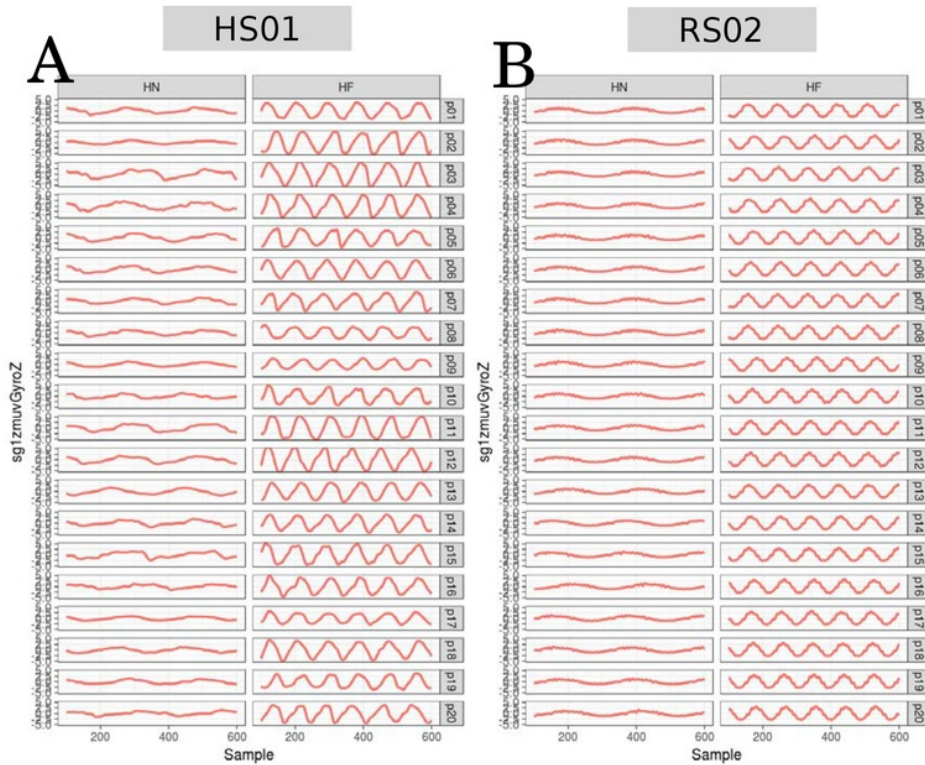


Fig. E.2 Time series for horizontal arm movements (sg1) Time series for sg0zmuvGyroZ for twenty participants (p01 to p20) for horizontal movements in normal (HN) and horizontal faster (HF) velocity with sensors attached to the participant wrist (HS01) and to the humanoid wrist (RS02). R code to reproduce the figure is available from Xochicale (2018).

Additional results for HHI experiment

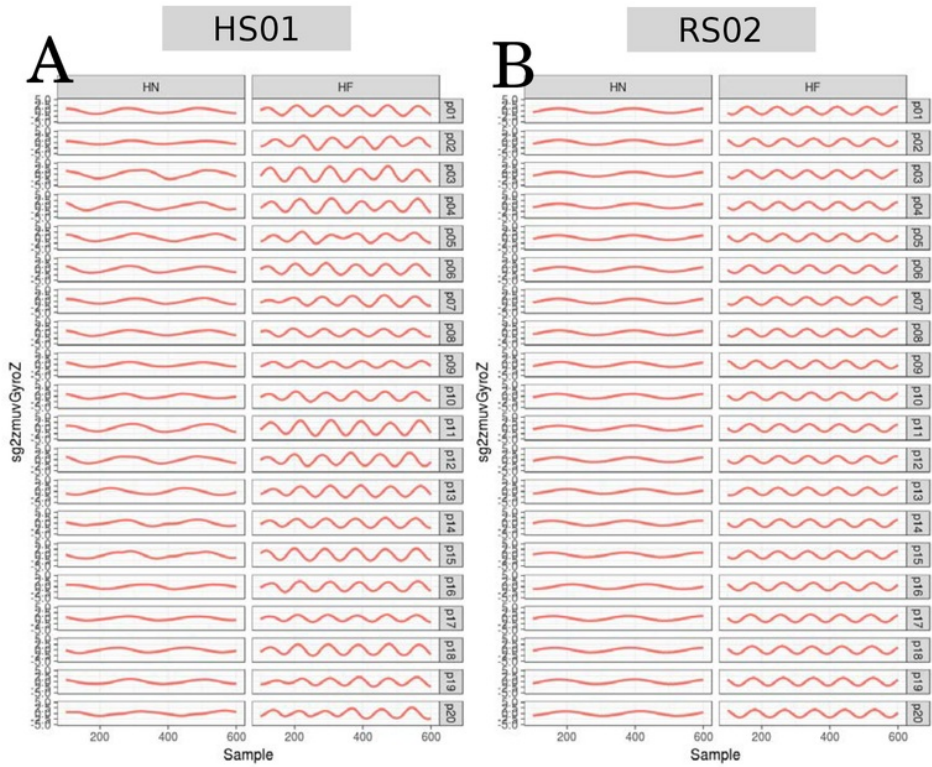


Fig. E.3 Time series for horizontal arm movements (sg2) Time series for sg0zmuvGyroZ for twenty participants (p_{01} to p_{20}) for horizontal movements in normal (HN) and horizontal faster (HF) velocity with sensors attached to the participant wrist (HS01) and to the humanoid wrist (RS02). R code to reproduce the figure is available from Xochicale (2018).

E.1 Time Series

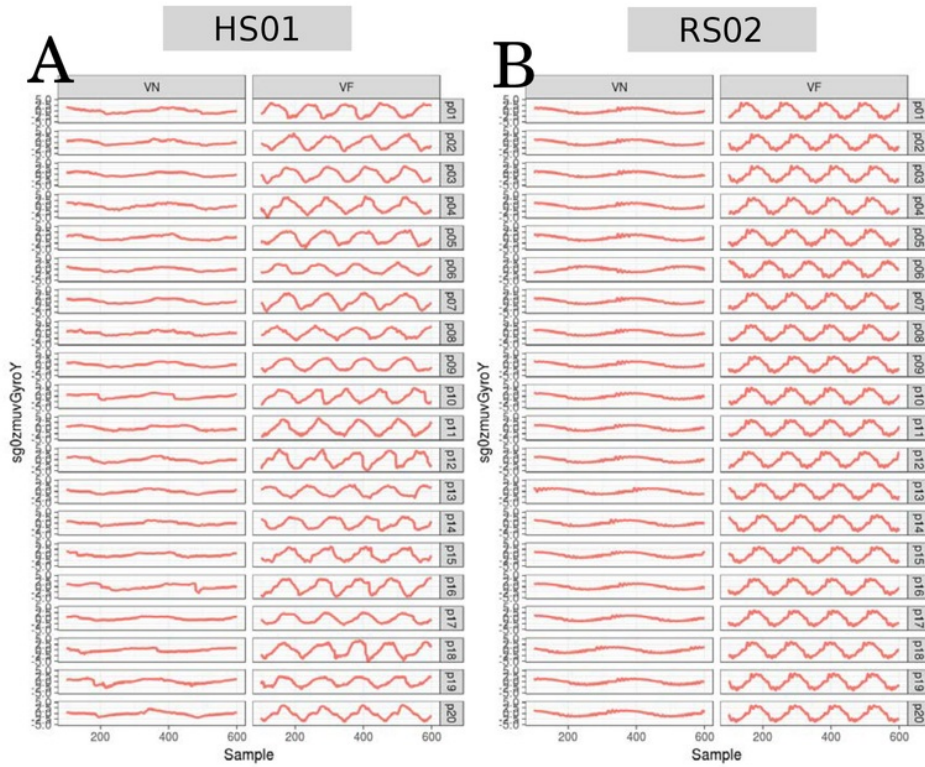


Fig. E.4 Time series for vertical arm movements (sg0) Time series for sg0zmuvGyroY for twenty participants (*p*01 to *p*20) for vertical movements in normal (HN) and horizontal faster (HF) velocity with sensors attached to the participant wrist (HS01) and to the humanoid wrist (RS02). R code to reproduce the figure is available from Xochicale (2018).

Additional results for HHI experiment

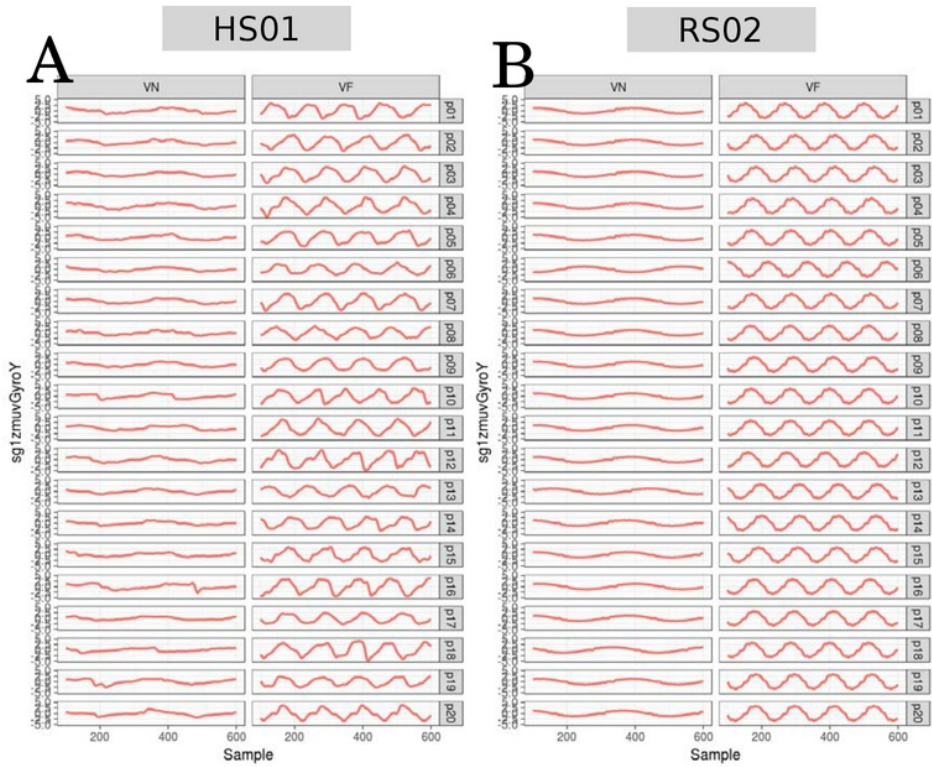


Fig. E.5 Time series for vertical arm movements (sg1) Time series for sg0zmuvGyroY for twenty participants (p_{01} to p_{20}) for horizontal movements in normal (HN) and horizontal faster (HF) velocity with sensors attached to the participant wrist (HS01) and to the humanoid wrist (RS02). R code to reproduce the figure is available from Xochicale (2018).

E.1 Time Series

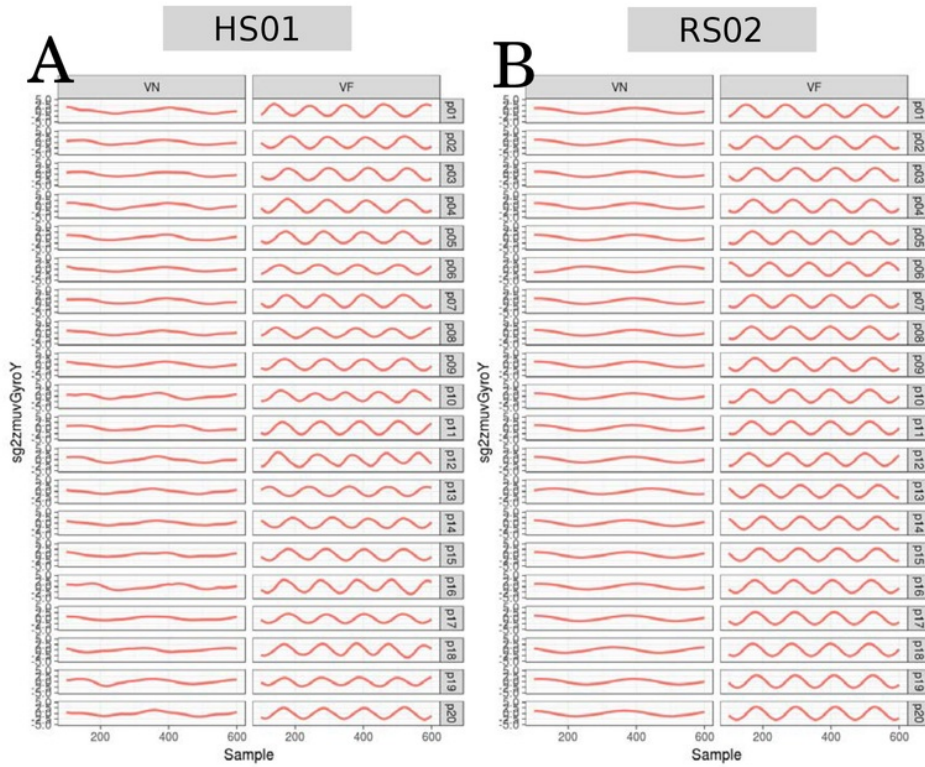


Fig. E.6 Time series for vertical arm movements (sg2) Time series for sg2zmuvGyroY for twenty participants ($p01$ to $p20$) for vertical movements in normal (HN) and horizontal faster (HF) velocity with sensors attached to the participant wrist (HS01) and to the humanoid wrist (RS02). R code to reproduce the figure is available from Xochicale (2018).

E.2 Embedding parameters

E.2.1 Minimum dimension embedding values

Minimum embedding dimensions for horizontal and vertical arm movements are presented in Figs. E.7 and E.8, respectively. For remained results with window size lengths
120 of time series data, we refer the reader to download the data and code at Xochicale (2018).

E.2 Embedding parameters

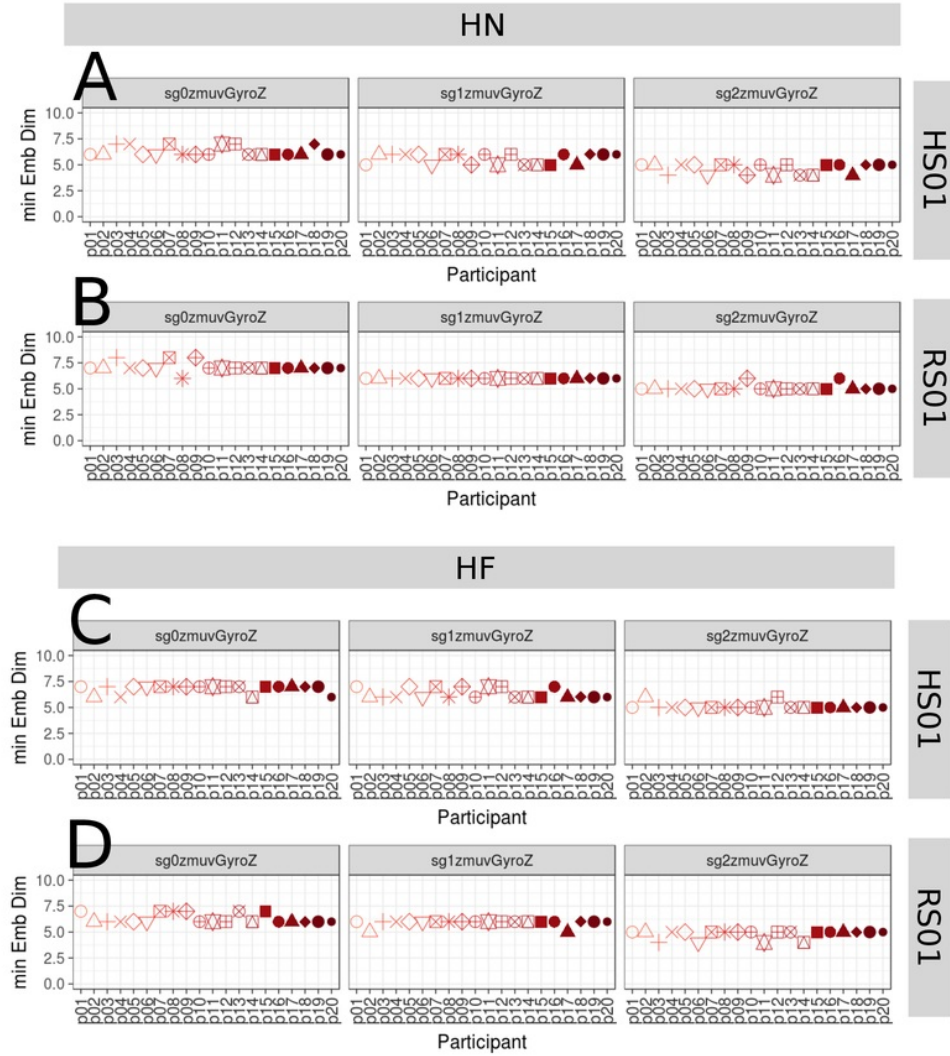


Fig. E.7 Minimum embedding dimensions for horizontal arm movements. (A, B) Horizontal Normal (HN), (C, D) Horizontal Faster (HF) movements, (A, C) sensor attached to participants (HS01), and (B, D) sensor attached to robot (RS01). Minimum embedding dimensions are for twenty participants (p01 to p20) with three smoothed signals (sg0zmuvGyroZ, sg1zmuvGyroZ and sg2zmuvGyroZ) and window lenght of 10-sec (500 samples). R code to reproduce the figure is available from Xochicale (2018).

Additional results for HHI experiment

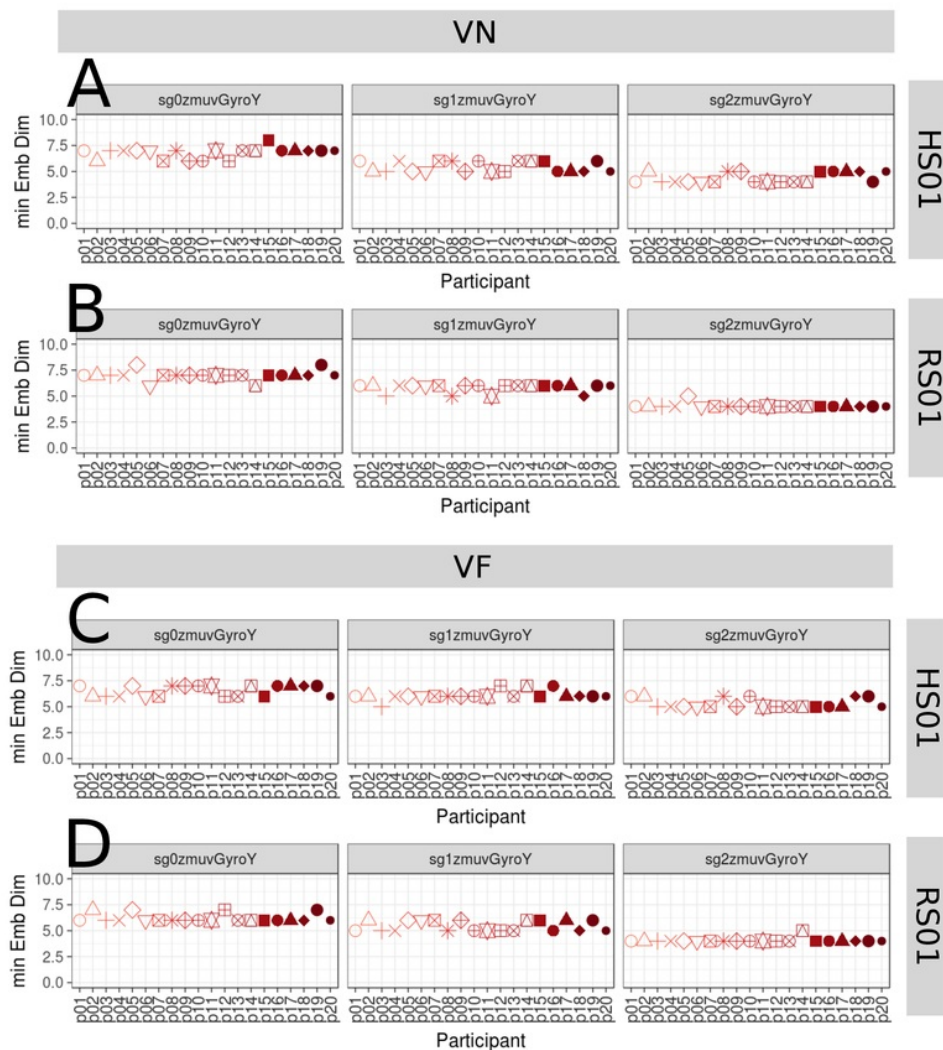


Fig. E.8 Minimum embedding dimensions for vertical arm movements. (A, B) Vertical Normal (VN), (C, D) Vertical Faster (VF) movements, (A, C) sensor attached to participants (HS01), and (B, D) sensor attached to robot (RS01). Minimum embedding dimensions are for twenty participants (p01 to p20) with three smoothed signals (sg0zmuvGyroY, sg1zmuvGyroY and sg2zmuvGyroY) and window length of 10-sec (500 samples). R code to reproduce the figure is available from Xochicale (2018).

E.2 Embedding parameters

E.2.2 Minimum delay embedding values

First minimum AMI values for horizontal and vertical arm movements are presented in Figs. E.9 and E.10, respectively. For remained results with window size lengths of time series data, we refer the reader to download the data and code at Xochicale (2018).¹²⁰

Additional results for HHI experiment

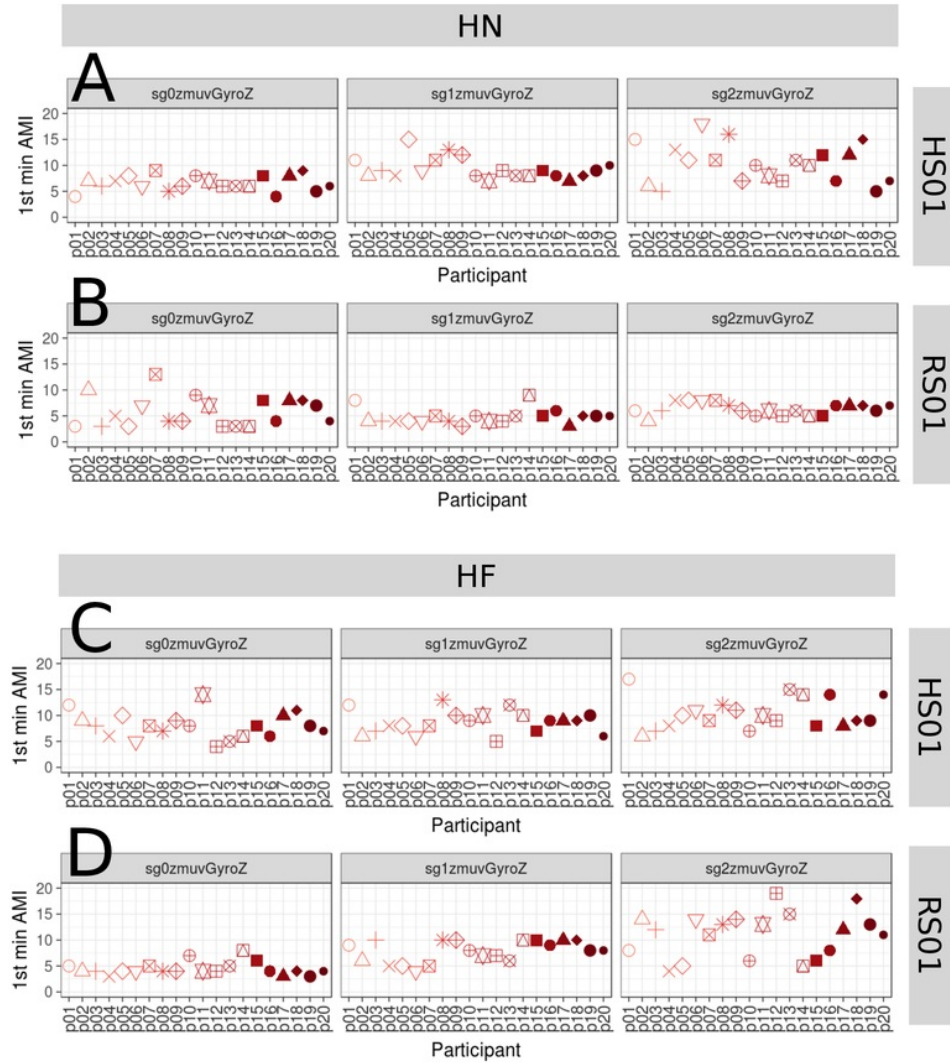


Fig. E.9 First minimum AMI values for horizontal arm movements. (A, B) Horizontal Normal (HN), (C, D) Horizontal Faster (HF) movements, (A, C) sensor attached to participants (HS01), and (B, D) sensor attached to robot (RS01). First minimum AMI values are for twenty participants (p01 to p20) with three smoothed signals (sg0zmuvGyroZ, sg1zmuvGyroZ and sg2zmuvGyroZ) and window lenght of 10-sec (500 samples). R code to reproduce the figure is available from Xochicale (2018).

E.2 Embedding parameters

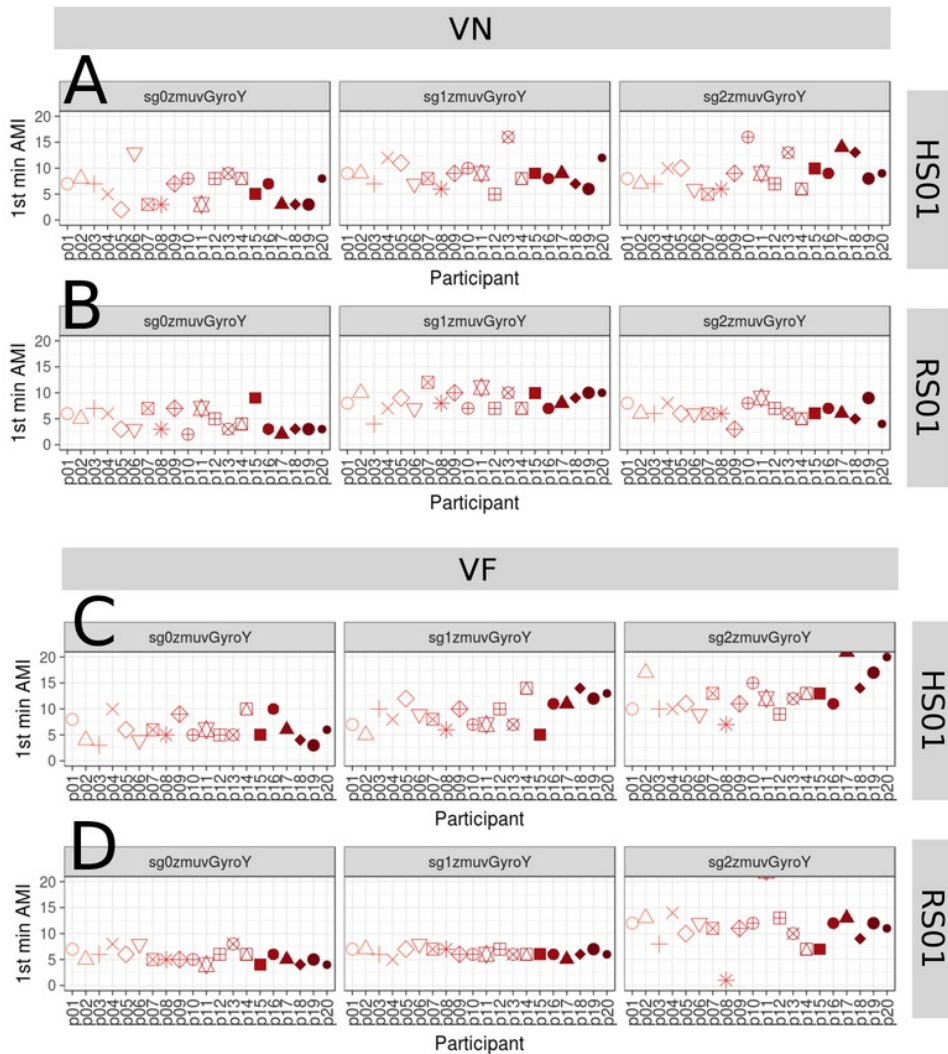


Fig. E.10 First minimum AMI values for vertical arm movements. (A, B) Vertical Normal (VN), (C, D) Vertical Faster (VF) movements, (A, C) sensor attached to participants (HS01), and (B, D) sensor attached to robot (RS01). First minimum AMI values are for twenty participants (p01 to p20) with three smoothed signals (sg0zmuvGyroZ, sg1zmuvGyroZ and sg2zmuvGyroZ) and window lenght of 10-sec (500 samples). R code to reproduce the figure is available from Xochicale (2018).

E.3 RSSs

Reconstructed state spaces of participant $p01$, $p02$ and $p03$ for horizontal arm movements (Figs. E.11 and E.12) and vertical arm movements (Figs. E.13 and E.14). For remained results with window size lengths of time series data, we refer the reader to download the data and code at Xochicale (2018).

E.3 RSSs

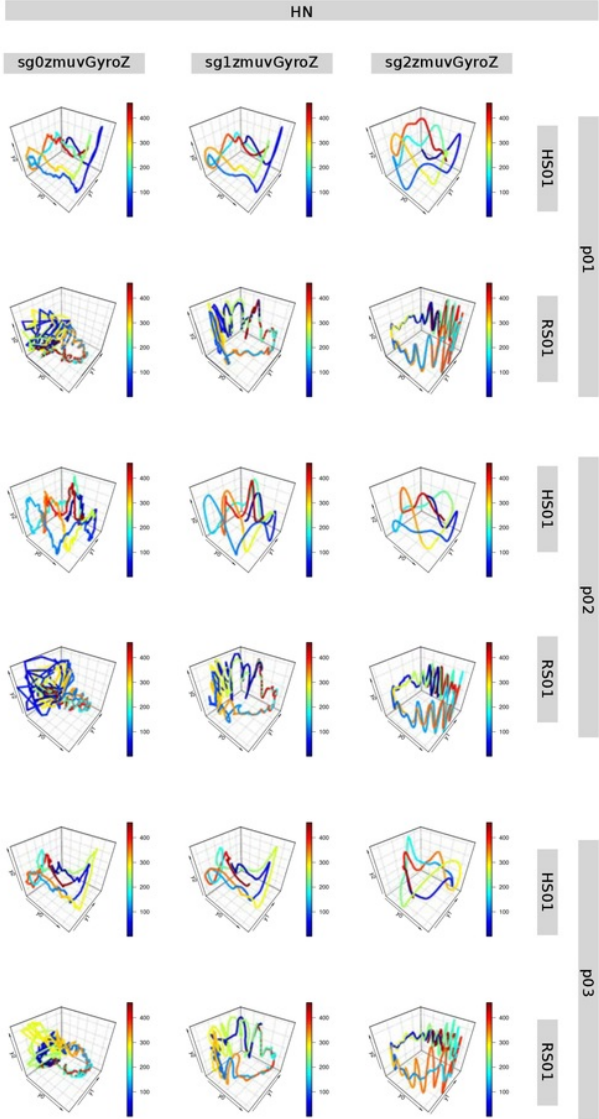


Fig. E.11 RSSs for horizontal normal arm movements. Reconstructed state spaces of participant $p01$, $p02$ and $p03$ for horizontal movements with raw-normalised ($sg0zmuvGyroZ$), n_{16} -normalised-smoothed 1 ($sg1zmuvGyroZ$) and normalised-smoothed 2 ($sg2zmuvGyroZ$) time series of the sensors attached to the participant (HS01) and other sensor attached to the robot (RS01). Reconstructed state spaces were computed with embedding parameters $m = 6$, $\tau = 8$. R code to reproduce the figure is available from Xochicale (2018).

Additional results for HHI experiment

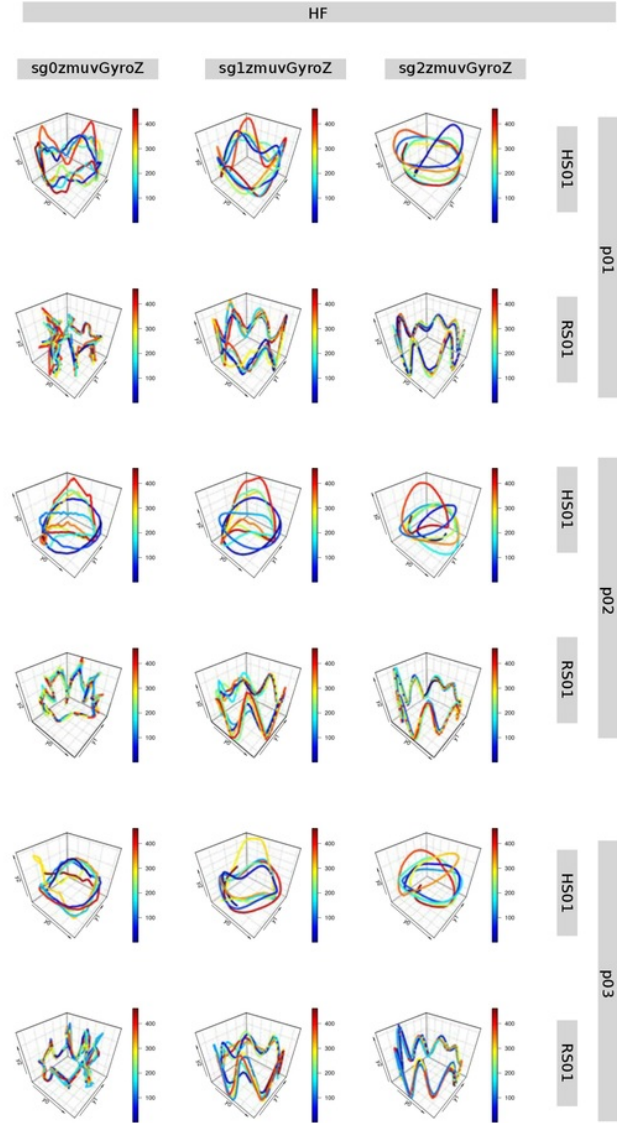


Fig. E.12 RSSs for horizontal faster arm movements. Reconstructed state spaces of participant $p01$, $p02$ and $p03$ for horizontal faster movements with raw-normalised ($sg0zmuvGyroZ$), normalised-smoothed 1 ($sg1zmuvGyroZ$) and normalised-smoothed 2 ($sg2zmuvGyroZ$) time series of the sensors attached to the participant (HS01) and other sensor attached to the robot (RS01). Reconstructed state spaces were computed with embedding parameters $m = 6$, $\tau = 8$. R code to reproduce the figure is available from Xochicale (2018).

E.3 RSSs

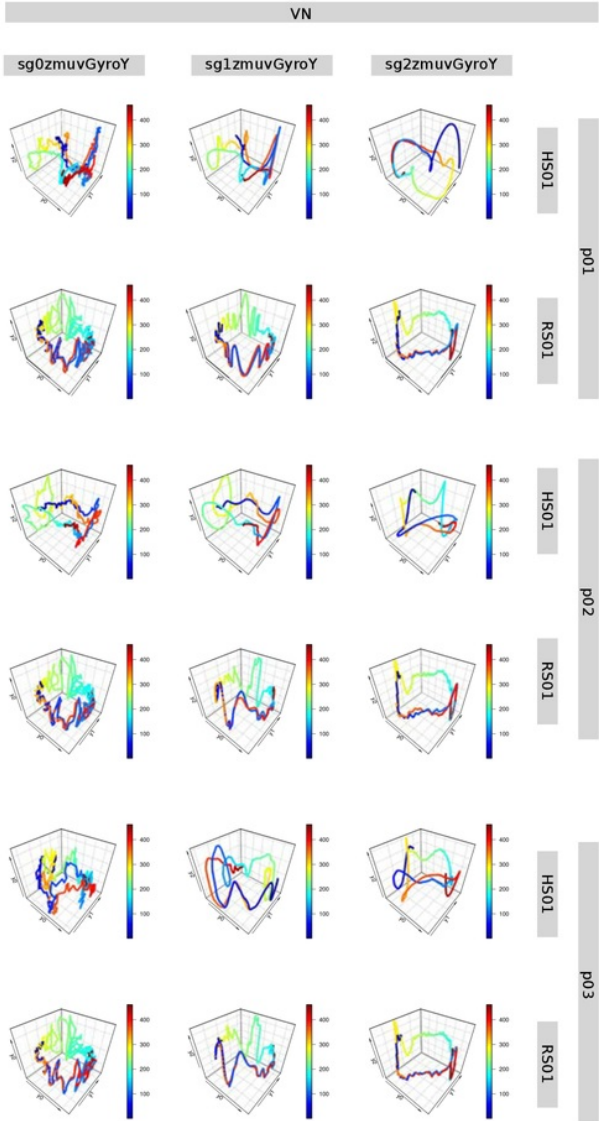


Fig. E.13 RSSs for vertical normal arm movements. Reconstructed state spaces of participant $p01$, $p02$ and $p03$ for horizontal movements with raw-normalised ($sg0zmuvGyroY$), n₁₆-normalised-smoothed 1 ($sg1zmuvGyroY$) and normalised-smoothed 2 ($sg2zmuvGyroY$) time series of the sensors attached to the participant (HS01) and other sensor attached to the robot (RS01). Reconstructed state spaces were computed with embedding parameters $m = 6$, $\tau = 8$. R code to reproduce the figure is available from Xochicale (2018).

Additional results for HHI experiment

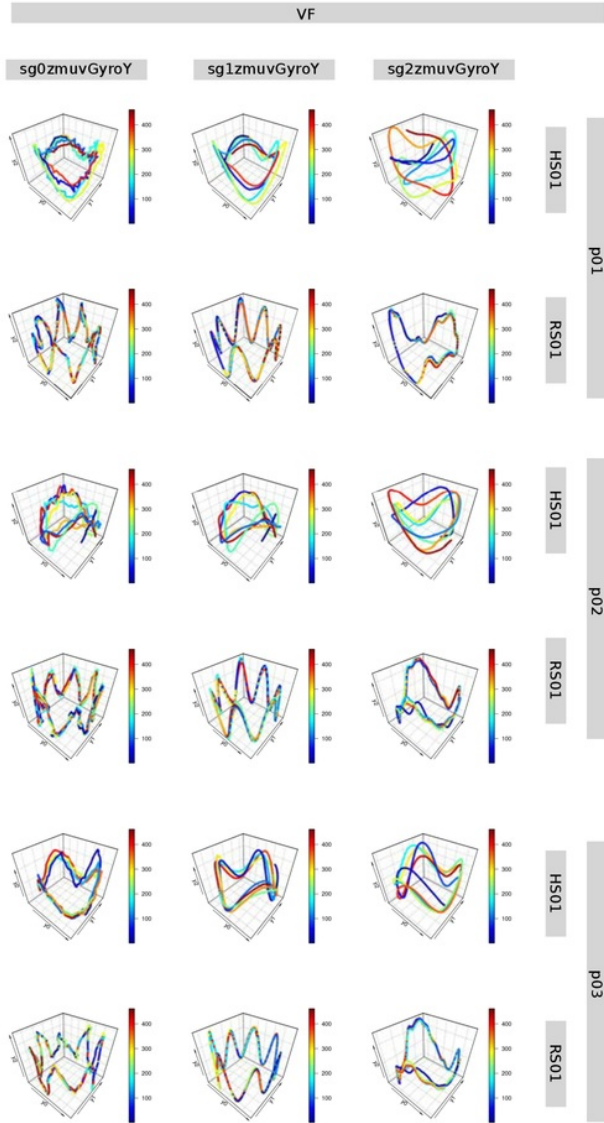


Fig. E.14 RSSs for vertical faster arm movements. Reconstructed state spaces of participant $p01$, $p02$ and $p03$ for horizontal faster movements with raw-normalised ($sg0zmuvGyroY$), n_{16} normalised-smoothed 1 ($sg1zmuvGyroY$) and normalised-smoothed 2 ($sg2zmuvGyroY$) time series of the sensors attached to the participant (HS01) and other sensor attached to the robot (RS01). Reconstructed state spaces were computed with embedding parameters $m = 6$, $\tau = 8$. R code to reproduce the figure is available from Xochicale (2018).

E.4 RPs

Recurrence Plots participant $p01$, $p02$ and $p03$ for horizontal arm movements (Figs. E.15, E.16) and vertical arm movements (Figs. E.17, E.18). For remained results with window size lengths of time series data, we refer the reader to download the data and code at Xochicale (2018).

Additional results for HHI experiment

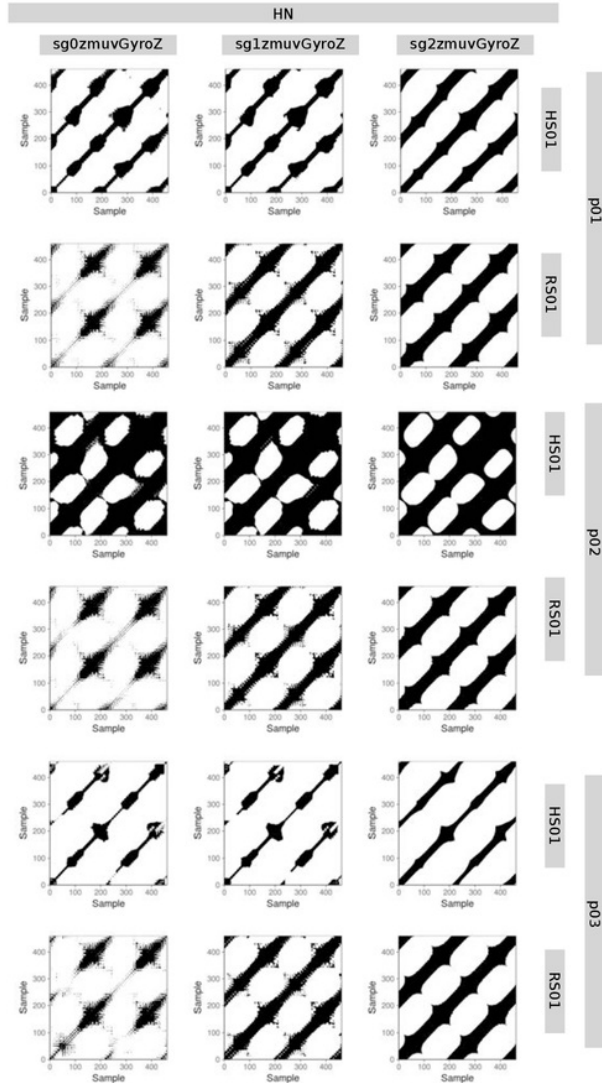


Fig. E.15 RPs for horizontal normal arm movements. Recurrence plots of participant $p01$, $p02$, $p03$ for horizontal normal movements with time series of raw-normalised ($sg0zmuvGyroZ$), normalised-smoothed 1 ($sg1zmuvGyroZ$) and normalised-smoothed 2 ($sg2zmuvGyroZ$), and sensor $HS01$ attached to the participant and to the robot ($RS01$). Recurrence plots were computed with embedding parameters $m = 6$, $\tau = 8$ and $\epsilon = 1$. R code to reproduce the figure is available from Xochicale (2018).

E.4 RPs

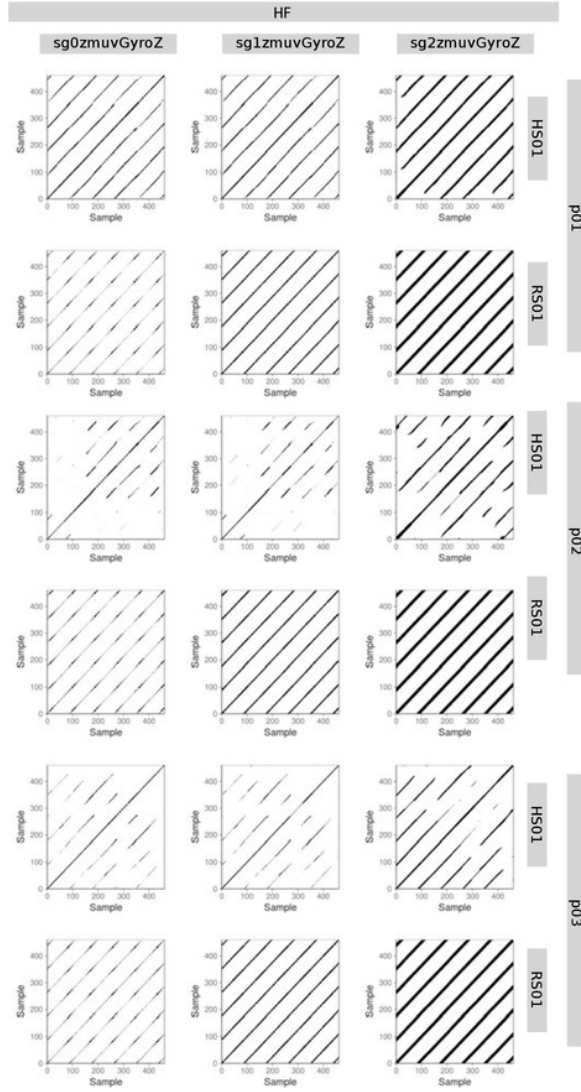


Fig. E.16 RPs for horizontal faster arm movements. Recurrence plots of participant $p01$, $p02$, $p03$ for horizontal faster movements with time series of raw-normalised ($sg0zmuvGyroZ$), normalised-smoothed 1 ($sg1zmuvGyroZ$) and normalised-smoothed 2 ($sg2zmuvGyroZ$), and sensors attached to the participant ($HS01$) and to the robot ($RS01$). Recurrence plots were computed with embedding parameters $m = 6$, $\tau = 8$ and $\epsilon = 1$. R code to reproduce the figure is available from Xochicale (2018).

Additional results for HHI experiment

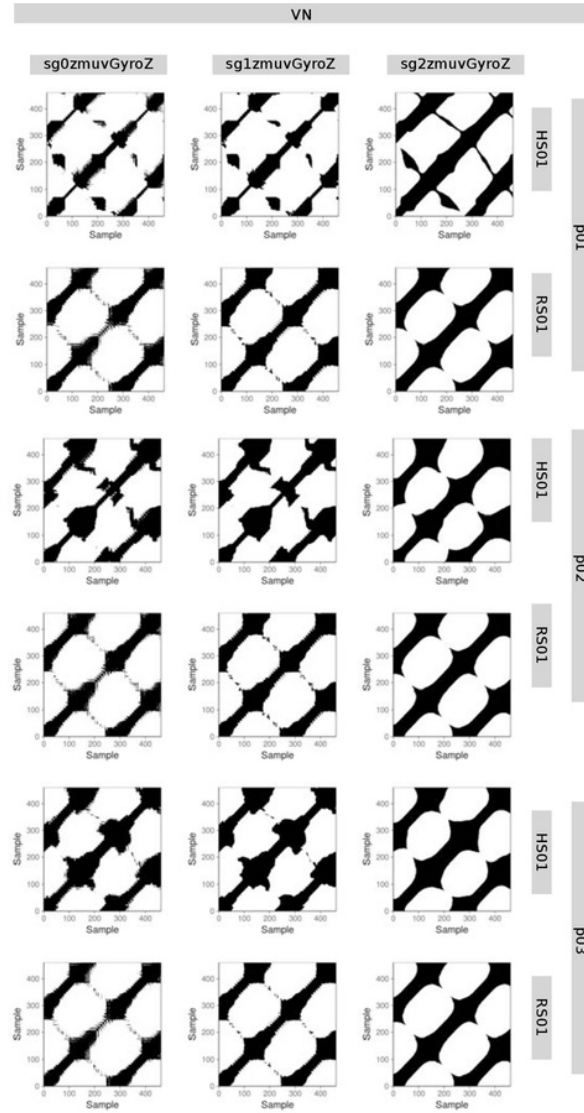


Fig. E.17 RPs for vertical normal arm movements. Recurrence plots of participant $p01$, $p02$, $p03$ for vertical normal movements with time series of raw-normalised ($sg0zmuvGyroY$), normalised-smoothed 1 ($sg1zmuvGyroY$) and normalised-smoothed 2 ($sg2zmuvGyroY$), and sensors attached to the participant ($HS01$) and to the robot ($RS01$). Recurrence plots were computed with embedding parameters $m = 6$, $\tau = 8$ and $\epsilon = 1$. R code to reproduce the figure is available from Xochicale (2018).

E.4 RPs

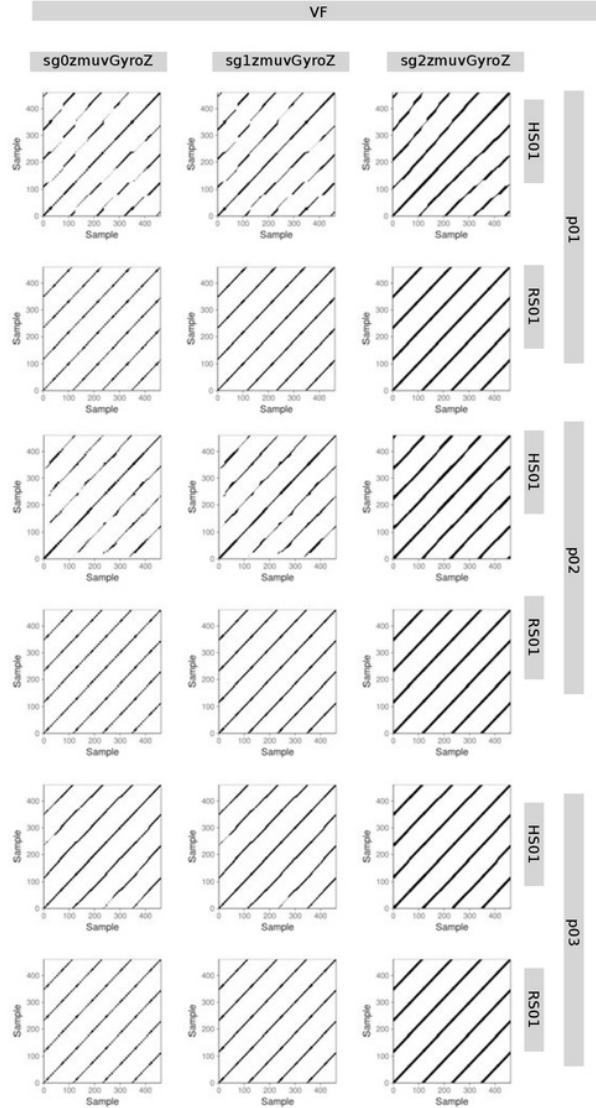


Fig. E.18 RPs for vertical faster arm movements. Recurrence plots of participant $p01$, $p02$, $p03$ for vertical faster movements with time series of raw-normalised ($sg0zmuvGyroY$), normalised-smoothed 1 ($sg1zmuvGyroY$) and normalised-smoothed 2 ($sg2zmuvGyroY$), and sensors attached to the participant (HS01) and to the robot (RS01). Recurrence plots were computed with embedding parameters $m = 6$, $\tau = 8$ and $\epsilon = 1$. R code to reproduce the figure is available from Xochicale (2018).

Additional results for HHI experiment

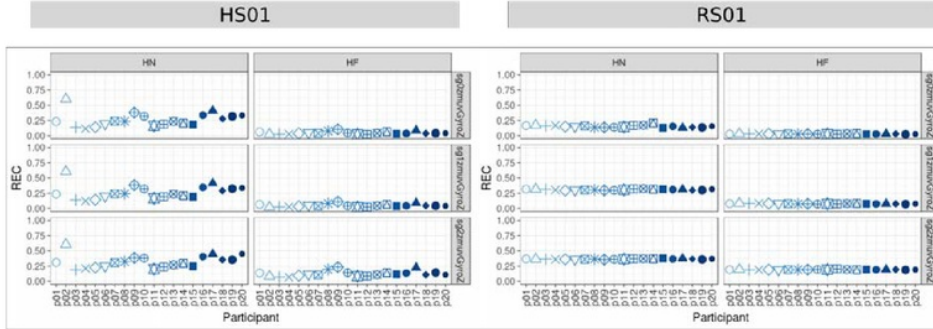


Fig. E.19 **REC values for horizontal arm movements.** REC values (representing % of black dots in the RPs) for 20 participants performing HN and HF movements with sensors HS01, RS01 and three smoothed-normalised axis¹ of GyroZ (sg0zmuvGyroZ, sg1zmuvGyroZ and sg2zmuvGyroZ). REC values were computed with embedding parameters $m = 6$, $\tau = 8$ and $\epsilon = 1$ R code to reproduce the figure is available from Kochicale (2018).

E.5 RQAs

E.5.1 REC values

REC values, representing the % of black dots in the RPs, are shown in Figs. E.19 and E.20.

E.5 RQAs

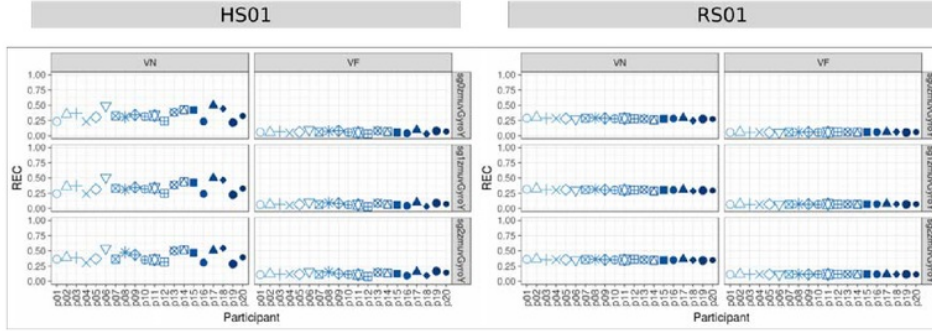


Fig. E.20 REC values for vertical arm movements. REC values (representing % of black dots in the RPs) for 20 participants performing VN and VF movements with sensors HS01, RS01 and three smoothed-normalised axis 1 of GyroY (sg0zmuvGyroY, sg1zmuvGyroY and sg2zmuvGyroY). REC values were computed with embedding parameters $m = 6$, $\tau = 8$ and $\epsilon = 1$. R code to reproduce the figure is available from Kochicale (2018).

E.5.2 DET values

DET values, representing predictability and organisation of the RPs. 163 are shown in Figs. E.21 and E.22.

Additional results for HHI experiment

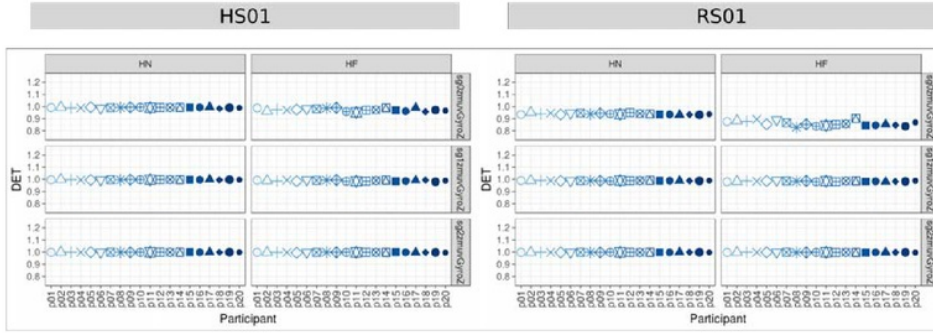


Fig. E.21 DET values for horizontal arm movements. DET values (representing predictability and organisation of the RPs) for 20 participants performing HN and HF movements with sensors HS01, RS01 and three smoothed-normalised \mathbf{z} axis of GyroZ (sg0zmuvGyroZ, sg1zmuvGyroZ and sg2zmuvGyroZ). DET values were computed with embedding parameters $m = 6$, $\tau = 8$ and $\epsilon = 1$. R code to reproduce the figure is available from Xochicale (2018).

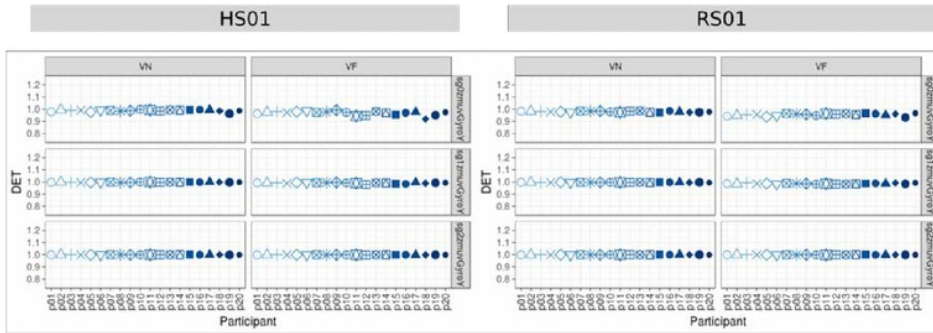


Fig. E.22 DET values for vertical arm movements. DET values (representing predictability and organisation of the RPs) for 20 participants performing VN and VF movements with sensors HS01, RS01 and three smoothed-normalised \mathbf{x} axis of GyroY (sg0zmuvGyroY, sg1zmuvGyroY and sg2zmuvGyroY). DET values were computed with embedding parameters $m = 6$, $\tau = 8$ and $\epsilon = 1$. R code to reproduce the figure is available from Xochicale (2018).

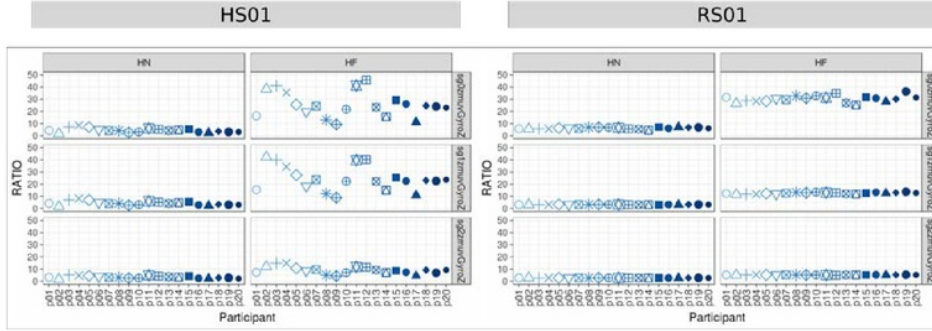


Fig. E.23 RATIO values for horizontal arm movements. RATIO (representing dynamic transitions) for 20 participants performing HN and HF movements with sensors HS01, RS01 and three smoothed-normalised axis 1 of GyroZ (sg0zmuvGyroZ, sg1zmuvGyroZ and sg2zmuvGyroZ). RATIO values were computed with embedding parameters $m = 6$, $\tau = 8$ and $\epsilon = 1$. R code to reproduce the figure is available from Kochicale (2018).

E.5.3 RATIO values

RATIO values, representing dynamic transitions, are shown in Figs. E.23 and E.24. 163

Additional results for HHI experiment

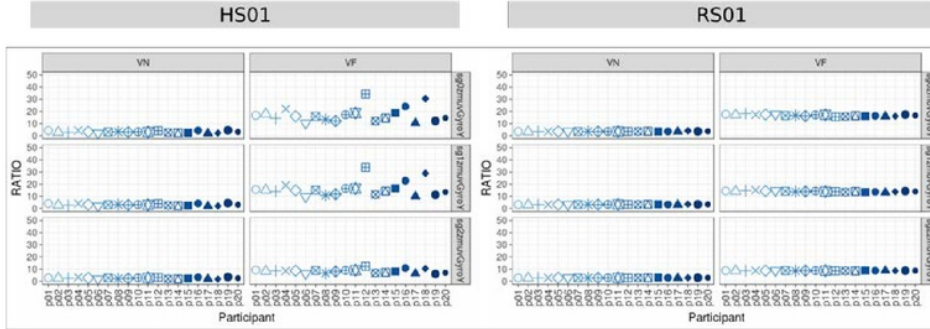


Fig. E.24 RATIO values for vertical arm movements. RATIO (representing dynamic transitions) for 20 participants performing VN and VF movements with sensors HS01, RS01 and three smoothed-normalised axis ① GyroY ($sg0zmuvGyroY$, $sg1zmuvGyroY$ and $sg2zmuvGyroY$). RATIO values were computed with embedding parameters $m = 6$, $\tau = 8$ and $\epsilon = 1$. R code to reproduce the figure is available from Kochicale (2018).

E.5.4 ENTR values

ENTR values, representing the complexity of the ructure in time series, are shown in Figs. E.25 and E.26.

E.5 RQAs

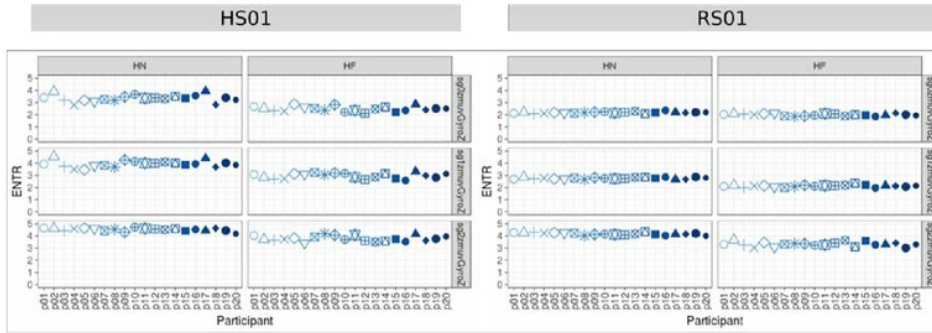


Fig. E.25 ⁶² ENTR values for horizontal arm movements. ENTR values (representing the complexity of the deterministic structure in time series) for 20 participants performing HN and HF movements with sensors HS01, RS01 and three smoothed-normalised axis of GyroZ (sg0zmuvGyroZ, sg1zmuvGyroZ and sg2zmuvGyroZ). ENTR values were computed with embedding parameters $m = 6$, $\tau = 8$ and $\epsilon = 1$. R code to reproduce the figure is available from Xochicale (2018).

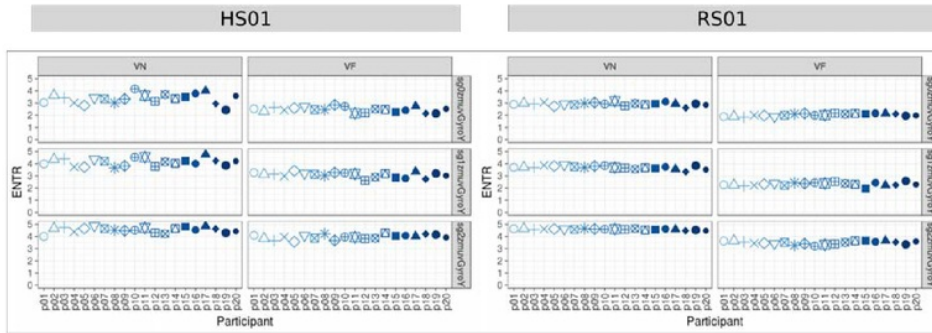
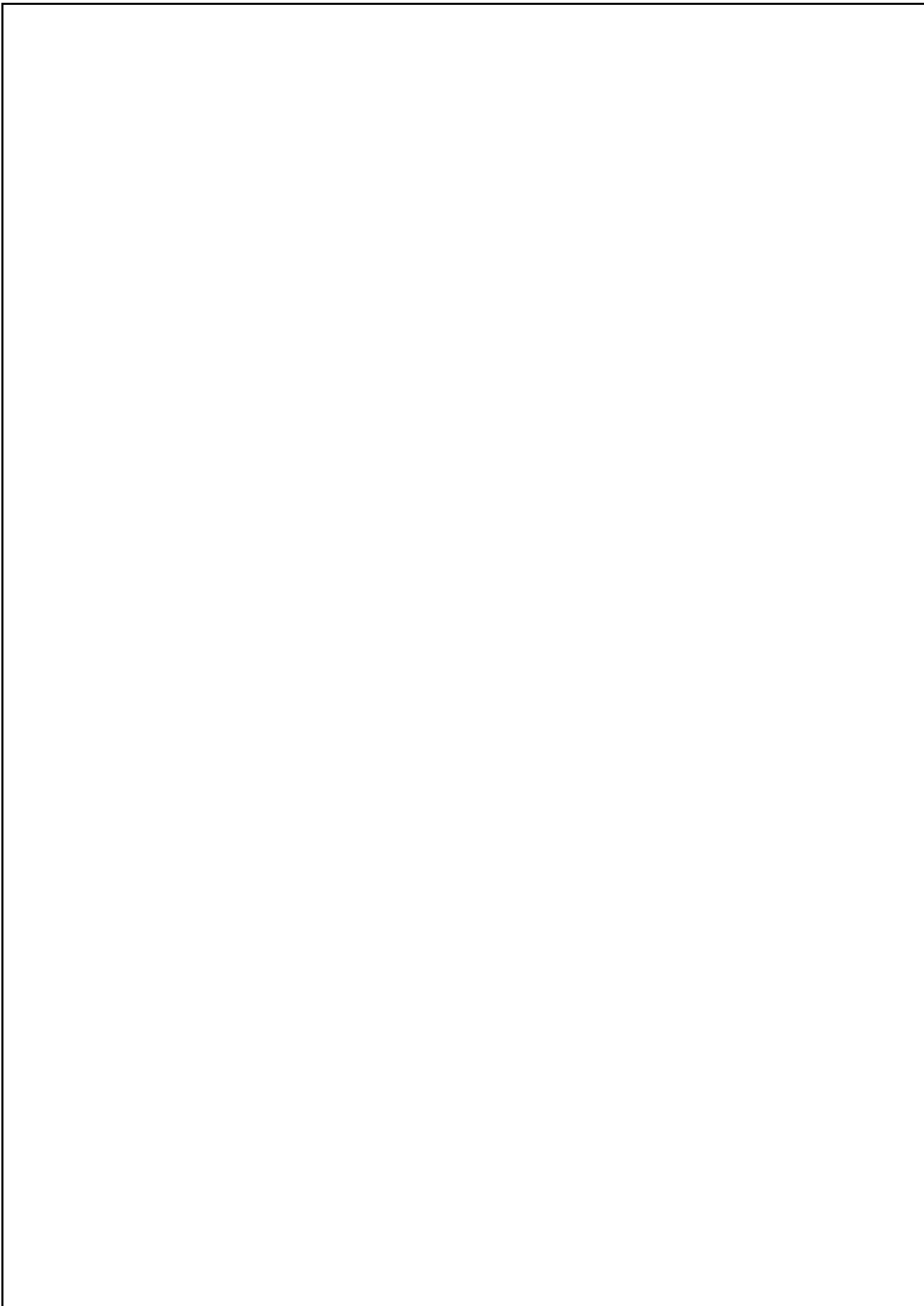


Fig. E.26 ⁶² ENTR values for vertical arm movements. ENTR values (representing the complexity of the deterministic structure in time series) for 20 participants performing VN and VF movements with sensors HS01, RS01 and three smoothed-normalised axis of GyroY (sg0zmuvGyroY, sg1zmuvGyroY and sg2zmuvGyroY). ENTR values were computed with embedding parameters $m = 6$, $\tau = 8$ and $\epsilon = 1$. R code to reproduce the figure is available from Xochicale (2018).



38

References

- Aguirre, L. A. and Letellier, C. (2009). Modeling nonlinear dynamics and chaos: A review. *Mathematical Problems in Engineering*, 11(12):1–22.
- 35 Amato, I. (1992). Chaos breaks out at nih, but order may come of it. *Science*, 256(5065):1763–1764.
- 55 Anguita, D., Ghio, A., Oneto, L., Parra, X., and Reyes-Ortiz, J. L. (2013). A public domain dataset for human activity recognition using smartphones. In *21th European Symposium on Artificial Neural Networks, Computational Intelligence and Machine Learning, ESANN 2013*.
- 104 Azami, H. and Escudero, J. (2016). Amplitude-aware permutation entropy: Illustration in spike detection and signal segmentation. *Computer Methods and Programs in Biomedicine*, 128:40 – 51.
- 61 Bandt, C. and Pompe, B. (2002). Permutation entropy: A natural complexity measure for time series. *Phys. Rev. Lett.*, 88:174102.
- Bartlett, R., Wheat, J., and Robins, M. (2007). Is movement variability important for sports biomechanists? *Sports Biomechanics*, 6(2):224–243. PMID: 17892098.
- 49 Benzeghiba, M., Mori, R. D., Deroo, O., Dupont, S., Erbes, T., Jouvet, D., Fissore, L., Laface, P., Mertins, A., Ris, C., Rose, R., Tyagi, V., and Wellekens, C. (2007). Automatic speech recognition and speech variability: A review. *Speech Communication*, 49(10):763 – 786. Intrinsic Speech Variations.
- 143 Bernstein, N. (1967). *The co-ordination and regulation of movements*. Pergamon-Press.
- 83 Bonnet, V., Ramdani, S., Azevedo-Coste, C., Fraisse, P., Mazzà, C., and Cappozzo, A. (2014). Integration of human walking gyroscopic data using empirical mode decomposition. *Sensors*, 14(1):370–381.
- 45 Bradley, E. and Kantz, H. (2015). Nonlinear time-series analysis revisited. *Chaos: An Interdisciplinary Journal of Nonlinear Science*, 25(9):097610.
- 63 Bruijn, S. M., van Dieën, J. H., Meijer, O. G., and Beek, P. J. (2009). Is slow walking more stable? *Journal of Biomechanics*, 42(10):1506 – 1512.
- 203 Bryce, R. and Sprague, K. (2012). Revisiting detrended fluctuation analysis. *Scientific reports*, 2:315.

References

- ³ Caballero, C., Barbado, D., and Moreno, F. (2013). El procesado del desplazamiento del centro de presiones para el estudio de la relación complejidad/rendimiento observada en el control postural en bipedestación. *Revista Andaluza de Medicina del Deporte*, 6(3):101 – 107.
- Caballero, C., Barbado, D., and Moreno, F. J. (2014). Non-linear tools and methodological concerns measuring human movement variability: An overview. *European Journal of Human Movement*, 32:31–81.
- ⁴⁴ Cao, L. (1997). Practical method for determining the minimum embedding dimension of a scalar time series. *Physica D: Nonlinear Phenomena*, 110:43–50.
- ² Carroll, J. P. and Freedman, W. (1993). Nonstationary properties of postural sway. *Journal of biomechanics*, 26(4):409–416.
- ⁴⁰ Casdagli, M., Eubank, S., Farmer, J., and Gibson, J. (1991). State space reconstruction in the presence of noise. *Physica D: Nonlinear Phenomena*, 51(1):52 – 98.
- ¹⁰³ Cavanaugh, J. T., Kochi, N., and Stergiou, N. (2010). Nonlinear analysis of ambulatory activity patterns in community-dwelling older adults. *The Journals of Gerontology: Series A*, 65A(2):197–203.
- ³ Chen, W., Wang, Z., Xie, H., and Yu, W. (2007). Characterization of surface emg signal based on fuzzy entropy. *IEEE Transactions on Neural Systems and Rehabilitation Engineering*, 15(2):266–272.
- Chen, W., Zhuang, J., Yu, W., and Wang, Z. (2009). Measuring complexity using fuzzyen, apen, and sampen. *Medical Engineering and Physics*, 31(1):61 – 68.
- ⁴⁵ Chiari, L., Rocchi, L., and Cappello, A. (2002). Stabilometric parameters are affected by anthropometry and foot placement. *Clinical Biomechanics*, 17(9):666 – 677.
- ¹¹ Coffey, N., Harrison, A., Donoghue, O., and Hayes, K. (2011). Common functional principal components analysis: A new approach to analyzing human movement data. *Human Movement Science*, 30(6):1144 – 1166.
- ⁷ Comotti, D., Galizzi, M., and Vitali, A. (2014). nememsi: One step forward in wireless attitude and heading reference systems. In *2014 International Symposium on Inertial Sensors and Systems (ISISS)*, pages 1–4.
- Corso, G., Prado, T. L., Lima, G. Z. d. S., and Lopes, S. R. (2017). A novel entropy recurrence quantification analysis. *ArXiv e-prints*.
- ¹² Costa, M., Goldberger, A. L., and Peng, C.-K. (2002). Multiscale entropy analysis of complex physiologic time series. *Phys. Rev. Lett.*, 89:068102.
- Costa, M., Priplata, A. A., Lipsitz, L. A., Wu, Z., Huang, N. E., Goldberger, A. L., and Peng, C.-K. (2007). Noise and poise: Enhancement of postural complexity in the elderly with a stochastic-resonance-based therapy. *EPL (Europhysics Letters)*, 77(6):68008.

References

- ⁴⁶ Daubechies, I., Lu, J., and Wu, H.-T. (2011). Synchrosqueezed wavelet transforms: An empirical mode decomposition-like tool. *Applied and Computational Harmonic Analysis*, 30(2):243 – 261.
- ¹²⁹ de Vries, J., Visser, G., and Prechtel, H. (1982). The emergence of fetal behaviour. i. qualitative aspects. *Early Human Development*, 7(4):301 – 322.
- ⁴⁸ Delignières, D., Deschamps, T., Legros, A., and Caillou, N. (2003). A methodological note on nonlinear time series analysis: Is the open-and closed-loop model of collins and de luca (1993) a statistical artifact? *Journal of Motor Behavior*, 35(1):86–96. PMID: 12724102.
- ¹⁹ Dhingra, R. R., Jacono, F. J., Fishman, M., Loparo, K. A., Rybak, I. A., and Dick, T. E. (2011). Vagal-dependent nonlinear ²⁵¹ability in the respiratory pattern of anesthetized, spontaneously breathing rats. *Journal of Applied Physiology*, 111(1):272–284. PMID: 21527661.
- ² Dingwell, J. B. and Cusumano, J. P. (2000). Nonlinear time series analysis of normal and pathological human walking. *Chaos: An Interdisciplinary Journal of Nonlinear Science*, 10(4):848–863.
- Dingwell, J. B. and Kang, H. G. (2007). Differences between local and orbital dynamic stability during human walking. *Journal of biomechanical engineering*, 129(4):586—593.
- Donker, S. F., Roerdink, M., Greven, A. J., and Beek, P. J. (2007). Regularity of center-of-pressure trajectories depends on the amount of attention invested in postural control. *Experimental Brain Research*, 181(1):1–11.
- ² Duarte, M. and Sternad, D. (2008). Complexity of human postural control in young and older adults during prolonged standing. *Experimental Brain Research*, 191(3):265–276.
- ¹³³ Eager, D., Pendrill, A.-M., and Reistad, N. (2016). Beyond velocity and acceleration: jerk, snap and higher derivatives. *European Journal of Physics*, 37(6):065008.
- ² Eckmann, J.-P., Kamphorst, S. O., and Ruelle, D. (1987). Recurrence plots of dynamical systems. *EPL (Europhysics Letters)*, 4(9):973.
- ¹ Emrani, S., Gentimis, T., and Krim, H. (2014). Persistent homology of delay embeddings and its application to wheeze detection. *IEEE Signal Processing Letters*, 21(4):459–463.
- ⁵⁴ Ferdenzi, C., Roberts, S. C., Schirmer, A., Delplanque, S., Cekic, S., Porcherot, C., Cayeux, I., Sander, D., and Grandjean, D. (2013). Variability of affective responses to odors: Culture, gender, and olfactory knowledge. *Chemical Senses*, 38(2):175–186.
- ¹³⁹ Flandrin, P., Gonçalvès, P., and Rilling, G. (2004). Detrending and denoising with empirical mode decompositions. In *2004 12th European Signal Processing Conference*, pages 1581–1584.

References

- 110 Flash, T. and Hogan, N. (1985). The coordination of arm movements: an experimentally confirmed mathematical model. *Journal of Neuroscience*, 5(7):1688–1703.
- 31 Frank, J., Mannor, S., and Precup, D. (2010). Activity and gait recognition with time-delay embeddings. *AAAI Conference on Artificial Intelligence*, pages 407–408.
- 128 Fraser, A. M. and Swinney, H. L. (1986). Independent coordinates for strange attractors from mutual information. *Phys. Rev. A*, 33:1134–1140.
- 19 Garcia, C. A. and Sawitzki, G. (2016). *nonlinearTseries: Nonlinear Time Series Analysis*. R package version 0.2.4 — For new features, see the 'Changelog' file (in the package source).
- 44 Garcia, S. P. and Almeida, J. S. (2005). Nearest neighbor embedding with different time delays. *Phys. Rev. E*, 71:037204.
- 179 Garland, J., Bradley, E., and Meiss, J. D. (2016). Exploring the topology of dynamical reconstructions. *Physica D: Nonlinear Phenomena*, 334:49 – 59. Topology in Dynamics, Differential Equations, and Data.
- 33 Gates, D. H. and Dingwell, J. B. (2007). Peripheral neuropathy does not alter the fractal dynamics of stride intervals of gait. *Journal of Applied Physiology*, 102(3):965–971. PMID: 17110519.
- Gates, D. H. and Dingwell, J. B. (2008). The effects of neuromuscular fatigue on task performance during repetitive goal-directed movements. *Experimental Brain Research*, 187(4):573–585.
- 102 Gibson, J. F., Farmer, J. D., Casdagli, M., and Eubank, S. (1992). An analytic approach to practical state space reconstruction. *Physica D: Nonlinear Phenomena*, 57(1):1 – 30.
- 27 Goldberger, A. (1996). Non-linear dynamics for clinicians: chaos theory, fractals, and complexity at the bedside. *The Lancet*, 347(9011):1312 – 1314.
- Goldberger, A. L., Peng, C.-K., and Lipsitz, L. A. (2002). What is physiologic complexity and how does it change with aging and disease? *Neurobiology of Aging*, 23(1):23 – 26.
- Goldberger, A. L., Rigney, D. R., and West, B. J. (1990). Chaos and fractals in human physiology. *Scientific American*, 262(2):42–49.
- 172 Gören [149], Salah, A. A., and Akin, H. L. (2013). A robotic fitness coach for the elderly. In Augusto, J. C., Wichert, R., Collier, R., Keyson, D., Salah, A. A., and Tan, A.-H., editors, *Ambient Intelligence*, pages 124–139, Cham. Springer International Publishing.
- 59 Gouaillier, D., Hugel, V., Blazevic, P., Kilner, C., Monceaux, J., Lafourcade, P., Marnier, B., Serre, J., and Maisonnier, B. (2009). Mechatronic design of nao humanoid. In Proceedings of the 2009 IEEE International Conference on Robotics and Automation, ICRA'09, pages 2124–2129, Piscataway, NJ, USA. IEEE Press.

References

- Guastello, S. J. and Gregson, R. A. M. (2011). *Nonlinear Dynamical Systems Analysis for the Behavioral Science Using Real Data*. CRC Press.
- 42 Guney-su, A., Arnrich, B., and Ersoy, C. (2015). Children's rehabilitation with humanoid robots and wearable inertial measurement units. In *Proceedings of the 9th International Conference on Pervasive Computing Technologies for Healthcare, PervasiveHealth '15*, pages 249–252, ICST, Brussels, Belgium, Belgium. ICST (Institute for Computer Sciences, Social-Informatics and Telecommunications Engineering).
- 95 Guney-su, A., Siyli, R. D., and Salah, A. A. (2014). Auto-evaluation of motion imitation in a child-robot imitation game for upper arm rehabilitation. In *The 23rd IEEE International Symposium on Robot and Human Interactive Communication*, pages 199–204.
- 75 Gómez-García, J. A., Godino-Llorente, J. I., and Castellanos-Dominguez, G. (2014). Non uniform embedding based on relevance analysis with reduced computational complexity: Application to the detection of pathologies from biosignal recordings. *Neurocomputing*, 132(Supplement C):178 – 158. Innovations in Nature Inspired Optimization and Learning Methods Machines learning for Non-Linear Processing.
- 18 Harbourne, R. T. and Stergiou, N. (2009). Movement variability and the use of nonlinear tools: Principles to guide physical therapist practice. *Physical Therapy*, 89(3):267–282.
- 11 Hatze, H. (1986). Motion variability—its definition, quantification, and origin. *Journal of Motor Behavior*, 18(1):5–16. PMID: 15136282.
- 31 Hausdorff, J. M. (2009). Gait dynamics in parkinson's disease: Common and distinct behavior among stride length, gait variability, and fractal-like scaling. *Chaos: An Interdisciplinary Journal of Nonlinear Science*, 19(2):026113.
- 18 Hausdorff, J. M., Peng, C. K., Ladin, Z., Wei, J. Y., and Goldberger, A. L. (1995). Is walking a random walk? evidence for long-range correlations in stride interval of human gait. *Journal of Applied Physiology*, 78(1):349–358. PMID: 7713836.
- 132 Herzfeld, D. J. and Shadmehr, R. (2014). Motor variability is not noise, but grist for the learning mill. *nature neuroscience*, 17(2):149.
- 22 Huang, N. E., Shen, Z., Long, S. R., Wu, M. C., Shih, H. H., Zheng, Q., Yen, N.-C., Tung, C. C., and Liu, H. H. (1998). The empirical mode decomposition and the hilbert spectrum for nonlinear and non-stationary time series analysis. *Proceedings of the Royal Society of London A: Mathematical, Physical and Engineering Sciences*, 454(1971):903–995.
- 197 Huffaker, R., Bittelli, M., and Rosa, R. (2017). *Nonlinear Time Series Analysis with R*. Oxford University Press.
- 8 Ioffe, S. and Szegedy, C. (2015). Batch normalization: Accelerating deep network training by reducing internal covariate shift. *CoRR*, abs/1502.03167.

References

- ⁸² Iwanski, J. S. and Bradley, E. (1998). Recurrence plots of experimental data: To embed or not to embed? *Chaos: An Interdisciplinary Journal of Nonlinear Science*, 8(4):861–871.
- ¹³⁸ Kabiraj, L., Saurabh, A., Wahi, P., and Sujith, R. I. (2012). Route to chaos for combustion instability in ducted laminar premixed flames. *Chaos: An Interdisciplinary Journal of Nonlinear Science*, 22(2):023129.
- ¹²⁷ Kanai, R. and Rees, G. (2011). The structural basis of inter-individual differences in human behaviour and cognition. *Nature Reviews Neuroscience*, 12(4):231.
- ⁵³ Kantz, H. and Schreiber, T. (2003). *Nonlinear Time Series Analysis*. Cambridge University Press, New York, NY, USA.
- Kennel, M. B., Brown, R., and Abarbanel, H. D. I. (1992). Determining embedding dimension for phase-space reconstruction using a geometrical construction. *Phys. Rev. A*, 45:3403–3411.
- ⁸⁹ Kitagawa, G. and Gersch, W. (1984). A smoothness priors-state space modeling of time series with trend and seasonality. *Journal of the American Statistical Association*, 79(386):378–389.
- ⁵⁷ Klonowski, W. (2002). Chaotic dynamics applied to signal complexity in phase space and in time domain. *Chaos, Solitons and Fractals*, 14(9):1379 – 1387.
- ¹⁰⁹ Klonowski, W. (2007). From conformons to human brains: an informal overview of nonlinear dynamics and its applications in biomedicine. *Nonlinear Biomedical Physics*, 1(1):5.
- ¹¹⁹ Klonowski, W. (2009). Everything you wanted to ask about eeg but were afraid to get the right answer. *Nonlinear Biomedical Physics*, 3(1):2.
- ⁴⁰ Krakovská, A., Mezeiová, K., and I, H. B. (2015). Use of False Nearest Neighbours for Selecting Variables and Embedding Parameters for State Space Reconstruction. *Journal of Complex Systems*, 2015.
- ¹¹⁸ Krüger, M., Eggert, T., and Straube, A. (2013). Age-related differences in the stabilization of important task variables in reaching movements. *Motor Control*, 17(3):313–320.
- ⁵ Kurz, M. J. and Hou, J. G. (2010). Levodopa influences the regularity of the ankle joint kinematics in individuals with parkinson’s disease. *Journal of Computational Neuroscience*, 28(1):131–136.
- Kurz, M. J., Markopoulou, K., and Stergiou, N. (2010). Attractor divergence as a metric for assessing walking balance. *Nonlinear dynamics, psychology, and life sciences*, 14(2):151–164.
- ¹⁴ Lake, D. E. and Moorman, J. R. (2011). Accurate estimation of entropy in very short physiological time series: the problem of atrial fibrillation detection in implanted ventricular devices. *American Journal of Physiology-Heart and Circulatory Physiology*, 300(1):H319–H325. PMID: 21037227.

References

- 155 Letellier, C. (2006). Estimating the shannon entropy: Recurrence plots versus symbolic dynamics. *Phys. Rev. Lett.*, 96:254102.
- 81 Liao, F., Wang, J., and He, P. (2008). Multi-resolution entropy analysis of gait symmetry in neurological degenerative diseases and amyotrophic lateral sclerosis. *Medical Engineering and Physics*, 30(3):299 – 310.
- 88 MacDonald, S. W., Nyberg, L., and Bäckman, L. (2006). Intra-individual variability in behavior: links to brain structure, neurotransmission and neuronal activity. *Trends in Neurosciences*, 29(8):474 – 480.
- 15 Madeleine, P. and Madsen, T. (2009). Changes in the amount and structure of motor variability during a deboning process are associated with work experience and neck–shoulder discomfort. *Applied Ergonomics*, 40(5):887 – 894.
- Madeleine, P., Mathiassen, S. E., and Arendt-Nielsen, L. (2008). Changes in the degree of motor variability associated with experimental and chronic neck–shoulder pain during a standardised repetitive arm movement. *Experimental Brain Research*, 185(4):689–698.
- 68 Mandic, D. P., u. Rehman, N., Wu, Z., and Huang, N. E. (2013). Empirical mode decomposition-based time-frequency analysis of multivariate signals: The power of adaptive data analysis. *IEEE Signal Processing Magazine*, 30(6):74–86.
- 28 Marwan, N. (2008). A historical review of recurrence plots. *The European Physical Journal Special Topics*, 164(1):3–12.
- Marwan, N. (2011). How to Avoid Potential Pitfalls in Recurrence Plot Based Data Analysis. *International Journal of Bifurcation and Chaos*, 21:1003.
- 36 Marwan, N., Romano, M. C., Thiel, M., and Kurths, J. (2007). Recurrence plots for the analysis of complex systems. *Physics Reports*, 438(5):237 – 329.
- Marwan, N. and Webber, C. L. (2015). Mathematical and computational foundations of recurrence quantifications. In Webber, C. L. and Marwan, N., editors, *Recurrence Quantification Analysis: Theory and Best Practices*, chapter 1, pages 3–43. Springer, Cham, 1 edition.
- 101 Mathiassen, S. E. (2006). Diversity and variation in biomechanical exposure: What is it, and why would we like to know? *Applied Ergonomics*, 37(4):419 – 427. Special Issue: Meeting Diversity in Ergonomics.
- 126 Mert, A. and Akan, A. (2018). Emotion recognition from eeg signals by using multivariate empirical mode decomposition. *Pattern Analysis and Applications*, 21(1):81–89.
- 11 Miller, D. J., Stergiou, N., and Kurz, M. J. (2006). An improved surrogate method for detecting the presence of chaos in gait. *Journal of Biomechanics*, 39(15):2873 – 2876.
- 187 Mori, H. and Kuniyoshi, Y. (2012). Is the developmental order of fetal behaviors self-organized in an uterine environment? In *2012 IEEE International Conference on Development and Learning and Epigenetic Robotics (ICDL)*, pages 1–2.

References

- ⁴¹ Müller, H. and Sternad, D. (2004). Decomposition of variability in the execution of goal-oriented tasks: three components of skill improvement. *Journal of Experimental Psychology: Human Perception and Performance*, 30(1):212.
- Newell, K. and Corcos, D. (1993). *Variability and Motor Control*. Human Kinetics Publishers.
- ¹⁰⁸ Newell, K. M. and Slifkin, A. B. (1998). The nature of movement variability. In Piek, J. P., editor, *Motor behavior and human skill : a multidisciplinary approach*, chapter 7, pages 143–160. Champaign, IL : Human Kinetics.
- ⁸⁷ Packard, N. H., Crutchfield, J. P., Farmer, J. D., and Shaw, R. S. (1980). Geometry from a time series. *Phys. Rev. Lett.*, 45:712–716.
- ⁹⁶ Pecora, L. M., Moniz, L., Nichols, J., and Carroll, T. L. (2007). A unified approach to attractor reconstruction. *Chaos: An Interdisciplinary Journal of Nonlinear Science*, 17(1):013110.
- ¹²⁵ Pellecchia, G. L. and Shockley, K. (2015). Application of recurrence quantification analysis: Influence of cognitive activity on natural fluctuations. In Riley, M., Van Orden, G., and (U.S.), N. S. F., editors, *Tutorials in Contemporary Nonlinear Methods for the Behavioral Sciences*, chapter 3, pages 95–141. National Science Foundation.
- ¹⁴ Peng, C., Havlin, S., Stanley, H. E., and Goldberger, A. L. (1995). Quantification of scaling exponents and crossover phenomena in nonstationary heartbeat time series. *Chaos: An Interdisciplinary Journal of Nonlinear Science*, 5(1):82–87.
- ¹⁰⁷ Peng, H., Zhou, C., Hu, H., Chao, F., and Li, J. (2015). Robotic dance in social robotics – a taxonomy. *IEEE Transactions on Human-Machine Systems*, 45(3):281–293.
- ⁵² Pincus, S. (1995). Approximate entropy (apen) as a complexity measure. *Chaos: An Interdisciplinary Journal of Nonlinear Science*, 5(1):110–117.
- Pincus, S. M. (1991). Approximate entropy as a measure of system complexity. *Proceedings of the National Academy of Sciences of the United States of America*, 88(6):2297–2301.
- ¹¹⁷ Pretoni, E. (2007). *Innovative methods for the analysis of sports movements and for the longitudinal monitoring of individual motor skills*. PhD thesis, Politecnico di Milano.
- ²⁶ Pretoni, E., Ferrario, M., Donà, G., Hamill, J., and Rodano, R. (2010). Motor variability in sports: A non-linear analysis of race walking. *Journal of Sports Sciences*, 28(12):1327–1336. PMID: 20853204.
- Pretoni, E., Hamill, J., Harrison, A. J., Hayes, K., Emmerik, R. E. V., Wilson, C., and Rodano, R. (2013). Movement variability and skills monitoring in sports. *Sports Biomechanics*, 12(2):69–92. PMID: 23898682.

References

- 70 Press, W. H., Teukolsky, S. A., Vetterling, W. T., and Flannery, B. P. (1992). *Numerical Recipes in C (2Nd Ed.): The Art of Scientific Computing*. Cambridge University Press, New York, NY, USA.
- 154 Quintana-Duque, J. and Saupe, D. (2013). *Evidence of Chaos in Indoor Pedaling Motion using Non-linear Methods*. Number July in Performance Analysis of Sport. Routledge.
- 162 Quintana-Duque, J. C. (2012). Non-linear dynamic invariants based on embedding reconstruction of systems for pedaling motion. In Byshko, R., editor, *Sportinformatik 2012 : 9. vom 12.- 14. Sept. 2012 in Konstanz : Beiträge*, pages 28–38. Universität.
- Quintana-Duque, J. C. (2016). *Non-linear methods for the quantification of cyclic motion*. PhD dissertation, University of Konstanz, Konstanz, Germany.
- 80 Rajendra Acharya, U., Paul Joseph, K., Kannathal, N., Lim, C. M., and Suri, J. S. (2006). Heart rate variability: a review. *Medical and Biological Engineering and Computing*, 44(12):1031–1051.
- 116 Rangarajan, G. and Ding, M. (2000). Integrated approach to the assessment of long range correlation in time series data. *Phys. Rev. E*, 61:4991–5001.
- 124 Rehman, N. and Mandic, D. P. (2010). Multivariate empirical mode decomposition. *Proceedings of the Royal Society of London A: Mathematical, Physical and Engineering Sciences*, 466(2117):1291–1302.
- 2 Rhea, C. K., Silver, T. A., Hong, S. L., Ryu, J. H., Studenka, B. E., Hughes, C. M. L., and Haddad, J. M. (2011). Noise and complexity in human postural control: Interpreting the different estimations of entropy. *PLOS ONE*, 6(3):1–9.
- Richman, J. S. and Moorman, J. R. (2000). Physiological time-series analysis using approximate entropy and sample entropy. *American Journal of Physiology-Heart and Circulatory Physiology*, 278(6):H2039–H2049. PMID: 10843903.
- Riley, M., Balasubramaniam, R., and Turvey, M. (1999). Recurrence quantification analysis of postural fluctuations. *Gait and Posture*, 9(1):65 – 78.
- 37 Rosenstein, M. T., Collins, J. J., and Luca, C. J. D. (1993). A practical method for calculating largest lyapunov exponents from small data sets. *Physica D: Nonlinear Phenomena*, 65(1):117 – 134.
- Rosenstein, M. T., Collins, J. J., and Luca, C. J. D. (1994). Reconstruction expansion as a geometry-based framework for choosing proper delay times. *Physica D: Nonlinear Phenomena*, 73(1):82 – 98.
- 79 Samà, A., Ruiz, F. J., Agell, N., Pérez-López, C., Català, A., and Cabestany, J. (2013). Gait identification by means of box approximation geometry of reconstructed attractors in latent space. *Neurocomputing*, 121:79–88.
- 69 Sandlund, J., Röijezon, U., Björklund, M., and Djupsjöbacka, M. (2008). Acuity of goal-directed arm movements to visible targets in chronic neck pain. *Journal of Rehabilitation Medicine*, 40(5):366–374.

References

- 115 Sandlund, J., Srinivasan, D., Heiden, M., and Mathiassen, S. E. (2017). Differences in motor variability among individuals performing a standardized short-cycle manual task. *Human Movement Science*, 51:17 – 26.
- 123 Savitzky, A. and Golay, M. J. E. (1964). Smoothing and differentiation of data by simplified least squares procedures. *Analytical Chemistry*, 36:1627–1639.
- 100 Schafer, R. W. (2011). On the frequency-domain properties of savitzky-golay filters. In *2011 Digital Signal Processing and Signal Processing Education Meeting (DSP/SPE)*, pages 54–59.
- 122 Schumacher, A. (2004). Linear and nonlinear approaches to the analysis of r-r interval variability. *Biological Research For Nursing*, 5(3):211–221. PMID: 14737922.
- 32 Seifert, L., Leblanc, H., Herault, R., Komar, J., Button, C., and Chollet, D. (2011). Inter-individual variability in the upper-lower limb breaststroke coordination. *Human Movement Science*, 30(3):550 – 565.
- 94 Shoaib, M., Bosch, S., Incel, O. D., Scholten, H., and Havinga, P. J. M. (2016). Complex human activity recognition using smartphone and wrist-worn motion sensors. *Sensors*, 16(4).
- 5 signal R developers (2014). *signal: Signal processing*.
- 5 Sosnoff, J. J., Valantine, A. D., and Newell, K. M. (2006). Independence between the amount and structure of variability at low force levels. *Neuroscience Letters*, 392(3):165 – 169.
- 16 Sosnoff, J. J. and Voudrie, S. J. (2009). Practice and age-related loss of adaptability in sensorimotor performance. *Journal of Motor Behavior*, 41(2):137–146. PMID: 19201684.
- 67 Stergiou, N. (2016). *Nonlinear Analysis for Human Movement Variability*. CRC Press.
- 16 Stergiou, N. and Decker, L. M. (2011). Human movement variability, nonlinear dynamics, and ¹²⁴⁹iology: Is there a connection? *Human Movement Science*, 30(5):869 – 888. EWOMS 2009: The European Workshop on Movement Science.
- 35 Stergiou, N., Harbourne, R., and Cavanaugh, J. (2006). Optimal movement variability: a new theoretical perspective for neurologic physical therapy. *Journal of neurologic physical therapy : JNPT*, 30(3):120—129.
- 177 Stergiou, N., Kent, J. A., and McGrath, D. (2016). Human movement variability and aging. *Kinesiology Review*, 5(1):15–22.
- 78 Stins, J., Michielsen, M., Roerdink, M., and Beek, P. (2009). Sway regularity reflects attentional involvement in postural control: Effects of expertise, vision and cognition. *Gait and Posture*, 30(1):106 – 109.

References

- 86 Svendsen, J. H. and Madeleine, P. (2010). Amount and structure of force variability during short, ramp and sustained contractions in males and females. *Human Movement Science*, 29(1):35 – 47.
- 87 Takens, F. (1981). Detecting strange attractors in turbulence. *Dynamical Systems and Turbulence, Warwick 1980: Proceedings of a Symposium Held at the University of Warwick 1979/80*, pages 366–381.
- 39 Tononi, G., Edelman, G. M., and Sporns, O. (1998). Complexity and coherency: integrating information in the brain. *Trends in Cognitive Sciences*, 2(12):474 – 484.
- 114 Trullna, L., Giuliani, A., Zbilut, J., and Webber, C. (1996). Recurrence quantification analysis of the logistic equation with transients. *Physics Letters A*, 223(4):255 – 260.
- 121 Tsuchida, S., Terada, T., and Tsukamoto, M. (2013). A system for practicing formations in dance performance supported by self-propelled screen. In *Proceedings of the 4th Augmented Human International Conference*, AH '13, pages 178–185, New York, NY, USA. ACM.
- 1 Uzal, L. C., Grinblat, G. L., and Verdes, P. F. (2011). Optimal reconstruction of dynamical systems: A noise amplification approach. *Phys. Rev. E*, 84:016223.
- Uzal, L. C. and Verdes, P. F. (2010). Optimal Irregular Delay Embeddings. In *Dynamics Days South America 2010*. National Institute for Space Research.
- 29 Vaillancourt, D. E. and Newell, K. M. (2002). Changing complexity in human behavior and physiology through aging and disease. *Neurobiology of Aging*, 23(1):1 – 11.
- Vaillancourt, D. E. and Newell, K. M. (2003). Aging and the time and frequency structure of force output variability. *Journal of Applied Physiology*, 94(3):903–912. PMID: 12571125.
- 170 Vaillancourt, D. E., Slifkin, A. B., and Newell, K. M. (2001). Regularity of force tremor in parkinson's disease. *Clinical Neurophysiology*, 112(9):1594 – 1603.
- 3 Vaillancourt, D. E., Sosnoff, J. J., and Newell, K. M. (2004). Age-related changes in complexity depend on task dynamics. *Journal of Applied Physiology*, 97(1):454–455. PMID: 15220326.
- 77 Vakharia, V., Gupta, V., and Kankar, P. (2015). A multiscale permutation entropy based approach to select wavelet for fault diagnosis of ball bearings. *Journal of Vibration and Control*, 21(16):3123–3131.
- 24 van Dieën, J. H., Koppes, L. L., and Twisk, J. W. (2010). Postural sway parameters in seated balancing: their reliability and relationship with balancing performance. *Gait and Posture*, 31(1):42 – 46.
- 32 Wagner, H., Pfusterschmied, J., Klous, M., von Duvillard, S. P., and Müller, E. (2012). Movement variability and skill level of various throwing techniques. *Human Movement Science*, 31(1):78 – 90.

References

- Webber, C. L. and Zbilut, J. P. (1994). Dynamical assessment of physiological systems and states using recurrence plot strategies. *Journal of Applied Physiology*, 76(2):965–973. PMID: 8175612.
- Webber, C. L. and Zbilut, J. P. (2005). Recurrence quantification analysis of nonlinear dynamical systems. In Riley, M. A. and Orden, G. C. V., editors, *Tutorials in contemporary nonlinear methods for behavioral science*, chapter 2, pages 26–94. National Science Foundation.
- Wijnants, M. L., Bosman, A. M., Hasselman, F., Cox, R. F., and Van Orden, G. C. (2009). 1/f scaling in movement time changes with practice in precision aiming. *Nonlinear Dynamics, Psychology, and Life Sciences*, 13(1):79–98. cited By 88.
- Wolf, A., Swift, J. B., Swinney, H. L., and Vastano, J. A. (1985). Determining lyapunov exponents from a time series. *Physica D: Nonlinear Phenomena*, 16(3):285 – 317.
- Wu, H. G., Miyamoto, Y. R., Castro, L. N. G., Ölveczky, B. P., and Smith, M. A. (2014). Temporal structure of motor variability is dynamically regulated and predicts motor learning ability. *Nature neuroscience*, 17(2):312.
- Wu, M.-C. and Hu, C.-K. (2006). Empirical mode decomposition and synchrogram approach to cardiorespiratory synchronization. *Phys. Rev. E*, 73:051917.
- Wu, Z. and Huang, N. E. (2004). A study of the characteristics of white noise using the empirical mode decomposition method. *Proceedings of the Royal Society of London A: Mathematical, Physical and Engineering Sciences*, 460(2046):1597–1611.
- Wu, Z. and Huang, N. E. (2009). Ensemble empirical mode decomposition: A noise-assisted data analysis method. *Advances in Adaptive Data Analysis*, 01(01):1–41.
- Xochicale, M. (2018). *GitHub repository for code and data of PhD thesis: Nonlinear Analyses to Quantify Movement Variability in Human-Humanoid Interaction*. <https://github.com/mxochicale/phd-thesis-code-data>.
- Yang, C. and Wu, C. Q. (2011). A robust method on estimation of lyapunov exponents from a noisy time series. *Nonlinear Dynamics*, 64(3):279–292.
- Yao, C.-Z. and Lin, Q.-W. (2017). Recurrence plots analysis of the cny exchange markets based on phase space reconstruction. *The North American Journal of Economics and Finance*, 42:584 – 596.
- Zbilut, J. P. and Webber, C. L. (1992). Embeddings and delays as derived from quantification of recurrence plots. *Physics Letters A*, 171(3):199 – 203.
- Zunino, L., Zanin, M., Tabak, B. M., Pérez, D. G., and Rosso, O. A. (2009). Forbidden patterns, permutation entropy and stock market inefficiency. *Physica A: Statistical Mechanics and its Applications*, 388(14):2854 – 2864.

ORIGINALITY REPORT



PRIMARY SOURCES

- | | | |
|---|---|------|
| 1 | edocs.fu-berlin.de
Internet Source | 1 % |
| 2 | www.eurjhm.com
Internet Source | 1 % |
| 3 | dspace.umh.es
Internet Source | <1 % |
| 4 | Khondekar, Mofazzal Hossain, Dipendra Nath Ghosh, Koushik Ghosh, and Anup Kumar Bhattacharjee. "Complexity in Solar Irradiance From the Earth Radiation Budget Satellite", <i>IEEE Systems Journal</i> , 2015.
Publication | <1 % |
| 5 | www.unomaha.edu
Internet Source | <1 % |
| 6 | "Recurrence Quantification Analysis", Springer Nature America, Inc, 2015
Publication | <1 % |
| 7 | Miguel P. Xochicale, Chris Baber, Mourad Oussalah. "Towards the Quantification of | <1 % |

Human-Robot Imitation Using Wearable Inertial Sensors", Proceedings of the Companion of the 2017 ACM/IEEE International Conference on Human-Robot Interaction - HRI '17, 2017

Publication

8

[edoc.hu-berlin.de](#)

Internet Source

<1 %

9

[etheses.bham.ac.uk](#)

Internet Source

<1 %

10

Hermann Müller. "Decomposition of Variability in the Execution of Goal-Oriented Tasks: Three Components of Skill Improvement.", Journal of Experimental Psychology Human Perception & Performance, 2004

Publication

11

[opus.bath.ac.uk](#)

Internet Source

<1 %

12

[kar.kent.ac.uk](#)

Internet Source

<1 %

13

[journal.frontiersin.org](#)

Internet Source

<1 %

14

[www.scitepress.org](#)

Internet Source

<1 %

15

[espace.library.uq.edu.au](#)

Internet Source

<1 %

16	eprints.qut.edu.au Internet Source	<1 %
17	Submitted to University of Birmingham Student Paper	<1 %
18	ulir.ul.ie Internet Source	<1 %
19	www.frontiersin.org Internet Source	<1 %
20	Springer Proceedings in Physics, 2016. Publication	<1 %
21	Miguel P. Xochicale, Chris Baber. "Towards the Analysis of Movement Variability in Human-Humanoid Imitation Activities", Proceedings of the 5th International Conference on Human Agent Interaction - HAI '17, 2017 Publication	<1 %
22	Feng, Xiaoyi, Shouyang Wang, Shuai Wang, and Xun Zhang. "Exploring the relationship between crude oil spot and futures prices: New perspective from multi-scale decomposition", International Journal of Energy and Statistics, 2014. Publication	<1 %
23	Christopher K. Rhea. "Noise and Complexity in Human Postural Control: Interpreting the	<1 %

Different Estimations of Entropy", PLoS ONE, 03/17/2011

Publication

-
- | | | |
|-----------------|---|------|
| 24 | qspace.library.queensu.ca | <1 % |
| Internet Source | | |
| 25 | harpgroup.org | <1 % |
| Internet Source | | |
| 26 | Submitted to University of Western Sydney | <1 % |
| Student Paper | | |
| 27 | Karwowski, W.. "A Review of Human Factors Challenges of Complex Adaptive Systems: Discovering and Understanding Chaos in Human Performance", <i>Human Factors The Journal of the Human Factors and Ergonomics Society</i> , 2012. | <1 % |
| Publication | | |
| 28 | d-nb.info | <1 % |
| Internet Source | | |
| 29 | Max J. Kurz. "Levodopa influences the regularity of the ankle joint kinematics in individuals with Parkinson's disease", <i>Journal of Computational Neuroscience</i> , 10/13/2009 | <1 % |
| Publication | | |
| 30 | lup.lub.lu.se | <1 % |
| Internet Source | | |
-

31	theses.ncl.ac.uk	<1 %
Internet Source		
32	Submitted to Coventry University	<1 %
Student Paper		
33	lib.dr.iastate.edu	<1 %
Internet Source		
34	Hermann Müller, Dagmar Sternad. "Decomposition of Variability in the Execution of Goal-Oriented Tasks: Three Components of Skill Improvement.", Journal of Experimental Psychology: Human Perception and Performance, 2004	<1 %
Publication		
35	digitalcommons.unomaha.edu	<1 %
Internet Source		
36	scholar.sun.ac.za	<1 %
Internet Source		
37	www.biomed.bas.bg	<1 %
Internet Source		
38	Submitted to University of Sheffield	<1 %
Student Paper		
39	repository.tudelft.nl	<1 %
Internet Source		
40	www.nonlin-processes-geophys.net	<1 %
Internet Source		

41	Submitted to University of Portsmouth Student Paper	<1 %
42	Submitted to University of Lancaster Student Paper	<1 %
43	www.mdpi.com Internet Source	<1 %
44	hal.archives-ouvertes.fr Internet Source	<1 %
45	Submitted to University of Western Australia Student Paper	<1 %
46	Submitted to University of Hong Kong Student Paper	<1 %
47	tel.archives-ouvertes.fr Internet Source	<1 %
48	documentatiecentrum.kortermaarkrachtig.com Internet Source	<1 %
49	prosodylab.org Internet Source	<1 %
50	cswww.essex.ac.uk Internet Source	<1 %
51	ipag.univ-rouen.fr Internet Source	<1 %

Afshin Samani. "Permuted Sample Entropy",

- 52 Communications in Statistics Simulation and Computation, 09/2010 <1 %
Publication
-
- 53 www.researchgate.net <1 %
Internet Source
-
- 54 cms2.unige.ch <1 %
Internet Source
-
- 55 www.safaribooksonline.com <1 %
Internet Source
-
- 56 Shoaib, Muhammad, Stephan Bosch, Ozlem Incel, Hans Scholten, and Paul Havinga. "Complex Human Activity Recognition Using Smartphone and Wrist-Worn Motion Sensors", Sensors, 2016. <1 %
Publication
-
- 57 www.waset.org <1 %
Internet Source
-
- 58 www.recurrence-plot.tk <1 %
Internet Source
-
- 59 Submitted to Vrije Universiteit Brussel <1 %
Student Paper
-
- 60 L. Seifert, H. Leblanc, R. Herault, J. Komar, C. Button, D. Chollet. "Inter-individual variability in the upper–lower limb breaststroke coordination", Human Movement Science, 2011 <1 %
Publication

-
- 61 Albertas Skurvydas. "Extension and flexion torque variability in ACL deficiency", Knee Surgery Sports Traumatology Arthroscopy, 02/08/2011 **<1 %**
Publication
-
- 62 sensorimotor.mcmaster.ca **<1 %**
Internet Source
-
- 63 ses.library.usyd.edu.au **<1 %**
Internet Source
-
- 64 link.springer.com **<1 %**
Internet Source
-
- 65 Meie Shen, Wei-Neng Chen, Jun Zhang, Henry Shu-Hung Chung, O. Kaynak. "Optimal Selection of Parameters for Nonuniform Embedding of Chaotic Time Series Using Ant Colony Optimization", IEEE Transactions on Cybernetics, 2013 **<1 %**
Publication
-
- 66 repositorio-aberto.up.pt **<1 %**
Internet Source
-
- 67 "Learning To Live Together: Promoting Social Harmony", Springer Nature, 2019 **<1 %**
Publication
-
- 68 Submitted to London School of Economics and Political Science **<1 %**
Student Paper

69	pure.ltu.se Internet Source	<1 %
70	fias.uni-frankfurt.de Internet Source	<1 %
71	"Computer Information Systems and Industrial Management", Springer Nature, 2016 Publication	<1 %
72	Submitted to University of South Florida Student Paper	<1 %
73	shura.shu.ac.uk Internet Source	<1 %
74	Elizabeth Bradley, Holger Kantz. "Nonlinear time-series analysis revisited", Chaos: An Interdisciplinary Journal of Nonlinear Science, 2015 Publication	<1 %
75	www.byo.ics.upm.es Internet Source	<1 %
76	syrtoproject.eu Internet Source	<1 %
77	Submitted to National Taiwan Normal University Student Paper	<1 %
78	metis-app.vu.nl Internet Source	<1 %

79	www.esade.edu Internet Source	<1 %
80	Submitted to Auckland University of Technology Student Paper	<1 %
81	Submitted to University of Western Ontario Student Paper	<1 %
82	Tommy P. Keane, Nathan D. Cahill, Jeff B. Pelz. "Eye-movement sequence statistics and hypothesis-testing with classical recurrence analysis", Proceedings of the Symposium on Eye Tracking Research and Applications - ETRA '14, 2014 Publication	<1 %
83	eprints.whiterose.ac.uk Internet Source	<1 %
84	Submitted to IIT Delhi Student Paper	<1 %
85	IFMBE Proceedings, 2009. Publication	<1 %
86	Hiroshi Endo. "Gender differences in hand stability of normal young people assessed at low force levels", Ergonomics, 03/2011 Publication	<1 %
	elib.dlr.de	

87	Internet Source	<1 %
88	digitalcommons.usu.edu Internet Source	<1 %
89	www.math.aau.dk Internet Source	<1 %
90	Submitted to University of Westminster Student Paper	<1 %
91	www.cs.tut.fi Internet Source	<1 %
92	Lipika Kabiraj, Aditya Saurabh, Pankaj Wahi, R. I. Sujith. "Route to chaos for combustion instability in ducted laminar premixed flames", Chaos: An Interdisciplinary Journal of Nonlinear Science, 2012 Publication	<1 %
93	www.ncbi.nlm.nih.gov Internet Source	<1 %
94	www.swell-project.net Internet Source	<1 %
95	Submitted to University of Queensland Student Paper	<1 %
96	egr.uri.edu Internet Source	<1 %

- 97 Marwan, Norbert, and Charles L. Webber. "Mathematical and Computational Foundations of Recurrence Quantifications", Understanding Complex Systems, 2015. <1 %
Publication
-
- 98 Radhakrishna, R.K.A.. "Nonlinear measures of heart rate time series: influence of posture and controlled breathing", Autonomic Neuroscience: Basic and Clinical, 20001002 <1 %
Publication
-
- 99 www.scribd.com <1 %
Internet Source
-
- 100 Submitted to Imperial College of Science, Technology and Medicine <1 %
Student Paper
-
- 101 content.iospress.com <1 %
Internet Source
-
- 102 Submitted to University of Strathclyde <1 %
Student Paper
-
- 103 dspace.lboro.ac.uk <1 %
Internet Source
-
- 104 elib.suub.uni-bremen.de <1 %
Internet Source
-
- 105 dyuthi.cusat.ac.in <1 %
Internet Source

- 106 Guneysu, Arzu, Recep Doga Siyli, and Albert Ali Salah. "Auto-evaluation of motion imitation in a child-robot imitation game for upper arm rehabilitation", The 23rd IEEE International Symposium on Robot and Human Interactive Communication, 2014. <1 %
Publication
-
- 107 repository.essex.ac.uk <1 %
Internet Source
-
- 108 psychsoc.gerontologyjournals.org <1 %
Internet Source
-
- 109 Submitted to University of Sydney <1 %
Student Paper
-
- 110 www.journal-labphon.org <1 %
Internet Source
-
- 111 hal.univ-lorraine.fr <1 %
Internet Source
-
- 112 Submitted to Universitas Brawijaya <1 %
Student Paper
-
- 113 mdpi.com <1 %
Internet Source
-
- 114 www.math.uni-bremen.de <1 %
Internet Source
-
- 115 www.ise.vt.edu <1 %
Internet Source

116	www.jneurosci.org	<1 %
Internet Source		
117	Giulia Dona. "Application of functional principal component analysis in race walking: An emerging methodology", Sports Biomechanics, 11/2009	<1 %
Publication		
118	Submitted to University of Wisconsin, Madison	<1 %
Student Paper		
119	Submitted to 2642	<1 %
Student Paper		
120	pdfs.semanticscholar.org	<1 %
Internet Source		
121	dl.acm.org	<1 %
Internet Source		
122	brn.sagepub.com	<1 %
Internet Source		
123	edepot.wur.nl	<1 %
Internet Source		
124	tesisenxarxa.net	<1 %
Internet Source		
125	ione.psy.uconn.edu	<1 %
Internet Source		

Submitted to University of Nottingham

126

Student Paper

<1 %

127

serval.unil.ch

Internet Source

<1 %

128

M Javorka. "The effect of orthostasis on recurrence quantification analysis of heart rate and blood pressure dynamics", *Physiological Measurement*, 01/01/2009

Publication

<1 %

129

Submitted to University of Durham

Student Paper

<1 %

130

"The Theory of the Moiré Phenomenon",
Springer Nature America, Inc, 2007

Publication

<1 %

131

Shuhei Tsuchida, Tsutomu Terada, Masahiko
Tsukamoto. "A system for practicing
formations in dance performance supported by
self-propelled screen", *Proceedings of the 4th
Augmented Human International Conference
on - AH '13*, 2013

Publication

<1 %

132

Submitted to St. Mary's College Twickenham

Student Paper

<1 %

133

Submitted to Harper Adams University College

Student Paper

<1 %

- 134 espace.curtin.edu.au <1 %
Internet Source
- 135 Complex Dynamical Systems in Education, 2016. <1 %
Publication
- 136 mobile.repository.ubn.ru.nl <1 %
Internet Source
- 137 www.pik-potsdam.de <1 %
Internet Source
- 138 Submitted to Indian Institute of Technology, Madras <1 %
Student Paper
- 139 www.gmat.unsw.edu.au <1 %
Internet Source
- 140 Submitted to The University of Manchester <1 %
Student Paper
- 141 Joseph S. Iwanski. "Recurrence plots of experimental data: To embed or not to embed?", Chaos An Interdisciplinary Journal of Nonlinear Science, 1998 <1 %
Publication
- 142 oparu.uni-ulm.de <1 %
Internet Source
- 143 www.ideals.illinois.edu <1 %
Internet Source

-
- 144 Marwan, N.. "Recurrence plots for the analysis of complex systems", Physics Reports, 200701 **<1 %**
Publication
-
- 145 www.dpmms.cam.ac.uk **<1 %**
Internet Source
-
- 146 Studies in Computational Finance, 2002. **<1 %**
Publication
-
- 147 www.dtic.mil **<1 %**
Internet Source
-
- 148 Jonas Sandlund, Divya Srinivasan, Marina Heiden, Svend Erik Mathiassen. "Differences in motor variability among individuals performing a standardized short-cycle manual task", Human Movement Science, 2017 **<1 %**
Publication
-
- 149 Submitted to Heriot-Watt University **<1 %**
Student Paper
-
- 150 open.bu.edu **<1 %**
Internet Source
-
- 151 Wei-neng Chen, Jun Zhang. "Ant colony optimization for determining the optimal dimension and delays in phase space reconstruction", Proceedings of the 13th annual conference on Genetic and evolutionary computation - GECCO '11, 2011 **<1 %**
Publication

-
- 152 www.cosic.esat.kuleuven.be <1 %
Internet Source
-
- 153 www.bartneck.de <1 %
Internet Source
-
- 154 www.uni-konstanz.de <1 %
Internet Source
-
- 155 rsta.royalsocietypublishing.org <1 %
Internet Source
-
- 156 Vega, I., Ch. Schütte, and T.O.F. Conrad.
"Finding metastable states in real-world time
series with recurrence networks", *Physica A
Statistical Mechanics and its Applications*,
2016.
Publication <1 %
-
- 157 nabytek-chodura.cz <1 %
Internet Source
-
- 158 www3.fi.mdp.edu.ar <1 %
Internet Source
-
- 159 Ezio Preatoni. "Motor variability in sports: A
non-linear analysis of race walking", *Journal of
Sports Sciences*, 10/2010 <1 %
Publication
-
- 160 "Proceedings of the 20th Congress of the
International Ergonomics Association (IEA
2018)", Springer Nature America, Inc, 2019 <1 %

- 161 www.ece.iit.edu <1 %
Internet Source
- 162 Herrmann, Christian. "Robotic Motion Compensation for Applications in Radiation Oncology", Universität Würzburg, 2013. <1 %
Publication
- 163 A. E. Adeniji, O. I. Olusola, A. N. Njah. "Comparative study of chaotic features in hourly wind speed using recurrence quantification analysis", AIP Advances, 2018 <1 %
Publication
- 164 docs.di.fc.ul.pt <1 %
Internet Source
- 165 Xu Jianyuan, Teng Yun, Lin Xin. "Study of Polluted Insulator Flashover Forecasting Based on Nonlinear Time Series Analysis", 2008 International Conference on High Voltage Engineering and Application, 2008 <1 %
Publication
- 166 Casdagli, M.. "State space reconstruction in the presence of noise", Physica D: Nonlinear Phenomena, 199108 <1 %
Publication
- 167 es.scribd.com <1 %
Internet Source

- 168 file.scirp.org <1 %
Internet Source
- 169 Submitted to Nanyang Technological University, Singapore <1 %
Student Paper
- 170 Submitted to University of Southern California <1 %
Student Paper
- 171 psthomas.com <1 %
Internet Source
- 172 arastirma.boun.edu.tr <1 %
Internet Source
- 173 Submitted to Universiti Selangor <1 %
Student Paper
- 174 158.197.33.91 <1 %
Internet Source
- 175 Z O Guimarães-Filho. "Characterizing electrostatic turbulence in tokamak plasmas with high MHD activity", Journal of Physics Conference Series, 09/01/2010 <1 %
Publication
- 176 Goldberger, A.L.. "What is physiologic complexity and how does it change with aging and disease?", Neurobiology of Aging, 200201/02 <1 %
Publication

177

Submitted to University of Chichester

Student Paper

<1 %

178

Jorge A. Gómez-García, Juan I. Godino-Llorente, Germán Castellanos-Dominguez.

"Non uniform Embedding based on Relevance Analysis with reduced computational complexity: Application to the detection of pathologies from biosignal recordings",
Neurocomputing, 2014

Publication

<1 %

179

[epubs.siam.org](http://pubs.siam.org)

Internet Source

<1 %

180

goce4interior.dgfi.tum.de

Internet Source

<1 %

181

Brian A. Hargreaves. "Time-optimal multidimensional gradient waveform design for rapid imaging", *Magnetic Resonance in Medicine*, 01/2004

Publication

<1 %

182

Submitted to Indian Institute of Science, Bangalore

Student Paper

<1 %

183

Small, . "Time series embedding and reconstruction", *World Scientific Series on Nonlinear Science Series A*, 2005.

Publication

<1 %

- 184 Joan Serrà. "Cross recurrence quantification for cover song identification", New Journal of Physics, 09/15/2009 <1 %
- Publication
-
- 185 www.research-collection.ethz.ch <1 %
- Internet Source
-
- 186 Pier Luigi Gentili, Hiroshi Gotoda, Milos Dolnik, Irving R. Epstein. "Analysis and prediction of aperiodic hydrodynamic oscillatory time series by feed-forward neural networks, fuzzy logic, and a local nonlinear predictor", Chaos: An Interdisciplinary Journal of Nonlinear Science, 2015 <1 %
- Publication
-
- 187 dblp.dagstuhl.de <1 %
- Internet Source
-
- 188 Submitted to Da Yeh University <1 %
- Student Paper
-
- 189 Understanding Complex Systems, 2015. <1 %
- Publication
-
- 190 Barbado Murillo, David, Rafael Sabido Solana, Francisco J. Vera-Garcia, Narcis Gusi Fuertes, and Francisco J. Moreno. "Effect of increasing difficulty in standing balance tasks with visual feedback on postural sway and EMG: Complexity and performance", Human <1 %

Movement Science, 2012.

Publication

191	hci.sbg.ac.at	<1 %
192	www.medien.ifi.lmu.de	<1 %
193	journals.plos.org	<1 %
194	youtube.com	<1 %
195	www.norg.uminho.pt	<1 %
196	Submitted to Fakultat fur Maschinenwesen der Technischen Universitat Munchen	<1 %
197	Student Paper	
198	www.utgjiu.ro	<1 %
199	Internet Source	
200	civil.colorado.edu	<1 %
201	raeng.co.uk	<1 %
202	Internet Source	
203	projekter.aau.dk	<1 %
204	theses.ucalgary.ca	<1 %
205	Internet Source	

<1 %

-
- 202 ro.ecu.edu.au <1 %
Internet Source
-
- 203 www.eneuro.org <1 %
Internet Source
-
- 204 Submitted to Oxford Brookes University <1 %
Student Paper
-
- 205 IFMBE Proceedings, 2010. <1 %
Publication
-
- 206 s-space.snu.ac.kr <1 %
Internet Source
-
- 207 Vacas-Jacques, Paulino, and Marija Strojnik. "", Infrared Spaceborne Remote Sensing and Instrumentation XV, 2007. <1 %
Publication
-
- 208 www.ruthschulz.com <1 %
Internet Source
-
- 209 "Wearable Robotics: Challenges and Trends", Springer Nature, 2017 <1 %
Publication
-
- 210 www.federalregister.gov <1 %
Internet Source
-
- 211 Reinoud J. Bootsma. "Dynamics of trajectory

formation and speed/accuracy trade-offs",
Behavioral and Brain Sciences, 06/1997

<1 %

Publication

212 Z. Q. ZHAO. "IDENTIFYING SPATIAL PATTERNS AND DYNAMICS OF CLIMATE CHANGE USING RECURRENCE QUANTIFICATION ANALYSIS: A CASE STUDY OF QINGHAI-TIBET PLATEAU", International Journal of Bifurcation and Chaos, 2011

<1 %

Publication

213 NORBERT MARWAN. "HOW TO AVOID POTENTIAL PITFALLS IN RECURRENCE PLOT BASED DATA ANALYSIS", International Journal of Bifurcation and Chaos, 2011

<1 %

Publication

214 darwin.bth.rwth-aachen.de

<1 %

Internet Source

215 wwwdocs.fce.unsw.edu.au

<1 %

Internet Source

216 Ramdani, S.. "On the use of sample entropy to analyze human postural sway data", Medical Engineering and Physics, 200910

<1 %

Publication

217 S. Dia. "Using Recurrence Plots for Determinism Analysis of Blade-Disk Tribometer", Experimental Techniques, 01/2012

<1 %

- 218 digital.library.adelaide.edu.au <1 %
Internet Source
-
- 219 KOH, MIN-SUNG, DANILO P. MANDIC, and ANTHONY G. CONSTANTINIDES. "THEORY OF DIGITAL FILTER BANKS REALIZED VIA MULTIVARIATE EMPIRICAL MODE DECOMPOSITION", *Advances in Adaptive Data Analysis*, 2014.
Publication
-
- 220 users.cms.caltech.edu <1 %
Internet Source
-
- 221 DISHAN HUANG. "A NEW APPLICATION OF ENSEMBLE EMD AMELIORATING THE ERROR FROM INSUFFICIENT SAMPLING RATE", *Advances in Adaptive Data Analysis*, 2011
Publication
-
- 222 roar.uel.ac.uk <1 %
Internet Source
-
- 223 hal.inria.fr <1 %
Internet Source
-
- 224 www.econjournals.com <1 %
Internet Source
-
- 225 Włodzimierz Klonowski. "From conformons to <1 %

human brains: an informal overview of nonlinear dynamics and its applications in biomedicine", Nonlinear Biomedical Physics, 2007

Publication

- | | | |
|-----|---|--------|
| 226 | www.aag.asn.au
Internet Source | $<1\%$ |
| 227 | <p>Berenice Rojo-Garibaldi, David Alberto Salas-de-León, María Adela Monreal-Gómez, Norma Leticia Sánchez-Santillán et al. "Nonlinear analysis of the occurrence of hurricanes in the Gulf of Mexico and the Caribbean Sea", Nonlinear Processes in Geophysics, 2018</p> <p>Publication</p> | $<1\%$ |
| 228 | www.gandsnut.net
Internet Source | $<1\%$ |
| 229 | <p>Joan E. Deffeyes, Regina T. Harbourne, Wayne A. Stuberg, Nicholas Stergiou.</p> <p>"Approximate entropy used to assess sitting postural sway of infants with developmental delay", Infant Behavior and Development, 2011</p> <p>Publication</p> | $<1\%$ |
| 230 | www illc uva nl
Internet Source | $<1\%$ |
| 231 | d28rz98at9flks.cloudfront.net
Internet Source | $<1\%$ |

232	oro.open.ac.uk Internet Source	<1 %
233	people.sc.fsu.edu Internet Source	<1 %
234	M. Faggini. "Visual Recurrence Analysis: Application to Economic Time series", New Economic Windows, 2007 Publication	<1 %
235	Michael Small. "Transforming Time Series into Complex Networks", Lecture Notes of the Institute for Computer Sciences Social Informatics and Telecommunications Engineering, 2009 Publication	<1 %
236	tdx.cat Internet Source	<1 %
237	www.cmsim.org Internet Source	<1 %
238	oa.upm.es Internet Source	<1 %
239	"Game Theory for Security and Risk Management", Springer Nature America, Inc, 2018 Publication	<1 %
240	www.ambarish.com	

<1 %

-
- 241 Lecture Notes in Computer Science, 2006. <1 %
Publication
- 242 Breanna E. Studenka, Adam C. King, Karl M. Newell. "Differential time scales of change to learning frequency structures of isometric force tracking.", Journal of Experimental Psychology: Human Perception and Performance, 2014 <1 %
Publication
- 243 www.arlis.org <1 %
Internet Source
- 244 www.hcibib.org <1 %
Internet Source
- 245 Jonathan B. Dingwell. "Nonlinear time series analysis of normal and pathological human walking", Chaos An Interdisciplinary Journal of Nonlinear Science, 2000 <1 %
Publication
- 246 Vlahogianni, E.I.. "Statistical characteristics of transitional queue conditions in signalized arterials", Transportation Research Part C, 200712 <1 %
Publication
-

247

Internet Source

<1 %

248

www.jucs.org

Internet Source

<1 %

249

Nicholas Stergiou, Leslie M. Decker. "Human movement variability, nonlinear dynamics, and pathology: Is there a connection?", Human Movement Science, 2011

Publication

<1 %

250

doc.gold.ac.uk

Internet Source

<1 %

251

Minxing Yu, Jiang Wang, Haitao Yu, Yingmei Qin. "Effect of Time Delay on the Variability of Output Pattern of CPG Network", 2018 37th Chinese Control Conference (CCC), 2018

Publication

<1 %

252

Fusaroli, Riccardo, and Kristian Tylén. "Investigating Conversational Dynamics: Interactive Alignment, Interpersonal Synergy, and Collective Task Performance", Cognitive Science, 2015.

Publication

<1 %

253

ilearnrw.eu

Internet Source

<1 %

254

Bellie Sivakumar. "Chaos in Hydrology", Springer Nature, 2017

<1 %

- 255 www.badania-gospodarcze.pl <1 %
Internet Source
- 256 Karunasinghe, D.S.K.. "Chaotic time series prediction with a global model: Artificial neural network", Journal of Hydrology, 20060530 <1 %
Publication
- 257 eprints.soton.ac.uk <1 %
Internet Source
- 258 academic.hep.com.cn <1 %
Internet Source
- 259 Chelani, Asha B. Devotta, Sukumar. "Nonlinear analysis and prediction of coarse particulate matter concentration in ambient air.", Journal of the Air & Waste Management As, Jan 2006 Issue <1 %
Publication
- 260 Saif Nalband, Aditya Sundar, A. Amalin Prince, Anita Agarwal. "Feature selection and classification methodology for the detection of knee-joint disorders", Computer Methods and Programs in Biomedicine, 2016 <1 %
Publication
- 261 pure.roehampton.ac.uk <1 %
Internet Source

M. Victoria Caballero-Pintado, Mariano Matilla-

- 262 García, Manuel Ruiz Marín. "Symbolic recurrence plots to analyze dynamical systems", *Chaos: An Interdisciplinary Journal of Nonlinear Science*, 2018 <1 %
Publication
-
- 263 Soehle, Martin, Bernadette Gies, Peter Smielewski, and Marek Czosnyka. "Reduced complexity of intracranial pressure observed in short time series of intracranial hypertension following traumatic brain injury in adults", *Journal of Clinical Monitoring and Computing*, 2013. <1 %
Publication
-
- 264 Michael S. O'Brien, Catherine G. Constable, Robert L. Parker. "Frozen-flux modelling for epochs 1915 and 1980", *Geophysical Journal International*, 1997 <1 %
Publication
-
- 265 ira.lib.polyu.edu.hk <1 %
Internet Source
-
- 266 research.aalto.fi <1 %
Internet Source
-
- 267 Witt, Annette, and Bruce D. Malamud. "Quantification of Long-Range Persistence in Geophysical Time Series: Conventional and Benchmark-Based Improvement Techniques", *Surveys in Geophysics*, 2013. <1 %

- 268 arxiv.org Internet Source <1 %
-
- 269 Ouyang, G.. "Using recurrence plot for determinism analysis of EEG recordings in genetic absence epilepsy rats", Clinical Neurophysiology, 200808 <1 %
Publication
-
- 270 Paul van Geert. "Unfolding Potential as Dynamic Emergence: A View From the Theory of Complex, Nonlinear Dynamic Systems", Journal of Cognitive Education and Psychology, 2014 <1 %
Publication
-
- 271 Martin L. Tanaka. "Separatrices and basins of stability from time series data: an application to biodynamics", Nonlinear Dynamics, 12/09/2008 <1 %
Publication
-
- 272 Michael J. Richardson. "Distinguishing the noise and attractor strength of coordinated limb movements using recurrence analysis", Biological Cybernetics, 02/06/2007 <1 %
Publication
-
- 273 T. E. KARAKASIDIS. "RECURRENCE QUANTIFICATION ANALYSIS OF TEMPERATURE FLUCTUATIONS IN A HORIZONTAL ROUND HEATED TURBULENT <1 %

JET", International Journal of Bifurcation and Chaos, 2009

Publication

-
- 274 Yin, Yi, and Pengjian Shang. "Multiscale recurrence plot and recurrence quantification analysis for financial time series", Nonlinear Dynamics, 2016. <1 %
- Publication
-
- 275 Anisoara Paraschiv-Ionescu. "Nonlinear Analysis of Physiological Time Series", Advanced Biosignal Processing, 2009 <1 %
- Publication
-
- 276 Eleni I. Vlahogianni. "Temporal Evolution of Short-Term Urban Traffic Flow: A Nonlinear Dynamics Approach", Computer-Aided Civil and Infrastructure Engineering, 10/2008 <1 %
- Publication
-
- 277 www.bdigital.unal.edu.co <1 %
- Internet Source
-
- 278 www.science.gov <1 %
- Internet Source
-
- 279 SYED, MUJAHID N., PANDO G. GEORGIEV, and PANOS M. PARDALOS. "SEIZURE MANIFOLD OF THE EPILEPTIC BRAIN: A STATE SPACE RECONSTRUCTION APPROACH", BIOMAT 2012, 2013. <1 %
- Publication

- 280 Pavlos, G.P.. "Evidence for chaotic dynamics in the Jovian magnetosphere", Planetary and Space Science, 200404/05 <1 %
Publication
-
- 281 cs.upm.ro <1 %
Internet Source
-
- 282 Junhai Ma. "The Study of the Chaotic Behavior in Retailer's Demand Model", Discrete Dynamics in Nature and Society, 2008 <1 %
Publication
-
- 283 documents.mx <1 %
Internet Source
-
- 284 repositorio.ufpe.br <1 %
Internet Source
-
- 285 carl-witt.de <1 %
Internet Source
-
- 286 Samani, Afshin, Svend Erik Mathiassen, and Pascal Madeleine. "Cluster-based exposure variation analysis", BMC Medical Research Methodology, 2013. <1 %
Publication
-
- 287 bioinformatics.oxfordjournals.org <1 %
Internet Source
-
- 288 Hasson, C.J.. "Influence of embedding parameters and noise in center of pressure <1 %

recurrence quantification analysis", Gait & Posture, 200804

Publication

-
- 289 Faes, Luca, Silvia Erla, and Giandomenico Nollo. "Compensating for instantaneous signal mixing in transfer entropy analysis of neurobiological time series", 2012 Annual International Conference of the IEEE Engineering in Medicine and Biology Society, 2012. <1 %
- Publication
-
- 290 docplayer.net <1 %
- Internet Source
-
- 291 www.bemservizi.unito.it <1 %
- Internet Source
-
- 292 Claxton, Laura J., Jennifer M. Strasser, Elise J. Leung, Joong Hyun Ryu, and Kathleen M. O'Brien. "Sitting infants alter the magnitude and structure of postural sway when performing a manual goal-directed task : Adaptive Postural Sway in Sitting Infants", Developmental Psychobiology, 2014. <1 %
- Publication
-
- 293 onlinelibrary.wiley.com <1 %
- Internet Source
-
- 294 www.newcastle.edu.au <1 %
- Internet Source

-
- 295 West, B.J.. "The independently fractal nature of respiration and heart rate during exercise under normobaric and hyperbaric conditions", *Respiratory Physiology & Neurobiology*, 200502 <1 %
Publication
-
- 296 archive.org <1 %
Internet Source
-
- 297 medicaljournals.se <1 %
Internet Source
-
- 298 pub.uni-bielefeld.de <1 %
Internet Source
-
- 299 Riva, F., M.J.P. Toebe, M. Pijnappels, R. Stagni, and J.H. van Dieën. "Estimating fall risk with inertial sensors using gait stability measures that do not require step detection", *Gait & Posture*, 2013. <1 %
Publication
-
- 300 "Cognitive Workload and Fatigue in Financial Decision Making", Springer Nature America, Inc, 2016 <1 %
Publication
-
- 301 mtg.upf.edu <1 %
Internet Source
-
- 302 Peng, Hua, Huosheng Hu, Fei Chao, Changle

Zhou, and Jing Li. "Autonomous Robotic Choreography Creation via Semi-interactive Evolutionary Computation", International Journal of Social Robotics, 2016.

<1 %

Publication

303 IFMBE Proceedings, 2014.

<1 %

Publication

304 "Progress in Motor Control", Springer Nature America, Inc, 2014

<1 %

Publication

305 core.ac.uk

<1 %

Internet Source

306 Wagner, H.. "Movement variability and skill level of various throwing techniques", Human Movement Science, 201202

<1 %

Publication

307 Porporato, A.. "Multivariate nonlinear prediction of river flows", Journal of Hydrology, 20010715

<1 %

Publication

308 digitalcommons.wku.edu

<1 %

Internet Source

309 www.dai-labor.de

<1 %

Internet Source

310 "Approximate Recurrence Quantification Analysis (aRQA) in Code of Best Practice", Springer Proceedings in Physics, 2016.

<1 %

- 311 David R. Bickel. "Robust and efficient estimation of the mode of continuous data: the mode as a viable measure of central tendency", Journal of Statistical Computation and Simulation, 2003 <1 %
- Publication
-
- 312 "Translational Recurrences", Springer Nature America, Inc, 2014 <1 %
- Publication
-
- 313 A. C. ILIOPOULOS. "GLOBAL LOW DIMENSIONAL SEISMIC CHAOS IN THE HELLENIC REGION", International Journal of Bifurcation and Chaos, 2010 <1 %
- Publication
-
- 314 Christopher S. Thaxton, W. P. Anderson, Chuanhui Gu, Borko Stosic, Tatijana Stosic. "Detrended fluctuation analysis and entropy-complexity causality analysis of temperatures in an urbanized mountain stream", Stochastic Environmental Research and Risk Assessment, 2017 <1 %
- Publication
-
- 315 Steffen Schulz. "The altered complexity of cardiovascular regulation in depressed patients", Physiological Measurement, 03/01/2010 <1 %

- 316 Rathleff, M.S.. "Inverse relationship between the complexity of midfoot kinematics and muscle activation in patients with medial tibial stress syndrome", *Journal of Electromyography and Kinesiology*, 201108 <1 %
- Publication
-
- 317 Gaudez, C., M.A. Gilles, and J. Savin. "Intrinsic movement variability at work. How long is the path from motor control to design engineering?", *Applied Ergonomics*, 2016. <1 %
- Publication
-
- 318 Agarwal, Ravi P., Erdal Karapınar, Donal O'Regan, and Antonio Francisco Roldán-López-de-Hierro. "Multidimensional Fixed Point Theorems on G-Metric Spaces", *Fixed Point Theory in Metric Type Spaces*, 2015. <1 %
- Publication
-
- 319 L.D. Zhang. "Real Urban Traffic Flow Chaotic Phase Space Study", 2008 11th International IEEE Conference on Intelligent Transportation Systems, 10/2008 <1 %
- Publication
-
- 320 Dimitris Vassiliadis. "Systems theory for geospace plasma dynamics", *Reviews of Geophysics*, 2006 <1 %
- Publication
-

- 321 Advances in Intelligent Systems and Computing, 2013. <1 %
Publication
-
- 322 NIELS WESSEL. "NONLINEAR METHODS OF CARDIOVASCULAR PHYSICS AND THEIR CLINICAL APPLICABILITY", International Journal of Bifurcation and Chaos, 2007 <1 %
Publication
-
- 323 Stergiou, N.. "Human movement variability, nonlinear dynamics, and pathology: Is there a connection?", Human Movement Science, 201110 <1 %
Publication
-
- 324 Reik V Donner. "Recurrence networks—a novel paradigm for nonlinear time series analysis", New Journal of Physics, 03/15/2010 <1 %
Publication
-
- 325 Submitted to University of Wales Institute, Cardiff <1 %
Student Paper
-

Exclude quotes

On

Exclude matches

Off

Exclude bibliography

On